भौमिक एवं ग्रहीय पर्यावरण के ऊर्ज विज्ञान, गतिकी, एवं रसायन शास्त्र की वैज्ञानिक समझ, तथा समाज पर इनकी विवक्षा

वैज्ञानिक उपलब्धियाँ

Scientific understanding of the energetics, dynamics and chemistry of the terrestrial and planetary environments and implications to the society

SCIENTIFIC ACCOMPLISHMENTS

2024-2025

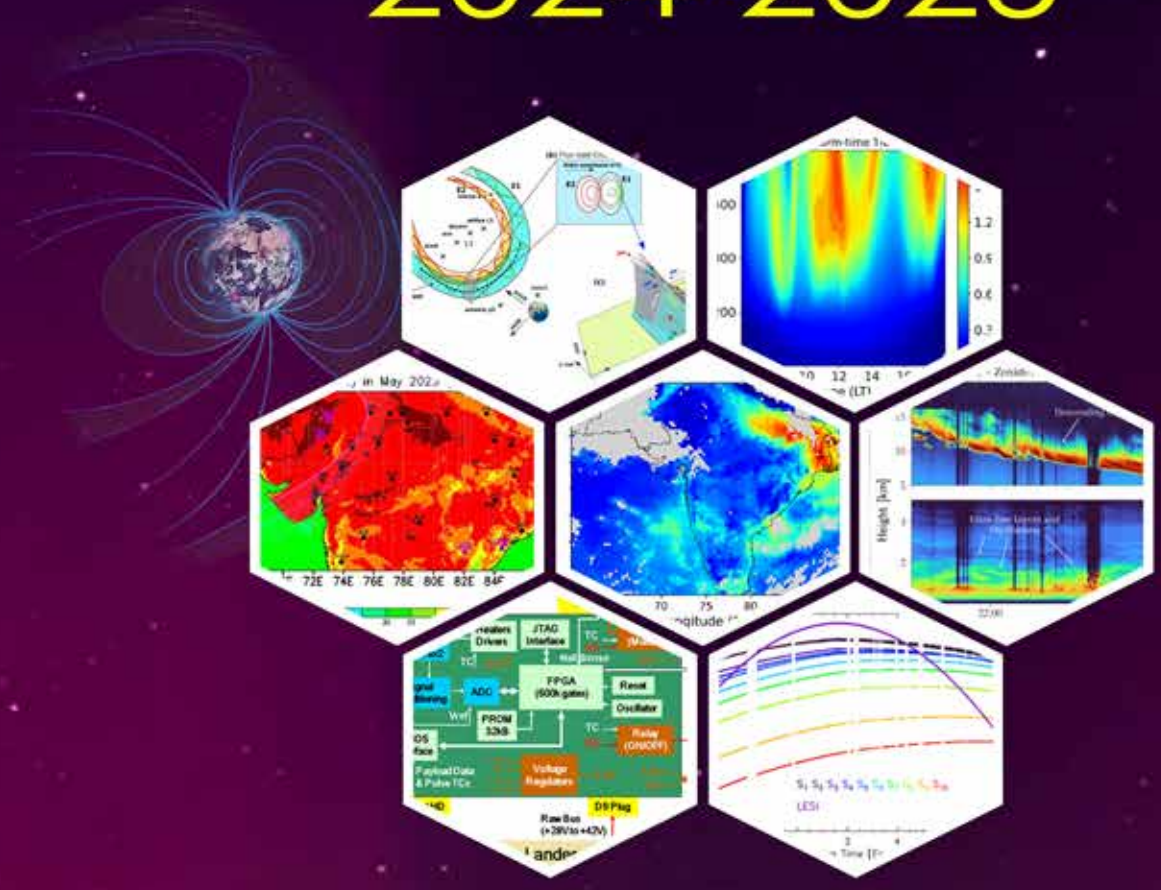

अंतरिक्ष भौतिकी प्रयोगशाला
विक्रम साराभाई अंतरिक्ष केंद्र
तिरुवनन्तपुरम

SPACE PHYSICS LABORATORY
Vikram Sarabhai Space Centre
Thiruvananthapuram

MBLP ATRF NAM ADB ITMP PSB ATD PCC ADM

वैज्ञानिक सलाहकार समिती एसपीएल
Scientific Advisory Committee of SPL

अध्यक्ष / Chairman

Dr. T. K. Alex, Hon. Distinguished Professor, ISRO HQ

सदस्य / Members

Prof. Dipankar Banerjee, Director, IIST

Prof. A. P. Dimri, Director, IIG

Sri. Ganesh Pillai M, Scientific Secretary, ISRO HQ

Dr. Amit Kumar Patra, Director, NARL

Prof. N. V. Chalapthi Rao, Director, NCESS

Dr. Saleem H, Dy. Director, AVN, VSSC

Dr. Tirtha Patim Das, Director, SPO, ISRO HQ

Prof. S. K. Satheesh, Chairman, DCCC, IISc, Bangalore

Prof. K. Mohan Kumar, Emeritus Professor, CUSAT

Prof. R. Sridharan, Former Director, SPL (Emeritus Scientist, PRL)

Prof. P. Balarama Rao, Former Director, NARL

Prof. A. Jayaraman, Former Director, NARL

Prof. Animesh Maitra, Calcutta University

Dr. Raj Kumar, Satish Dhawan Professor, SAC

Dr. S. Seetha, Former Director, SSPO, ISRO HQ

Dr. Tarun Kumar Pant, Director, SPL (Member Secretary)

वैज्ञानिक उपलब्धियाँ
Scientific Accomplishments

2024-2025

विक्रम साराभाई अंतरिक्ष केंद्र
Vikram Sarabhai Space Centre

भारतीय अंतरिक्ष अनुसंधान संगठन
Indian Space Research Organisation


GOVERNMENT OF INDIA
DEPARTMENT OF SPACE
VIKRAM SARABHAI SPACE CENTRE

भारत सरकार
अंतरिक्ष विभाग
विक्रम साराभाई अंतरिक्ष केंद्र
तिरुवनंतपुरम - 695 022, भारत
दूरभाष : 0471-2565567/2704412
फैक्स : 0471-2704105
ईमेल : director@vssc.gov.in

ए राजराजन
A Rajarajan
विशिष्ट वैज्ञानिक व
Distinguished Scientist &
निदेशक/Director

Government of India
Department of Space
Vikram Sarabhai Space Centre
Thiruvananthapuram - 695 022, India
Phone : +91-471-2565567/2704412
Fax : +91-471-2704105
Email : director@vssc.gov.in

FOREWORD

The Space Physics Laboratory (SPL) at Vikram Sarabhai Space Centre has always been striving to excel and advance in the research areas of atmospheric, space, and planetary sciences through a seamless integration of space- and ground-based observations, theory, and modeling. Through its carefully designed scientific programmes, SPL continues to contribute meaningfully to the realization of ISRO's long-term scientific vision while deepening our understanding of the Earth-Atmosphere system, the Sun–Earth connection, and planetary environments. SPL's strength lies in its capability for the development of scientific payloads and experimental systems, encompassing conceptualization, design, fabrication, qualification, and deployment, supported by close synergy with other entities within VSSC. Complementing this, SPL has created sustained academic partnerships with universities and national research institutions, resulting in nationwide ground-based observational networks and successful execution of coordinated field campaigns across the country. These collective efforts are aimed at addressing fundamental questions and processes that have far-reaching implications for climate, weather, space weather, and societal applications.

The year 2024–25 marked a period of exceptional scientific momentum for SPL. The successful performance of SPL payloads on Chandrayaan-3, RAMBHA-LP and ChaSTE, continues to result in new perspectives on Lunar thermal properties and the lunar near-surface plasma environment, laying an essential scientific foundation for sustained human exploration of the Moon. Observations from Aditya-L1 provided new insights into solar transients and turbulence, while integrated Sun–Earth studies of the intense May 2024 geomagnetic storm revealed various new aspects of the complex coupling that governs space weather impacts on near-Earth environments. Significant advances were made through exploration of the ionosphere–magnetosphere coupling, atomic oxygen variability relevant to satellite drag, volcanic influences on climate, monsoon convection, aerosol–climate interactions, satellite remote-sensing algorithms, and regional CO_2 flux inversion. Looking ahead, SPL has initiated several forward-looking programmes that reflect its evolving scientific ambition. These include the development of advanced Rayleigh Lidar systems, the establishment of an extraterrestrial sample analysis laboratory, the deeper lunar thermal probe (TAAP), and the realization of four scientific payloads for the Venus Orbiter Mission. Together, these initiatives position SPL to address frontier scientific questions related to planetary evolution, atmospheric coupling across scales, and space weather processes in the coming decade.

The vibrancy of SPL's research ecosystem is evident from the publication of over eighty papers in high-impact peer-reviewed journals. Equally important is the Laboratory's strong commitment to nurturing the next generation of scientists through the ISRO Research Fellowship and Post-Doctoral schemes supported by ISRO and national initiatives such as the INSPIRE Faculty Scheme, Ramanujan Fellowship, National Post-Doctoral Fellowship, and DST Women Scientist Fellowship.

The Scientific Advisory Committee, comprising eminent scientists, provides invaluable guidance through its annual review of SPL's activities and future plans. I am pleased to acknowledge that the Committee's guidance has consistently helped align SPL's research directions with emerging scientific opportunities and national priorities. As SPL/VSSC remains committed to not only pursue but also translate its scientific understanding into capability and societal relevance, I commend the scientists, engineers, technical staff, students and collaborators of SPL for their dedication and excellence, and I wish the Laboratory continued success in the years ahead.

(A. Rajarajan)

SCIENTIFIC DISCIPLINES AND ACTIVITIES

From the Director

Annual accomplishments are not merely a record of activities, but a reflection of institutional growth, learning, and maturity. For SPL the year 2024–25 was a year of notable advances across research, mission support, infrastructure development, and human resource nurturing. This report captures the collective efforts and achievements of our scientific, technical, and administrative teams during the year under review. It is a privilege to present this Annual Accomplishment Report, and I am honored to assume this responsibility at a time when SPL as an institute continues to build upon a strong legacy of scientific excellence in space and Earth system sciences.

This year, extensive analysis of Chandrayaan-3 Lander payload data continued yielding new results. While the RAMBHA-LP revealed daytime electron densities of 300–650 cm^{-3} and electron temperatures of 3000–8000 K, ChaSTE observations indicated a mean vertical temperature gradient of 3.8 ± 0.24 K cm^{-1} in the upper 10 cm of regolith, with thermal diffusivity indicating two distinct layers separated at ~6 cm depth. These findings provide vital insights into the electromagnetic environment near surface and subsurface heat transfer and thermal properties of the high-latitude lunar regolith. The two-way radio occultation experiment using S-band signals from Chandrayaan-2 has revealed, for the first time, the electron density profile of the lunar ionosphere within the geomagnetic tail, showing unusually high plasma densities (~2.5×10^4 cm^{-3}) around 4km and above influenced by localized lunar magnetic fields. As one knows, experiments onboard ISRO's Chandrayaan 1 & 2 orbiter missions by SPL have unambiguously established the dynamic nature of Moon's surface bound exosphere, its' composition and altitudinal extant. In fact, SPL's CHACE-2 payload onboard CH-2 continues to provide data as the orbiter is still functioning. In this context, during the extreme geomagnetic storm of May, 2024 ISRO's CHACE-2 onboard Chandrayaan-2 provided the first observational confirmation of a more than tenfold increase in lunar exospheric densities, caused by solar wind ion sputtering from Coronal Mass Ejection impacts on the Moon. Investigation of the Mars Orbiter Mission (MOM) radio signal data for October 2021 provided solar wind velocities (100–150 km s^{-1}) and electron densities (~10^{10} m^{-3}) in the solar coronal region. These estimates have been shown to be consistent with theoretical trends but lower than previous studies owing to the weak solar activity during the observation period.

ISRO's Aditya-L1, the satellite for the study of Sun and Solar Wind, hosts two very important payloads conceived by SPL, VSSC and developed with the support of other entities in VSSC and LEOS, namely Plasma Analyzer Package for Aditya (PAPA) and dual-sensor fluxgate MAGnetometer (MAG). The dual-sensor fluxgate magnetometer (MAG) has been successfully monitoring the magnetic field changes associated with the solar wind arriving at L1. In fact, the MAG has captured some key solar transient events, that have revealed some new aspects on the transitions from anisotropic to quasi-isotropic turbulence in solar wind during extreme solar activity. At the same time, the PAPA performing nominally, has been providing continuous solar wind and particle flux data in various energy bins. The first results from PAPA are currently in the peer review process for publication. While these results enhance understanding of solar wind dynamics near Earth, more such results are expected in near future as these payloads continue to operate regularly and providing data.

The geomagnetic storm that occurred during May, 2024, was one of the strongest ones to occur in the space age. SPL carried out extensive studies on this event from source to terrestrial ionosphere using data obtained through a combination of satellite & ground-based observations and modelling. First, the numerical simulations using multiple heliospheric and coronal models successfully reproduced the near-simultaneous arrival of multiple Coronal Mass Ejections (CMEs) causing the geomagnetic storm. This validated the models' capability to accurately predict CME arrival times and velocities during complex solar storms. Following this, multipoint observations from Aditya-L1 (MAG payload) and other spacecrafts revealed a large-scale internal magnetic reconnection within an ICME (interplanetary CME) flux rope—triggered by interacting CMEs—forming an extensive current

sheet over 200 earth radii. This study demonstrated how internal reconnection reshapes magnetic structures of ICMEs and drives severe space weather impacts on Earth such as that during May 2024 event.

The CMEs during the May 2024 event led to the commencement of extreme geomagnetic storm, when SPL's HF radar and ionosonde observations at Thumba detected very large and oscillating prompt penetration electric fields (PPEF) of magnetospheric origin, producing significant plasma drift variations and formation of F3 layers. Observations using GPS, Digisonde, and physics-based ionospheric modeling over Thumba during the May 2024 storm revealed that fluctuating prompt penetration electric fields, together with storm-time meridional wind reversals, jointly produced strong daytime Vertical Total Electron Content (VTEC) enhancements, undulations, and F3 layers demonstrating the coupled influence of electrodynamic and neutral wind processes on the Indian equatorial ionosphere.

During the same event, analysis of satellite observations (SWARM-A and GOLD) revealed a strong super-fountain and extremely variable Equatorial Ionization Anomaly driven by enhanced electric fields and accompanied by increased electron temperatures in the evening equatorial ionosphere, highlighting the complex and localized impacts of intense geomagnetic disturbances. One can say that perhaps these studies from SPL on the space weather events of May 2024 are most comprehensive covering regions from near Sun interplanetary space, L1 point, magnetosphere to Earth's upper atmosphere. These measurements and studies have significant implications in our efforts for evolving a more realistic space situational awareness.

It is important to mention that in recent years an understanding is evolving that the ionosphere responds very significantly to forcing due to atmospheric processes occurring below it, especially during quiet geophysical conditions. Realizing this, research studies have been taken up at SPL to understand this very aspect of Atmosphere-ionosphere coupling initiating an active collaboration between two divisions of SPL that traditionally explore two different regions of atmosphere. In one such study, the multi-instrument atmospheric, ionospheric observations and modeling using COSMO for Thumba revealed that tropical cyclones can significantly disturb the equatorial and low-latitude ionosphere through gravity wave activity and alter the electrodynamics. In another important study using ground- and space-based observations of ionospheric parameters such as TEC and ionospheric densities, distinct pre-seismic anomalies about nine days before the 2021 Haiti earthquake (a major earthquake) were brought forth, suggesting a plausible ionospheric response linked to the event, underscoring the need for multi-parameter studies in earthquake-prone regions. SPL also made notable advancements in modelling domain through the development of a robust Large Eddy Simulation (LES) framework for predicting the diurnally evolving atmospheric boundary layer (ABL) under the transient influence of a solar eclipse. This first-of-its-kind modelling framework enabled direct investigation of the time-evolving turbulence characteristics in response to transient and dynamically varying incoming solar radiation. Broadening its modelling capabilities to extreme weather events, SPL effectively employed the COSMO model to elucidate the critical role of boundary-layer dynamics in the persistence of severe heat waves over the central Indian region.

Atmospheric and climate research is a crucial and significant component of SPL's research and is aimed at understanding weather patterns, genesis and evolution of cyclones, monsoon and water cycle, aerosols and regional climate changes, among many other important aspects. By studying these, we strive to improve weather modeling and forecasting for evolving better adaptation and mitigation strategies. Using multi-year C-band polarimetric Doppler Weather radar from Thumba and satellite data, SPL characterized the morphology and diurnal cycle of convective storms over the Indian region, improving the understanding of monsoon variability. Radar observations over the central Himalayan region during the Asian Summer Monsoon reveal generally weak vertical motions, except for a distinct downdraft layer around 10–11 km altitude, offering new insights into air mass transport and uplift processes within the monsoon system. The instantaneous shortwave and longwave radiative effects of deep convective cloud-cores over the tropics have been derived using multi-year (2012–2018) simultaneous observations of SAPHIR and ScaRaB on board the Megha-Tropiques satellite.

Extensive Regional Climate Model simulations have been done highlighting that aerosol–radiation interactions significantly reduce surface solar radiation and sensible heat flux, especially over the Indo-Gangetic Plain, impacting hydroclimate and air quality. Analysis of observations and model simulations from SPL have revealed that the stratospheric water vapor injected by the Hunga-Tonga Hunga Ha'apai eruption caused significant stratospheric cooling and concurrent strong surface warming over the Indian region, demonstrating the strong radiative impact of volcanic water vapor on regional climate. Based on long-term RH200 rocket observations from Thumba and reanalysis data, a new quasi-periodic oscillation in the tropical upper stratosphere has been identified and the potential sources for this new phenomenon have been proposed. Similarly, analysis of 43 years of reanalysis and satellite data reveals that the Brewer–Dobson Circulation strengthens during the westward phase of the Quasi–Biennial Oscillation, particularly in the Northern Hemisphere, influencing ozone and water vapor distributions and causing measurable variations in stratospheric radiative forcing. Analysis of ERA5 reanalysis data (1981–2021) reveals that the poleward expansion of the Hadley circulation has caused a corresponding

poleward migration of subtropical marine stratocumulus clouds over the northeast Pacific, southeast Pacific, and southeast Atlantic, providing new insights into the (a) long-term climatic impacts of Hadley cell expansion on low-level cloud distribution and (b) profound implication in earth radiation budget.

SPL achieved significant scientific advances in aerosol science through integrated satellite, ground-based, and modelling studies. SPL developed robust retrieval algorithms for Aerosol Optical Depth from INSAT-3DR, enabling accurate geostationary monitoring of regional and temporal aerosol variability, and characterized dust aerosols using the Infrared Difference Dust Index from INSAT-3D. Machine learning–based cloud screening algorithms were implemented for OceanSat-3 OCM-3 imagery to improve aerosol and ocean colour products. Important contributions were made to understand the aerosol–climate interactions through energy-balance decomposition of aerosol-induced surface temperature changes. Comprehensive investigations into aerosol microphysics and chemistry revealed light-scattering and absorption enhancements, black carbon mixing states, and secondary organic aerosol formation under varying air-mass regimes in tropical coastal and continental environments. Regional aerosol characterization studies quantified hygroscopic growth and winter haze amplification over IGP, and speciated radiative forcing over the northern Indian Ocean.

As one understands, estimating CO_2 fluxes is challenging because of the multi-channel exchange of CO_2 between the atmosphere, land, and oceans. In a significant development, SPL has developed an inverse modelling framework to estimate CO_2 fluxes over India using satellite observations. This framework has improved representation of transport and atmospheric mixing in the tropical/monsoon region, thereby reducing errors in attributing observed CO_2 concentrations to surface fluxes.

Along with the payload developmental activities, SPL also undertakes Technology Development Projects that are important from the point of view of the long-term science goals of SPL and relevance to ISRO's programs. In this context, SPL completed four Technology Development Projects (TDPs) and initiated several others. For 2025 the key achievements include successful development of a (a) Standalone Sun Tracking Radiometer (SSTR) for AOD measurements, (b) a high-altitude aerosol sampling system, (c) Micropulse lidar capable of ultrathin clouds and cloud layers detection up to an altitude of 18 km from ground, and (d) a VLF-ELF receiver capable of detecting the changes in ionospheric D-region during quiet and thunderstorm conditions, having direct implications in atmosphere ionosphere coupling. All these four systems have been field tested and are deployed for regular measurements.

SPL has published over 80 peer-reviewed research papers during 2024-2025. SPL is leading Scientific collaborations with national and international institutions, such as IRF Kiruna Sweden for Venus Orbiter Mission & University of Tokyo/JAXA, for Akatsuki mission that have strengthened the scope of SPL's planetary and atmospheric research. Nationally, SPL collaborates with over more than 40 universities and national institutes to operate its network of ground-based observations systems. At present SPL operates three projects/networks in collaboration. These are (1) Aerosol Radiative Forcing Over India (ARFI) Project of ISRO-GBP focusing on the study of aerosols, (2) Network of Boundary Layer Experiments (NOBLE) Project of ISRO-GBP focusing on atmospheric boundary layer & atmospheric dynamics and (3) Indian Network for Space Weather Impact Monitoring (INSWIM) focusing on the ionosphere across the country during varying space weather conditions. In addition, SPL conducts multi-institutional field experiments from time to time involving balloon and ship-borne measurements. In addition to these research activities, SPL also continues its critical operational role as an integral member of ISRO's Inter-Centre Weather Forecasting Expert Team, successfully delivering short-range COSMO-based weather forecasts in support of all PSLV, GSLV, and LVM launch missions from SHAR. While SPL's senior members actively contribute to the research programs of leading national institutes and universities through their advisory roles, SPL as an institute is evolving to better respond to the emerging national and global challenges in serving the society.

We are thankful to Dr. T. K. Alex (Chairman, SPL-SAC) and members of the scientific advisory committee of SPL for meticulously steering our scientific and technical developments to meet our institutional aspirations over the years. We have always made our best efforts to implement all the recommendations made by the SPL-SAC.

All our accomplishments owe it to the visionary leadership at VSSC and ISRO. Shri. A. Rajarajan, Director, VSSC has been a constant motivator and a strong driving force pushing us to constantly pursue our scientific goals. We are extremely thankful to Dr. V. Narayanan, Chairman, ISRO for his constant guidance and support to our research and development programs, and inspiration to think of better ways to carry forward SPL's scientific legacy keeping in view ISRO's long term goals.

तरुण कुमार पन्त

तरुण कुमार पंत / Tarun Kumar Pant
निदेशक, एसपीएल/Director, SPL

सम्मान / RECOGNITIONS

Suresh Babu S

- Elected as Fellow of National Academy of Science India (FNASc).
- Represented Government of India in the 62nd session of Intergovernmental Panel on Climate Change (IPCC) at Hangzhou, China, during 24 – 28 February, 2025.

Rubia R

- Young Scientist Award, International Union of Radio Science (URSI) Regional conference on Radio Science, Uttarakhand, India, 2024.

अकादमिक उत्कृष्टता / ACADEMIC EXCELLENCE

Swathi B, Sathiyamoorthy V

- Best Paper Award, "Roll clouds over the Arabian Sea and their association with monsoon activity", International Symposium on Tropical Meteorology (INTROMET-2025), Indian Institute of Tropical Meteorology, Pune, 18-20 November 2025.

Siddarth Shankar Das

- Felicitated by VSSC_ISRO for highest number of publications in refereed journals as first author during 2010-2024

Vijayakumar S Nair

- Top cited paper award India in Environmental Science by Institute of Physics (IOP) Publishing's, UK (2024)

Mukunda Gogoi, Suresh Babu S, Tandule Chakradhar Rao

- Best Paper Award for "AI-Enhanced Multi-Wavelength Multi-Pixel aerosol retrieval from OCM-2 on-board Oceansat-2 satellite", Satellite Technology Day Symposium, U. R. Rao Satellite Centre, Bengaluru, April 21, 2025.

Anjana U, Kishore Kumar K

- Best paper award at International Symposium on Tropical Meteorology (INTROMPET-2025) held at IITM Pune.

Reuben Samson Yaqub

- Best Poster Award, "First Measurements of D-region plasma density over dip equatorial region using in-house developed VLF receiver", 40th PSSI National Symposium on Plasma Science and Technology for Sustainable Future, IIT Tirupati. 27-29 December 2025.

अंतरराष्ट्रीय यात्रा अनुदान / INTERNATIONALTRAVEL GRANTS

Ayisha M Ashruf

- SCOSTEP Visiting Scholar Fellowship 2025 (SVS 2025).

Indu Venugopal

- AGU 2025 Student Travel Grant.

Shibotosh Biwsas

- "Vella Fellowship" from Los Alamos National Laboratory (LANL), USA, for the Los Alamos space weather summer school 2025.
- Summer school on "Cross-scale Coupling of Heliophysics Systems", University of L'Aquila, Italy, May 12-16, 2025.

अंतर्वस्तु / Contents

प्रकाशन / PUBLICATIONS

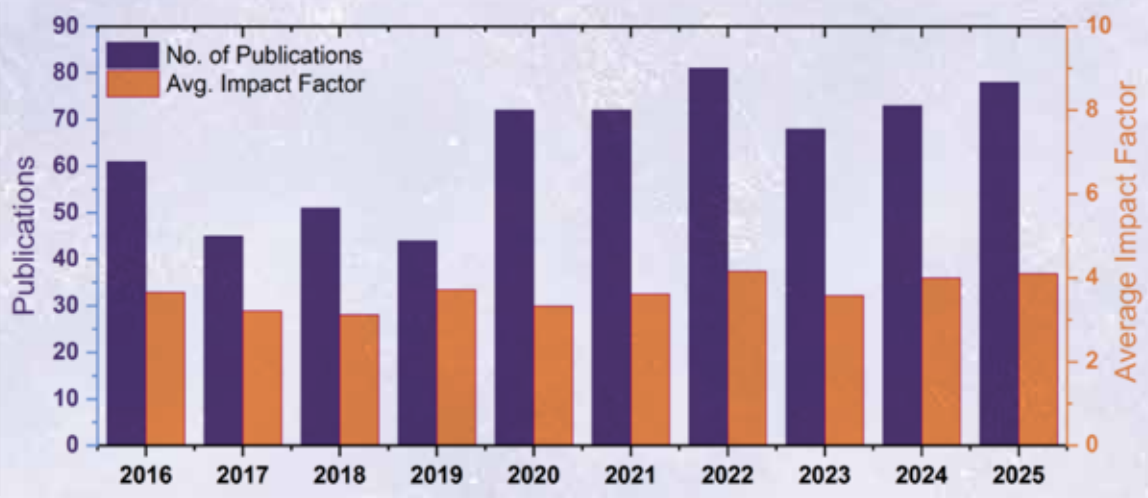

पीएच.डी. सम्मानित/Ph.D. AWARDED

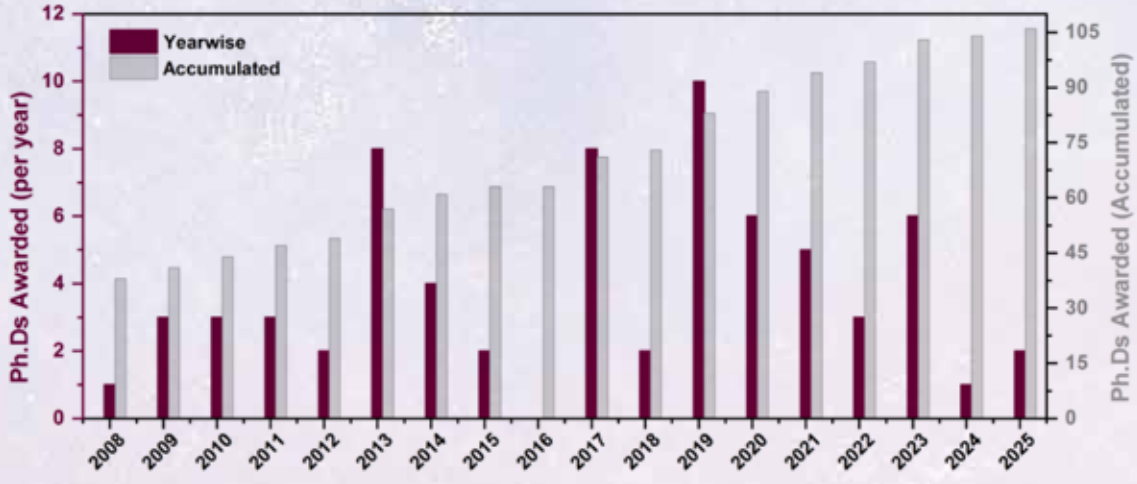

Veenus Venugopal

- "Impacts of Brewer-Dobson Circulation on the Distribution of Stratospheric Ozone and Water Vapour", University of Kerala, September 2025 [Supervisor: Siddarth Shankar Das].

Richa Naja Jain

- "A study on solar wind dynamics and its impact on near-Earth space environment using Radio Science techniques", University of Kerala, Thiruvananthapuram, July 2025 [Supervisor: Raj Kumar Choudhary].

माईक्रो तरंग एवं परिसीमा स्तर भौतिकी
MICROWAVE AND BOUNDARY LAYER PHYSICS

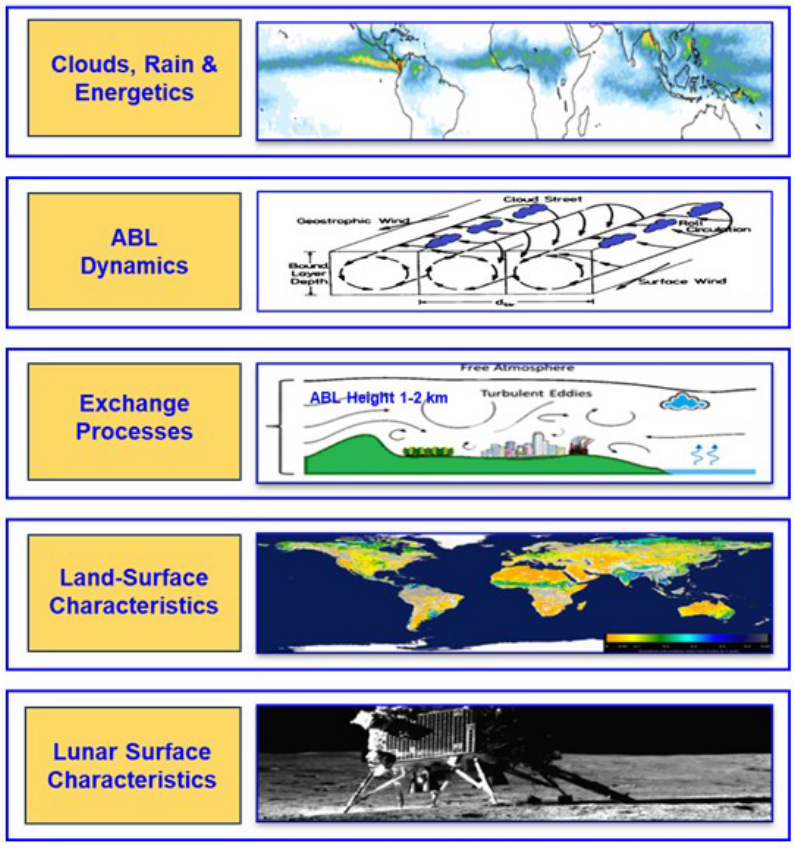

एमबीएलपी शाखा वायुमंडलीय परिसीमा परत (एबीएल) के पृष्ठीय अभिलक्षणों, संरचना एवं गतिकी तथा मुक्त क्षोभमंडल, मेघों, संवहन, अवक्षेपण के साथ इसके युग्मन और पृथ्वी एवं अन्य ग्रहीय पिंडों के माइक्रोवेव सुदूरसंवेदन पर ध्यान केंद्रित करती है। इस शाखा के मुख्य लक्ष्य हैं: (i) पृष्ठ-वायु अन्योन्यक्रिया प्रक्रियाओ, एबीएल के दैनिक प्रादर्भाव व प्रदूषक प्रकीर्णन में एबीएल प्रक्रियाओं की भूमि का सहित सुस्पष्ट भौगोलिक पर्यावरण के बारे में समझ को बढ़ाना (ii) मेघों, अवक्षेपण एवं भूवायुमंडल प्रणाली की ऊर्जिकी से संबंधित समझ को सुधारना, एवं (iii) ग्रहों के सतहों की अंतरिक्षवाहित तथा भू-आधारित माइक्रोवेव सुदूर संवेदन से पृष्ठीय गुणधर्मों, वायुमंडलीय जल बाष्प, मेघ अभिलक्षणों एवं अवक्षेपण, तथा वायुमंडल के माध्यम से माइक्रोवेव संचरण पर उनके संभाव्य प्रभावों का अध्ययन।

The MBLP branch focuses on the surface characteristics, structure and dynamics of the atmospheric boundary layer (ABL) and its coupling with free-troposphere, clouds, convection, precipitation, and microwave remote sensing of the Earth and other planetary bodies. The main objectives are: (i) to improve the understanding of the ABL processes under distinct geographical environments, including surface-air interaction processes, diurnal evolution of ABL, and the role of ABL processes in pollutant dispersal, (ii) improve the understanding on clouds, precipitation and energetics of the Earth-atmosphere system, and (iii) space-borne and ground based microwave remote sensing of planetary surface and atmosphere for deriving the surface properties, atmospheric water vapour, cloud characteristics and precipitation, including their potential impact on microwave propagation through the atmosphere.

वैज्ञानिक टीम / Science Team
सत्यमूर्ती वी. / Sathiyamoorthy V.
किरण कुमार एन. वी. पी. / Kiran Kumar N. V. P.
निज़ी मात्यू / Nizy Mathew
संतोष एम. / Santosh M.
रंजू आर. / Renju R.
शैलेन्द्र कुमार / Shailendra Kumar
एड्विन वी डेविस / Edwin V. Davis[&]
राजीव के. / Rajeev K[##]

तकनीकी टीम / Technical Team
दिनकर प्रसाद वज्जा / Dinakar Prasad Vajja
प्रमोद पी. पी. / Pramod P. P.
लाली पी. टी. / Lali P. T.

अनुसन्धान सहयोगी / Research Associate
नयमा वल्सा स्करिया / Nayama Valsa Scariah[*]

अनुसंधान अध्येता / Research Fellows
स्वाती बी./ Swathi B.
सार्थक तिवारी / Sarthak Tiwari [**]
अश्वती आर. एस. / Aswathy R. S.[$]
फात्तिमा षिरिन पी. टी. / Fathima Shirin P. T.[#]

[*] *Joined in June 2025*
[**] *Joined in July 2024*
[&] *Joined in December 2025*
[#] *Relieved in June 2025*
[$] *Relieved in July 2025*
[##] *Superannuated in May 2025*

Atmospheric Boundary-Layer Studies

Boundary-Layer Roll Clouds over the Arabian Sea during the Indian Summer Monsoon Season

A unique type of low-level boundary layer clouds known as roll clouds are observed over the Arabian Sea during the peak summer monsoon season of July-August. They are observed along the flow path of the Arabian Sea branch of the monsoon low-level jet (LLJ). Adjacent bands of the roll clouds are found to be separated by a distance of about 10 km and they stretch for about a few hundred kilometers. They cover a wide area of the central and north Arabian Sea and adjoining west coast of India but failed to garner the attention of the meteorological community. Main reason for this

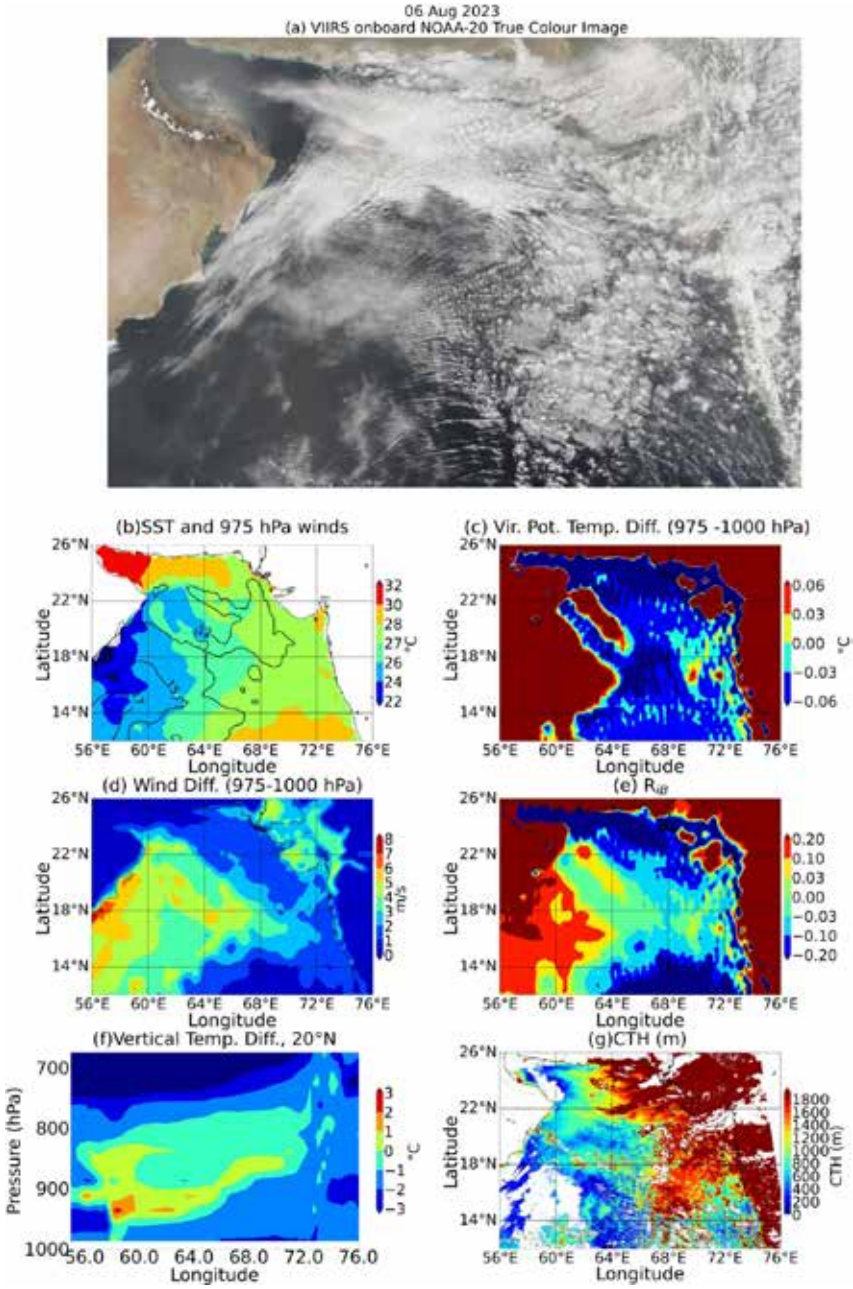

Figure 1: (a) VIIRS onboard NOAA-20 satellite true colour image of 06 August 2023 (b) SST (°C) in shades and 975 hPa wind speed (ms-1) in contours, (c)Virtual potential temperature difference between 975 and 1000 hPa levels (°C) (θv975 – θv1000) (d) wind difference (ms-1) between 975 hPa and 1000 hPa levels (e) bulk Richardson number [RiB] (f) Temperature difference (°C) between adjacent vertical pressure levels along 20°N and (g) Cloud top height (CTH in m) from VIIRS onboard NOAA-20 satellite [Swathi and Sathiyamoorthy, Sci. Rep., 2025].

is that these are low-level clouds, confined to the boundary layer and can't be distinguished from the surface in infrared satellite imageries.

An attempt has been made in this study to understand the mechanism behind their formation using ten years (2005-2014) of high-resolution NOAA-20 satellite imageries and ECMWF reanalysis data. Near-surface vertical wind shear associated with the LLJ (dynamical instability) causes the formation of counter rotating roll vortices. Roll clouds form over the ascending regions and cloud-free condition prevails over the descending regions of the roll vortices. The LLJ carries cold air from the oceanic upwelling region to the exit region with relatively warmer sea surface temperature (SST). This causes thermal instability, which further strengthens the roll cloud formation on the exit region of the LLJ. Roll clouds do not form over the entrance region of the LLJ with stable atmospheric condition.

To understand the role of different instabilities on the formation of roll clouds, thermal instability, dynamic instability and bulk Richardson number (R_{iB}) are calculated between 975 hPa and 1000 hPa levels. Few case studies were made during the peak monsoon season of 2023 whenever roll clouds are clearly seen without the obstruction of mid- and upper-level clouds. Result for one case (August 06, 2023) is provided in Fig. 1 (a-g). True colour image obtained by Visible Infrared Imaging Radiometer Suite (VIIRS) onboard NOAA-20 satellite for 06 August 2023 (Fig. 1a) are analysed. Over the southwest corner of the Arabian Sea (entrance region), cloud-free condition prevails. On the central Arabian sea (exit region) clouds in the form of unbroken straight lines (roll clouds) are seen initially. Further away along the flow path of the LLJ, roll clouds break into individual clouds which appear as string of pearls. Further away, they grow and evolve as closed convective cloud cells (C4).

Roll clouds are found over the regions with moderate wind difference of about 3-5 ms^{-1} with marginally negative temperature difference ranging from -0.03° C to -0.06° C (Fig. 1 c-d) between 975 hPa and 1000 hPa levels. Roll clouds are found over near neutral regions with $-0.03 < R_{iB} < 0$. Roll clouds evolve into C4 over marginally unstable regions with $-0.1 < R_{iB} < -0.03$ on the exit side of the LLJ. Cloud-free condition is found over statically stable regions with $R_{iB} > 0$. (Fig. 1e)

Roll clouds are advected by the LLJ. They grow in size and break into individual cells and further evolve into C4 due to change in instability and gradual increase in the height of lower tropospheric thermal inversion (Fig. 1 f-g). Roll clouds are formed far away from the Western Ghats Mountain without the orographic lifting of monsoon winds. Roll clouds and C4 occupy a large part of the Arabian Sea. They are freely advected over the west Indian states of Gujarat and Rajasthan and adjoining regions of Pakistan due to the absence of orography to block the LLJ. But these clouds are blocked over northern parts of the west coast of India by Western Ghats. They are accumulated and lifted on the windward side of the Western Ghats and provide light to moderate rainfall of 5-25 $mmday^{-1}$ on clear roll days.

Clouds, Precipitation and Energetics of the Earth-Atmosphere System

Understanding the Regional Differences in Cloud Characteristics over South Asia during Indian Summer Monsoon Season using CloudSat Observations

Clouds influence the radiation balance of the earth–atmosphere system. They reflect a fraction of the incoming shortwave solar radiation and block a fraction of the outgoing longwave radiation and thus their characteristics needs to be understood. The attenuation corrected radar reflectivity factor (Z_e) data provided by Cloud Profiling Radar (CPR) onboard CloudSat operating at 94 GHz was used to investigate the characteristics of different types of cloud systems, namely deep convective core (DCC), deep convective system (DCS) and intense convective system (ICS) during 2006 to 2018. Two-dimensional Z_e and height thresholds were used for cloud system identification. DCCs are identified as individual CPR vertical profile, whose tops cross 12-km altitude with base height below 3-km with Z_e > -28 dBZ, 0 dBZ and 10 dBZ at 12 km, 11 km and 9 km altitudes, respectively. DCSs are defined as clouds with a minimum cloud base height (CBH < 2-km) and maximum cloud top height (CTH > 8-km), whereas ICSs consist of at least one pixel with Z_e > 10 dBZ in the continuous area of Z_e.

The relative occurrence of different cloud system types in each 1°lon. ×1lat. grid box during the Indian summer monsoon season has been studied (Fig.2). One of the important features is the difference in their geographical distribution. DCSs are mostly concentrated at the land dominated and topographic areas along with Myanmar, northeast India, Himalayan foothills, central India and Western Ghats. ICSs are concentrated along the Himalayan foothills and Western Ghats. The analysis of the vertical reach based on the different Z_e thresholds showed that cloud top over the oceanic areas is

characterized by the cloud-sized particles whereas over the land and orographic areas, cloud tops are dominated by the precipitation-sized particles. The spatial distribution of cloud systems revealed wide variation in the zonal and meridional directions over the South Asia.

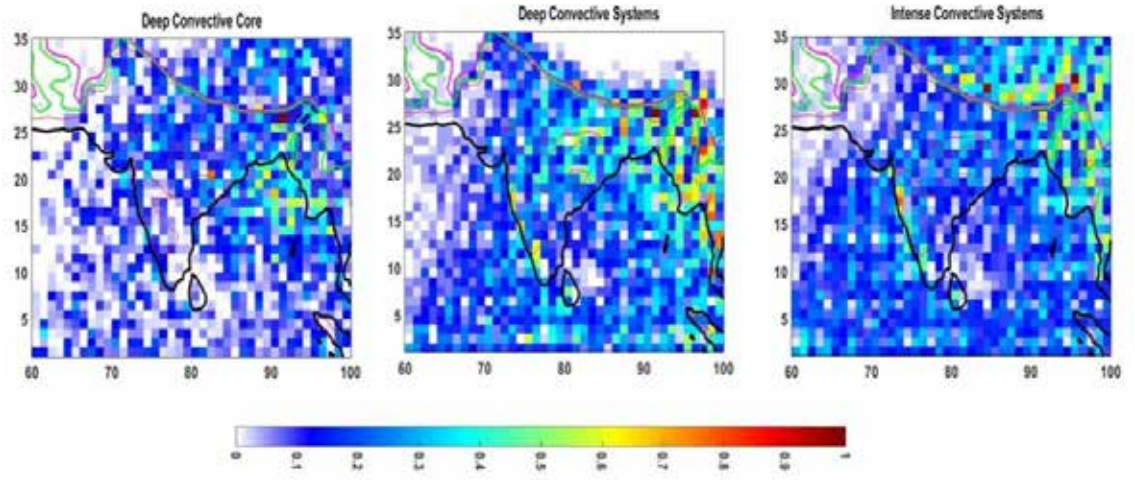

Figure 2: Relative occurrence of (left) deep convective cores, (middle) deep convective systems and (right) intense convective systems in each 1°lon. ×1° lat. box over South Asia during the Indian summer monsoon season of June to September. Relative occurrence of each cloud types is calculated with respect to the maximum numbers of cloud type occurrence in each 1° lon. ×1° lat. grid box [Kumar, Theor. Appl. Climatol., 2025].

Spatial Distribution of Slopes of Radar Reflectivity below the Freezing Level over South Asia using Radar Reflectivity Profiles of TRMM Precipitation Radar

Spatial distribution of slopes of radar reflectivity (SRR) in the lower troposphere (between maximum Z_e in 4-6 km altitude and 1.5-3 km altitude) has been examined for the south Asian region during the Indian summer monsoon season (June to September) of 1998-2013. SRR is calculated by applying linear regression approach on individual attenuation corrected radar reflectivity (Z_e) profiles of the Tropical Rainfall Measuring Mission (TRMM)-Precipitation Radar (PR). Variation in Z_e over a specific area is the result of balance between moisture content in the atmosphere and the strength of updraft. Moist atmosphere with weak updraft at lower levels can lead to accretion or collision of raindrops leading to increased drop size especially over the oceanic shallow cumulus regions. Increase in drop size in the lower atmosphere leads to increase in Z_e towards the surface. However, in a dry lower atmosphere, raindrops either evaporate or break into small raindrops, resulting in a decrease in drop size and reduction in Z_e towards the surface.

PR radar reflectivity profiles with slopes greater (less) than zero indicate that Z_e decreases (increases) towards the surface. Also, variation in Z_e can be interpreted as loss or gain in the raindrop masses (change in the hydrometeor size) due to evaporation, break-up or collision-coalescence process under different meteorological conditions. Fig. 3a shows the spatial distribution of negative SRRs in 1° lon. × 1° lat. boxes and the colour-bar indicates the fraction of PR profiles with negative SRRs. It is observed that more than 70% of TRMM-PR profiles have negative SRRs over ocean compared to land area (<30%). The Arabian Sea and the Equatorial Indian Ocean consist of the highest fraction of negative SRRs (~70–90%). Head Bay of Bengal and adjoining land areas have nearly equal numbers of PR profiles with positive and negative SRRs. The spatial distribution of extreme Z_e slopes (<−1dBZ km^{-1} and > 1dBZ km^{-1}) show nearly similar trends, but the differences are higher among the land and ocean (Fig. 3 b-c). Again, oceanic areas consist of a higher fraction (>80%) of negative slopes, whereas land-dominated areas have a higher fraction of positive slopes (>75%). The spatial distribution of positive and negative SRRs in convective and stratiform precipitations exhibiting the land-ocean difference is significant in convective precipitation compared to stratiform precipitation (Fig.3 e-h). In stratiform precipitation, high fraction of negative slope corresponds to the shallow precipitation areas over the Arabian Sea and the effect of land-ocean contrast is less significant.

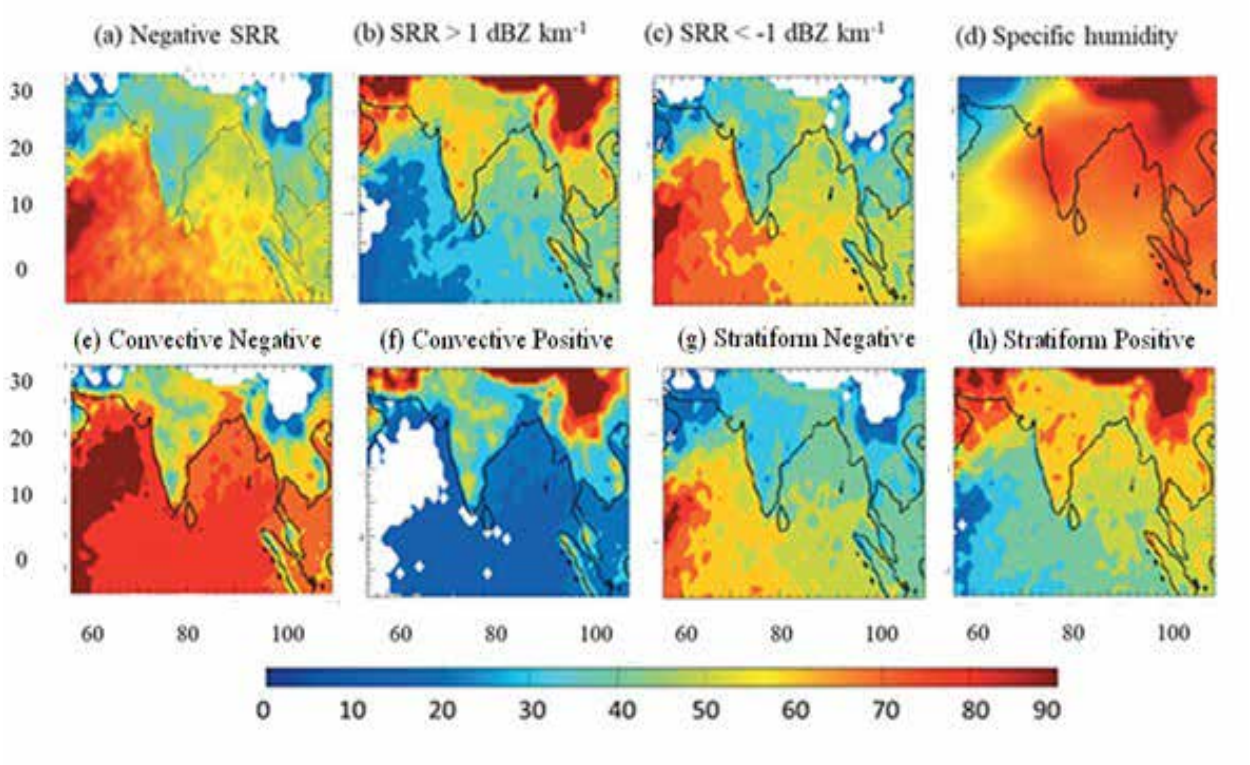

Figure 3: (a) Spatial distribution of TRMM PR radar reflectivity negative slopes. (b) Percentage of PR profiles with extreme positive slope of >1 dBZ km^{-1}. (c) Percentage of PR profiles with extreme negative slopes of <1 dBZ km^{-1}. (d) Surface relative humidity (%) during JJAS months using NCEP reanalysis data. Spatial distribution of PR profiles with (e) negative slopes in convective precipitation (f) positive slopes in convective precipitation (g) negative slopes in stratiform precipitation and (h) positive slopes in stratiform precipitation. Study period is 1998-2013 [Kumar, Remote Sens. Lett., 2024].

Precipitation Structure and Convective Intensity over South Asia during Active and Break Spells of the Indian Summer Monsoon

Precipitation structure (PS) and convective intensity (CI) of precipitation features (PF) are investigated using the multiple sensors onboard Tropical Rainfall Measuring Mission (TRMM) and Global Precipitation Measurement (GPM) satellites during active and break (ACT and BRK) spells of Indian summer monsoon season during 1999-2021 period. Fig. 4 and Fig. 5 show the spatial distribution of different parameters embedded in the PFs indicating their CI (maximum height of 40 dBZ [MH40], flash rate corresponding to lightning activity [Fl rate], minimum polarization corrected temperature at 37GHz [Min37PCT], maximum radar reflectivity factor near the surface (MaxdBZ), vertical depth (maximum height of 20 dBZ (MH20) and minimum IR brightness temperature (MinIR) and structure (size and surface volumetric rainfall contribution) during ACT spell. ACT spells have low MinIR over most parts of India and Bay of Bengal compared with BRK spells which indicates that the clouds are mostly deeper during ACT spells except in a few regions. Bay of Bengal has the lowest MinIR during both ACT and BRK spells (Fig. 4 and Fig 5). Bay of Bengal has the deepest clouds with cloud-sized hydrometeors at higher altitudes but they have shallow precipitation tops (MH20 < 6-km) and moderate CI (MH40 < 4-km, Fl-rate < 5 min^{-1}). During ACT spells, Western Ghats is covered with PFs having shallow precipitation tops but with high near-surface rainfall intensity without lightning activity. However, during BRK spells, larger and deeper PFs are observed over south India with significant lightning activity when compared to ACT spells. During BRK spells, CI is high over the South India and Eastern Ghats (MH20 > 7 km and MH40 > 6 km) with high near-surface rainfall intensity (MaxdBZ > 40 dBZ) and lightning activity (>15 FL min^{-1}).

Higher volumetric surface rainfall distribution is oriented in a slant east-west direction between Myanmar coast and northwest India during ACT spells, whereas, it is oriented east–west along the foothills of Himalayas and over Head Bay of Bengal during BRK spells.

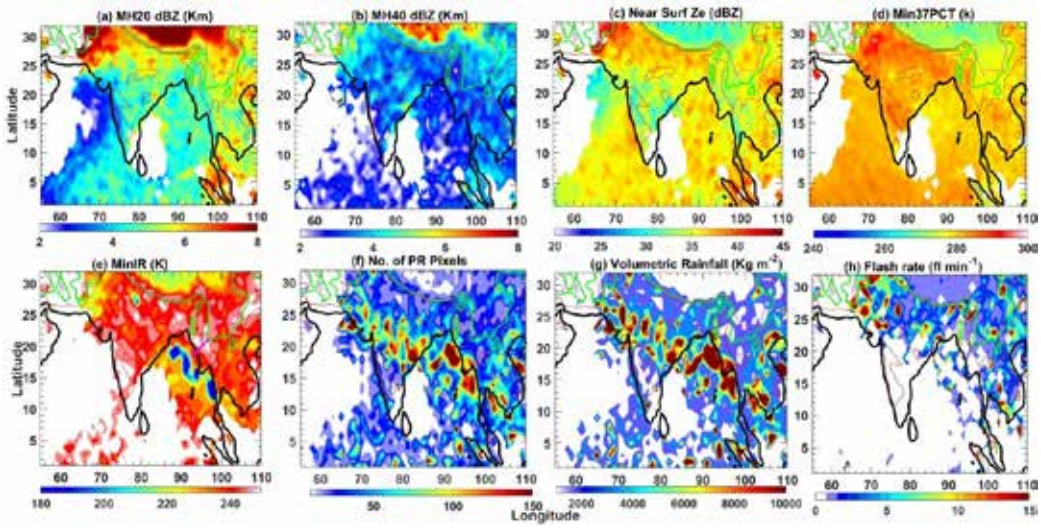

Figure 4: Spatial distribution of PFs and convective intensity during the active spells in each 1° lon. x1°lat. grid box during Indian summer monsoon season of 1999-2021. (a) Maximum height of 20 dBZ using TRMM and GPM PR radar reflectivity which shows the depth of the PF, (b) Maximum height of 40 dBZ using TRMM and GPM PR showing convective intensity of the PF, (c) maximum surface radar reflectivity (in dBZ) using TRMM and GPM PR indicating the intensity of PF, (d) minimum polarisation corrected temperature using TRMM TMI and GPM GMI and (e) minimum infrared brightness temperature using TRMM VIRS; (f) number of TRMM/GPM PR pixels ≥ 20 dBZ in PFs (g) total volumetric surface rainfall (in kg.m^{-2}) (h) lightning flash count (min-1) from TRMM LIS sensor [Kumar, Int. J. Clim., 2025].

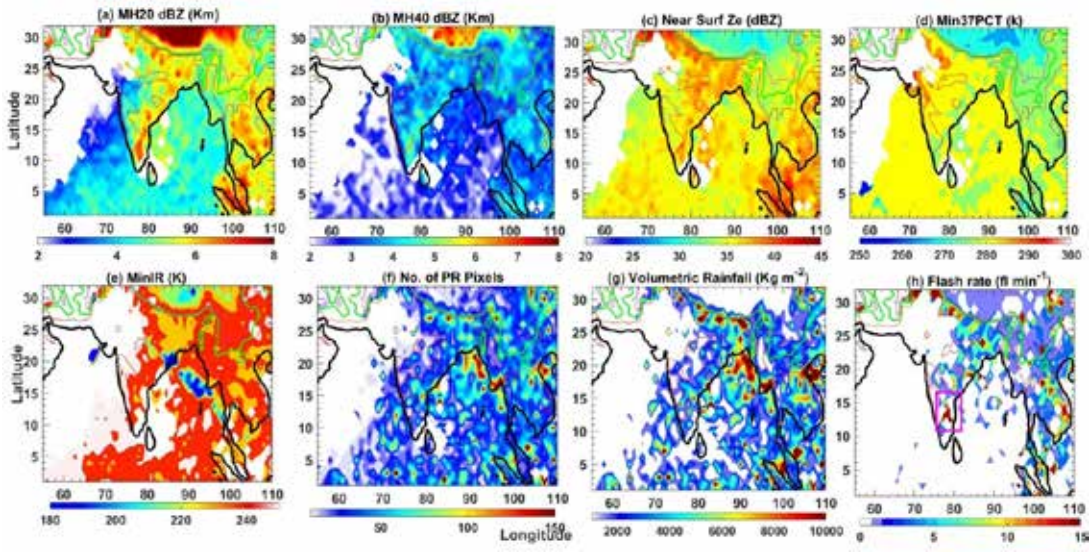

Figure 5: Similar to Figure 4 but for break spells [Kumar, Int. J. Clim., 2025]

Differences in Convective Variability during Active and Break Monsoon Spells over the South Asian Region using 25-years (1998-2022) of Satellite Observation

In this study spatial distribution of four types of extreme convective echoes (ECE) namely, deep convective core (DCC), wide convective core (WCC), deep-wide convective core (DWC) and broad stratiform region (BSR) are studied during active (ACT) and break (BRK) spells of the Indian summer monsoon using 25-years (1998-2022) of precipitation radar data from TRMM and GPM satellite missions. Different ECEs are defined based on three-dimensional attenuation corrected radar reflectivity (Z_e) from space-based precipitation radar, precipitation echo top height (ETH) and areal extent. DCCs are defined as the continuous region of Z_e greater than 30 dBZ with ETH more than 8-km altitude. WCCs are three-dimensional continuous convective area with Z_e greater than 30 dBZ having spatial coverage more than 800 km^2 at any altitude. DWCs are the contiguous area with Z_e greater than 30 dBZ at 8 km altitude and must have

a spatial extent greater than 800 km^2 and BSRs are regions of contiguous stratiform radar echo covering at least 40,000 km^2.

Spatial distribution of different ECEs and extreme convective ETH (Fig.6 and Fig.7) shows regional differences between ACT and BRK spells. DCCs and WCCs show significant differences over the west India, peninsular India and off west coast of India whereas BSRs show major differences over central India and north Bay of Bengal between ACT and BRK spells. Northeastern Himalayas shows least difference between the two spells. Peninsular India has larger and deeper DCCs during BRK spells. DCCs and DWCs over western foothills of Himalayas are deeper during ACT spells but absent during BRK spells. The Arabian Sea has larger but shallower WCCs compared to Bay of Bengal. Difference in horizontal extent and ETH between ACT and BRK is minimal over the Arabian Sea. Bay of Bengal has the largest as well as deepest WCCs during both ACT and BRK spells. ETH of the DCCs over the Western Himalayan Foothills and adjoining regions are deeper during the ACT spells but their spatial extent is small. Changes in the circulation, updraft, atmospheric moisture content and moisture advection are mainly affecting the horizontal extent and depth of ECEs over the monsoon region. These parameters show significant fluctuations between ACT and BRK spells and affect horizontal extent and depth of ECEs.

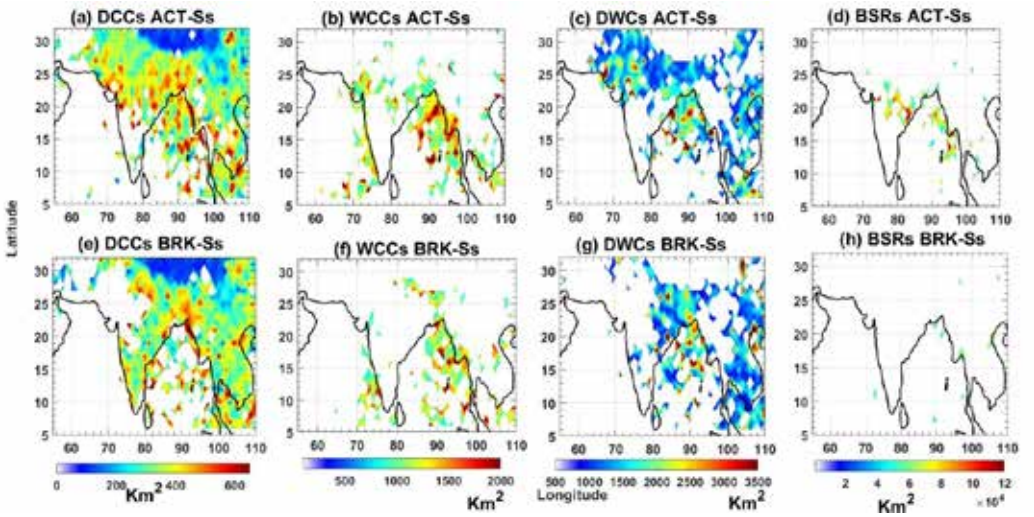

Figure 6: Spatial distribution of extreme convective echo area (in km^2) during (top row) active spells (a) DCC, (b) WCC, (c) DWC and (d) BSR and during (bottom row) break spells (e) DCC, (f) WCC, (g) DWC and (h) BSR. Analysis period is the Indian summer monsoon season of 1998-2022 [Kumar, Theor. Appl. Climatol., 2024].

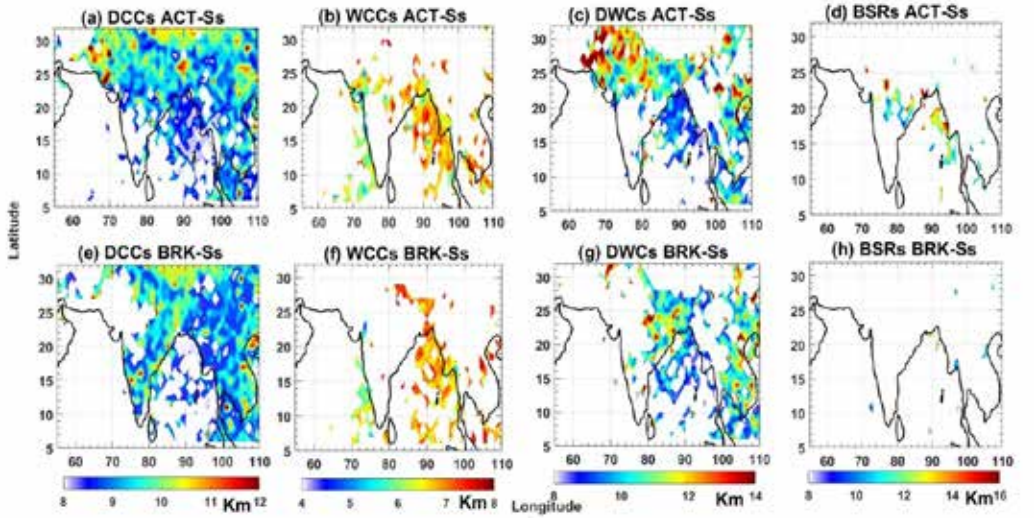

Figure 7: Spatial distribution of extreme convective echo top height (km) during (top row) active spells (a) DCC, (b) WCC, (c) DWC and (d) BSR and during (bottom row) break spells (e) DCC, (f) WCC, (g) DWC and (h) BSR. Analysis period is the Indian summer monsoon season of 1998-2022 [Kumar, Theor. Appl. Climatol., 2024].

Lunar Surface Studies

Operational Insights and Measurements of ChaSTE onboard Chandrayaan-3 Lander

Chandra's Surface Thermophysical Experiment (ChaSTE) instrument was developed and qualified to measure the temperature and thermal conductivity of the top 10cm layer of the lunar regolith. In the absence of a touchdown sensor or camera surveillance, the temperature variation of the lowest temperature sensor (S_{10}) was monitored in near-real time using telemetry focusing on sudden temperature variations to confirm the penetration of ChaSTE into the lunar regolith.

During penetration operation, temperature sensor 'S_{10}' close to the tip of the thermal probe showed a significant temperature drop from stroke 201mm to 215 mm along with a consistent increase in the penetration motor current (Fig. 8). The rate of temperature reduction was 2.3° C per minute, which was one order higher than the rate of temperature reduction observed between the strokes of 77mm to 201mm (0.16° C per minute). The simultaneous reduction in temperature and the increase in motor current at a stroke of 201mm are attributed to the advancement of the ChaSTE probe into the regolith.

Further, penetration commands were executed to continue the advancement of the ChaSTE thermal probe into the regolith. Data recording could not be performed between strokes 267mm to 297mm, for 14 hours, due to parallel mission operations. The probe was fully penetrated into the regolith at the stroke of 303mm, with the sensors positioned from the surface (S_1) to 100mm (S_{10}) below the surface. Throughout the penetration operation, the motor current was observed to be nominal, indicating expected levels of penetrative resistance of the regolith. This confirmed the absence of obstacles such as boulders and stones in the ChaSTE penetration point in the landing site.

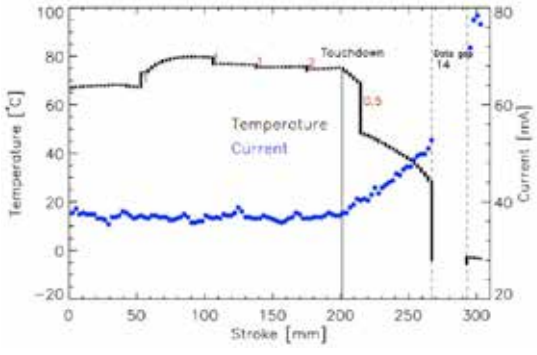

Figure 8: Variation of current (mA) drawn by the ChaSTE penetration motor and the temperature (C) measured by temperature sensor S_{10} for different strokes of probe penetration. The residence times between strokes (in hours) are mentioned in red digits. Touch-down refers to the touchdown of regolith by S_{10} [Mathew et al., Adv. Space Res., 2025a].

Temperature Measurements by ChaSTE/ Chandrayaan-3

ChaSTE penetration operation was completed by 15:36 UTC of 25 August 2023. Subsequent to stabilization of the transients, the initial temperature recorded by S_1 and S_{10}were 56.8°C and −5.5°C, respectively. The initial temperature of all other sensors located between S_1 and S_{10} also falls within these bounds. S_1 reached a maximum of 67°C during the third day after the start of the temperature record, which also has a maximum Sun elevation angle of 19°. A decreasing trend could be seen in the S_1 temperature measurement. However, S_{10} initially increased and then continued to stabilise at 21°C, since it is the farthest from the surface of the regolith. All other sensors exhibited similar behaviour with respect to their relative positions from the surface.

The temperature measured by ChaSTE were higher than those expected from the numerical simulations and measurements done by LRO, though the phase of temperature changes were in accordance with of the effective solar irradiance of the lunar surface (LESI), which is the solar irradiance perpendicular to the surface of Moon (Fig. 9). The reflection of solar radiaton. IR emission and IR absorption by lander module, slope of local terrain and the heat emitted by the lander engines may be the reasons for the higher surface temperature observed. Higher subsurface temperature may be attributed to the shunting effect of ChaSTE probe. The heat shutting by the ChaSTE probe to the subsurface is being investigated using numerical simulations.

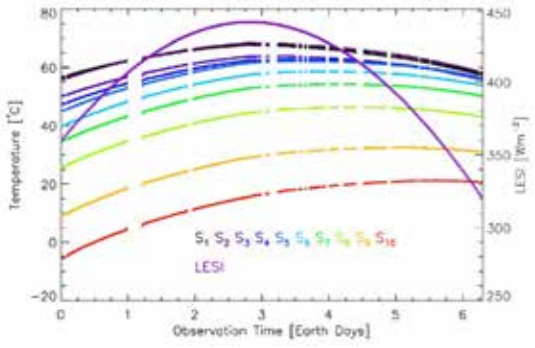

Figure 9: Temperature (°C) variation during Lunar day time measured by ChaSTE sensors (S_1 to S_{10}) placed at different depths of the regolith. Variation of LESI (Wm^{-2}) is also shown. Breaks in the plots are data gaps [Mathew et al., Adv. Space Res., 2025a].

Estimation of Packing Density of Lunar Regolith by ChaSTE/Chandrayaan-3

The force required for the penetration of ChaSTE thermal probe into the lunar regolith depended on the bulk density of the lunar soil. The current drawn by the penetration motor was recorded, which was directly related to the penetration force applied. The loads required for different depths of penetration were estimated from laboratory experiments with lunar simulant for known packing densities. By analysing the measured currents of the penetration motor and the load variation for different depths of penetration for varying packing densities, the penetration forces at the ChaSTE insertion point at the landing site was inferred. The observed variation of penetration force with depth in the lunar regolith byChaSTE falls within the curves corresponding to the laboratory experiments with packing densities of 1930 kgm^{-3} and 1950 $kg.m^{-3}$ (Fig. 10). Hence, the average packing density of the regolith within a depth of ~140 mm at the ChaSTE penetration point was estimated to be 1940 ±10kgm^{-3}.

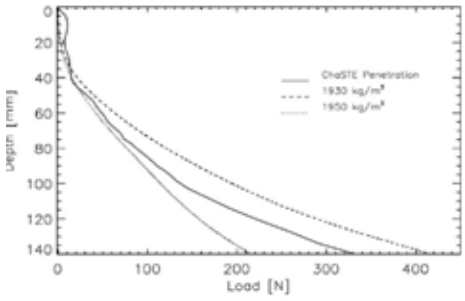

Figure 10: Variation of penetration load (N) with depth (mm). ChaSTE penetration was performed on actual lunar surface at landing site, whereas lab tests (1930 kgm^{-3} & 1950 kgm^{-3}) were performed on lunar simulant of near uniform grain size enclosed in a container [Mathew et al., Adv. Space Res., 2025a].

The packing density estimated by the ChaSTE at the landing site is on the higher side when compared to the observations by earlier lunar landing experiments such as Apollo missions around this depth. The displacement of fluffy surface regolith layer by the exhaust from the lander module, meteor impact at the landing site, etc. may be the likely reasons for the estimated higher packing density.

Estimation of Thermal Conductivity of the Lunar Regolith by ChaSTE

ChaSTE made the first in-situ estimation of thermal conductivity of lunar regolith at southern high-latitude. After the commissioning phase, continuous temperature measurements were carried out by ChaSTE for ~150 earth hours. After this, two heating experiments were conducted to estimate the thermal conductivity of the lunar regolith by activating the coil heater which was wound on the 9thtemperature sensor located at a depth of 80 mm below the lunar surface. The power drawn by the heater in these experiments was 0.1 W. During the first experiment conducted at 02:07 UTC on 1September 2023, the heater was turned on and the surrounding regolith was heated for 3.5 hours until a steady heat flow to the regolith was maintained. Then the heater was switched off for about 10 hours. The heater was turned on again for 2 hours (the heating duration was revised after the analysis of the first heating experiment data). The temperature variation observed by the sensors during the two heating experiments are studied (Fig.11). Temperature variation with the natural logarithm of time for the two experiments were calculated. The slopes of the heating curves were estimated where the relationship is linear. The estimated slopes were 3.235 Ks^{-1} and 3.130 Ks^{-1}, respectively for the two heating experiments. The slopes were mapped back to thermal conductivities using the relationship established (Fig. 12), through laboratory experiments with a one-to-one probe and by using standard hot wire method. The estimated thermal conductivities of the lunar regolith are 0.0115$Wm^{-1}K^{-1}$and 0.0124 $Wm^{-1}K^{-1}$, with uncertainties of 0.0008 Wm^{-1} $K^{-1}$and 0.0009 W $m^{-1}K^{-1}$, respectively.

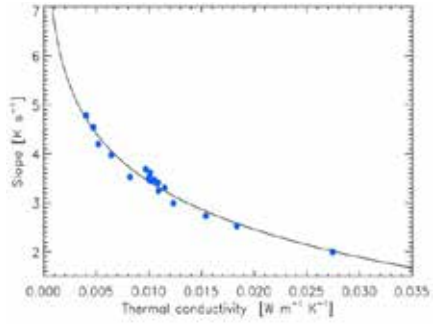

Figure11: Variation of thermal conductivity ($Wm^{-1}K^{-1}$) with slope (Ks^{-1}) for different self-heating curves of ChaSTE lab experiments [Mathew et al., Sci.Rep., 2025].

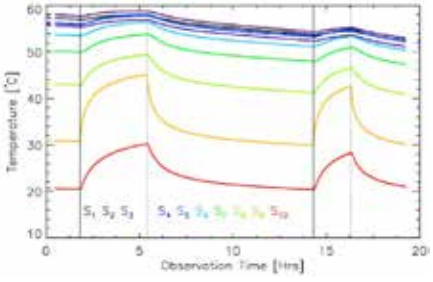

Figure12: Temperature variation observed by ChaSTE sensors during thermal conductivity heating experiments. Vertical lines represent time of heater ON (solid lines) and heater OFF (dotted lines) [Mathew et al., Adv. Space Res., 2025a].

Phase progression of the diurnal temperature variation at subsurface lunar regolith

The average vertical temperature gradient observed is ~3.7°C/cm at ~09:30 Lunar Local Time (LT). A noticeable increase in temperature gradient below ~6 cm depth points to a difference in regolith layer properties above and below this depth. Sub-zero temperature exists within the 10 cm layer prior to ~10 LT. The daytime temperature variations measured by ten temperature sensors and a systematic phase delay in the peaking of the temperature with depth was observed (Fig. 13). The warmest temperature was attained at 12 LT near the surface while that it was attained at 14:40 LT at 10 cm depth.

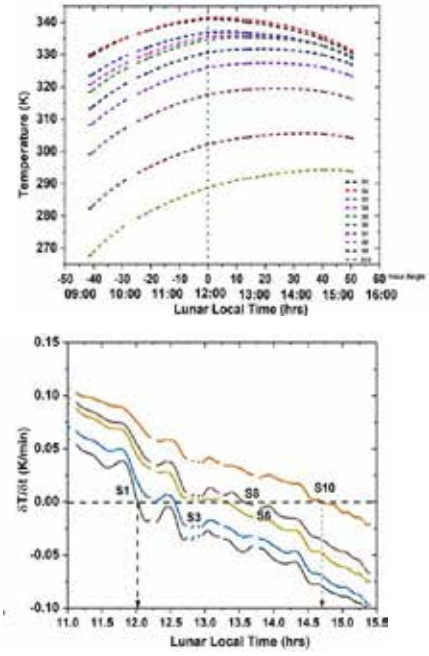

Figure 13: Daytime variations of lunar regolith temperature at different depths as measured by the temperature sensors on ChaSTE thermal probe from surface (S1 is top-most sensor) to 10 cm depth with depth spacing of 6mm, 6mm, 6mm, 6 mm, 8mm, 10 mm,17 mm, 18mm and 17mm (S10 is bottom-most sensor) (left panel). Phase delay in the peaking of temperature at 5 depths measured by the sensors S1 (~ 0.7 cm), S3 (~1.9 cm), S6 (~3.9 cm), S8 (~6.6 cm) and S10 (~10 cm) (right panel) [Renju et al., Mon. Not. R. Astron. Soc., 2025].

The daytime temperature variations, the significant lapse rate changes with depth and phase progression of the diurnal variation observed up to 10 cm depth, provided important insight on the influence of surface heat flux further deeper into the regolith layer as well as the thermal properties of the high latitude region. The phase delay in attaining temperature maximum at different depth was used to determine the diffusivity and thermal properties such as thermal conductivity and thermal inertia of the regolith.

The daytime variations of the in-situ measured temperature were affected by local topography and the infrared emission from the lander. The temperature of the lander body varied in the range of 290 K to 350K (Fig. 14). Correspondingly the estimated infrared radiation emitted would be 400Wm^{-2} to 750Wm^{-2}. Downwelling part of this radiation will be absorbed by the lunar surface and can act as a heat source in addition to the solar radiation. The potential impact of the lander in modifying the thermal characteristics of the landing site is found to be critical for planning the future lander missions.

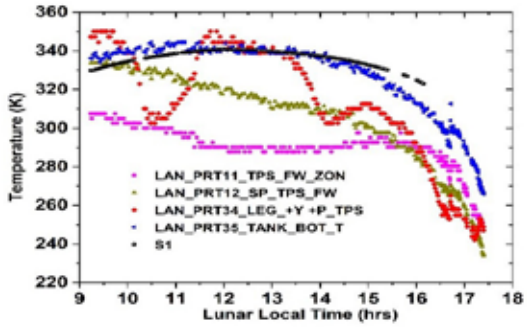

Figure 14: Temperature variation measured by the RTD sensors attached to the legs of the lander during the Chandrayaan-3 lander experiment and measured by S1 sensor in the ChaSTE probe (black line) during the daytime [Renju et al., Mon. Not. R. Astron. Soc., 2025].

Technology Development Activities

Development of Thermophysical Analysis of lunAr Polar regolith (TAAP) payload for LuPEX/Chandrayaan-5 Mission

The TAAP payload onboard LuPEX/Chandrayaan-5 is a follow-on of the ChaSTE/Chandrayaan-3 mission. It is aimed to understand the thermophysical characteristics of the lunar regolith at the polar region. Illumination conditions over the polar region are strongly influenced by topography due to low solar elevation angle. Surface and near-surface thermal environment can vary in complex ways with time of day and season. It is designed to measure the temperature profile of the regolith up to a depth of 20 cm and estimate thermal conductivity of the regolith at two depths. It is planned to measure the thermal profile continuously for a longer period when compared to the ChaSTE/Chandrayaan-3. The observations over the pole along with measurements from other previous missions (including ChaSTE/Chandrayaan-3) at different latitudes will provide a holistic view of the thermal structure of the moon.

Ongoing Activities and Future Projections

- Understanding the boundary-layer characteristics over distinct geographical regions of India by expanding the NOBLE network over arid region, core monsoon region and narrow mountain gaps with strong exit winds.
- Long-term changes in dynamic and thermodynamic parameters that support the formation and maintenance of boundary layer low-level roll clouds and closed convective cloud cells over the Arabian Sea during summer and their impact on monsoon activity.
- Climatological assessment of boundary-layer coastal low-level jet along the East Indian coast.
- Identification and characterization of overshooting deep convective clouds over the tropics using SAPHIR payload onboard Megha-Tropiques satellite.
- Understanding the influence of soil moisture on pre-monsoon thunderstorm activity over India using NISAR observations.
- Study the three-dimensional distribution of cloud and precipitation over the Indian sub-continent and adjoining seas using space-borne radar data, DWR data and in-situ observations.
- Quantification of the shunting effects and shadows on the lunar regolith temperature using ChaSTE/ Chandrayaan-3 data and forthcoming TAAP/LUPEX missions.

Publications in Peer-Reviewed Journals

1. Kumar, S., "Investigation of radar reflectivity profiles below the freezing level over South East South Asia using TRMM and Megha-Tropiques satellites", Remote Sensing Letters, https://doi.org/10.1080/2150704X.2024.2427913, 2024.
2. Kumar, S., "Regional differences in cloud characteristics at different depth, intensity and horizontal scale over South Asia during Indian summer monsoon using CloudSat and reanalysis data", Theoretical and Applied Climatology, https://doi.org/10.1007/s00704-024-05203-2, 2024.
3. Pant, T. K., Manju G., Mathew N., Pradeepkumar P., Paul J., Sreelatha P., Thampi S., Mridula N., Mosarraf Hossain Md., Vajja D. P., Aasik V., Satheesh Chandran M., Antony K. J., Renju R., Singhal T., Pramod P. P., Sajeev R., Suresh R., Sunitha K., John J., Thamarai V., Chaudhary T., Mehra M. M., Prasad K. D., "Chandrayaan-3 Lander Payloads and Science", Journal of Aerospace Sciences and Technologies, https://doi:10.61653/joast.v76i3a.2024.1006, 2024.
4. Chauhan, M. K., Singh, N., Singh, J., Rajput, A., Nandan, H., Rajeev, K., Kiran Kumar, N, V, P., "Evaluating the parameterization schemes and exploring the potential of XGboost Machine Learning tool for downward longwave radiation", Journal of Geophysical Research: Atmospheres, https://doi.org/10.1029/2024JD043115, 2025.
5. Kumar, S., "Differences in the convective variability during active and break spells over South Asian region using 25 years of satellite observations and reanalysis data", Theoretical and Applied Climatology, https://doi.org/10.1007/s00704-025-05627-4, 2025.
6. Kumar, S., "Precipitation Structure and Convective Intensity Over South-East South Asia During Active and Break Spells of the Indian Summer Monsoon Using TRMM, GPM, Megha-Tropiques Satellites and Reanalysis Data", International Journal of Climatology, https://doi.org/10.1002/joc.8758, 2025.
7. Mathew, N., Durga Prasad K., Mohammad F., Aasik V., Vajja D. P., Ram Prabhu M., Satheesh Chandran M., Subhajayan K. P., Antony K. J., Pramod P. P., Chandan K., Mathew D., Suresh R., Subramanian U. A., Sathiyamoorthy V., Unnithan M. V., Preethakumari V., Ramdas V., Salas A., Ajeeshkumar P. S., Naik N., Paul V., Reddy P. K., Ambily G., Kannan K., Dhanya M. B., Mishra S., Lali P. T., Sunitha K., Jash S., Singhal T., Janmejay K., Mishra M. K., Renju R., Suresh Raju C., Bhardwaj A., "Thermal conductivity of high latitude lunar regolith measured by Chandra's Surface Thermophysical Experiment (ChaSTE) onboard Chandrayaan-3 lander", Scientific Reports, 15(1), 7535. https://doi.org/10.1038/s41598-025-91866-4, 2025.
8. Mathew, N., Prabhu, M. R., Aasik, V., Mohammad, F., Vajja, D. P., Pramod, P. P., Antony, K. J., Satheesah Chandran, M., Subhajayan, K. P. and Sathiyamoorthy, V. "Operational Insights and Measurements of ChaSTE on the Chandrayaan-3 Vikram Lander", Advances in Space Research, https://doi.org/10.1016/j.asr.2025.05.024, 2025a.
9. Mathew, N., Prasad K. D., Vajja D. P., Aasik V., Mohammad F., Pramod P. P., Satheesh Chandran M., Antony K. J., Ram Prabhu M., Dhanya M. B., Unnithan M. V., Thomas S. G., Kumar C., Mathew D., Suresh R., Subhajayan K. P., Ajeeshkumar P. S., Reddy P. K., Jash S., Kannan K., Sunitha K., Mishra S., Kumar J., Sathiyamoorthy V., Bhardwaj A., "Chandra's surface thermophysical experiment (ChaSTE) onboard

Chandrayaan-3 Lander", Advances in Space Research, https://doi.org/10.1016/j.asr.2025.01.022, 2025b.

10. Moya-Álvarez, A, S., Silva, Y., Villalobos-Puma, E., Saavedra-Huanca, M., Carlos Del Castillo, Kumar, S. and Valdivia-Prado, J. M., "Extreme Precipitation Events Associated with Summer Rains in the Western Slope of the Peruvian Andes Using a Numerical Modeling and Weather Radar Data: Case Studies", Pure and Applied Geophysics, https://doi.org/10.1007/s00024-025-03834-8, 2025.
11. Renju, R., Suresh Raju, C. and Mishra, M. K., "High resolution thermal profiles of lunar regolith over a southern high latitude location using in-situ observations from ChaSTE/Chandrayaan-3 Lander", Monthly Notices of the Royal Astronomical Society, https://doi.org/10.1093/mnras/staf380, 2025.
12. Swathi, B. and Sathiyamoorthy, V., "Unique roll clouds along the flow path of the Indian summer monsoon low-level jet over the Arabian sea", Scientific Reports, https://doi.org/10.1038/s41598-025-97849-9, 2025.

Scientific/Technical Reports

1. Renju, R., Koushik N, Shiju, G. T., Vajja, D. P., Pramod, P. P., Kiran, J. A., Satheesh, C.M., Sreejith, K. J., Vipin V. V., Fazil M., 'Preliminary Design Review Document: Thermophysical Analysis of lunar Polar regolith (TAAP)'. Chandrayaan-5/LuPEX mission. SPL-TAAP-PDR-CHN5-DOC-25-01-00.
2. Santosh, M., 'An advanced deep learning-based technique to retrieve high resolution profiles of water vapor and temperature from atmospheric refractivity. Potential Application to Global Navigation Satellite System (GNSS) Radio Occultation. Model Design & Model Validation with in-situ data-Part-I', ISRO-VSSC-TR-0760-0-25.
3. Santosh, M. 'An advanced deep learning-based technique to retrieve high resolution profiles of water vapor and temperature from atmospheric refractivity. Application to Global Navigation Satellite System (GNSS) Radio Occultation data-Part-II', ISRO-VSSC-TR-0761-0-25.

Presentation in Symposia/Conferences/Workshops

1. Fathima Shirin, P.T., Kirankumar, N. V. P., Prabhakar, S., Sathiyamoorthy, V. and Sunil Kumar, S. V., 'Estimating the Influence of Clouds on Surface Radiation Balance over a Tropical Station using Ground-Based Observations', Second Frontiers Symposium in Earth, Environmental and Sustainability Sciences-2025, IISER, Trivandrum, February 08, 2025.
2. Mathew, N., Mohammad F., Aasik V., Subhajayan K. P., Ram Prabhu M., Antony K. J., Kannan K., Pramod P. P., Jash S., Vajja D. P., Satheesh Chandran M., Mathew D., Sathiyamoorthy V.Lakshmi V. M. , 'In situ measurement of temperature profile of high latitude lunar surface regolith by ChaSTE onboard Chandrayaan-3 during the penetration operation', Global Space Exploration Conference (GLEX 2025), New Delhi, May 7–9, 2025.
3. Renju, R., "Soil Moisture Retrieval over different regions of India from Sentinel-1/SAR observations", CEOS WGCV Synthetic Aperture Radar Calibration & Validation Workshop-2024, Space Applications Centre, Ahmedabad, November 12-15, 2024.
4. Rincy Roy, Swathi, B. and Sathiyamoorthy, V., 'Investigating Fog occurrence over the south peninsular India using INSAT-3D Imager data', The International Symposium on Tropical Meteorology (INTROMET-2025), Indian Institute of Tropical Meteorology, Pune, November 18-20, 2025.
5. Santosh, M. and Ghosh, A. K., 'Coastal Low-Level Jets along the Eastern India: Morphology, Seasonality, and Diurnal Variability', The International Symposium on Tropical Meteorology (INTROMET-2025), Indian Institute of Tropical Meteorology, Pune, November 18-20, 2025.
6. Santosh, M. and John, H., 'An advanced deep learning-based technique to retrieve high resolution profiles of moisture and temperature from atmospheric refractivity - Potential Application to GNSS-RO', The International Symposium on Tropical Meteorology (INTROMET-2025), Indian Institute of Tropical Meteorology, Pune, November 18-20, 2025.
7. Kumar, S., 'Precipitation structure and convective intensity during active and break spells over South Asia using multiple satellite-based observations. The International Symposium on Tropical Meteorology (INTROMET-2025), Indian Institute of Tropical Meteorology, Pune, November 18-20, 2025.
8. Swathi, B. and Sathiyamoorthy, V., 'Roll clouds over the Arabian Sea and their association with monsoon activity', The International Symposium on Tropical Meteorology (INTROMET-2025), Indian Institute of Tropical Meteorology, Pune, November 18-20, 2025.

ऐरोसॉल ट्रेस गैस तथा रेडिएटिव फोर्सिंग
AEROSOLS TRACE GASES AND RADIATIVE FORCING

एसपीएल की ऐरोसॉल, ट्रेस गैस एवं विकिरणी प्रभाव (एटीआरएफ) शाखा का ध्येय ऐरोसॉलों और ट्रेस गैसों के भैतिक / रासायनिक गुणधर्मों की वैज्ञानिक समझ विकसित करना है, जिसमें ऐसी प्रक्रियाएं शामिल है जो जलवायु परिवर्तनों का कारण बनने वाले उनके त्रिविमीय वायुमंडलीय वितरण और विकिरण के साथ संबंधों को नियंत्रित करती हैं। इस शाखा के प्राथमिक लक्ष्य हैं: (i) अंतरिक्ष-वाहित और भू-आधारितप्रेक्षणों के संयोजन से भारतीय उपमहाद्वीप, निकटवर्ती महासागरों के साथ-साथ हिमालय एवं ध्रुवीय वातावरणों का ऊपर स्थित ऐरोसॉल और ट्रेस गैसों के दिगीय एवं समयानुसार विभेदित आंकड़ों के संग्रह का विकास, (ii) ऐरोसॉल और ट्रेस गैसों के जलवायु प्रभावों से संबन्धित विशिष्ट वैज्ञानिक समस्याओं का अध्ययन करनेवाले विषयगत बहु-मंचीय (जहाज, वायुयान और उच्च तुंगतावाला गुब्बारा) क्षेत्र परीक्षणों का आयोजन, (iii) पृथ्वी एवं ग्रहीय वायुमंडलों में ऐरोसॉलों और ट्रेस गैसों के सुदूर संवेदन केलिए पुनःप्राप्ति कलन-विधियों और अंतरिक्ष-वाहित संवेदकों का विकास, (iv) स्थलीय और ग्रहीय वायुमंडलों में एरोसोल और गैसों को मापने के लिए उपकरणों का विकास और (v) संभावित जलवायु प्रभावों के आकलन के लिए क्षेत्रीय जलवायु मॉडलों के साथ एरोसोल और ट्रेस गैस डेटा का एकीकरण।

Aerosols, Trace gases and Radiative Forcing (ATRF) branch of SPL aims at scientific understanding of the physical/chemical properties of aerosols and trace gases, involving processes that control their three-dimensional atmospheric distribution and interaction with radiation leading to climate changes. The primary objectives are (i) development of spatially and temporally resolved aerosol and trace gas database over the Indian subcontinent, adjoining oceans as well as the Himalayan and Polar environments by combining the space-borne and ground-based observations, (ii) conducting thematic multi-platform (ship, aircraft and high altitude balloon) field experiments addressing specific problems pertinent to the climate impact of aerosols and trace gases, (iii) development of retrieval algorithms and space-borne sensors for the remote sensing of aerosols and trace gases in earth and planetary atmospheres,(iv) development of instruments for measuring aerosols and gases in the terrestrial and planetary atmospheres and (v) assimilation of the aerosol and trace gas data with regional climate models for the assessment of potential climate impact.

वैज्ञानिक टीम / Science Team
सुरेश बाबू एस / Suresh Babu S.
विजयकुमार एस नायर / Vijayakumar S. Nair
प्रशांत हेग्डे / Prashant Hegde
मुकुंदा गोगोई / Mukunda Gogoi
शोभन कुमार कोंपल्ली / Sobhan Kumar Kompalli
प्रिजित एस एस / Prijith S. S.
रेवती एस अजयकुमार / Revathy S. Ajayakumar
सुरेश कुमार रेड्डी बी / Suresh Kumar Reddy B.

तकनीकी टीम / Technical Team
अजीष कुमार पी एस / Ajeesh Kumar P. S.
संतोष केआर पांडे / Santosh KR Pandey

ईनस्पयर फाकल्टी / INSPIRE Faculties
रम्या सी बी / Ramya C. B.
लिमा सी बी / Lima C. B.

अनुसंधान/परियोजना सहयोगी/ Research / Project Associates
चक्राधर रॉव टी / Chakradhar Rao T.
अखिला आर एस / Akhila R. S.*
लेक्ष्मी एस आर / Lekshmi S. R.#

अनुसंधान अध्येता/Research Fellows
अनस इब्नु बशीर / Anas Ibnu Basheer
अतुल ए.के / Athul A. K.
नितिन बाबू / Nithin Babu
पार्वती आनंद / Parvathy Anand
शिबा शंकर गौड़ा / Shiba Shankar Gouda

**Relieved in December, 2025*
#Joined in June, 2025

Satellite Remote Sensing of Aerosols

Retrieval of Aerosol Optical Depth from INSAT-3DR for Accurate Geostationary Monitoring of Regional and Temporal Aerosol Dynamics

Accurate, high-frequency monitoring of Aerosol Optical Depth (AOD) is essential for understanding aerosol dynamics, regional transport pathways, and their environmental and climatic impacts. Geostationary satellites are uniquely suited for this task due to their ability to provide continuous observations over large domains. In this study, INSAT-3DR geostationary observations are utilised to retrieve sub-hourly AOD through a data-driven approach built on a physically interpretable machine learning (ML) framework. An eXtreme Gradient Boosting (XGBoost) ML model is developed using features derived from INSAT-3DR visible and infrared channels, with a novel fused AOD product employed as the target variable. This fused AOD integrates long-term MODIS observations (2014-2022) with extensive ground-based measurements from ARFINET and AERONET (62 stations) using a combined Support Vector Regression (SVR) and Gaussian Process Regression (GPR) scheme. The fused AOD shows strong agreement with ground observations (r = 0.955, RMSE = 0.06), and is generated for both Aqua and Terra overpass times across the study domain.

To ensure explicit interpretability in the retrieval system, SHAP (SHapley Additive exPlanations) analysis was conducted. The results confirm that the model relies on physically consistent features representing aerosol scattering, absorption, and thermal-contrast mechanisms, demonstrating that the ML model is grounded in radiative-transfer behavior rather than purely empirical correlations. The trained model exhibits strong performance in retrieving AOD from INSAT-3DR relative to the fused AOD ($r \approx 0.839$, $RMSE \approx 0.081$) and effectively captures regional aerosol hotspots, sub-hourly variability, and major pollution events (Fig.1). It reliably resolves key aerosol characteristics including diurnal evolution, seasonal patterns, and region-specific features such as high loading over the Indo-Gangetic Plain and coastal outflow zones. Site-specific RMSE values (~0.04 - 0.16) indicate that INSAT-3DR accurately reproduces both the magnitude and spatial variability of AOD,

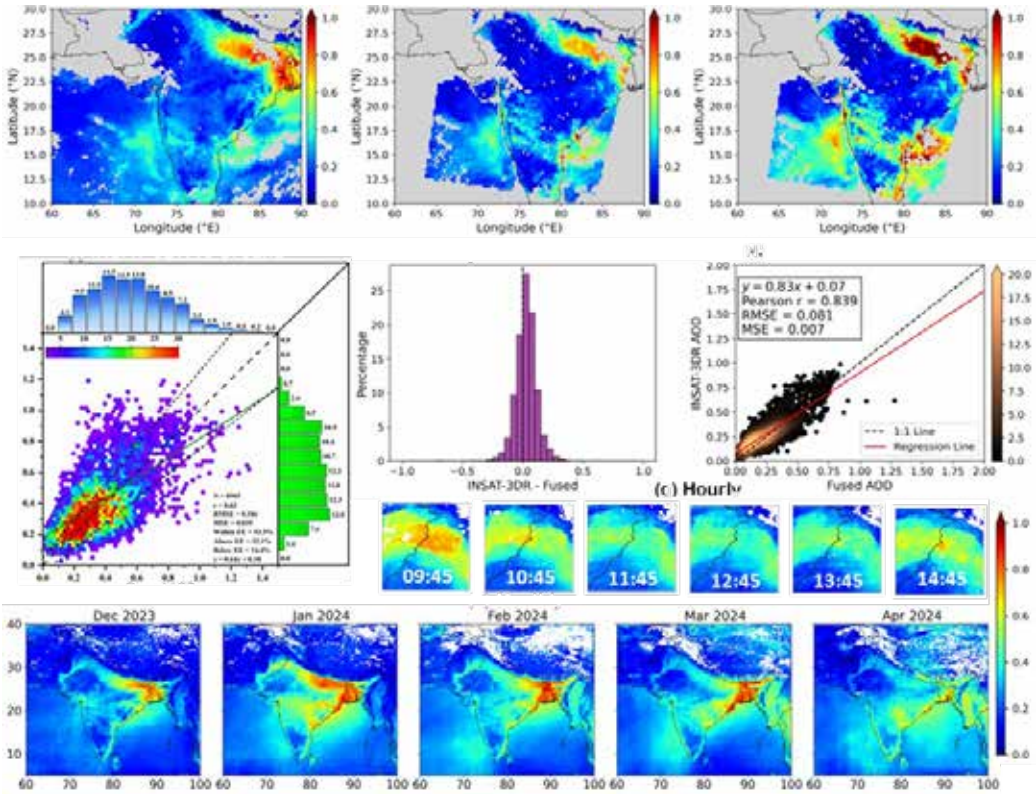

Figure 1: Comparative analysis of spatial distribution of (a) INSAT-3DR AOD, (b) Fused AOD and (c) MODIS AOD for a MODIS overpass on 21 December, 2021 at 05:30 UTC. (d) Scatter plot of INSAT-3DR AOD vs fused AOD. (e) Histogram of AOD differences (INSAT-3DR – fused). (f) Comparison between INSAT-3DR AOD and ground AOD. (g) Hourly variation of INSAT-3DR AOD over India on 08 November 2024 (IST). (h) Monthly variation of INSAT-3DR AOD [Tandule et al., Atmos. Environ., 2026].

with uncertainties well within acceptable limits for regional monitoring.

By enabling AOD retrievals at sub-hourly temporal resolution, this approach represents a significant advance in high-frequency aerosol observation. The developed framework provides critical inputs for air-quality assessment, short-term aerosol forecasting, and satellite-based emission source characterization. Moreover, the fusion-based training strategy and explainable ML architecture offer a scalable solution that can be readily adapted to future geostationary missions with similar spectral capabilities. Overall, this work establishes a robust and operationally relevant tool for routine aerosol surveillance and a valuable input to climate and chemical transport models.

Dust aerosol characterization using Infrared Difference Dust Index (IDDI) from INSAT-3D Imager

Geostationary satellites, with their capability to provide frequent observations of the same region, enable holistic analysis of dust aerosol transport and distribution and thereby facilitate accurate assessment of their impacts on climate. In this study, analysis of dust aerosol distribution and its absorbing efficiency over the Indian region has been carried out using the thermal IR measurements from the INSAT-3D Imager. Dust aerosol distribution is examined using the Infrared Difference Dust Index (IDDI), which is the measure of depression in thermal infrared (TIR) brightness temperature (BT) due to the presence of mineral dust aerosols in the atmosphere. IDDI is computed as the difference in BT in TIR-1 (BT_{TIR1}), in comparison with the reference BT ($BT_{TIR1,ref}$) in the same channel. Here, $BT_{TIR1,ref}$ is estimated as the maximum BT_{TIR1} during the previous 15 days, at same solar illuminating conditions, assuming at least one clear-sky condition with negligible aerosol amount within the reference period. Thus, $BT_{TIR1,ref}$ is the brightness temperature corresponding to the radiation emitted from the surface under the clear-sky condition. Computation of IDDI has been carried out on the pixels, which are not contaminated by the presence of clouds. Here, cloud pixels are identified using an algorithm incorporating five tests, which use BTs in four infrared channels of INSAT-3D Imager (mid-wave infrared, water-vapour channel, TIR-1 and TIR-2). Unlike the parameters from passive visible sensors, which are limited only to day-time, TIR based IDDI from INSAT-3D with high spatiotemporal resolution during both day and night enables continuous monitoring of the genesis and evolution of dust storm events. Analysis using IDDI from INSAT-3D shows wide spread distribution of dust aerosols over Indian subcontinent and surrounding oceanic regions during the severe dust storm events in May 2018 (Fig. 2a). Large amount of dust aerosols released into the atmosphere during the dust storm events enhances the absorption efficiency of the aerosol system, which is estimated as the ratio of IDDI (from INSAT-3D) to AOD at 550 nm (from MODIS), over south Asian region to as high as 20-25 K (Fig. 2b). Day-to-day variation of IDDI shows excellent agreement with dust aerosol optical depth (DAOD) estimated from Moderate Resolution Imaging Spectroradiometer (MODIS) and Second Modern-Era Retrospective analysis for Research and Applications (MERRA-2), underscoring the potential of this index for the spatiotemporal characterization of dust aerosols

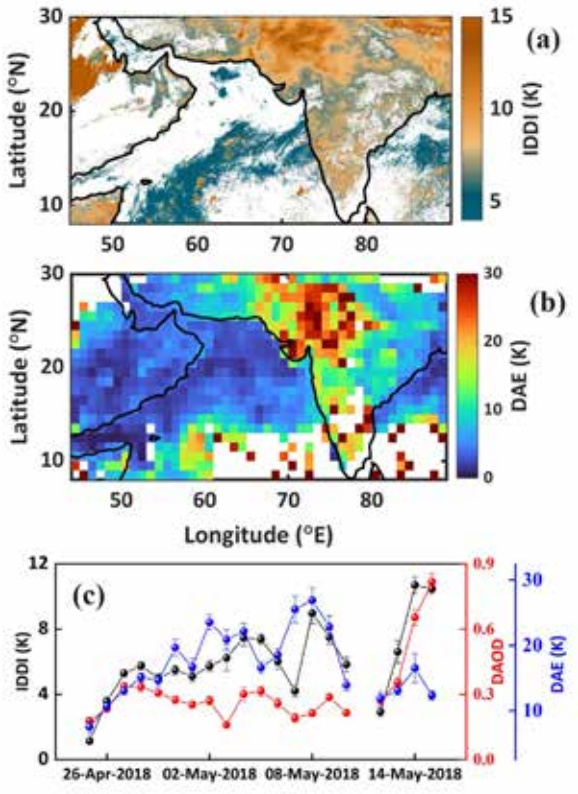

Figure 2: Spatial and temporal variation of dust aerosols over Indian region during the dust storm events in May 2018. Spatial distribution of (a) IDDI and (b) DAE estimated from INSAT-3D during the dust storm episodes from 07th to 09th May, 2018 and (c) day-to-day variation of IDDI and DAE from INSAT-3D and DAOD estimated from MODIS and MERRA-2 over Northwest India (72–77°E; 23–28°N) during the dust storm event. Markers represent mean values of IDDI (black), DAOD (red), and DAE (blue) and vertical bars denote corresponding standard errors [Lima et al., Int. J. Remote Sens., 2024].

(Fig.2c). Spatial distribution of dust aerosols and prevailing circulation pattern demonstrates long range transport of dust aerosols to far away locations. Presence of elevated aerosol layers with high particulate depolarization ratio, observed by Cloud Aerosol Lidar with Orthogonal Polarization (CALIOP), over these regions also corroborate the long-range dust aerosol transport. Enhancement in radiation absorption due to the wide spread distribution of dust aerosols would significantly alter the circulation dynamics and weather systems over South Asia.

Improved cloud screening of OceanSat-3 OCM-3 satellite imagery using machine learning algorithm

Clouds obstruct satellite observations, introducing ambiguities in the retrieval of various land, ocean, and atmospheric parameters. Especially, retrieving accurate aerosol properties and biogeochemical information from satellite remote sensing requires effective cloud screening. Reliable determination of these properties depends on the availability of cloud-free pixels. However, cloud detection becomes particularly challenging for sensors with the limited number of available spectral bands. Traditional approaches often rely heavily on the thermal infrared channels and pre-defined thresholds, which often fails in complex screens. Since Ocean Color Monitor-3 (OCM-3) onboard the OceanSat-3 (EOS-06) is not equipped with a thermal infrared band, accurate cloud detection remains a difficult and active area of research. In this context, the development of a robust, generalizable cloud detection framework is critical for improving downstream geophysical retrievals from Indian ocean-color missions.

In view of the above, a machine learning (ML)-based cloud screening algorithm is developed specially tailored for OCM-3. Using Support Vector Machine (SVM) and Random Forest (RF) classifiers trained on reflectance from visible and near-infrared bands and fused cloud indices (CI1 and CI2), the framework demonstrates the ability to detect both thick and thin clouds with high accuracy. Compared to adaptive thresholding (AT), which struggles over complex backgrounds and thin-cloud regimes, the ML models provide a more accurate separation of cloud and surface signatures through learned patterns. A unique strength of

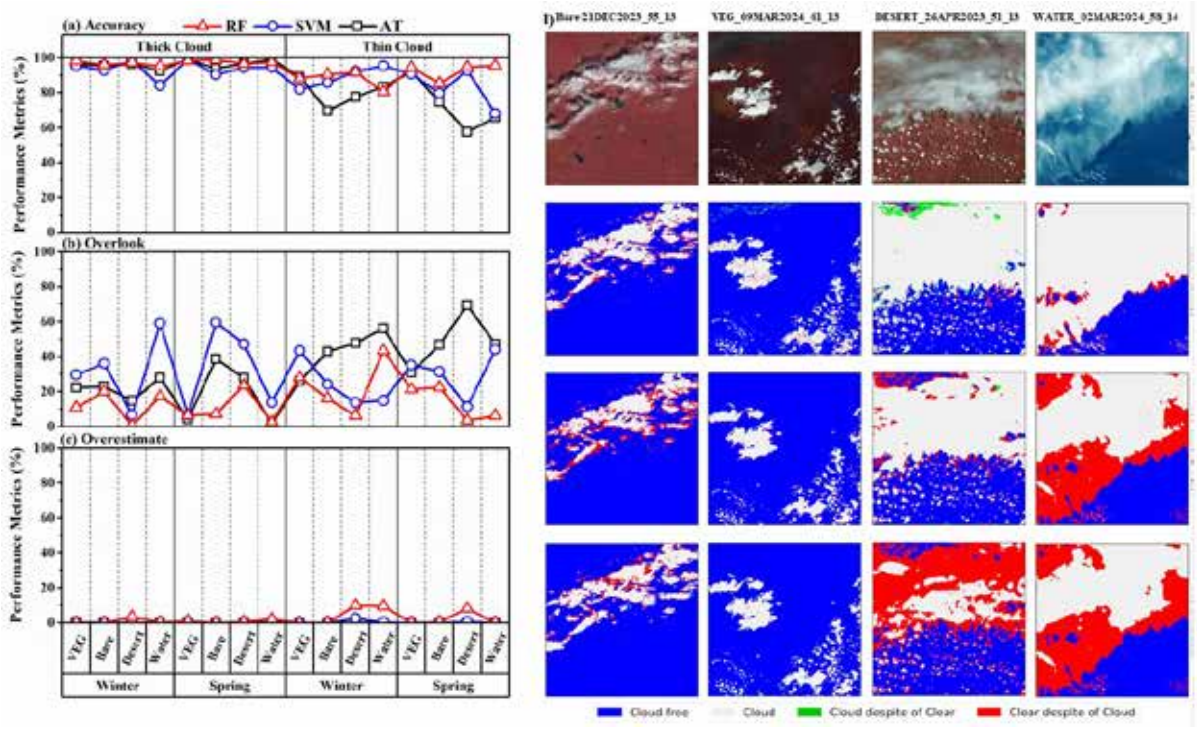

Figure 3: Variation of performance metrics (a) Accuracy, (b) Overlook, and (c) Overestimate of testing samples from RF, SVM and AT over VEG, Bare, Desert and Water surfaces. (d) Cloud masks from the random forest (RF), support vector machine (SVM) and adaptive threshold (AT) techniques over four underlying surfaces: Bare, VEG, Desert, and Water. Blue: Both VI and ML detected pixels are cloud-free, Grey: Both VI and ML detected pixels are cloudy, Green: The VI pixel is clear but the ML detected pixel is cloudy (overestimate), Red: The VI pixel is cloudy but the ML detected pixel is clear (overlook). The column headings specify the date, satellite path and row of the tile from which the 400 x 400-pixel grid is selected [Tandule et al., Remote Sens. Appl. Soc. Environ., 2025].

this work lies in its emphasis on generalizability across India's highly heterogeneous land surface types. As the Indian region is represented by highly heterogeneous land-surface properties, a diverse and surface-specific training dataset is constructed to develop the ML model, those carefully select scenes representing vegetated, desert/arid, bare/urban, and oceanic surfaces across winter (DJF) and spring (MAM). Visual inspection–based reference cloud masks ensure accurate labeling in the absence of coexistent cloud-mask products for OCM-3.

Systematic sensitivity analyses reveal that the integrated diverse underlying surface training strategy yields a generalized model capable of handling India's diverse landscapes, reducing both overestimation and overlook errors. The RF classifier emerges as the most robust, achieving ~94% accuracy for all cloud types and outperforming SVM and AT, particularly for thin clouds where threshold-based methods typically fail. As illustrated in Fig. 3a-c, the RF classifier consistently has high accuracy when compared with reference cloud masks across surface types, demonstrates physically meaningful feature contributions through SHAP values, and reproduces cloud fraction with high accuracy for both thick and thin clouds. This generalized ML framework therefore represents a significant advance for operational cloud masking in OCM-3 imagery. By enabling efficient cloud detection across India's complex surface diversity, the method enhances the reliability of subsequent aerosol and ocean-color retrievals. The approach also sets up a scalable framework for future Indian missions operating under similar spectral limitations.

Assessment of climate impacts due to aerosols

Energy-Balance Decomposition of the Aerosol-Induced Changes on Surface Temperature

Aerosol-radiation interactions decrease the solar radiation reaching the surface, which cools the surface and influences land-atmosphere interactions and affects the regional climate through various pathways. Discerning the aerosol effect on surface temperature is challenging due to the complexities associated with land-atmosphere interactions and various feedback processes. The Regional Climate Model (RegCM) simulations were carried out to understand the effects of aerosols on radiative and non-radiative fluxes at the surface. Direct radiative forcing due to aerosols at surface during winter, pre-monsoon, monsoon, and post-monsoon are -7.32±2.52, -12.3±5.08, -9.27±6.6, and -8.02 ± 3.13 Wm^{-2}, respectively. This instantaneous decrease in solar radiation at the surface modifies the energy balance and affects the surface temperature. Using the energy balance equation, aerosol-induced changes in surface temperature are decomposed into its radiative (shortwave (SW) and longwave) and non-radiative (sensible heat flux (SHF), latent heat flux (LHF), and ground flux) components for different seasons (Fig. 4). In general, aerosol-radiation interactions decrease the surface temperature over South Asia in all four seasons, which depends not only on the aerosol loading but also on the efficiency of land-atmosphere coupling as seen in the large heterogeneity of change in temperature per unit AOD. The IGP shows high aerosol loading, strong cooling, and high cooling efficiency (temperature reduction per unit AOD) in winter. Aerosol-induced changes in incoming longwave radiation cool the Indian region most prominently in winter, whereas these changes cause warming over west of South Asia. The SHF consistently compensates or balances the effect of aerosol-induced SW cooling throughout all the seasons. The decrease in SHF is more than 50% of the decrease in SW radiation due to aerosols over the Indo-Gangetic Plain (IGP). The LHF compensates for only 10% and 14% of the SW cooling during the pre-monsoon and monsoon seasons, respectively. Hence, less than 50% of the SW cooling is translated into the net surface temperature change, whereas the remaining is compensated with the decreased SHF and LHF. The decrease in SHF and surface temperature influences the evolution of the boundary layer and relative humidity. The maximum decrease in boundary layer height is observed during the pre-monsoon season. The shallow boundary layer prevailed during the winter season is further decreased due to aerosol-induced weakening of SHF over the IGP. The decrease in boundary layer height was as high as 100 m during winter over the IGP. Despite the decrease in evaporation due to surface cooling, relative humidity depicts an increase over South Asia. The impact of aerosol-induced weakening of SHF remains relatively unexplored despite its significant influence on the air quality and hydroclimate of the region. This is mostly attributed to the lack of simultaneous measurements of aerosols and boundary layer fluxes. Therefore, this study highlights the need for a dedicated campaign to investigate the role of

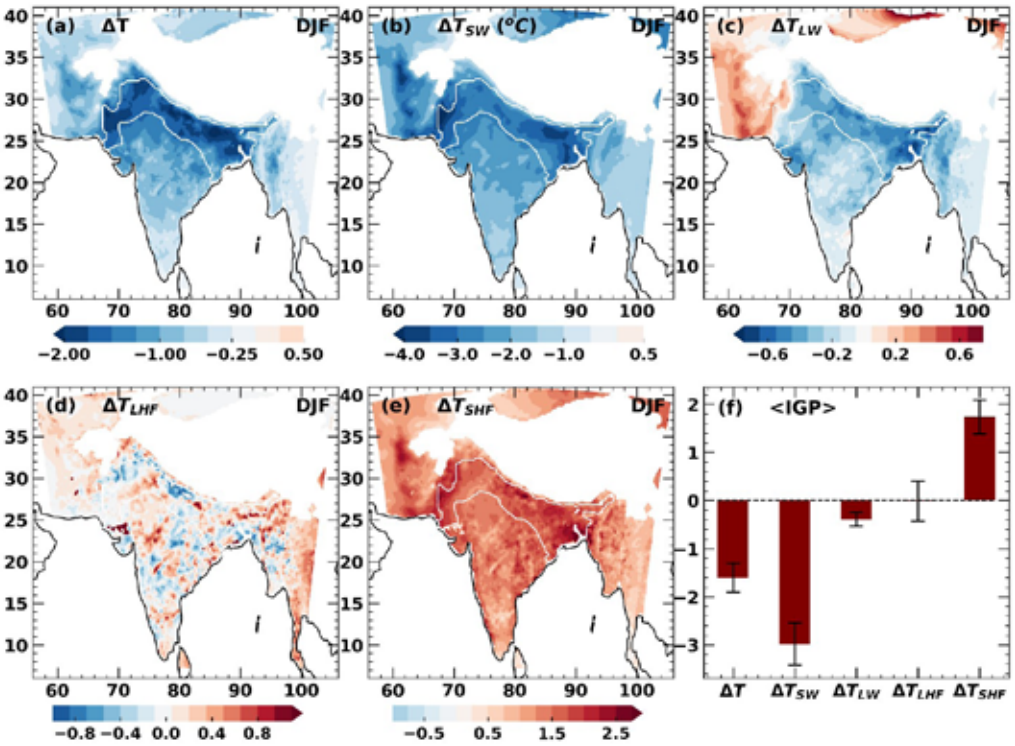

Figure 4: (a) The aerosol-induced change in net surface temperature over South Asia during winter (DJF). The change in surface temperature due to aerosol effects in (b) shortwave radiation, (c) longwave radiation, (d) latent heat flux, and (e) sensible heat flux, (f) the mean values all these parameters over the Indo-Gangetic Plain [Akhila et al. J. Geophy. Res., 2025].

aerosols in land-atmosphere interactions and their implications for air quality over the IGP during winter

Aerosol Microphysical Properties

Aerosol light-scattering enhancement and liquid water content in a tropical coastal atmosphere

Ambient relative humidity (RH) significantly influences aerosol behavior in the atmosphere by altering, optical scattering properties, aerosol liquid water content (ALWC), chemical composition, and mixing state. Understanding aerosol hygroscopicity is essential for evaluating aerosol-radiation and aerosol-cloud interactions, especially in humid tropical environments. This study investigated aerosol hygroscopic growth and associated scattering enhancement over Thumba, a tropical coastal location in peninsular India using measurement setup with dry (RH < 45%) and wet Nephelometers. Observations were carried out during winter (24 December 2019 to 04 January 2020) and the post-monsoon season (03-30 November 2020), with wet nephelometer RH varying between 60-85% in steps of 5%. Concurrent measurements of near-real-time non-refractory submicron (NR-PM1) aerosol chemical composition using aerosol mass-spectrometry technique, along with aerosol liquid water content estimated using a thermodynamic equilibrium model were used to examine the role of various chemical species in controlling aerosol hygroscopicity. The aerosol light-scattering enhancement factor (Fig. 5a), *f(RH)*, defined as the ratio of scattering coefficients measured at 550 nm under humidified and dry conditions, increased monotonically with RH, from 1.22-1.25 at 60% RH to ~1.45-1.48 at 85% RH *(i.e., f(RH=85%,550nm)*. Aerosol chemical composition strongly influenced hygroscopicity. Marginally higher light-scattering enhancement (5-8%) for aerosols was observed during the sea-breeze periods than the land-breeze periods due to the presence of more hygroscopic aerosols. Though organic aerosols (OA) are the dominant species, the light-scattering enhancement factor *f(RH)* correlated positively (Pearson's R~0.83-0.89) (Fig. 5b) with inorganic mass fractions, dominated by sulfate (and negatively with organics) indicating the aerosol swelling was intensified with increasing proportion of secondary aerosols. The hygroscopicity parameter derived from aerosol composition, κ_{chem}, showed maximum values during daytime owing to photochemical formation of secondary oxygenated OA and sulfate which depict higher water-uptake ability.

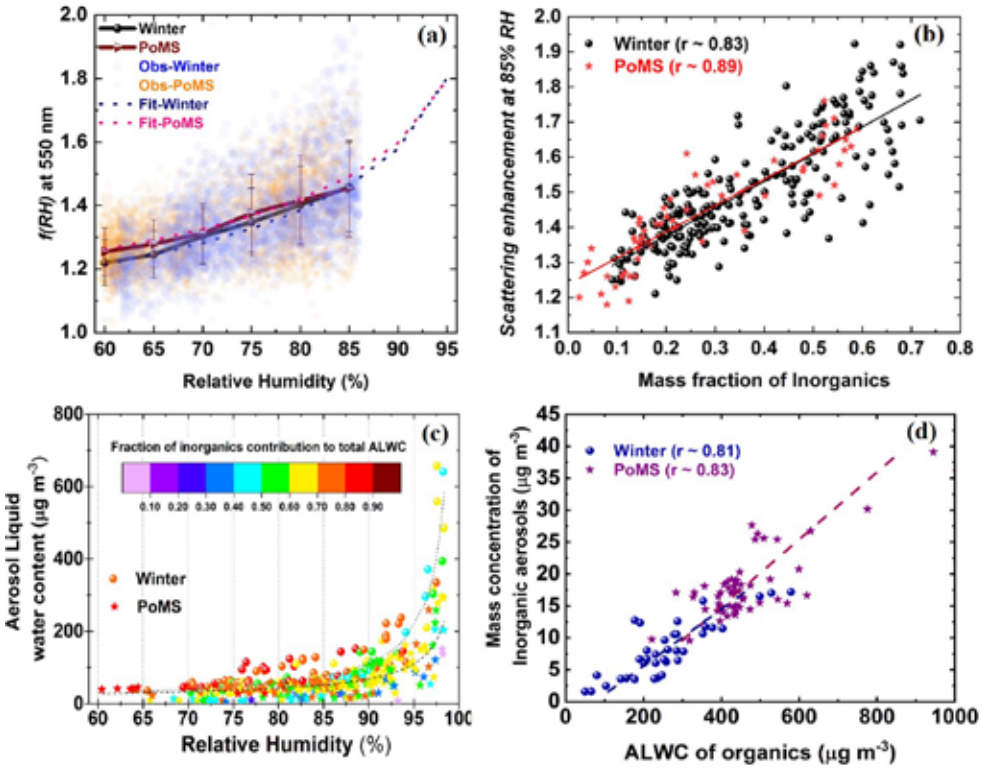

Figure 5: (a) Variation of mean aerosol light-scattering enhancement factors at 550 nm between the RH values ~ 60-85 % along with the individual observations, mean humidographs and γ-fit functions. Association between (b) f(RH=85%, 550nm) and the mass fractions of inorganics, (c) ambient RH and ALWC (with the points color-mapped with the fractional contribution of inorganic aerosols), and (d) ALWC of organics and the mass concentration of inorganics under elevated (>85%) ambient RH conditions. The linear fit and Pearson's correlation coefficient (r) are also given [Kompalli and Babu, Atmos. Res., 2026].

However, no clear linear relationship emerged between particle size (geometric mean diameter from particle number size distribution) and *f(RH)* which presented a complex picture concerning the relative dominance of aerosol size and composition in determining hygroscopicity. Model-estimated ALWC (which also represents critical role of ambient RH in influencing aerosol characteristics) depicted a non-linear increase at elevated RH levels (RH > 85%), resulting in mean mass growth factors (MGF) (the ratio of mass loading in dry and wet conditions) that increased from 3-4 at lower RH levels to values as high as 10-12 (Fig. 5c). Secondary inorganic aerosols contributed most to this growth, although organics (mainly highly oxidized OA) also exhibited substantial water uptake under high RH (>85%) levels. Importantly, the increased hygroscopicity and enhanced ALWC of organic aerosols ($ALWC_{organics}$) coincided with amplified production of inorganic aerosols (r>0.8) (Fig. 5d). Such presence of inorganics beyond their deliquescence RH implied their active heterogeneous aqueous-phase formation pathways facilitated by humid conditions and enhanced $ALWC_{organics}$. Overall, the study demonstrates that ambient humidity strongly regulates aerosol optical properties, chemical transitions, and secondary aerosol formation processes over humid tropical coastal environments. These findings highlight the importance of incorporating RH-dependent hygroscopic behavior into climate models and remote-sensing retrievals to improve accuracy in estimating aerosol radiative forcing and cloud activation potential.

Black carbon mixing state and light-absorption enhancement under different air mass regimes over a tropical coastal site

Changes in black carbon (BC) mixing state due to atmospheric aging contributes to enhanced light-absorption and hygroscopicity. Understanding BC microphysical properties, mixing state, and associated light-absorption behavior is crucial for assessing its climate impacts, especially over sensitive tropical coastal atmospheric environments. This study investigates refractory BC characteristics, using single-particle level laser-induced incandescence technique, at Thumba, a tropical coastal site in Peninsular India during

the period 2018-2021. The observations span four distinct airmass regimes-Marine (clean conditions), Continental (polluted), Mixed-1 and Mixed-2 (containing both marine and continental signatures). Concurrent observations of NR-PM_1 species (to identify processes governing coatings) and core-shell Mie modeling (to estimate absorption enhancement linked to BC coatings) were also used. The results reveal substantial variability in BC mass concentrations, size distributions, mixing state and associated impact on light-absorption (Fig. 6a) depending on the airmass conditions. It reflected varying source/sink strengths, aging processes of BC, and potential condensable coating material. Across all airmasses, BC particles were well-aged with mass median diameters (i.e., BC core sizes) ranging from 181 ± 8 nm to 202 ± 6 nm, suggesting the mixed, outflow-dominated BC sources. Significant coating on BC cores was observed, quantified by relative coating thickness (i.e., ratio of total coated BC particle and uncoated BC core sizes) (RCT ~ 1.3–1.6) in general. While Marine conditions depicted the thinnest coatings (RCT ≈ 1.34), the thickest coatings occurred during Continental and mixed periods (RCT ≥ 1.57), reflecting enhanced aging and availability of condensable material. The coatings on BC particles exhibited daytime enhancement (Fig. 6b), driven by photochemically produced condensable material, a contrasting diurnal pattern to that of other BC properties. Further, relative humidity (Fig. 6c) and photochemistry (Fig. 6d) strongly influenced BC mixing state. Submicron aerosol composition showed high organic aerosol (OA) contributions (58–67%), dominated by secondary OA (39–51%) (i.e., oxygenated organic aerosols-OOA is more abundant than primary hydrocarbon-like OA-HOA), with sulfate being the major inorganic component. Diurnal patterns of NR-PM_1 species confirmed photochemical formation of secondary aerosol coatings on BC (which involves sulfate and OOA), especially during daytime. Interestingly, the RCT on BC increased and/or remained invariant with increasing relative humidity (RH) until RH ≤82%, and subsequently showed a decline likely due to deliquescence and partial detachment of inorganic coating components. Despite this, coatings representing 30-50% of the BC core size persisted at high humidity (RH > 85%), suggesting that secondary organics remain adhered to BC under moist conditions. Such variations in BC mixing state affected light absorption properties. The absorption enhancement factor (E_{abs}) (the ratio of light-absorption cross-section between coated and uncoated BC) relative to uncoated BC ranged from 1.36 ± 0.14 during Marine periods to

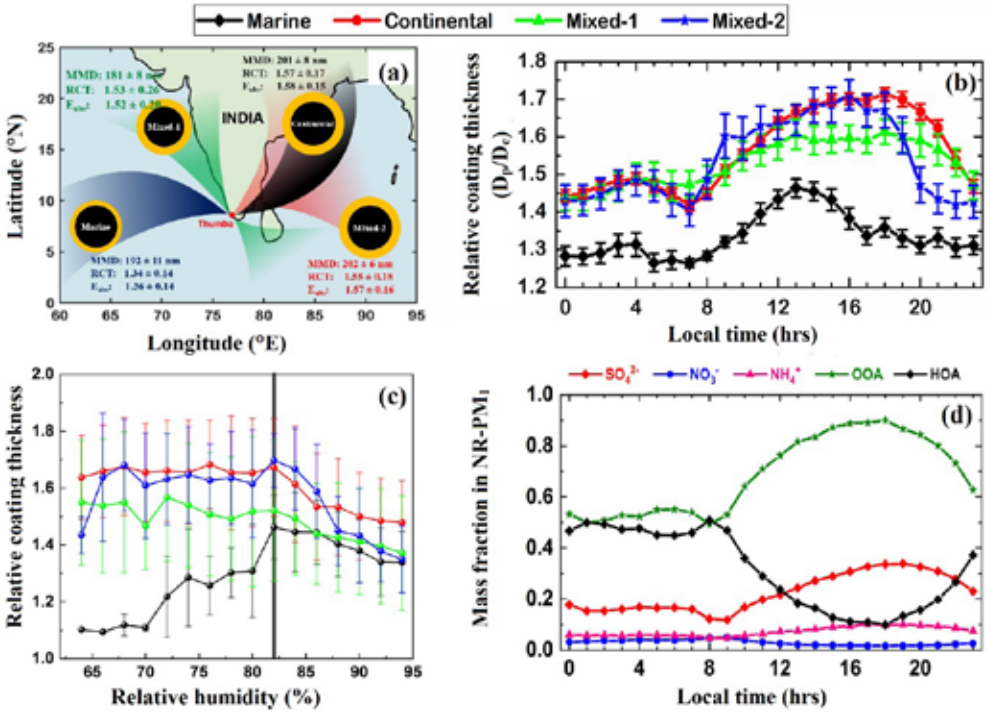

Figure 6: (a) A summary of BC microphysical characteristics (MMD -mass median diameter, RCT-relative coating thickness, and E_{abs} –light-absorption enhancement factor) over Thumba, (b) diurnal variation of RCT on BC cores under diverse airmass conditions, (c) variation of mean RCT with ambient RH (the vertical bar marks 82% RH which is deliquescence RH for inorganics), (d) diurnal pattern of non-refractory submicron aerosol species that are potential coating species for BC [Nithin et al., Atmos. Res., 2026].

1.58 ± 0.15 during Continental periods. Overall, the study demonstrates that unique tropical atmospheric processes, including long-range transport, secondary aerosol formation, humidity-driven changes, and meteorological conditions, significantly modify BC mixing state and its light-absorption behavior. These modifications lead to enhanced warming potential, highlighting the critical need to incorporate BC aging and mixing state dynamics into climate assessments for tropical regions.

Estimation of TOA flux and radiance based on the angular distribution of aerosol light scattering measurements

Estimating Top-of-Atmosphere (TOA) flux and radiance is essential for understanding Earth's radiation budget and climate. In this context, we have utilized polar nephelometer measurements of aerosol scattering coefficients at 17 angles (9 -170°), experimentally determined aerosol phase functions and calculated Legendre moments. These moments were then used to estimate TOA flux and radiance. The measurements conducted under diverse air mass conditions over a tropical coastal location, Thumba, revealed significant seasonal and diurnal variations in angular scattering patterns, with the highest scattering during winter and the lowest during the monsoon. Notably, a prominent secondary scattering mode, with varying magnitude across different seasons, was observed in the 20–30° angular range, highlighting the influence of different air masses and aerosol sources.

Aerosol phase function derived from the measured angular distributions of aerosol scattering coefficients indicated that the values (P_{meas}) possess similar patterns with the Henyey–Greenstein phase function (P_{HG}) derived theoretically across all seasons (Fig. 7a-d); however, P_{meas} shows distinct variations from P_{HG} at angles greater than 60°. This difference is more pronounced from May to November.

The collocated aerosol chemical composition in both fine and coarse modes was investigated to elucidate the underlying processes driving the observed discrepancies between actual and approximated phase functions. The distinct seasonality is identified in the dominant aerosol types. The aerosol system in the pre-monsoon and monsoon exhibited the presence of coarse-mode aerosols dominated by major ionic components (Na^+, Ca^{2+}, Cl^-) and trace elements (Al, Fe). Conversely, winter and post-monsoon

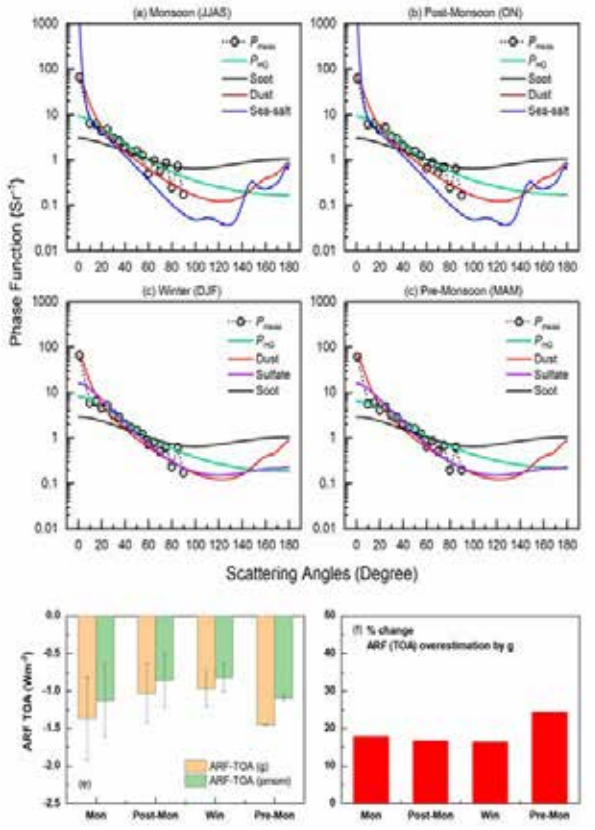

Figure 7: (a-d) Aerosol phase functions (P_{meas}) calculated from the observed angular scattering coefficients at different seasons. The Henyey-Greenstein Phase function (P_{HG}) derived from g is also shown. Additionally, the phase functions of different species (soot, dust, sea salt and sulfate) derived from their size distributions and refractive index values at 525 nm, are presented. (e) The diurnal average aerosol radiative forcing (ARF) at the TOA for each season estimated using P_{meas} and P_{HG}. (f) Percentage change in the ARF at the TOA between the two approaches [Jana et al., J. Quant. Spectrosc. Radiat. Transfer, 2025].

witnessed a considerable amount of fine-mode aerosols rich in NH_4^+, K^+, SO_4^{2-}, MSA^-, oxalate, OC, and EC. Interestingly, OC and SO_4^{2-} were present in both modes in all the seasons, albeit with varying magnitudes. However, the presence of the other dominant species differed from season to season, which was directly reflected in the variations observed in the angular pattern of light scattering and derived phase function. These observations highlighted the critical role played by aerosol microphysical properties in affecting their optical properties and the importance of size-segregated aerosol chemical composition measurements, where the presence of very large coarse-mode non-spherical aerosols caused increased oscillations in the phase function beyond 60° during the pre-monsoon and monsoon seasons. As a result, TOA fluxes and radiances derived using the P_{HG} showed

a significant difference, up to 24% in seasons with substantial coarse-mode aerosol presence, compared to those derived using the Legendre moments of the phase function (Fig. 7e-f). Therefore, TOA flux and radiance estimates using Legendre moments are generally more accurate in the presence of complex aerosol scattering characteristics, particularly for non-spherical or coarse-mode aerosols, while the P_{HG} may yield less accurate results due to its simplified representation of scattering behavior. Overall, this study highlights the importance of incorporating angular scattering measurements in diverse environments apart from size-segregated aerosol chemistry with a focus on process-level studies for accurate radiative transfer calculations and robust satellite remote sensing applications.

Aerosol Chemistry

Impact of sea- and land-breeze circulations on formation of secondary organic aerosols in the tropical coastal atmosphere

Secondary organic aerosols (SOA) consist of tiny particles produced when gases in the air undergo chemical reactions, and these particles influence air quality, climate, and human health. However, the molecular characteristics and formation processes of SOA in such environments remain unexplored, especially over tropical coastal atmosphere, where land-breeze (LB) and sea-breeze (SB) circulations significantly influence the distribution and transformation processes of SOA. The present study investigates the sources and formation processes of SOA during SB and LB circulations at Thumba (8.5° N, 76.9° E), located on the southwest coast of tropical peninsular India during pre-monsoon period (19 March - 12 April 2019). PM_{10} were collected on day (11:30–16:30 LT) and night (00:30–05:30 LT) basis using high volume sampler (HVS) to examine the impact of land-sea breeze circulations on formation processes of SOA. PM_{10} samples were analyzed for water-soluble dicarboxylic acids, ω-oxoacids, and α-dicarbonyls compounds using gas chromatography (GC) technique. The study found that though the relative abundance of OC showed no significant difference between SB and LB, its subsets, water-soluble organic carbon (WSOC) and water-insoluble organic carbon (WIOC), exhibited notable differences (Fig. 8b-c). The abundance of oxalic acid (C_2) was the most common compound during both circulations, especially in the LB (Fig.8a).

Other abundant compounds included phthalic acid

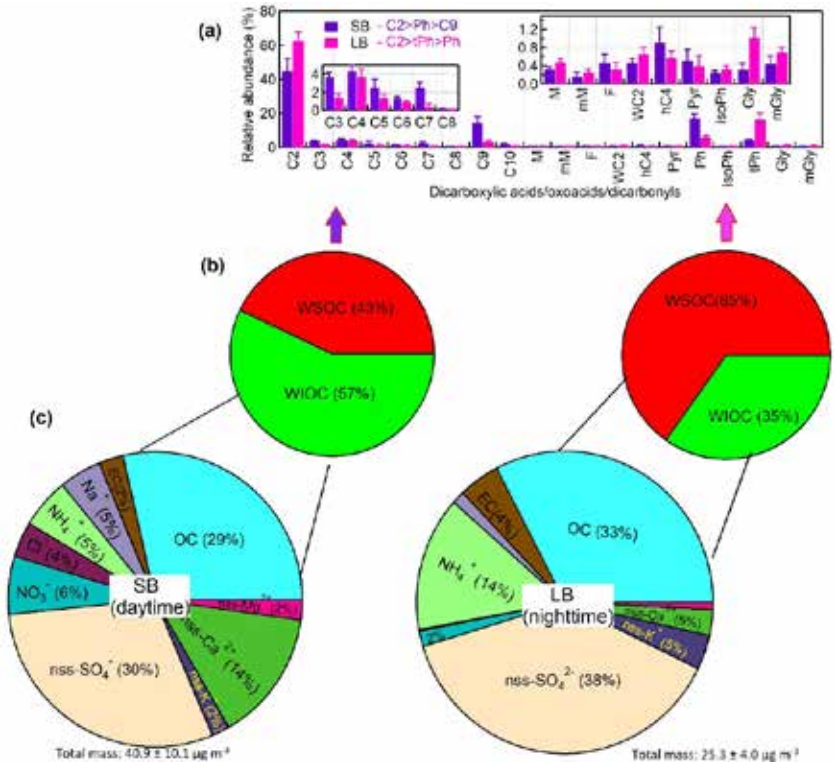

Figure 8: Relative abundances (%) in (a) molecular distributions of water-soluble organic compounds (b) water-soluble and water-insoluble organic carbon, and (c) chemical composition during SB and LB circulations at Thumba during premonsoon. Total mass is the sum of all measured chemical species, including water-soluble ionic species, EC and OC [Boreddy et al. ACS Earth Space Chem., 2025].

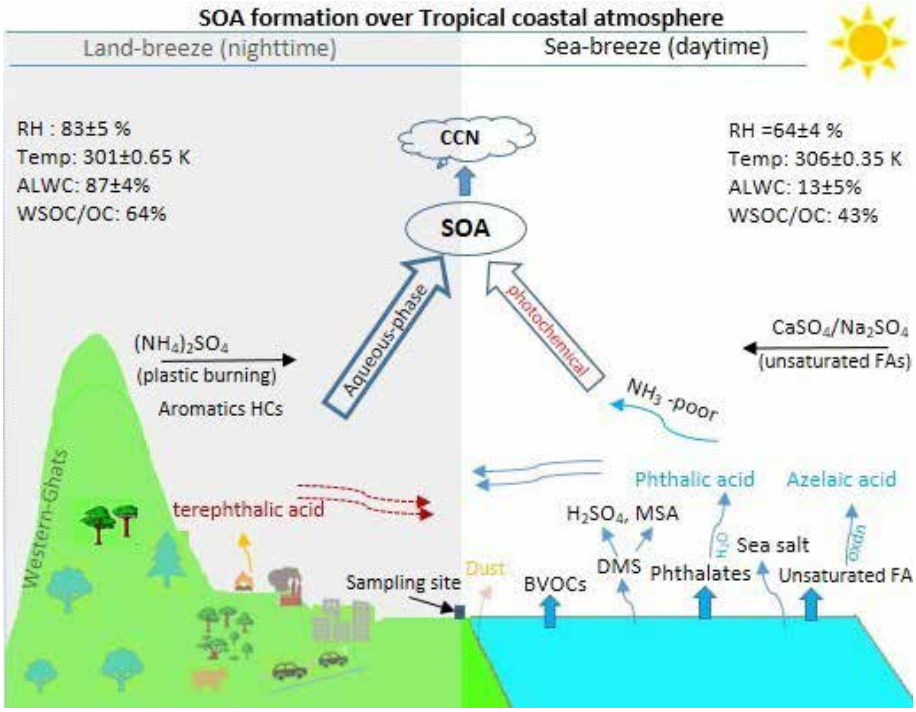

Figure 9:Illustration of SOA formation in the tropical coastal atmosphere [Boreddy et al., ACS Earth Space Chem., 2025].

(ph; an oxidation product of aromatic acids) and azelaic acid (C_9; a tracer of biogenic unsaturated fatty acids), being more common during the SB. The presence of high levels of terephthalic acid (tPh; a tracer of plastic burning) during the LB indicated the influence of plastic burning in nearby areas. Markers of sunlight-driven reactions, such as fumaric-to-maleic (F-to-M) and malonic-to-succinic (C_3-to-C_4) acids, were almost twice as high during the SB, suggesting stronger photochemical activity. In contrast, C_2-to-$\Sigma(C_2–C_{10})$ and WSOC-to-OC ratios were higher during LB, suggesting secondary oxidation in an aqueous medium. ISORROPIA-II revealed that the LB had higher humidity levels and more aerosol liquid water content (ALWC) further supports the aqueous-phase formation of SOA (Fig.9).

Overall, SOA formation in Thumba is influenced by photochemical processes of marine-derived-organic precursors, such as unsaturated fatty acids and hydrolysis of phthalates, and related biogenic precursors during SB. However, the aqueous-phase formation of SOA relates to human-induced pollutants, including plastic burning dominant, during LB. The overwhelming contribution of terephthalic acid during LB highlights the urgent need to understand airborne-nanoplastics and their potential climate effects, particularly in tropical coastal atmospheres.

Chemical Evolution of Size-Resolved Aerosols during Air-Mass Transition over the Tropical Western Ghats and Peninsular India

Atmospheric aerosols significantly influence regional climate and air quality through their direct radiative effects and indirect effects on cloud properties. The Western Ghats (WG), a globally recognized biodiversity hotspot and key modulator of the Indian monsoon, experiences pronounced seasonal shifts in air-mass regimes. This study investigates the size-segregated chemical composition of aerosols at Ponmudi (8.8°N, 77.1°E, 960 m a.s.l.), a high-altitude site in the southern WG, during the continental-to-marine air-mass transition phase (January–April 2020–2021), which is dominated by continental outflow during the northeast monsoon.

Size-segregated aerosol samples were collected using a high-volume cascade impactor with five stages capturing particles in the following size ranges: <1.1, 1.1–2.0, 2.0–3.3, 3.3–7.0, and >7.0 µm, operated at 566 L min^{-1}. Samples were analysed for organic carbon (OC), elemental carbon (EC), water-soluble organic carbon (WSOC), major water-soluble ions, and trace metals. Air-mass origins were classified into three types using seven-day HYSPLIT back-trajectories: Indo-Gangetic Plain (IGP), East Asia + Bay of Bengal (EA+BoB), and mixed Bay of Bengal + Arabian Sea

(BoB+AS) (Fig. 10). Aerosol liquid water (ALW) was estimated using the ISORROPIA-II model for inorganic components and κ-Köhler theory for organic contributions. Source apportionment was performed using EPA PMF 5.0 on 110 size-resolved samples. Coarse-mode aerosol mass dominated throughout the study period, exceeding fine-mode mass by more than a factor of two, with both fractions increasing progressively from winter to pre-monsoon. Fine-mode aerosols were enriched in secondary inorganic species (primarily $(NH_4)_2SO_4$), EC and WSOC, while coarse-mode aerosols contained elevated concentrations of sea-salt (Na, Cl^-) and crustal components. Air-mass composition varied distinctly by origin: IGP air masses were dominated by anthropogenic sulphates and crustal species, whereas EA+BoB air masses showed highly oxidised organics (elevated OM/OC ratios) mixed with marine aerosols. PMF analysis resolved nine distinct factors, including aged secondary sulphate, biomass-burning-influenced mixed aerosols, sea-salt, and mineral dust. Mass closure analysis revealed high OM/OC conversion factors (up to ~2.2) in EA+BoB air masses, confirming extensive photochemical oxidation during long-range atmospheric transport. The aerosol system over the WG during the transition phase comprises a complex mixture of long-range-transported aged continental emissions, urban-valley pollutants from local convection, and marine aerosols. Cloud processing and aqueous-phase chemistry significantly enhance secondary sulphate, organic species, and ALW content, particularly in fine-mode particles. These chemically processed aerosols can substantially alter hygroscopicity, cloud condensation nuclei (CCN) activity, and regional radiative forcing over this ecologically sensitive high-altitude ecosystem. The findings underscore the critical need for continued monitoring to comprehensively assess impacts on monsoon dynamics and air quality in this biodiverse region.

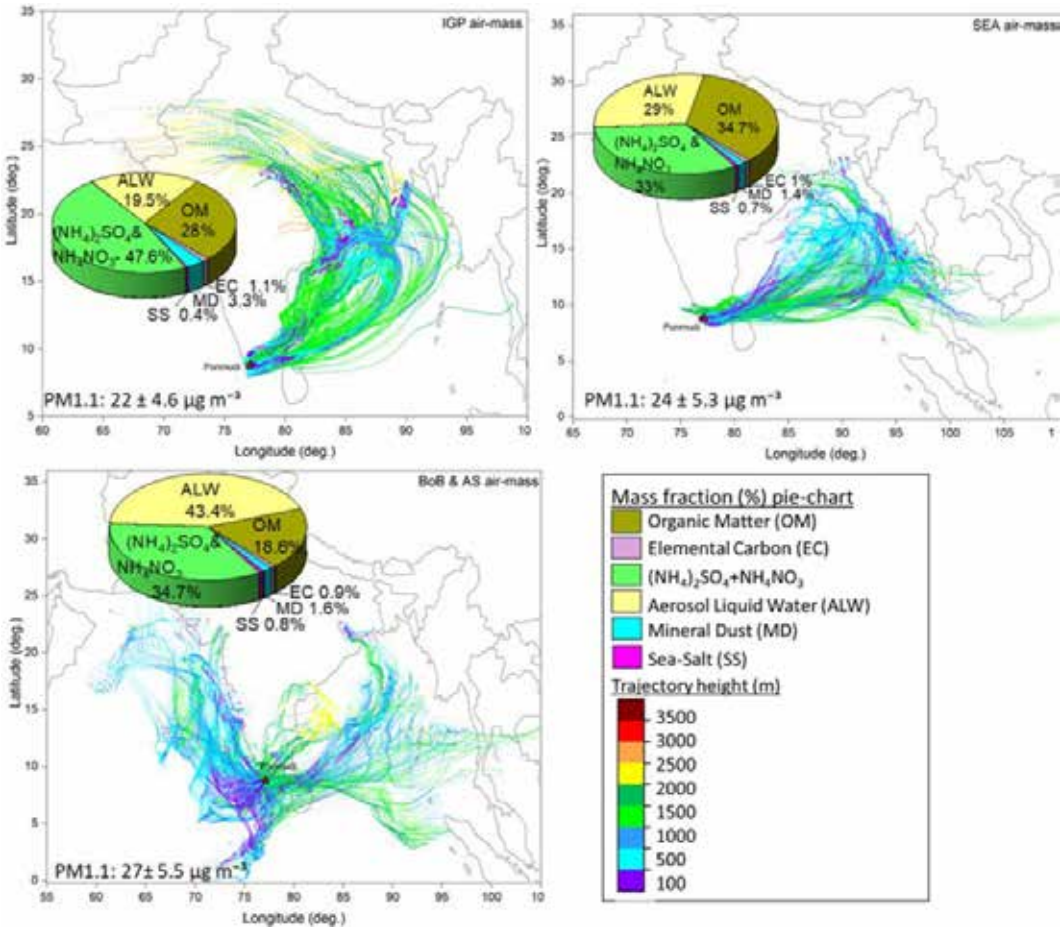

Figure 10: Seven-day backward air mass trajectories, along with their corresponding heights, arriving at Ponmudi during the sampling campaign. The trajectories are classified into three types as presented in each panel based on air mass direction. The mass fraction of fine aerosol mass associated with the respective trajectories is given as pie charts [Aswini et al., Atmos. Res. 2025].

Regional Characterization of Aerosols

Winter haze amplification by aerosol hygroscopic growth

Every year during winter, the densely populated Indo-Gangetic Plain (IGP) in Northern India experiences increasingly prolonged and widespread occurrences of fog, leading to a 2-fold increase in the number of days with poor visibility (less than 0.5 km) over this region. This frequent occurrence of widespread winter haze over Northern India is largely appear to originate from exceedingly high concentrations of fine particulate matter from anthropogenic emissions. However, the underlying mechanisms driving winter haze in Northern India are not well understood. The present study employed a synergy of satellite and reanalysis data from 2006 to 2021 to assess the role of hygroscopic growth of aerosol optical depth (AOD) in winter haze over the eastern Indo-Gangetic Plain. A method has been developed to extract dry AOD (AOD_{dry}) from ambient AOD (AOD_{amb}) to elucidate the origin of winter haze. About 31% of severe haze episodes (AOD > 0.85) occurring under ambient humidity conditions decrease to below 5% for dry conditions, indicating the critical role of particle hygroscopic growth. The spatio-temporally averaged extinction enhancement factor (AOD_{amb}/ AOD_{dry}) of 1.8 indicates the likelihood of a large fraction of water-soluble aerosols over eastern IGP under high relative humidity conditions suggesting their potential role as cloud condensation nuclei (CCN) affecting haze and fog processes. The estimated trend of AOD_{amb} (0.012 yr^{-1}) is about twice to that of the trend in AOD_{dry} (0.005 yr^{-1}) accompanied by concurrent increasing trends in surface and column humidity (Fig. 11). The mean aerosol radiative forcing at the surface ($\Delta F_{surface}$ = -38.1 ± 9.3 Wm^{-2}) and in the atmosphere ($\Delta F_{atmosphere}$ = 24.2 ± 6.2 Wm^{-2}) under ambient conditions varied by -9.6 Wm^{-2} (34%) and 6.8 Wm^{-2} (39%), compared to those in dry conditions (-28.5 ± 6.4 Wm^{-2} and 17.4 ± 3.9 Wm^{-2}), respectively. The mean radiative forcing at the top of the atmosphere (ΔF_{TOA}) varied by only -2.7 Wm^{-2} (25%) lesser for ambient conditions (-13.9 ± 0.10 Wm^{-2}) compared to those under dry conditions (-11.2 ± 0.07 Wm^{-2}), suggesting that change in radiative forcing at the TOA due to hygroscopic growth is relatively small by factors up to 1.6 compared to that at the surface and in the atmosphere. The net surface cooling effect due to aerosol direct radiative impact can further increase relative humidity in the boundary layer. This surface cooling effect coupled with high moisture and enriched inorganic and water-soluble organic aerosols (through secondary transformations from oxidation of primary anthropogenic emission) lead to increased aerosol liquid water content (ALWC) and hygroscopic growth, creating positive-feedback on regional meteorology. Thus, ubiquitous winter haze over the eastern Indo-Gangetic Plain is exacerbated by hygroscopic growth under high anthropogenic aerosol emissions, further aggravated through aerosol-radiation feedback. These results will be valuable in devising haze forecasts, implementing effective mitigation policies, and representing aerosol hygroscopicity in climate models.

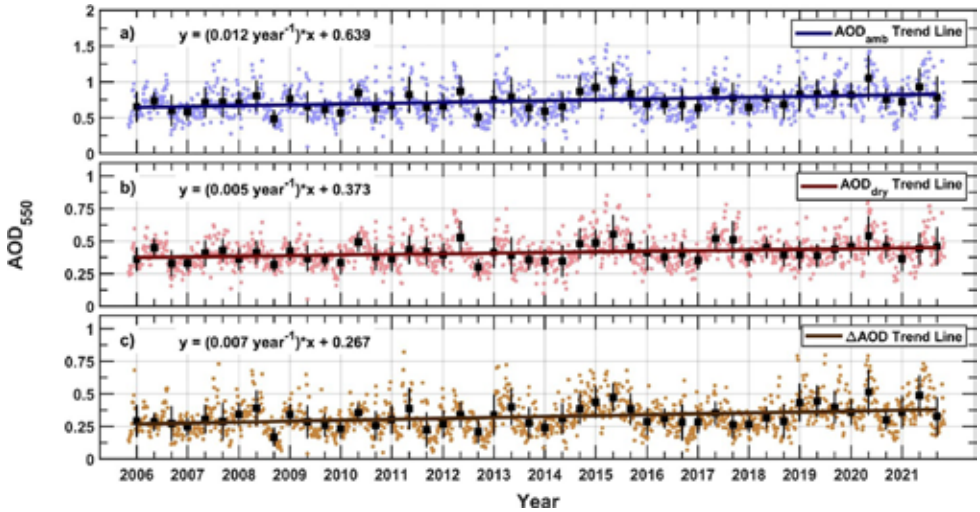

Figure 11: Long-term linear trends in AOD_{550} under a) ambient and b) dry conditions along with trend of c) amplified AOD_{550} (ΔAOD_{RH}) due to hygroscopic growth over eastern Indo-Gangetic Plain during winter 2006–2021. The daily mean values are indicated by coloured circle markers, and the monthly mean values with standard deviation are indicated by black square markers with vertical lines. Trends are reported with a confidence level greater than 95% [Kallihosur et al., Comm. Earth Environ., 2025].

Speciated aerosol direct radiative forcing over the northern Indian Ocean during the south Asian outflow in the winter 2018 ICARB experiment

The anthropogenic aerosols are one of the major uncertain components of the climate system. In this regard, there is a growing interest within the climate and atmospheric science community of the importance of acquiring quantitative data on anthropogenic aerosol changes, particularly over the south Asian and adjoining oceanic areas. In this context, a comprehensive assessment of the speciated and spectral aerosol direct radiative forcing (DRF) over the southeastern Arabian Sea and equatorial Indian Ocean is made during the Integrated Campaign for Aerosols, gases, and Radiation Budget (ICARB-2018) experiment. The strength of the work lies in combining multi-instrument shipborne measurements with chemical speciation and radiative-transfer modelling, which together help in clearly separating the contributions of water-soluble inorganic ions (WSAI), organic carbon (OC), black carbon (BC), sea-salt, and dust to the total aerosol loading and radiative forcing. Such a detailed examination of aerosol species over the open ocean especially during the period of intense continental outflow is rare and important observational gap in understanding South Asian aerosol - radiation interactions.

The spatial variability in columnar AOD and absorbing/scattering coefficients highlights the strong north - south gradient shaped by continental outflow with ~ 89% contribution from anthropogenic component near-coastal regions and 46% even south of the equator. Water-soluble anthropogenic ions (WSAI) emerge as the primary contributor to columnar AOD across most of the northern Indian Ocean, likely due to their higher scaling distance (-28.4°) compared to organic carbon (OC, -15.5°) and black carbon (BC, -12.63°). Speciated aerosol radiative forcing estimates indicate that BC drives the highest surface forcing near coastal regions, while WSAI dominates in far oceanic regions. In the equatorial Indian Ocean, WSAI exerts the highest surface forcing (-3.5 ±2.6 W m^{-2}), followed by BC (-3.3 ±1.7 W m^{-2}) and OC (-1.5 ±1.0 W m^{-2}). BC also plays a dominant role in atmospheric heating rates over the equatorial Indian Ocean, contributing approximately 67 % (Fig. 12). These observations reveal the importance of addressing anthropogenic pollution sources, especially form industrial and transportation sectors. Mitigation efforts targeting these specific aerosol species could lead significant improvement in regional air quality and climate outcomes.

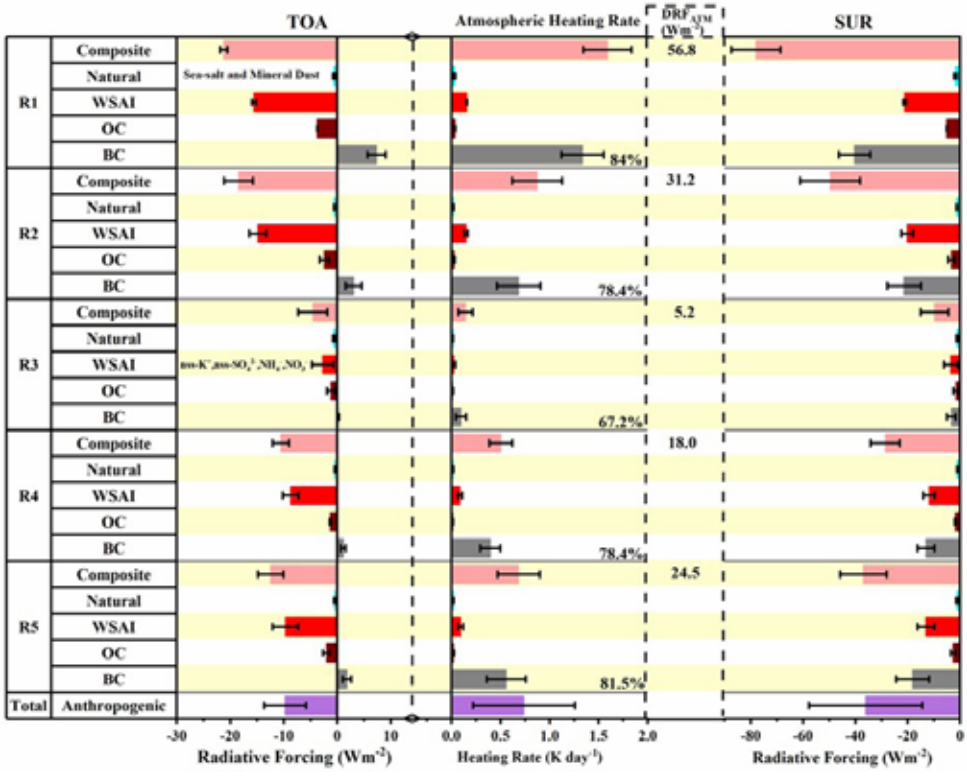

Figure 12: Spectrally integrated direct shortwave aerosol radiative forcing for various species; composite, natural, WSAI, OC, BC [Gogoi et al., Atmos. Environ., 2025].

Technical Activities

Design and development of a LED-based hand-held Multi-wavelength Sun Photometer

A cost-effective, user-friendly handheld multi-channel LED-based sun photometer (MLP) is developed to expand the coverage and accessibility of aerosol optical depth measurements across India. The novelty of this instrument is the addition of low bandwidth (<30 nm) Light Emitting Diodes (LED) as the opto-electric transducer. These LEDs function as photodetectors by absorbing photons and generating photocurrents. The wavelength dependent optical responses of the LEDs enable the replacement of the traditional band pass interference filter – lens – photodiode combination with narrow-band LEDs in sun photometers, thereby reducing the cost. Three LEDs of different colors (wavelengths) are used in the MLP, and the spectral response characterization of the LED sensors was performed using a monochromator. The optical non-linearity of the LEDs was also tested and found that the device's response varies linearly (R^2 = ~ 0.98) with different flux levels.

It is a portable and standalone instrument and is comprised of 2 segments: (i) a multi-channel Optics unit and (ii) a Data logger module packed in single housing. 9V rechargeable batteries power the unit. The uniquely designed optics tube holds three (expandable to six) optical sensors (LEDs) and a temperature sensor. The optics tube is fabricated from a metallic block and has pockets to hold the various optical components. The optical channels are machined on the cylindrical block such that they maintain extreme parallelism. For measurements, a dedicated optical window on one side of the block and parallel to the optical axis is provided for visual check of solar alignment. A real-time peak signal display on LCD also helps in precise alignment.

The data logger contains all the required logic and electronic circuitry to operate the sun photometer as a standalone unit. It is a microcontroller based embedded system, which schedules the timing and control operations, data acquisition, and memory storage and provides an interface to PC for data download. The integrated GPS helps automatic geo-tagging and time stamping on data, a feature that minimizes the reconfiguration of these parameters when moving the unit to a new location.

The main functions of the instrument are to measure the direct solar flux at different wavelengths, acquire and save the data along with time stamping and location tagging and download the data to PC when prompted.

Figure 13: Image of MLP.

The image of the handheld LED sun photometer is shown in Fig. 13. Its dimensions are 180x140x60 mm and weighs less than 1 kg. Several field trials were conducted to assess the performance of the MLP. Comparison of MLP Aerosol Optical Depth (AOD) with ground-based MWR, Microtops and satellite-based MODIS AOD showed excellent agreement, validating the performance of the system and the accuracy of AOD estimation. These are depicted in Fig.14 (a), (b) and (c).

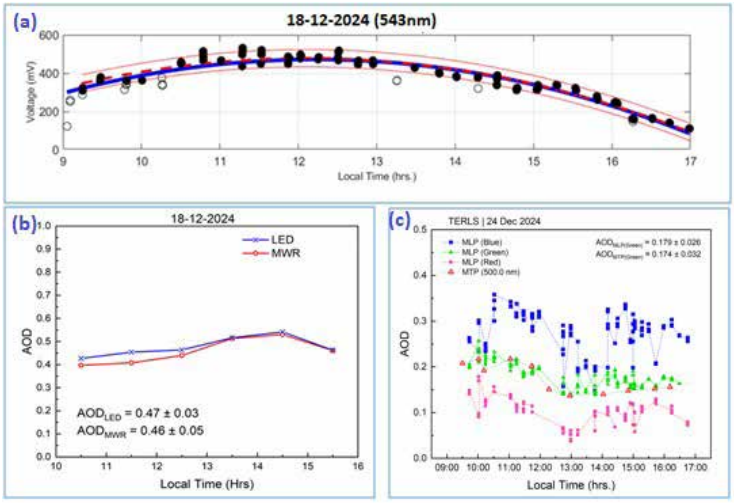

Figure 14: (a) MLP measured raw voltage vs time. (b) MLP and MWR AOD comparison. (c) MLP and Microtops AOD comparison.

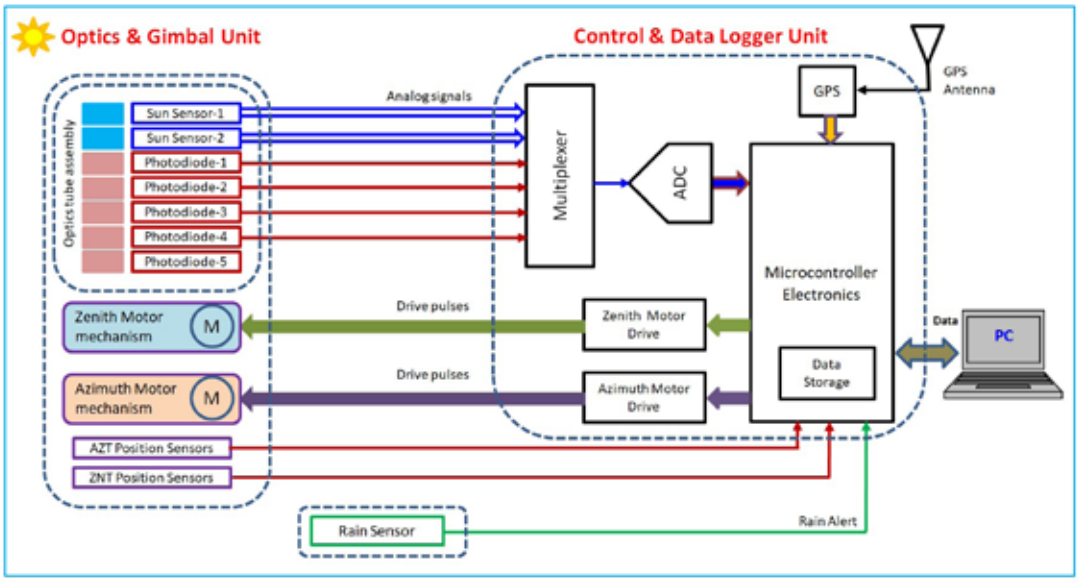

Figure 15: Block diagram of μ-MWR.

Development of Compact Solar Radiometer (μ-MWR)

A miniature version of solar radiometer (μ-MWR) has been developed. The salient features of this instrument are (i) compact and lightweight, (i) automatic sun tracking and data acquisition, (iii) 5/6 optical channels/wavelengths, (iv) almanac and sun sensor-based sun seeking algorithm, (v) provision for direct sun and almucantar measurements. The schematic block diagram of μ-MWR is shown in Fig.15. It consists of an Optics & Gimbal unit and a Control & data logger unit.

The multi-channel optics unit is integrated to the Gimbal mechanism for sun tracking and measurements. Five individual optics tubes are arranged in parallel with the main optical axis. Each of them consists of an interference filter, lens assembly and a silicon photodiode and hence eliminates the requirement of a filter wheel-based wavelength scanning mechanism. It is also equipped with two sun sensors (4-quadrant photodiodes) for aiding the solar tracking. These are having ±45° and ±5° field of view for coarse and fine sun alignment, respectively.

The control and data logger unit is a microcontroller based embedded system and it hosts various algorithms such as Solar Position algorithm, Sun tracking algorithm and Data acquisition algorithm for the standalone operation of the radiometer.

The μ-MWR starts automatically at sunrise time, and estimates the position of the sun by using a Solar Position Algorithm by using the GPS data. Subsequently, it positions the optic unit to the estimated solar angles by driving the motorized Gimbal. Thereafter, the feedback from the sun sensors is used for precise alignment to the sun and subsequent tracking. Solar flux measurements are carried out at selected interval after locking the optical axis with the sun. In addition, the unit is programmed to enter into sleep mode during rain and at sunset.

Design and development of a Compact Snow Depth and Snow Temperature Profiler

A cost-effective instrument is developed for the accurate measurement of snow depth, and thermal state of snow pack, which is essential for snow accumulation, snow atmosphere interaction and snow melt analysis. The system uses two sensors for the continuous measurement of snow depth using ultrasonic and laser techniques. Additionally, a set of four calibrated PT100 temperature sensors is integrated for the continuous and instantaneous measurement of snow temperature at different snow layers. Accurate data logging in terms of position and time information, along with the snow depth and snow-temperature data, is supported by aiding a miniature GPS receiver. The prototype of the system is very compact and lightweight. For the real-time transmission of data from the remote field to the nearby station, the developed system includes a wireless module having transmission range up to 1.5 km. The schematic of the snow profiler is given in Fig.16.

The major unique features of the system include the

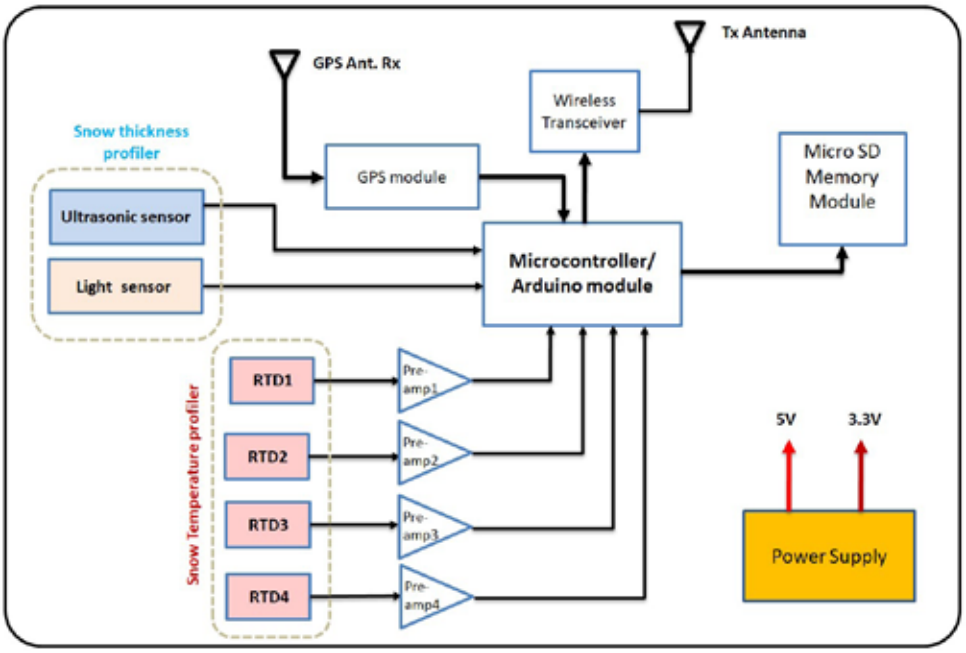

Figure 16: Block diagram of snow profiler.

application of dual sensors (ultrasonic and laser) for accurate snow-depth measurements; the use of four PT100 RTD sensors, which are stable, accurate, and provide excellent linearity, to measure snow temperature at different layers; unique wireless data transmission capability up to a distance of 1.5 km; the use of miniaturized sensors to make the system cost-effective, portable, and suitable for low-power consumption; an onboard data storage facility with memory capacity up to 16 GB; and the integration of a miniature GPS receiver for accurate position and time tagging of the acquired data.

Ongoing Activities and Future Projections

- Investigating the role of large-scale atmospheric oscillations on winter aerosol dynamics across the Indo-Gangetic Plain
- Investigating the Impact of Greening and Enhanced Cloudiness on Aerosol Direct Radiative Forcing and Its Influence on Net Primary Productivity over Northwest India
- Assessing the aerosol contributions to the anomalous weakening of surface warming trend over India using satellite observations and Regional Climate Modelling
- Development of Satellite-Based Polarized Radiometry Algorithm for Accurate Retrieval of Aerosol Optical Depth
- Conducting of high-altitude balloon flight experiments for collecting aerosol samples from the upper troposphere and lower stratosphere
- Engineering Model development of Sun-Tracking Solar Radiometer for Dust Optical Depth Retrievals on Future Mars Lander Missions
- Laboratory-model development of a quartz crystal microbalance for aerosol measurements in both planetary and terrestrial atmospheres
- Quantification of atmospheric aerosol impacts on free-space optical communication over Indian region based on ARFINET data
- Molecular level analysis of atmospheric organic aerosols using NMR spectroscopy
- Design and development of a laboratory-scale photochemical chamber for studying reaction processes involving atmospheric aerosols

Publications in Peer-Reviewed Journals

1. Kompalli, S.K. and Babu, S.S., "Aerosol light-scattering enhancement and liquid water content in a tropical coastal atmosphere", Atmospheric Research, https://doi.org/10.1016/j.atmosres.2025.108615, 2026.
2. Nithin, B., Kompalli, S.K., and Babu, S.S., "Black carbon mixing state and light-absorption enhancement under different air mass regimes over a tropical coastal site", Atmospheric Research, https://doi.org/10.1016/j.atmosres.2025.108641, 2026.
3. Tandule, C.R., Gogoi, M.M., Gauda, S.S. and Babu, S.S., "Retrieval of aerosol optical depth from INSAT-3DR for accurate geostationary monitoring of regional and temporal aerosol dynamics", Atmospheric Environment, https://doi.org/10.1016/j.atmosenv.2025.121730, 2026.
4. Akhila, R. S., Nair, V. S., Basheer, A. I., Parottil, A., and Babu, S. S, "Energy-balance decomposition of the aerosol-induced changes on surface temperature over South Asia", Journal of Geophysical Research: Atmospheres, https://doi.org/10.1029/ 2024JD043123, 2025.
5. Aswini, A. R., Deshmukh, D. K., Ramya, C. B., Hegde, P., and Babu, S. S., "Size-speciated aerosol chemistry during continental-to-marine transition, Western Ghats", Atmospheric Research, https://doi.org/10.1016/j.atmosres.2024.107826, 2025.
6. Abdullah, B.H., Singh, P., Vaishya, A., Prasad, P., Rastogi, S., Gogoi, M.M., and Babu, S.S., "Decadal analysis of black carbon aerosols over the central Indo-Gangetic Plain: trends, source regions, and policy impact", Atmospheric Research, https://doi.org/10.1016/j.atmosres.2025.108271, 2025.
7. Boreddy, S.K.R., Parvathy, P., Kumar, D., Hegde, P., and Babu, S. S. "Secondary organic aerosol formation in the tropical coastal atmosphere: impact of land- and sea-breeze circulations", ACS Earth and Space Chemistry, https://doi.org/10.1021/acsearthspacechem.5c00028, 2025.
8. Das, B., Pathak, B., Bhattacharjee, U., Sahu, P.J., Kundu, A., Borgohain, A., Gogoi, M.M., Kundu, S.S., Bhuyan, K., and Bhuyan, P.K., "NPF-induced enhancement of Cloud Condensation Nuclei over an urban location in Eastern Himalayan Foothills: A campaign-based study", Atmospheric Environment, https://doi.org/10.1016/j.atmosenv.2025.121524, 2025.
9. Gogoi, M.M., Nair, V.S., Tandule, C.R., Hegde, P., Kompalli, S.K., and Babu, S.S., "Speciated and spectral aerosol direct radiative forcing over the northern Indian Ocean during the south Asian outflow in the winter 2018 ICARB experiment", Atmospheric Environment, https://doi.org/10.1016/j.atmosenv.2025.121457, 2025.
10. Jana, S., Gogoi, M.M., Ajith, T.C., Hegde, P., Kompalli, S.K., and Babu, S.S., "Estimation of TOA flux and radiance based on the angular distribution of aerosol light scattering measurements", Journal of Quantitative Spectroscopy and Radiative Transfer, https://doi.org/10.1016/j.jqsrt.2025.109365, 2025.
11. Kundu, A., Kundu, S.S., Borgohain, A., Gogoi, M.M., Babu, S.S., Sharma, S.K., and Gogoi, M., "Role of atmospheric boundary layer dynamics in driving surface black carbon concentrations over a high-altitude station in North-east India", Atmospheric Pollution Research, https://doi.org/10.1016/j.apr.2025.102420, 2025.
12. Meda, B. N. M., Sarangi, C., Ali, S., Viswanath M., Nair, V. S., Kumar, A., Jena, C., and Soni, V. K., "Spatiotemporal Variability and Radiative Forcing of Secondary Brown Carbon over India", ACS Environmental Scicence & Technology Air, https://doi.org/10.1021/acsestair.5c00120, 2025.
13. Pathak, B., Das, B., Sahu, P., Gogoi, M.M., Bhuyan, P.K., Baishya, K., Mahanta, P., Bhuyan, K., Biswas, J., Hazarika, R., Bora, S., Borah, M., Borgohain, R., Bhuyan, J., Bhuyan, K., and Hazarika, S., "Investigating spatial heterogeneity in aerosols chemical composition and implications for physico-optical properties over the North Eastern region of India", ACS Earth and Space Chemistry, https://doi.org/10.1021/acsearthspacechem.5c00197, 2025.
14. Reshmy, D. S., Swarnalatha, K., Gautam, S., Mathew, B. S., and Hegde, P., "Assessing air pollution in a

coastal urban setting: contributions of PM_{10}, vehicular emissions, and public health impacts", Journal of Atmospheric Chemistry, https://doi.org/10.1007/s10874-025-09483-4, 2025.

15. Tandule, C.R., Gogoi, M.M., and Babu, S.S., "Improved Cloud Screening of OceanSat-3 OCM-3 Satellite Imagery using Machine Learning", Remote Sensing Applications: Society and Environment, https://doi.org/10.1016/j.rsase.2025.101481, 2025.
16. Vishwakarma, Y.K., Bhardwaj, N., Ram, K., Gogoi, M.M., Banerjee, T., Mohanty, M., and Singh, R.S., "Bioaerosol emissions from solid waste processing facilities at urban environment and their impact on human health", Science of the Total Environment, https://doi.org/10.1016/j.scitotenv.2025.180049, 2025.
17. Ajith, T. C., Windwer, E., Li, C., Fang, Z., Kompalli, S.K., Nursanto, F. R., Olayemi, T.E., Ese, J.I., Sharpe, S.A.L., Fraund, M., Moffet, R.C., Laskin, A., Fry, J.L., and Rudich, Y., "Investigating new particle formation and growth over an urban location in the Eastern Mediterranean", Journal of Geophysical Research: Atmospheres, https://doi.org/ 10.1029/2024JD041802, 2024.
18. Harithasree, S., Sharma, K., Girach, I.A., Sahu, L.K., Nair, P.R., Singh, N., Flemming, J., Babu, S.S., Ojha, N., "Surface ozone over Doon valley of the Indian Himalaya: Characteristics, impact assessment, and model results'', Atmospheric Environment, https://doi.org/10.1016/j.aeaoa. 2024.100247, 2024.
19. Kallihosur, T., Nair, V. S., and Sinha, P. R., "Winter haze amplification by aerosol hygroscopic growth over eastern Indo- Gangetic Plain", Communication Earth Environment, https://doi.org/10.1038/s43247-024-01792-y, 2024.
20. Lima, C. B., Prijith, S. S., and Babu, S. S., "Characterisation of dust aerosols and their absorbing efficiency over South Asia using infrared observations from INSAT-3D Imager", International Journal of Remote Sensing, https://doi.org/10.1080/01431161.2024.2431176, 2024.

Presentation in Symposia/Conferences/Workshops

1. Kompalli, S.K., Nithin, B., Babu, S. S., "Black carbon mixing state and light-absorption enhancement across diverse outflow regions over India", 14th Asian Aerosol Conference (AAC 2025), Mumbai, December 01-04, 2025.
2. Ajayakumar, R.S., Kompalli, S.K., Williams, A., Lakshmikumar, T.V., Babu, S.S., "Drivers of surface ozone characteristics over a tropical coastal semi-urban site in Southern India", International Symposium on Tropical Meteorology (INTROMET-2025), IITM, Pune, November 18-20, 2025.
3. Anas Ibnu Basheer, Nair, V. S., Babu, S. S., "Investigating the effects of greening and cloud cover increase on aerosol direct radiative forcing over northwest India", 14th Asian Aerosol Conference (AAC 2025), Mumbai, December 01-04, 2025.
4. Ramya, C.B., Hegde, P., Deshmukh, D.K., Babu, S.S., "Unraveling the Formation Pathways of Secondary Organic Aerosols Based on Molecular Level Analysis over a Remote Location in Tropical Rain Forest", 16th International Commission on Atmospheric Chemistry and Global Pollution (iCACGP) Symposium and the 18th International Global Atmospheric Chemistry (IGAC) Science Conference (iCACGP-IGAC Conference 2024), World Trade Centre Kuala Lumpur (WTC KL), Kuala Lumpur, Malaysia, September 09-13, 2024.
5. Lekshmi S.R., "Structured Laser Beams for Robust Vertical Free-Space Optical Communication Links: A Numerical Study Using Scintillation Index Estimations", SCOPOSIS 2025, PRL, Ahmedabad, December, 08-12, 2025.
6. Tandule, C.R., Gogoi, M.M., Babu, S.S., "Role of mineral dust on net primary productivity over the Arabian Sea: Satellite remote sensing and model simulations", SOLAS Open Science Conference 2024, CSIR - National Institute of Oceanography, Goa, November, 11-13, 2024.
7. Srivastava, P., Naja, M., Joshi, H., Seshadri, T.R., Gogoi, M.M., Babu, S.S., Bhardwaj, P., Kumar, R., "Insights from about two decades of ground and space-based aerosol observations over the Central Himalayas", URSI-RCRS 2024, Bhimtal, October, 22 – 25, 2024.

8. Thejas, K. V., Nair V.S., and Sinha, P. R., "Aerosol-moisture-cloud interactions over Eastern Indo-Gangetic Plain during winter", IASTA National Aerosol Conference, Doon University, Dehradun, India, December 17-20, 2024.
9. Jasmine, M. K., Aloysius, M., Nair, V.S., "Impact of rainfall on reducing winter air pollution in the Indo-Gangetic Plain", IASTA National Aerosol Conference, Doon University, Dehradun, India, December 17-20, 2024.
10. Gogoi, M. M., Tandule, C.R., Babu, S.S., "AI-enhanced multi-wavelength multi-pixel aerosol retrieval from OCM-2 on-board Oceansat-2 satellite", Satellite Technology Day – 2025, U R Rao Satellite Centre, Bangalore, April 21, 2025.
11. Gogoi, M.M., and Babu, S.S., "Contrasting Aerosol Characteristics across the Western, Central, and Eastern Himalayas: Insights from Long-Term High-Altitude Observations", National Conference on Polar Sciences, NCPOR, Goa, September 16-18, 2025.
12. Prijith S. S., "Aerosol Climatology over the Oceanic regions around India from OceanSat-3", Review meeting of Oceansat-3 Utilization Projects, Space Application Centre, Ahmedabad, January 17, 2025.
13. C B Ramya., P. Hegde., Babu, S.S., "Molecular analysis of atmospheric aerosol particles–Method and Impact", National Conference on Critical and Strategic Minerals India 2025 (CASMIN 2025), Kochi, Kerala, December 4-5, 2025.
14. P. Anand., C B Ramya., P. Hegde., Babu, S.S., "Identification of molecular markers of organic aerosols using BSTFA derivatisation method", National Conference on Critical and Strategic Minerals India 2025 (CASMIN 2025), Kochi, Kerala, December 4-5, 2025.

Technical Reports

1. Ajeeshkumar, P.S. and Gogoi, M. M., "Design and development of handheld LED sun-photometer", ISRO-VSSC-TR-0105-0-25, 2025.

संख्यात्मक वायुमंडल प्रतिरूपण
Numerical Atmosphere Modelling

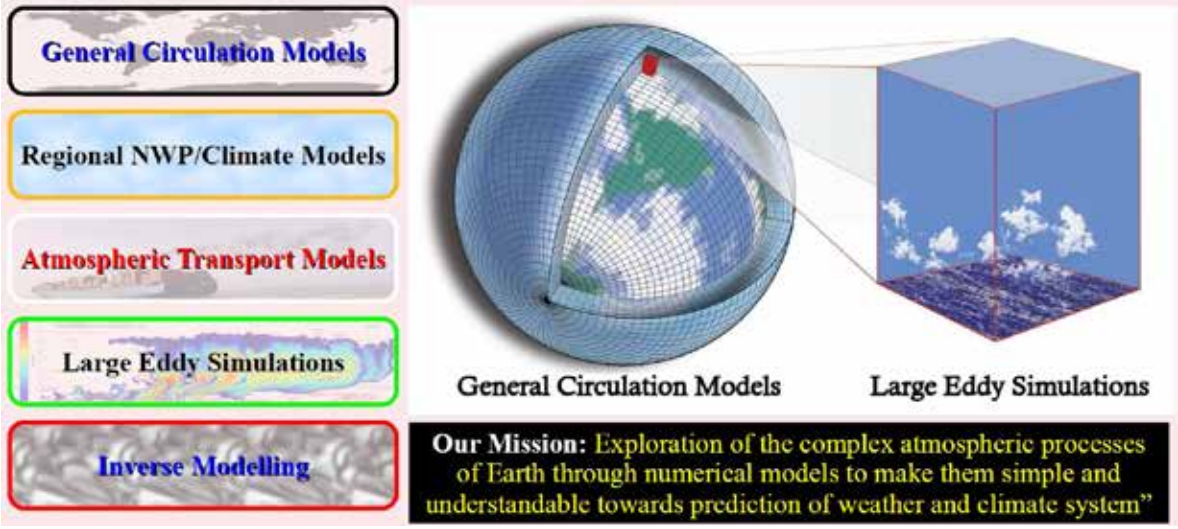

संख्यात्मक वायुमंडल प्रतिरूपण (एन ए एम) शाखा की वैज्ञानिक गतिविधियाँ संख्यात्मक मॉडलों की सहायता से पृथ्वी के वायुमंडल की जटिल भौतिक और रासायनिक प्रक्रियाओं की जाँच और अवलोकन पर केंद्रित हैं। इन जाँचों का अंतिम लक्ष्य सामाजिक अनुप्रयोगों के लिए जटिल वायुमंडलीय प्रक्रियाओं की हमारी समझ को बेहतर और सरल बनाना है। एनएमसी शाखा का दृष्टिकोण वायुमंडलीय मॉडलिंग में नई तकनीकों को अपनाना है जो प्राप्त करने योग्य और सार्थक हों। संख्यात्मक मॉडलों में सामान्य परिसंचरण मॉडल (जीसीएम), संख्यात्मक मौसम पूर्वानुमान (एनडब्ल्यूपी) और जलवायु मॉडल, वायुमंडलीय परिवर्तन मॉडल और एरोसोल सिमुलेशन शामिल हैं। एनएमसी शाखा कॉसमो मॉडल की मदद से शहरी क्षेत्र में किए गए अध्ययनों के अलावा लैनल मिशन को वास्तविक समय में छोटी दूरी की मौसम भविष्यवाणी सहायता भी प्रदान करती है।

The scientific activities of the Numerical Atmosphere Modelling (NAM) branch are focused on the investigation and exploration of the complex physical and chemical processes of the Earth's atmosphere with the aid of numerical models. The ultimate goal of these investigations is to improve and simplify our understanding of the complex atmospheric processes for societal applications. The gamut of numerical models used by the NAM branch includes general circulation models (GCMs), numerical weather prediction (NWP) and climate models, atmospheric transport models, and large eddy simulations. NAM branch also extends real-time short-range weather prediction support to the ISRO's launch missions undertaken from Sriharikota with the help of COSMO model.

वैज्ञानिक टीम / Science Team
बाला सुब्रहमण्यम डी / Bala Subrahamanyam D.
सिजीकुमार एस / Sijikumar S.
उमा के एन / Uma K. N.

अनुसन्धान सहयोगी / Research Associate
नित्या के / Nithya K.*

अनुसंधान अध्येता / Research Fellow
बुक्या सामा / Bukya Sama**
आदर्श जैन / Adarsh Jain
अक्षय एस / Akshay S.

परियोजना सहयोगी / Project Associate
नहान एन एच / Nahan N. H.#

Relieved from duties in October 2025
** Relieved from duties in February 2025*
#Joined in July 2025*

Investigation of the Solar Eclipse-induced Modulations in ABL through Large Eddy Simulations (LES) Framework

When the Moon blocks the Sun's light, even for a short time, it causes sudden changes in the Earth's atmosphere. These changes can reveal how sensitive the air near the surface is to variations in sunlight. While previous studies have extensively investigated the eclipse-induced modulations in temperature, pressure, wind patterns, and turbulence; numerical simulations of eclipse-induced atmospheric boundary layer (ABL) modulations remain limited. This study addresses this gap by employing a cutting-edge state-of-the-art meteorological modelling system, Parallelized Large Eddy Simulation Model (PALM), for carrying out the large eddy simulations (LES) experiments to meticulously recreate the lower atmospheric conditions over Thumba during an annular solar eclipse that transpired on 15 January 2010 (Fig. 1). It was one of the longest eclipses of the century, lasting nearly seven minutes at its peak. Two modelling scenarios $LES_{Control}$ and $LES_{Eclipse}$ were compared, where $LES_{Control}$ is a normal clear-sky day without an eclipse and $LES_{Eclipse}$ is the actual eclipse conditions with reduced solar radiation. The model was supported with weather data from ground stations and balloons, ensuring accuracy. The results reveal that during the eclipse, the sharp decline in solar irradiance caused significant cooling of air and soil temperatures, a drop in sensible heat flux, and a decrease in turbulence kinetic energy. These changes suppressed convection, lowered the ABL height, and weakened vertical mixing of heat and momentum. The study further highlights how the suppression of turbulence, evident from reduced eddy diffusivity (K_h and K_m), restricted the vertical growth of the ABL and delayed its post-eclipse recovery (Fig. 2). The $LES_{Eclipse}$ experiment, incorporating observational data, effectively captured these variations and provided a stark contrast to the $LES_{Control}$ experiment under typical clear-sky conditions. Notably, the eclipse-induced turbulence suppression led to a shallower mixed layer and a decrease in the altitude of maximum convection from approximately 1.5 km to 600 m. These findings underscore the complex interplay between solar radiation, turbulence, and ABL development, offering critical insights into boundary-layer processes under extreme radiative forcing conditions.

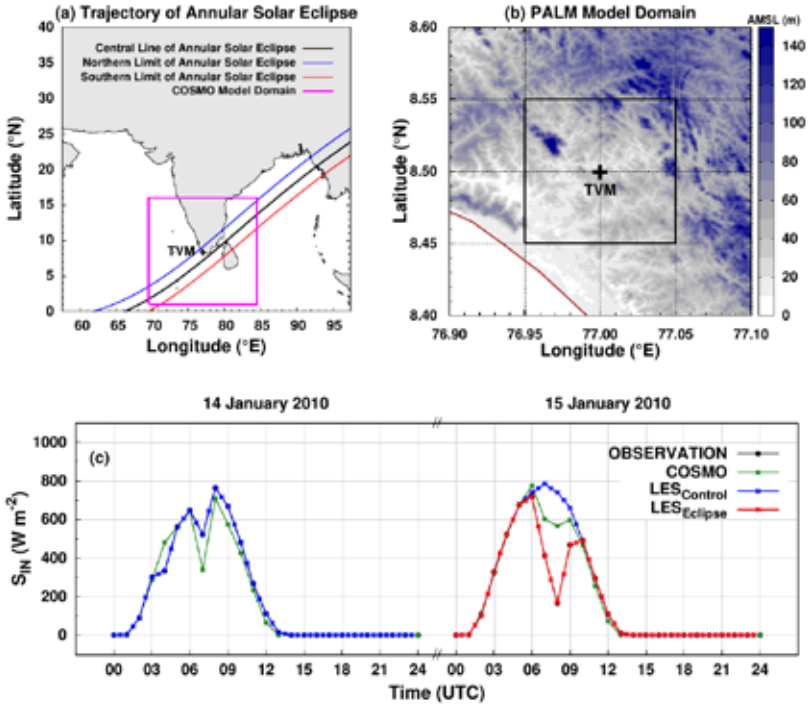

Figure 1: (a) Trajectory of the annular solar eclipse on 15 January 2010 across peninsular India, showing the central path of maximum annularity along with the northern and southern limits, respectively. The square box indicates the COSMO regional atmospheric model domain, centered over Thiruvananthapuram. (b) Computational domain of the PALM LES model, spanning 10.008 km×0.008 km. The background map represents surface elevation in meters above mean sea level (AMSL). (c) Hourly variations of solar irradiance (SIN) on 14 and 15 January 2010 as observed from an in situ automatic weather station over the experimental site. Concurrent variations from the COSMO model and two LES experiments (the $LES_{Control}$ and $LES_{Eclipse}$) are also depicted in the figure [Subrahamanyam, Sci. Rep., 2025].

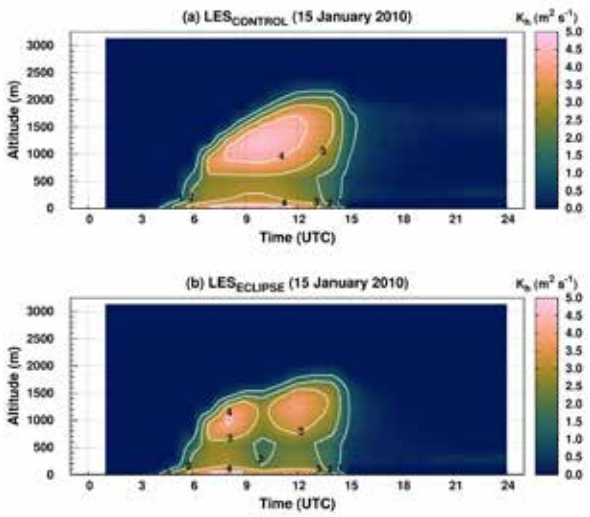

Figure 2. Time-altitude cross section of eddy diffusivity for heat (Kh) obtained from the (a) LESControl and (b) LESEclipse experiments of PALM for 15 January 2010 (Subrahamanyam, Sci. Rep., 2025).

Impact Analysis of the Severe Heat Waves on the ABL over the Central India through COSMO Model Simulations

The role of ABL processes in the prolonged persistence of heat waves over central India is analysed using high-resolution simulations from the COSMO regional weather prediction model. Central India frequently experiences severe heat waves during April – June. May 2023 has been chosen to serve as a representative extreme month for this analysis. Using hourly surface and atmospheric data from 26 inland stations for four contrasting locations (Jodhpur, Jalore, Jagdalpur, and Gopalpur, Fig.3)- the study evaluates the diurnal evolution of surface energy fluxes, turbulent characteristics, and ABL structure. Jodhpur and Jalore were selected as two representative stations, where extreme heat waves prevailed from 9 to 14 May 2023, and both these stations consistently recorded peak air temperatures above 40°C. Additionally, Jagadlpur and Gopalpur were chosen as another two representative stations, where the deciduous forest coverage was very high, and the heat waves were relatively less intense, with peak air temperatures remaining below 40°C. Model evaluation against IMD observations shows that COSMO reliably captures the occurrence, intensity, and spatial variability of heat waves (Fig. 3c and 3d). Results reveal clear differences in surface heating between arid, desert-like stations (Jodhpur and Jalore) and forested, moisture-rich ones (Jagdalpur and Gopalpur). During May, Jodhpur and Jalore exhibit intense solar insolation, reduced latent heat flux due to limited moisture, strong

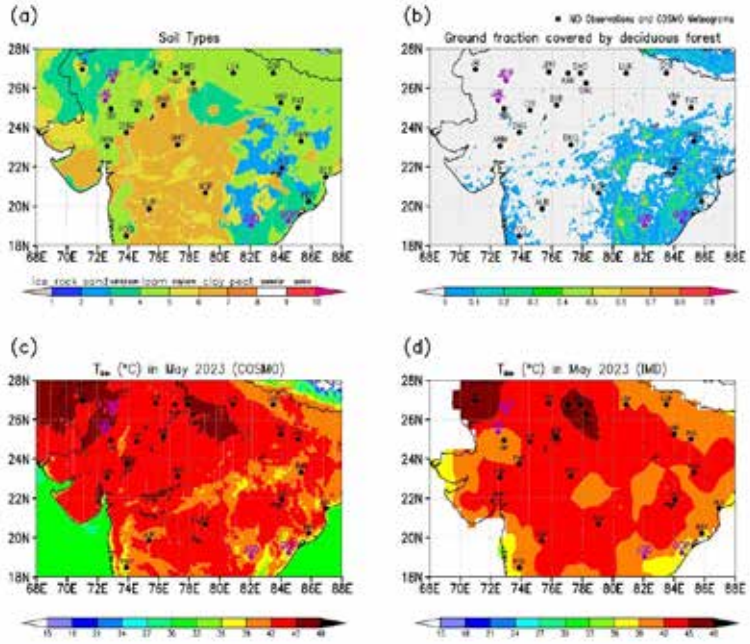

Figure 3: Geographical domain of the COSMO model over the central Indian region. (a) Spatial distribution of soil types over the study region, as prescribed in the COSMO model simulations, with locations of COSMO meteograms, together with IMD observation sites marked. (b) Ground fraction covered by deciduous forest, indicating the spatial variability in vegetation cover, highlighting key surface characteristics relevant to land-atmosphere interactions. (c) Spatial distribution of maximum air temperatures from COSMO model simulations and (d) corresponding IMD regridded observations for May 2023. Panels (c) and (d) highlight regional temperature variability and the overall agreement between simulated and observed fields [Jain and Subrahamanyam, J. Turbul., 2025].

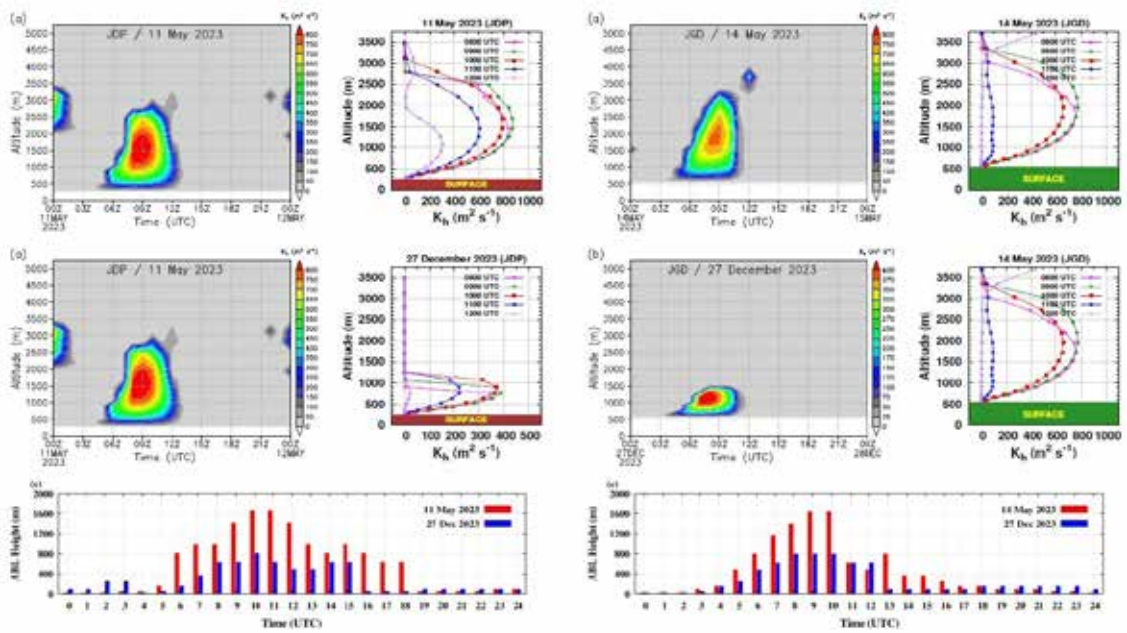

Figure 4: (Left Panel) Time-altitude cross-sections of eddy diffusivity for heat (K_h) over Jodhpur (JDP, witnessing severe heat wave conditions) from COSMO simulations on (a) 11 May 2023, a representative heat wave day, and (b) 27 December 2023, illustrating contrasting winter conditions; (c) shows the corresponding diurnal evolution of ABL heights inferred from the Kh profiles for both representative days. (Right Panel) Same as the Left Panel, but for Jagadlpur (JGD, witnessing mild heat wave conditions) [Jain and Subrahamanyam, J. Turbul., 2025].

sensible heat fluxes (~275 W m^{-2}), and high soil temperatures (>50°C), all contributing to vigorous convective activity. In contrast, dense vegetation at Jagdalpur and Gopalpur supports greater moisture availability and latent heating, moderating near-surface air temperatures and reducing heat wave severity.

A key focus of the study is the turbulent eddy diffusivity for heat (K_h), used to infer the vertical development of the ABL. Under strong heat wave conditions, K_h increases sharply during daytime, indicating intense vertical mixing (Fig. 4). Over Jodhpur and Jalore, the ABL grows rapidly after sunrise and deepens to 1.40 - 1.65 km, sustaining this height for several hours due to strong surface-driven convection. Conversely, at Jagdalpur and Gopalpur - despite reaching comparable midday heights (1.20 - 1.45 km) - the ABL collapses quickly in the late afternoon because weaker turbulence cannot maintain vertical mixing. During December, all four stations exhibit shallow, stable ABLs (<650 m) with markedly reduced K_h, reflecting suppressed convective processes under winter cooling. The contrasting behaviours highlight how land-surface characteristics, vegetation cover, moisture availability, and surface energy partitioning govern ABL evolution and, consequently, the intensity and persistence of heat waves. Overall, the study demonstrates that arid regions with sparse vegetation are more vulnerable to prolonged and severe heat waves due to their tendency to generate stronger sensible heating and deeper, more persistent ABLs. The findings underscore the importance of land–atmosphere interactions in shaping regional heat extremes and emphasize the usefulness of high-resolution modelling in improving heat wave predictability.

CO_2 variability over Thumba: Synergy of observation and model

Carbon dioxide (CO_2) is the most important greenhouse gas and its global mean concentration have enhanced by ~52% (422 ppm in 2024) as compared to the levels in pre-industrial era (~278 ppm in 1750). It has been noted that rapid industrial growth, very high level of traffic and energy consumption over India have led to increase in the concentration of greenhouse gases. In this study, we discuss the CO_2 variability and influencing factors based on the in-situ measurements (5 years; 2017–2021), atmospheric chemistry transport model (MIROC4-ACTM) simulations, and Orbiting Carbon Observatory (OCO-2) observations at a coastal station Thumba. Contrasting airmasses (continental and oceanic) on synoptic scale and land-sea breeze circulations on mesoscale make this site unique to study the CO_2 variations. The monthly mean variations in surface CO_2 using in situ measurements and model simulations along with model tracers of

fossil fuel and natural fluxes show a systematic seasonal variation (Fig. 5). A peak in pre-monsoon (April-May) and a dip in monsoon (September) with embedded increasing trend of 2.19 ppm yr^{-1} (2017-2021) is observed. The CO_2 levels rose from 412±2.9 ppm in April 2017 to 422±1.6 ppm in May 2021. Model simulated monthly variation is in excellent agreement with the observation with $r^2 = 0.89$. The model shows comparable or slightly higher trend of 2.47 ppm yr^{-1} as compared to the observations. Positive trend in fossil fuel tracer is 4.59 ppm yr^{-1} (i.e., 186% of trend in CO2, 2.47 ppm yr^{-1}) which is partially compensated with negative trend in natural tracers -2.12 ppm yr^{-1} (-86%). Trend in natural tracer is contributed by land-biospheric (-1.46 ppm y^{-1}; 69% of -2.12 ppm y^{-1}) and oceanic (-0.66 ppm y-1; 31% of -2.12 ppm y^{-1}) sinks. The diurnal mean pattern of ΔCO_2 shows that the mixing ratio of CO_2 is maximum at around 07:00 IST and the minimum is between 14:00 and 18:00 IST, followed by gradual increase after 19:00 IST (Fig. 6a and b). The diurnal amplitude is lower (~31 ppm) during monsoon and higher (~50 ppm) during winter. Interestingly, the rate of increase from the mid-night to early morning (00:00 – 07:00 IST) is 2.7 ppm hr^{-1} during pre-monsoon, which is much higher than that during other seasons (0.9 - 1.5 ppm hr^{-1}). Model reproduced broad pattern with higher values during night or early morning hours and minimum in the afternoon hours. The model simulated diurnal amplitude is much smaller (1.2 - 3.7 ppm) in contrast to the observed amplitude (~31 - 50 ppm). The larger diurnal amplitude observed at the site is due to mesoscale sea-land breeze circulation, which cannot be simulated in the model due to its coarse resolution of 2.8° × 2.8°.

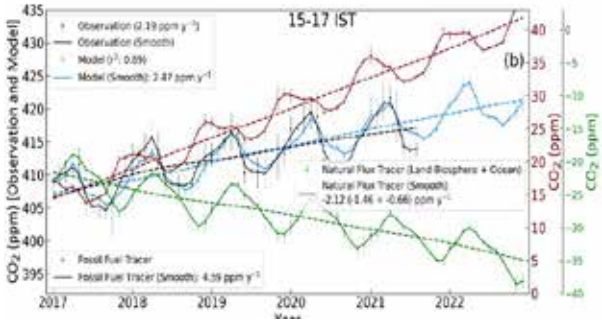

Figure 5: Monthly mean variations of CO2 based on observations (black) and simulations (blue). While scatter with error bar shows monthly mean with standard deviation, continuous curve shows smooth variation obtained by applying NOAA curve fitting method. Dashed curve shows the trend line. Variations in fossil fuel (brown) and natural tracers (green) are shown on right-y axes [Uma et al., Sci. Total Environ, 2024].

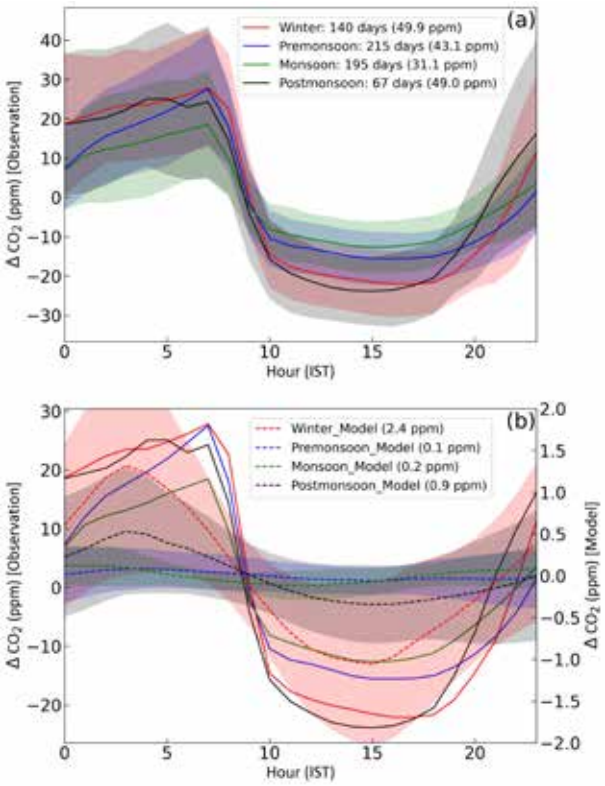

Figure 6: Mean diurnal patterns of CO2 over Thumba during different seasons during 2017 - 2021 based on observations (a) and model (b). Shaded region represents standard deviation. Here, ΔCO2 is obtained by removing daily mean from hourly values. Number of days of observation used for averaging is mentioned in the legend in (a). Solid lines in (b) are same as those in (a). Diurnal amplitude is inscribed in brackets in the respective legend [Uma et al., Sci. Total Environ, 2024].

Characteristics of Monsoon Convection and its Interaction with the Large-Scale Environment: Insights from Radar Observations and Reanalysis

Understanding the morphological, dynamical, and microphysical characteristics of monsoon convection over the gateway of the Indian summer monsoon (ISM), i.e., Kerala, is essential, as it dictates the propagation of the monsoon system over the entire country. The present study deals with the morphological characteristics of convective storms (CS), their propagation, and the diurnal cycle during the ISM using C-band weather radar from Thumba over a seven-year (2017-2023) period. The percentage occurrence of intense storms (>35 dBZ, 30 km^3) is found to be spread over all the sides, and 60-70% is observed over both the southwest and northeast sides of the radar (Fig. 7a). The maximum reflectivity is over the northeast side compared to the southwest side of the radar which shows that intense CS is situated over the

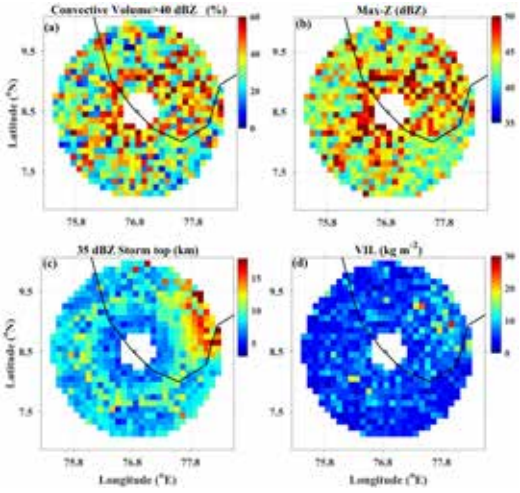

Figure 7: Spatial distribution of (a) % occurrence of convective volume of reflectivity > 40 dBZ, (b) Max-Z, (c) storm top, and (d) Vertical Integral of Liquid of the convective storms (CS) from 2017-2023 [Uma and Sama, Clim. Dyn., 2025].

leeward side of the Western Ghats compared to the coast and windward side (Fig. 7b). The spatial map of the 35 dBZ storm top (Fig. 7c) shows high values over the land (>14 km) (northeast of the radar) compared to the oceans and the coast. The Vertical Integral of Liquid (VIL) in Fig. 7d is less than 10 kg/m^2 over most of the radar domain, except for a few inland regions where it is near 20 kg/m^2. The percentage occurrence of congestus is 60%, deep is 39%, and overshooting CS is 1%. The percentage occurrence of D, C, and B/C CS is 89.5%, 10%, and 0.5%, respectively. The diurnal variation has a peak between 14:00 and 15:00 LT over the land and between 04:00-05:00 LT, 14:00-15:00 LT, and a small peak at 22:00 LT over the oceans (Fig.8). The dominant peak in the afternoon over the land is caused by the deep CS and the early morning peak over the oceans is predominantly caused by the congestus, followed by deep. The large-scale interaction in terms of stability, moisture, and dynamics are related to the properties of CS. The

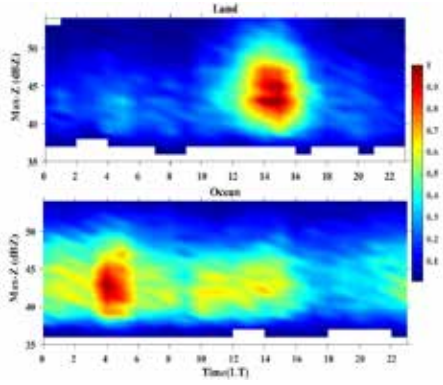

Figure 8: PDF of (a) Area of the CS, and (b) precipitation rate for different ranges of CAPE [Uma and Sama, Clim. Dyn., 2025].

mid-tropospheric moist environment supported by the positive moisture convergence is the main driving factor for intense CS compared to the stability over this region.

Impact of the Tropical Cyclones on the Upper Atmosphere: Bridging the Lower Atmospheric Simulations with the Ionospheric Measurements

Interest in the impact of tropical cyclones (TCs) on the upper atmosphere - particularly the ionosphere - has grown because these storms generate strong convection and atmospheric gravity waves that can propagate upward and disturb ionospheric plasma. Such disturbances can alter Total Electron Content (TEC) and produce Traveling Ionospheric Disturbances (TIDs), which directly affect satellite communication, GPS accuracy, and space-based navigation systems. As tropical cyclones over regions like the Arabian Sea are becoming more frequent and more intense, understanding their ionospheric signatures is also becoming increasingly important for forecasting their broader geophysical impacts. These effects occur even under geomagnetically quiet conditions, revealing a strong lower - upper atmospheric coupling that is not yet fully understood. This study investigates whether the extremely severe cyclonic storm Tauktae, which developed over the Arabian Sea in May 2021, generated measurable disturbances in the ionosphere, particularly TIDs. Using a combination of COSMO regional atmospheric model simulations and GPS-TEC observations from three InSWIM network stations (Kavaratti, Pune, and GMRT), the coupling mechanisms between the lower atmosphere and the ionospheric region under geomagnetically quiet conditions is analysed. COSMO simulations capture Tauktae's rapid intensification from a depression to an extremely severe cyclonic storm and reveal significant enhancements in tropospheric zonal winds, especially when the cyclone's eye was within ~400 km of a station (Fig. 9). The selected GPS-TEC data for cyclone-affected days (May 14-17) show substantial increases in deviations of TEC (dVTEC) compared to a non-cyclone day (May 05), with values consistently exceeding the quiet-time threshold of ±0.25 TECU.

As an extension of this investigation, focusing on two major 2017 cyclones - Mora (the Bay of Bengal, pre-monsoon) and Ockhi (the Arabian Sea, post-monsoon) – it is examined whether these TCs introduce detectable anomalies into the natural VTEC variations typically governed by

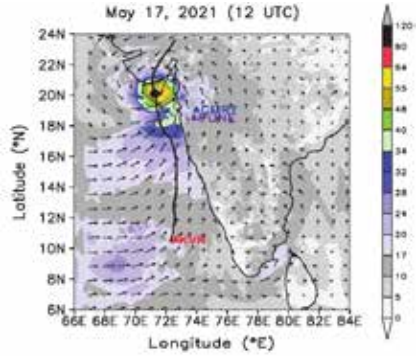

Figure 9. Spatial maps of the maximum sustained surface wind speed (in Knots) at 12 UTC, derived from COSMO model simulations for May 17, 2021 when the Tauktae was designated as an extremely severe cyclonic storm. The track of Cyclone Tauktae is marked with solid black lines. Additionally, three InSWIM network stations – KVR (Kavaratti), Pune, and GMRT – are depicted with filled triangles for geographical reference [Chowdhury et al., Adv. Space Res., 2025a].

solar radiation, geomagnetic activity, and seasonal patterns. To accurately isolate cyclone-induced effects, the study employs rigorous data screening to remove days affected by geomagnetic storms or other nearby cyclones. Control periods from the corresponding months in 2018 and 2019 (quiet years without relevant TCs) are used for comparison. The analysis shows that both Mora and Ockhi caused significant VTEC depletion, ranging from 7% to 19%, and that these reductions depended strongly on each cyclone's intensity and proximity to TVM. In this study, the average values of VTEC (AVTEC) for the period of 2017 to 2019 are analyzed and the daily peak values of AVTEC ($AVTEC_{max}$) are subjected to linear-trend analysis, which highlights that 2017 exhibits a much steeper decline during the cyclone periods than 2018 and 2019, indicating that TCs superimpose additional "contamination" on natural solar-cycle-driven VTEC trends. Statistical tests further confirm that the 2017 VTEC distributions significantly differ from those of the subsequent quiet years. Overall, the work highlights the dual role of cyclone intensity and distance from the observation site in shaping ionospheric perturbations, and emphasizes the importance of accounting for TCs in long-term ionospheric studies to avoid misleading interpretations of solar or geomagnetic influences.

COSMO Model Simulations in support of ISRO's Launch Missions and Daily Weather Forecast Summary dissemination

SPL contributes to launch operations at SDSC-SHAR through its role as a key member of ISRO's Inter-Centre Weather Forecast Expert Team. Using the COSMO regional NWP model, SPL contributes to the accurate short-range weather forecasts tailored to the requirements of PSLV, GSLV, LVM, and SSLV missions. During 2024-2025, the COSMO forecast has been provided for the following missions:

1. SSLV-D3/EOS-08 Mission : August 16, 2024
2. PSLV-C59/Proba-3 Mission : December 5, 2024
3. PSLV-C60/SPADEX Mission : December 30, 2024
4. GSLV-F15/NVS-02 Mission : January 29, 2025
5. PSLV-C61/EOS-09 Mission : May 18, 2025
6. GSLV-F16/NISAR Mission : July 30, 2025
7. LVM3 M5/CMS-03 Mission : November 2, 2025

In addition, daily weather summaries are shared through Ashoka intranet. Fig. 10 shows a sample weather forecast report. As on December 31, 2025, 258 forecast bulletins have been posted on intranet.

Today's (21-11-2025) Weather Outlook for THUMBA (8.50°N, 77.0°E)

PARAMETERS	FORECASTED VALUES	
	Minimum	Maximum
Temperature (°C)	24.0	29.6
Relative Humidity (%)	70.4	95.9
Wind Speed (m/s)	0.3	16.1
24 h accum. Rainfall (mm)	10.4	
Probability of Thunderstorms (50 km x 50 km)*		
0530 - 0830 IST	NIL	
0830 - 1130 IST	MODERATE	
1130 - 1430 IST	HIGH	
1430 - 1730 IST	MODERATE	
1730 - 2030 IST	LOW	
2030 - 2330 IST	LOW	
2330 - 0230 IST (next day)	LOW	
0230 - 0530 IST (next day)	NIL	

*NIL (0%), LOW (<20%), MODERATE (>20% and <60%), HIGH (>60% and <85%), VERY HIGH (>85%)

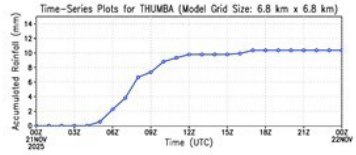

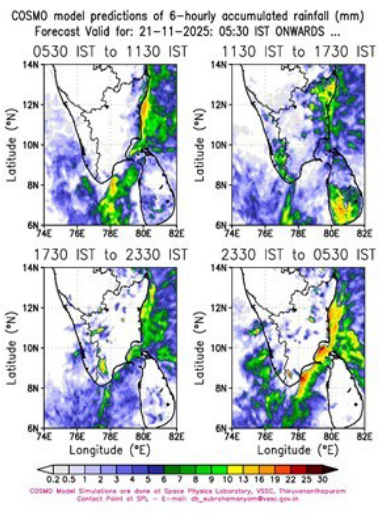

Figure 10: A sample Forecast Outlook of COSMO model simulations, being posted on a daily basis on Intranet portal of VSSC.

Ongoing Activities and Future Projections

- Investigation of the dynamical and microphysical characteristics of hail-producing thunderstorms using WRF model simulations
- Assessment of severe heat waves over the coastal regions and their simulations through the COSMO model and their impacts on boundary-layer dynamics
- Analysis of eddy diffusivity profiles towards formulation of a robust algorithm for identification of the top of atmospheric boundary layer during convective conditions
- Large Eddy Simulations of the diurnally evolving ABL for a detailed assessment of subgrid-scale processes
- Estimation of carbon fluxes over India using satellite observations and atmospheric inverse modelling
- Preparation and analysis of radar mosaics to track convection and precipitation over the Indian region

Publications in Peer-Reviewed Journals

1. Adarsh Jain and D. Bala Subrahamanyam, Why Some Heat Waves Last Longer: Insights on the Atmospheric Boundary Layer Characteristics over the Central India from High-Resolution Modelling, Journal of Turbulence, https://doi.org/10.1080/14685248.2025.2601202, 2025.
2. Bala Subrahamanyam, D., "Unveiling diurnal metamorphosis in the atmospheric boundary layer during an annular solar eclipse through large eddy simulations", Scientific Report, https://doi.org/10.1038/s41598-025-15252-w, 2025.
3. Swati Chowdhury, Bala Subrahamanyam, D., Choudhary, R. K., "First observational investigation on the temporal trends of Vertical Total Electron Content (VTEC) over an equatorial station: Discerning the impacts of Mora and Ockhi – Two tropical cyclones in 2017", Advances in Space Research, https://doi.org/ 10.1016/j.asr.2024.11.078, 2025.
4. Swati Chowdhury, Choudhary, R. K., Bala Subrahamanyam, D., "Did the "Tauktae" cyclone impact the upper atmosphere through traveling ionospheric disturbances? A case study over the Arabian Sea using measurements from InSWIM network stations", Advances in Space Research, https:/doi.org/10.1016/j.asr.2024.11.012, 2025.
5. Uma, K. N., Sama, B., "Characteristics of monsoon convection and its interaction with the large-scale environment over the gateway of the Indian summer monsoon: insights from radar observations and reanalysis", Climate Dynamics, https://doi.org/10.1007/s00382-025-07879-2, 2025.
6. Uma, K. N., Girach, I. A., Chandra N., Patra, P. K., Kiran Kumar, N. V. P., Nair, P. R., "CO_2 variability over a tropical coastal station in India: Synergy of observation and model", Science of the Total Environment, https://doi.org/10.1016/j.scitotenv.2024.177371, 2024.

Presentation in Symposium / Conferences / Workshop

1. Adarsh Jain and D. Bala Subrahamanyam, Atmospheric Boundary Layer Processes during Extreme Heat Waves in Central India: Insights from High-Resolution Modelling, International Symposium on Tropical Meteorology (INTROMET 2025), IITM, Pune, November, 18-20, 2025.
2. Akshay and S. Sijikumar, Sensitivity of vegetation-specific parameters in VPRM for estimating net-ecosystem exchange over India, International Symposium on Tropical Meteorology (INTROMET 2025), IITM, Pune, November, 18-20, 2025.
3. Nithya K., Sijikumar, S., Aneesh, S., "Forced Response in the Mean State and Interannual Variability of the Indian Summer Monsoon in Future Projections", The European Geosciences Union (EGU) General Assembly - 2025, Vienna, Austria, 27 April – 2 May, 2025.
4. Sama, B and Uma, K. N., "Dynamics of monsoon mesoscale convective systems over Thumba: Insights from ISRO C-band Polarimetric Doppler Weather Radar", International Workshsop on Technical and Scientific Aspects of iMST Radar and Lidar (MST16/iMST 3), University of Rostock, Rostock, Germany, September, 06-13, 2024.
5. Uma K. N., Sama, B., "Evaluation of mesoscale convective systems embedded within cyclones using weather radars over south east coast of India", 7th Conference of India Radar Meteorology (iRAD-2025), IIG, Mumbai, January, 06-08, 2025.

वायुमंडलीय गतिकी शाखा
Atmospheric Dynamics Branch

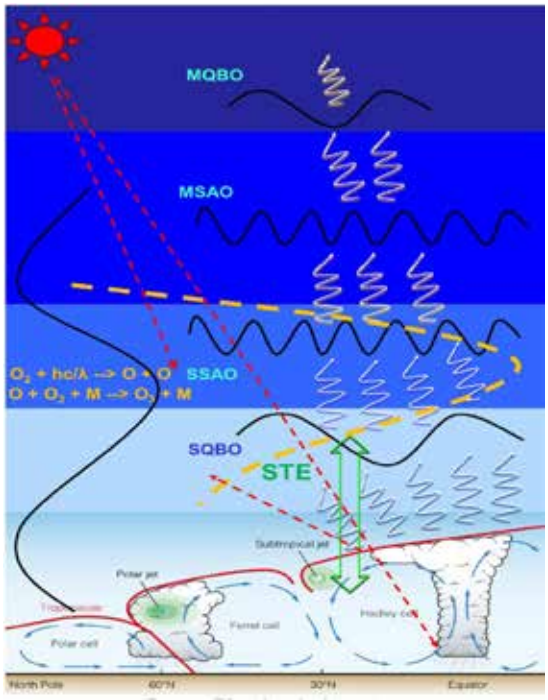

क्षोभमंड़ल से निम्न तापमंड़ल तक ऊर्ध्वाधर युग्मन सहित पृथ्वी के वायुमंड़ल की गति को बदलने के लिए उत्तरदायी वायुमंड़लीय प्रक्रमणों पर वायुमंड़लीय गतिकी शाखा (एडीबी) अग्रणी अनुसंधान का कार्य कर रही है। इस स्थूल उद्देश्य के साथ अनुसंधान गतिविधियों का लक्ष्य भू तथा अंतरिक्ष आधारित प्रेक्षणों का उपयोग करते हुए गूरुत्वीय तरंगों से सौर चक्र तक वायुमंड़लीय तरंगों तथा परिवर्तनीयों के स्पेक्ट्रम का मात्रीकरण करना है। वायुमंड़लीय तरंगों का अभिलक्षणन, उनके स्रोत व क्रियाविधि, संचरण अभिलक्षण, वायुमंड़ल युग्मन की भूमिका, अल्प दीर्घकालीन परिवर्तनशीलता तथा वैश्विक नमून में प्रतिनिधित्व के आधार पर किया जाता है। तरंगों और दोलनों पर अध्ययन के अलावा, वायुमंड़लीय गतिकी शाखा हवा, तापमान, ओज़ोन ओर जलबाष्प के समवर्ती मापनों का उपयोग करते हुए उष्णकटिबंधीय क्षोभमण्डलीय गतिकी और संबंधित समताप मंडल-क्षोभमंडल के बीच होने वाले विनिमय प्रक्रीयाओं पर शोध करती है। एडीबी शाखा में बादलों और जलवायु गतिशीलता के क्षेत्र में भी सक्रिय रुप से अध्ययन किया जाता है। हेडली और ब्रेवर-डॉब्सन परिचलन जैसे वृहत पैमाने पर वायुमंड़लीय संचार की विशेषता और उनके दीर्घकालिक विकास और जलवायु पर इनके प्रभावों पर जांच जारी है। हाल ही में, शुक्र ग्रह पर विशेष जोर देने के साथ ग्रहीय वायुमंड़लीय गतिशीलता को आगे बढ़ाने के लिए शाखा की गतिविधियों का विस्तार किया गया है।

Atmospheric Dynamics Branch is carrying out the front-line research on atmospheric processes responsible for vertical coupling of the Earth's atmosphere, right from the ground to mesosphere-lower thermosphere. With this broad objective, the research activities are aimed at quantifying the atmospheric motion spectra from gravity waves to solar cycle using ground and space-based observations and to quantify the various aspects of atmospheric waves such as their source mechanisms, propagation characteristics, role in atmosphere coupling, short and long-term variability and their representation or parameterization in global models. Apart from the studies on waves and oscillations, the branch focuses on the tropical tropopause dynamics and associated stratosphere-troposphere exchange processes making use of simultaneous measurements of wind, temperature, ozone and water vapour. The studies under the realms of cloud and climate dynamics are also actively pursued in the Branch. Large-scale circulations viz., Hadley and Brewer-Dobson Circulations are characterised and their long-term evolution and its impacts on climate are investigated. Recently, the Branch's horizon is extended to pursue Planetary Atmospheric Dynamics with special emphasis on the Venus and Mars.

वैज्ञानिक टीम / Science Team
किशोर कुमार के / Kishore Kumar K.
सिद्धार्थ शंकर दास / Siddarth Shankar Das
सुनिलकुमार एस वी / Sunilkumar S.V.
जयदेव प्रदीप / Jayadev Pradeep
कौशिक एन / Koushik N.
वरुण निकम् / Varun Nikam
सच्चिन प्रभाकर / Sachin Prabhakar

तकनीकी टीम/Technical Team
मणिकंठन नायर एन / Manikantan Nair N.
मोहम्मद नज़ीर एम / Mohammad Nazeer M.
पोन्निसै पेरूमाल जे / Ponnisai Perumal J.

अनुसंधान सहयोगी / Research Associate
ओइंद्रिला नाथ / Oindrila Nath

अनुसंधान अध्येता / Research Fellows
नबारुण पोड्डार / Nabarun Poddar
हादिया नावल सी के / Hadiya Nawal C. K.
वीनस वी / Veenus V.*
अंजना यू / Anjana U.#

**Relieved in December 2024*
#Relieved in February 2025

Middle Atmospheric Dynamics

The teleconnection between Brewer–Dobson Circulation (BDC) and Quasi–Biennial Oscillation (QBO): Implications on ozone and water vapor distribution

The response of the stratospheric BDC to QBO is evaluated using a composite of QBO cycles from 1979 to 2021. The BDC plays a crucial role in regulating the transport of ozone, water vapor as well as the trace gases between the troposphere and stratosphere. BDC is influenced by different atmospheric oscillations and extreme events, in troposphere as well as stratosphere. In an attempt to delineate the response of the meridional circulation, the BDC metrics derived from 43 years of climatological reanalysis dataset from ERA5 are used. The QBO phases are evaluated based on the zonal-mean zonal wind direction at 50 hPa pressure level.

The composite differences between westward and eastward QBO phases from 60˚S to 60˚N is estimated (Fig.1). The wave driving from E-P flux divergence (D) is plotted to see the strength of stratospheric meridional circulation (Fig. 1a). The

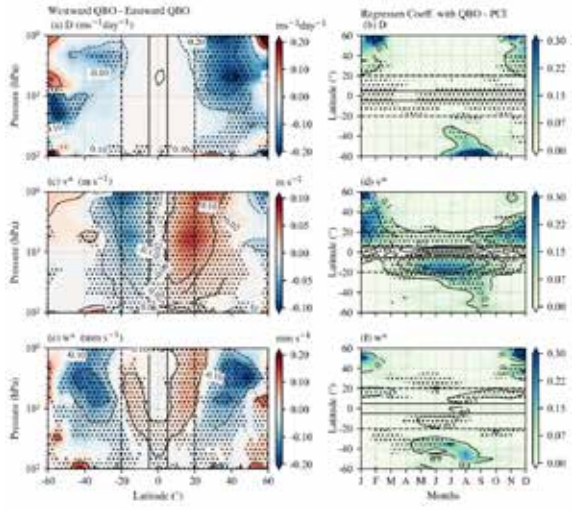

Figure 1: The composite differences between westward QBO and Eastward QBO for a deseasonalized wave driving, D, (a), residual meridional velocity, v (c) and residual vertical velocity, w* (e) along with the normalized regression coefficient of the respective variables (b, d, and e) with the first principal component of QBO. The dashed straight line drawn at – 20° S and 20° N denotes the region of QBO secondary meridional circulation. The filled contours are latitudinally scaled for better visibility of the extra-tropical anomalies. The dotted region indicates statistically significant regions with >90% confidence level [Veenus and Das, Clim. Dyn., 2025].*

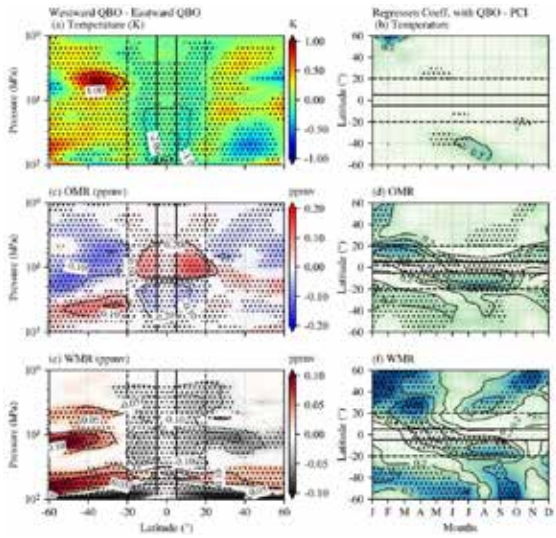

Figure 2: Same as Fig. 1, but for Temperature, ozone mixing ratio (OMR), and water vapor mixing ratio (WMR) from Aura Microwave Limb Sounder Observations [Veenus and Das, Clim. Dyn., 2025].

wave driving during the westward phase of QBO is higher compared to eastward QBO phase. This is reflected in an increased residual meridional transport. The residual meridional velocity (v*) shows air diverging towards high latitudes when the QBO phase is westward (Fig. 1c). This is reflected in more northward transport (positive values) in the NH and more southward transport (negative values) in the Southern Hemisphere (SH). In response to the meridional transport over the tropical region, the air is lifted up, while downwelling is observed at high latitudes (Fig. 1e). Fig. 2 shows the composited anomalies depicted between westward QBO and eastward QBO for temperature, ozone and water vapour. The temperature differences show the effect of enhanced downwelling in the extra-tropical regions in westward QBO (Fig. 2a). The cooling observed in the NH subtropics is in response to the thermal wind effect. The ozone mixing ratio shows well-marked QBO signatures in the lower and middle stratospheres. During the westward (eastward) QBO phase at 50 hPa, negative anomalies of 0.2 ppmv (positive, 0.2 ppmv) are observed over the tropical lower stratosphere (Fig. 2c). The water vapor is influenced by QBO at the stratospheric entry, where the cold point tropopause temperature is much lower in the westward phase of QBO, leading to a dry anomaly of 0.1 ppmv (Fig. 2e). The concentration changes lead the instantaneous radiative forcing to vary between 0.11 to 0.14 Wm^{-2} during QBO phases. The feedback of these radiatively active species is crucial for the understanding of QBO.

Assessing the impact of the Hunga Tonga-Hunga Ha'apai volcanic eruption on the structure of the Brewer–Dobson Circulation (BDC) : Possible Implications

The Hunga Tonga–Hunga Ha'apai (HTHH) volcanic eruption on 15 January 2022 drew significant attention to the Southern Hemisphere stratosphere. The eruption injected a plume reaching mesospheric altitudes, with overshooting tops of 50–55 km, and generated Tsunamis as well as seismic and internal gravity waves. It substantially altered stratospheric water vapor and ozone, key radiatively active constituents of the middle atmosphere. Complex feedbacks between water vapor and ozone contribute major uncertainties in stratospheric modeling. An estimated 146 Tg of water vapor, equivalent to about 10% of the stratospheric water vapor budget, was injected following the eruption, leading to a 13.7% increase in mean stratospheric water vapor within three months. In this context, the present study examines the impact of the abrupt enhancement in stratospheric water vapor on the strength of the Brewer–Dobson circulation.

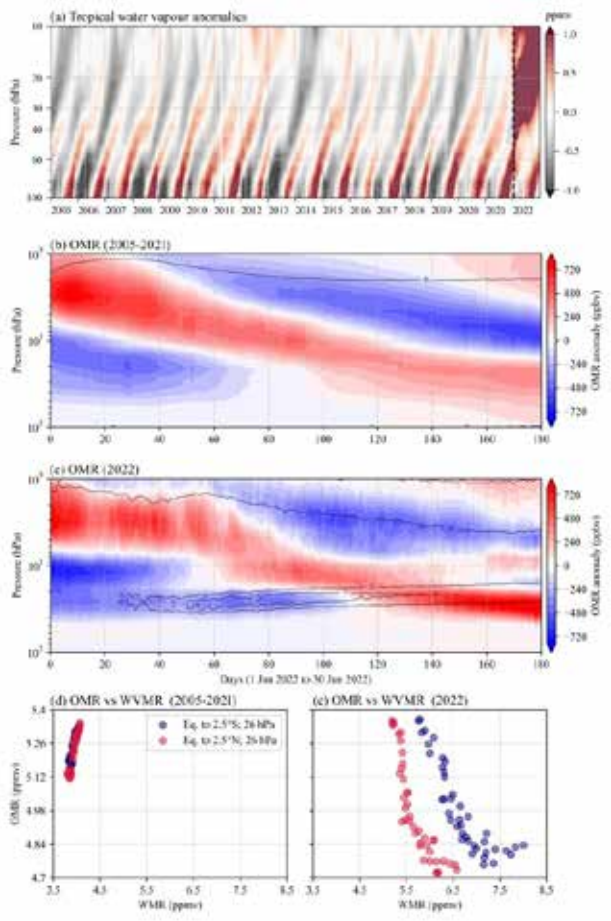

Figure 3: (a)Tropical water vapour anomalies showing the atmospheric tape recorder signal. The black vertical dashed line denotes the peak date of the HTHH eruption. The time-mean removed ozone mixing ratios: (b) climatological average and (c) for the year 2022. Black contours denote water vapour mixing ratios in ppmv. Values are zonally and latitudinally averaged for 2.5°S to 2.5°N. Scatter plot between OMR and WMR shown between days 80 to 120 for Equator to 2.5°S and Equator to 2.5°N at 26 hPa (d) climatology, and (e) for the year 2022 [Veenus and Das, Adv. Space Res., 2024].

The analysis reveals a clear disruption of the tropical stratospheric tape-recorder signal following the HTHH eruption (Fig. 3a), accompanied by pronounced changes in stratospheric water vapor and ozone. The ozone distribution in the stratosphere deviated markedly from its climatological pattern during the post-eruption period (Fig. 3b). Under climatological conditions, water vapor mixing ratios in the lower stratosphere rarely exceed 4–5 ppmv; however, values increased to nearly 8 ppmv within the first 100 days after the eruption and remained elevated at around 6 ppmv in subsequent months. This excess water vapor enhanced catalytic ozone destruction, leading to ozone depletion of about 300–400 ppbv (Fig. 3c). The depletion was strongest over the tropical region, consistent with the location of the erupted plume. While climatological conditions show a positive correlation between water vapor and ozone (Fig. 3d), an inverse relationship dominated in 2022, with ozone decreasing as water vapor increased (Fig. 3e). Such unusually low ozone mixing ratios, reaching 4.7–5 ppmv, have no precedent in the climatological record prior to this eruption.

Wave driving from May to September exhibited a marked reduction relative to climatology (Fig. 4). In the climatological mean, the Southern Hemisphere winter stratosphere is characterized by enhanced wave driving in the upper stratosphere (Fig. 4a), whereas in 2022 the wave activity was nearly absent (Fig. 4b). In the wave-breaking region near 10 hPa, wave forcing was substantially weakened, and the subtropical stratosphere was largely devoid of wave activity. Altered stratospheric wind patterns impeded wave propagation, as indicated by EP flux vectors, leading to reduced wave penetration into the upper stratosphere and a weakened circulation. The suppressed Brewer–Dobson circulation is reflected in reduced tropical upwelling and corresponding changes in diabatic heating rates. This anomalous reduction in tropical upwelling during 2022 became more pronounced after the spread of enhanced water vapor into the Southern Hemisphere.

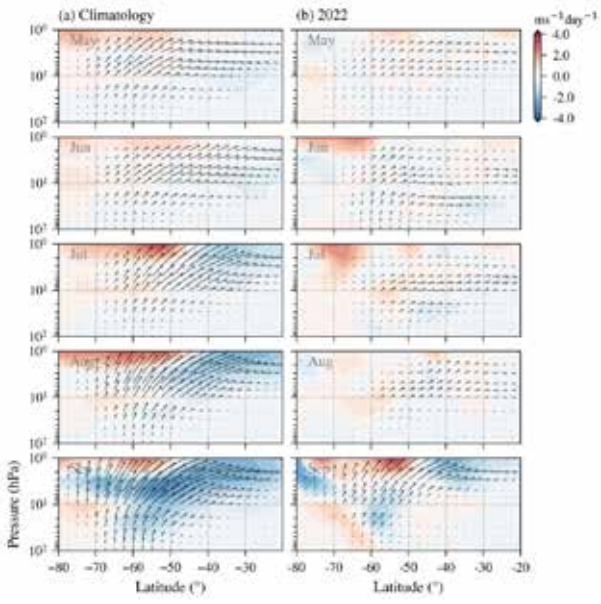

Figure 4. Monthly mean wave driving evaluated from EP flux divergence for (a) Climatology, and (b) for the year 2022. The vectors denote the components of the EP flux [Veenus and Das, Adv. Space Res. 2024].

Observational evidence of stratospheric cooling and surface warming due to an increase of stratospheric water vapor by Hunga-Tonga Hunga-Ha'apai volcanic eruption

Earlier studies have estimated the mean water vapor, which has profound impact on stratospheric thermal structure, entering the stratosphere having mixing ratio 3.5 ppmv with an annual cycle of 1.5 ppmv. Compared to these values water vapor injected by the HTHH volcanic eruption had resulted in a 10% increase in stratospheric water vapor budget and values as high as 12 ppmv were observed in the plume after dispersion. By June 2022, the spread of the water vapor ceased due to a decrease in the circulation's strength. The strength of BDC in NH branch weakened, while the SH it gained more strength in June. This led to the transport of the excess water vapor to the SH.

The enhanced water vapour that reached 20°N latitude did not advance further north. But the southern branch now moved forward to 30°S and beyond. The enhancement in water vapour in the stratosphere reached uniformly around 7–8 ppmv in the SH by August 2022. The water vapor was transported into the polar region by the end of the year 2022.The injected water vapor reached the Indian region by mid-March 2022. The values showed an increase in mixing ratios by 1.5 ppmv in the following months. The enhanced water vapour reached 10 hPa by July 2022 and stayed there during the second half of the year. A positive anomaly of ~ 1 ppmv was observed in the middle stratosphere, whereas in normal years the anomalies rarely cross 0.5 ppmv magnitude.

The temperature anomaly over the Indian region obtained from COSMIC-1 and 2 averaged between 25 and 30 km (Fig. 5). A negative anomaly was seen in the temperature that began in March 2022 and continued as long as in May. The most significant cooling was observed in the second half of March, which lasted up to the end of April and showed more than 4 K decrease in the stratospheric temperature over the Indian region. The decrease is more than 2 K from the standard deviation in March 2022. During the same period, stratospheric cooling was observed in ERA5 also (Fig. 5b) attributed the water vapor increase in the stratosphere. The surface temperature over the Indian region (5°N to 40°N; 60°E to 100°E) was examined (Fig. 5c) and the anomaly calculated by removing the mean of 1951 to 2022 (monthly mean removed) from each year showed an increase of ~3 K in the average surface temperature over the Indian region in the 2022 summer. The maximum surface temperature observed reached as high as 4 K.

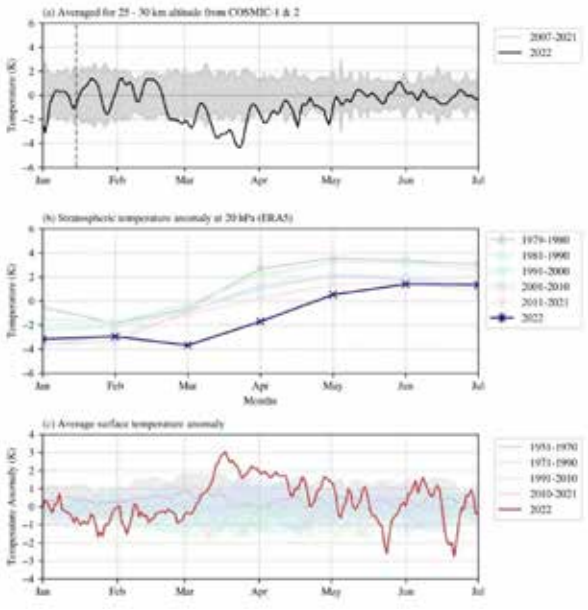

Figure 5: The stratospheric and tropospheric temperature anomaly from the COSMIC-1 &2 averaged for (a) 25 to 30 km over the Indian region. The shaded region represents the standard deviation of temperature anomaly from 2007 to 2021. (b) The stratospheric temperature anomaly from ERA5 from 1979 to 2022. (c) Daily gridded temperature anomaly from India Meteorological Department (IMD) from 1951 to 2022. Anomalies observed in the average of maximum and minimum temperatures in a day are plotted [Veenus and Das, Nat. Hazards, 2025].

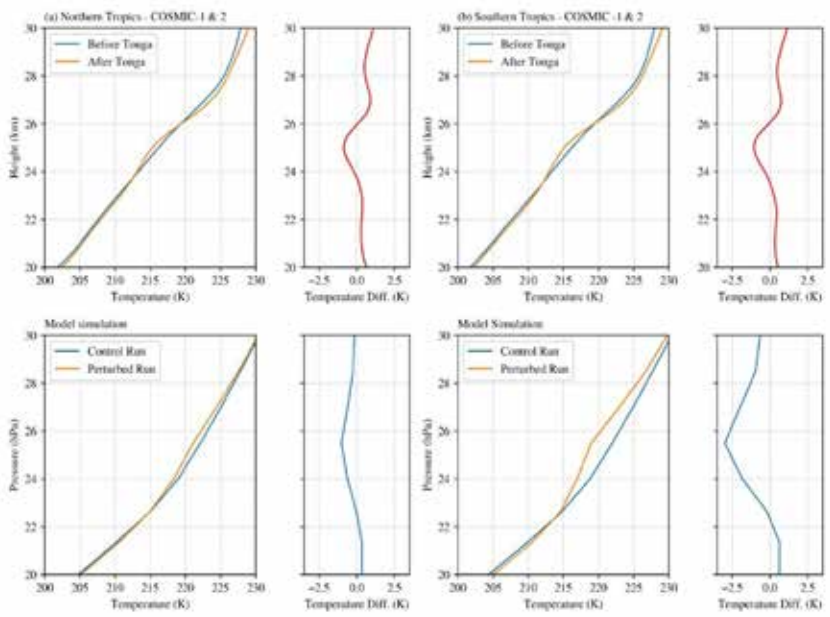

Figure 6: The tropical average temperature profiles before and after Tonga from COSMIC-1 and 2 along with the model simulated profiles; the controlled run and the Tonga-injected stratospheric water vapor perturbed run for (a) Northern Tropics and for (b) the Southern tropics [Veenus and Das, Nat. Hazards, 2025].

In addition, we did the simulations with the Konrad model during the observational period. The zonal mean profiles of WMR obtained from MLS and temperature from COSMIC-2 measurements were used to initialize the model. The model simulated the temperature profiles for both hemispheres (Fig. 6). The SH tropics showed a temperature anomaly of 3 K on the perturbed run compared with the control run. The NH tropics, where the water vapor was transported by BDC, was exhibiting a smaller cooling, with a magnitude of 1 K. The model simulation confirmed that the observed cooling is due to the water vapor in the stratosphere. The observed temperature deviations were confined to the 24–26 km levels, whereas the model showed a spread in heights, with 24–28 km in both hemispheres. As there were no other significant events in the time period, this cooling of the stratosphere was attributed to the substantial amount of water vapor covering the region.

Climate Dynamics

Impact of Hadley Circulation Expansion on the Distribution of low-level Clouds over its Descending Limbs

In the present study, the consequences of Hadley Circulation (HC) expansion on the distribution of subtropical marine stratocumulus clouds (SC), which are not reported hitherto, are investigated. Due to the large-scale descent of HC and other favourable conditions over the sub-tropics, large decks of SC are found to be squeezed within the boundary layer especially over the coastal regions of the subtropical north-east Pacific (NEP), south-east Pacific (SEP) and south Atlantic (SA). Cloud fraction dataset along with zonal and meridional winds during the years 1980-2022 from the state-of-the art ERA5 reanalysis are employed for the study. The zonally resolved HC boundaries are retrieved over each 10-degree longitude sector, using the zonally resolved meridional mass stream function computed from Helmholtz decomposed horizontal winds.

The regional maps of cloud fraction (CF) over the study regions along with the winds at 925 hPa level during their respective peak seasons are constructed (Fig.7). To identify the suitable metric for investigating the low-level clouds response to the HC expansion, the latitudinal distribution of CF over the study regions is constructed. Over all the three oceanic basins, it is noted that there exists a distinct maximum in the CF at 900 hPa as well as 925 hPa pressure level over the low latitude regions. Similarly, distinct poleward minima are also noted over all the three study regions. Initially, both latitude of maximum CF and the poleward latitude of minimum CF are considered for the analysis. It is noted that the time series of latitude of maximum low-level CF over two of the three study regions show relatively little variations. On the other hand, the time series of poleward latitude of minimum CF shows marked variability with time. After initial assessment, the poleward latitude of

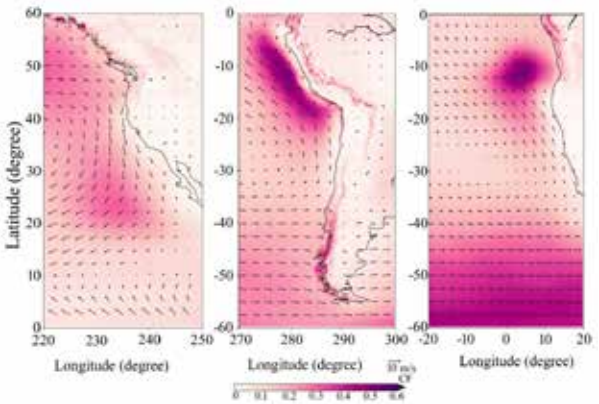

Figure 7: The regional maps of cloud fraction over the study regions along with the background winds at 925 hPa level during their respective peak seasons [Anjana and Kumar, Theor. Appl. Climatol., 2025].

minimum low-level CF at a given pressure level is considered for further analysis.

The results have emphatically shown that the sub-tropical marine SC over all the three study regions migrated towards poles with significant rates of 31.5, 70.38 and 68.8 km/decade over the NEP, SEP and SA, respectively (Fig.8). The regional HC boundaries also have shown significant poleward migration rates over these three regions. The descending region boundaries of HC exhibited poleward migration at the rates of 40.5, 51.8 and 41.1 km/decade over the NEP, SEP and SA basins, respectively. Though there are differences in magnitudes of migration rates in the descending region boundaries of HC and latitude of minimum CF over the study regions, all are showing significant poleward migration. The results indicate the co-variability of these two metrics and thus provide evidence for the impact of HC expansion on the low-level cloud poleward extension, which plays a crucial role in regulating Earth's radiation budget. It is noted that a fractional change in coverage of low-level clouds such as SC can affect the energy balance of the planet. The study thus provided new insights into the long-term changes in HC and their impact on marine SC distribution over its descending limbs.

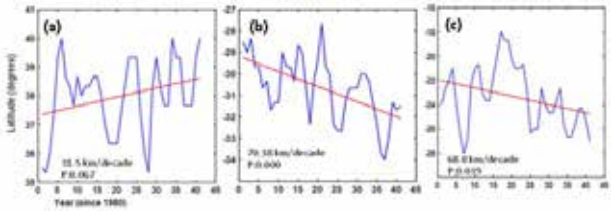

Figure 8: Time series of latitude of minimum cloud fraction at 925 hPa pressure level over the (a) NEP, (b) SEP and (c) SA during 1980–2022. The time series is smoothed using 3-point running mean. The estimated trends and p-values are given in the graphs [Anjana and Kumar, Theor. Appl. Climatol., 2025].

Cloud Dynamics

Characteristics of Vertical Air Motion during Summer Monsoon using ST Radar at Central Himalaya

The vertical motion (w) of air is an important dynamic variable that facilitates the study of different atmospheric processes across various scales. The w of air parcels determines the radiative-convective equilibrium in the troposphere by transport of heat and moisture and influences the structure of the troposphere across regions on earth. The vertical structure and temporal variability of w manifest the vertical exchange of mass and momentum between the upper troposphere and lower stratosphere. In this context, first observations on the characteristics of w during the Asian Summer Monsoon months, over the central Himalayan region using ST radar are presented here. Clear air zenith observation data have been extracted and analysed to determine the distribution w during 2022 and 2023. Convection, precipitation and SNR < -20 dB have been discarded from the present analysis.

Figure 9 shows the Contour Frequency Altitude Diagram (CFAD) indicating the percentage occurrence of w for each month composite of 2 years and its mean profiles (extreme right panel) for June, July, August, September, and October. The spread in percentage occurrence of the w above 6 km is observed to be less in the month of June and increases substantially in July, and August and reduces again in September and in October reaches bound similar to that of June. Below 6 km the percentage spread is similar for all 5 months with October showing the narrowest distribution. This shows the relatively greater w of air parcels in the most active monsoon months. From the monthly mean profiles, it is evident that the w generally follows similar trends for all the 5 months with the average value generally not exceeding 5 cm s^{-1}. A characteristic general downdraft below 6 km is noted for all the months which are strongest in the lower troposphere below 4 km in June and October. An intermonth variation of vertical velocity profiles is observed in the range 6–9 km that is in the mid-troposphere region with small magnitude (<2 cm s^{-1}) updrafts and downdrafts in June and July progressing to pronounced updrafts (>2 cm s^{-1}) for the later months. A relatively strong downdraft is found between 10 and 11 km which

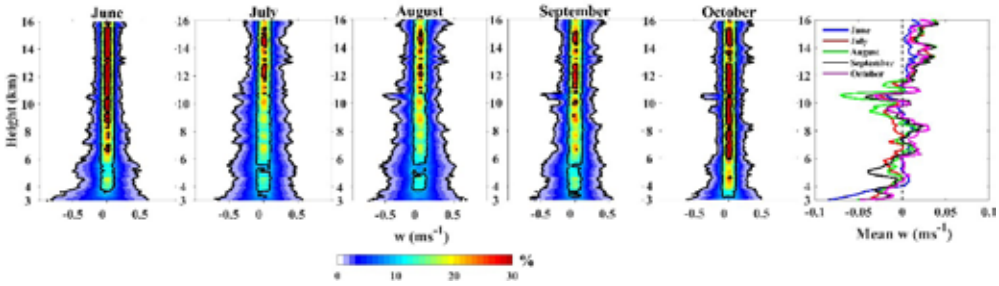

Figure 9: Contour Frequency Altitude Diagrams (CFADs) (CFAD) showing the percentage occurrence of vertical velocity for each month composite of 2 years (Solid black contour lines show 1%, 10% and 25% of occurrence) and the mean w profiles for each month (extreme right panel) in June, July, August, September, and October over Nainital [Poddar et al., Earth and Space Sci., 2025].

persist for all the months with increasing in magnitude from June (~2 cm s^{-1}) to August (~7 cm s^{-1}) and successively decreasing in September and October. This persistent layer of downdraft is a new feature that has been observed and has to be further studied with more datasets to understand its generative mechanism. Above 12 km, consistent updrafts persist in the upper troposphere for all the 5 months increasing in strength from June to a mean maximum value of ~5 cm s^{-1}.

Further analysis of sub-daily variability of vertical velocity for forenoon, afternoon, and evening periods for all the months showed notable variations in the mid-tropospheric region with barely any change in the upper troposphere above 12 km, indicating that the slow upward transport does not directly depend on the inter-period variability for any of the months. This zone of high variability in mean vertical velocity below 12 km and the zone of very less inter-period variability above that support the "two-step process" paradigm. These observations compounded with the location of the study being directly inside the Asian Summer Monsoon Anticyclone (ASMA) makes it possible to hypothesize that for air parcels to reach at least the lower level. Episodic convective systems are needed to trigger the vertical transport upward and then the slow ascent and "trapping" of this air is controlled by the dynamics. It is evident that during clear air conditions, direct downward transport of stratospheric air mass to troposphere is not possible except for some transient trigger event such as wave breaking activity or any local variability.

Space-Borne Dual Frequency Radar Observations of Precipitation Microphysics of Extremely Severe and Long-Lived Cyclonic Storm 'BIPARJOY'

Observations of Dual-frequency Precipitation Radar (DPR) on-board Global Precipitation Measurement (GPM) over an extremely severe cyclonic storm 'Biparjoy' that formed over the Arabian Sea in the month of June, 2023 are used to investigate the spatial pattern of microphysical processes of precipitating clouds embedded in the eye-wall, inner and outer rainband regions of the cyclone.

GPM-DPR provided the measurements of spatial pattern radar reflectivity (Z_e), rain rate, type of precipitation, median drop diameter, number concentration and latent heating at 2km altitude during the passage of cyclone 'Biparjoy' on 11 June, 2023 (Fig.10). By this time the TC was developed in to ESCS after spending 5 days in the AS. The eye of the cyclone with diameter around 50 km could be clearly seen from radar reflectivity pattern (Fig.10 a). The eye of the cyclone is represented by a black dot in the figure. The demarcations of the eye wall, inner and outer rainband regions of the cyclone also can be noted from the figure. The cyclone eye is thus surrounded by convective precipitation, which is organized in narrow rainbands. The maximum reflectivity was found to be around 50 dBZ at the south-east corner of eye wall region of the cyclone. This high reflectivity region coincides with the maximum rain rate (~60 mm/hr) regions (Fig. 10b), which in turn are associated with the convective type precipitation depicted in (Fig. 10c). The type of precipitation map depicted in Fig.10(c) show a large swath of stratiform precipitation with sparsely embedded convective regions near the eye as well as outer rain bands during this stage of TC. Fig. 10 (d-f) show the spatial structure of microphysical properties of the cyclone (D_m, N_w and latent heat). The median drop diameter is found to be in the range of 1.5 to 2 mm at 2km height (Fig. 10d) and the associated drop concentration is found to be in the range of 35 and 50 (Fig. 10e).

The spatial distribution of latent heating at 2 km height was obtained (Fig. 10f) and the maximum heating in rainband regions of the cyclone is

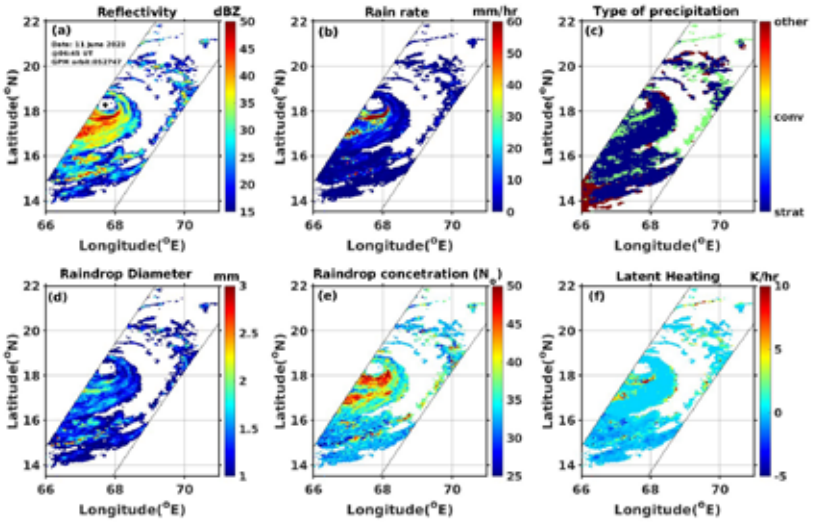

Figure 10: The GPM-DPR observed spatial patterns of (a) radar reflectivity, (b) rain rate, (c) type of precipitation, (d) median drop diameter, (e) number concentration and (f) latent heating at 2km during the passage of the cyclone 'Biparjoy' on 11 June 2023 [Subrahmanyam et al., J. Ind. Soc. Remote Sen. 2025].

observed to be more than 10 K/hr. The latent heating is one of the key factors that sustain TC systems that occur within them. This process involves the release of energy when water vapour condenses into liquid droplets, and the resulting precipitation fuels the cyclone, maintaining its intensity.

GPM observations (Ku-band radar) of the cyclone during four different epochs have been analysed (Fig.11). During 11 and 12 June, the GPM observations capture the eye of the cyclone but compared to 11 June, observations on 12June clearly capture the eye wall, inner and outer rain bands (Fig.11a and b). The vertical cross section corresponding to GPM obviations on 12 June shows the tall structures of radar reflectivity in three regions viz., outer rain band, inner rain band and the eye wall (Fig. 11f). The outer and inner rain band region is found to be separated by stratiform precipitation region with a clear bright band signature. The deep convective clouds with echo tops reaching high as ~17 km in the outer rain band region can also be noted. The GPM observations on 15 and 16 June 2023 at 14:33 and 04:06 UTC, respectively also show deep convective systems embedded in the cyclone's rain bands, which are interconnected by the stratiform precipitation regions. The significance of the present study lies in bringing out the spatial pattern of microphysical processes in the different regions such as eye-wall, inner and outer rainband of the cyclone and in discussing the potential physical mechanisms governing these processes.

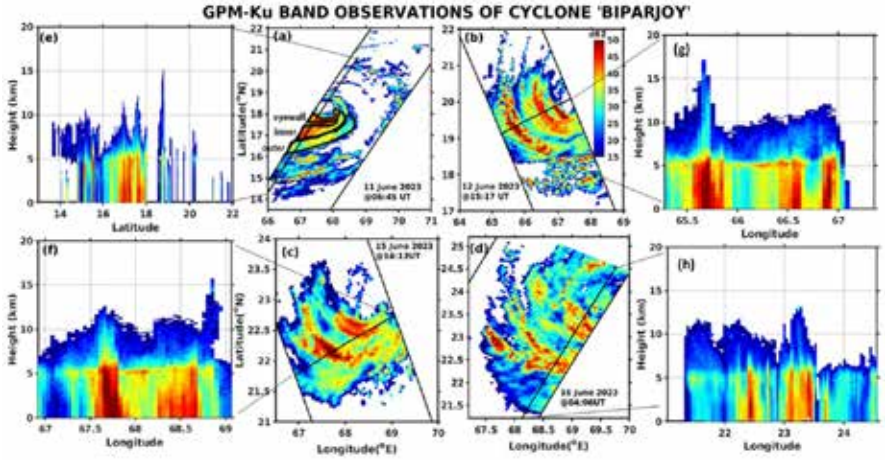

Figure11. GPM-Ku band radar observations of different stages of the cyclone 'Biparjoy' on (a) 11, (b) 12th, (c) 15, and (d) 16 June 2023, respectively. The regions of eye-wall, inner, and outer rainbands of cyclone are shown in figure (a). The height-latitude/longitude sections of selected regions are shown in panels (e-h) [Subrahmanyam et al., J. Ind. Soc. Remote Sen., 2025].

Planetary Atmospheric Dynamics

Studies on Venusian Atmospheric Models: Inputs for Venus Orbiter Mission

Comparative Analysis of Venusian Atmospheric Structure using Models and Observations

Given the major gap areas and uncertainties in the understanding of the atmosphere of Venus, it is essential to choose a reliable Venusian atmospheric model in the context of ISRO's Venus Orbiter Mission (VOM). An extensive comparative analysis of the Venusian atmospheric structure was carried out using two global atmospheric models of the Venus: (1) Venus Global Reference Atmosphere (Venus-GRAM 2021), an empirical model incorporating blended observational datasets; and (2) Venus Climate Database (VCD v2.3), a database of theoretical values generated by a physics-based atmospheric model. Inter-comparison of key atmospheric parameters (temperature, density and pressure) as given by the two models, was carried out in the 10-250 km altitude region, focusing on their spatial (latitudinal), diurnal (day-night), and seasonal (solar activity-induced) variabilities.

The models were further compared with available observational (in situ and remote sensing) datasets of the Venusian atmosphere from previous missions (Pioneer Venus, Magellan, Venus Express and Akatsuki). The analysis confirms overall inter-model agreement, with distinct discrepancies and strong spatio-temporal variabilities in the upper atmosphere above ~100 km (e.g., >140 K variability in temperature, and ~2 orders of magnitude variations in density and pressure at 200 km altitude). Solar activity is found to have a profound impact on the atmospheric structure above ~150 km altitude, with mean density and pressure increasing by nearly 1 order of magnitude, and mean temperature increasing by nearly ~50 K, from solar minima to maxima conditions. Comparison of the models with observations reveal significant deviations, with observations showing a tendency to lie up to ~70% beyond the combined variability ranges given by the models, indicating the need for additional safety margins to capture realistic atmosphere variations. Results of the study were provided as critical inputs to the URSC VOM Project team, as required for various mission-related aspects such as spacecraft design, thermal management and aero-breaking.

Chemical Composition of Venusian Atmosphere from Models and Observations

The chemical structure of the Venusian atmosphere is poorly constrained due to limited availability of observational data from past missions. In this context, two state-of-the-art atmospheric models, Venus-GRAM 2021 and VCD v2.3, were employed to conduct a comprehensive comparative analysis of Venus' atmospheric chemical composition across the 10-250 km altitude region. The study focused on number density profiles of major constituents such as CO_2 and N_2 (in the lower atmosphere), O and CO (in the upper atmosphere), as well as minor but chemically significant species, including H_2SO_4, SO_2, O_3 and OCS, characterizing their model-derived global, spatial, diurnal, and solar activity-induced variabilities.

Global mean analysis of both models shows the dominance of atomic oxygen (AO) above ~150 km altitude, with the combined variability range from the two models indicating nearly ~2 orders of magnitude variability in the AO number density at 200 km altitude. Solar activity is found to have a moderate impact on AO, with the mean number density varying within 1 order of magnitude from solar minima to maxima. In terms of latitudinal variability of AO, Venus-GRAM shows 60% higher equatorial mean number densities compared to the polar values, while VCD shows an opposite behavior. Model outputs for various species were further compared with observational datasets from previous missions, revealing pronounced spatio-temporal variabilities in the atmospheric composition, as well as notable inter-model differences and discrepancies between model predictions and observations. Inputs on the variabilities of key species such as AO and liquid sulphuric acid (H_2SO_4 aerosols & cloud particles) were shared to VOM Project, URSC, given their potential impact on spacecraft design, mission planning and operational aspects of ISRO's upcoming Venus Orbiter Mission.

Technical Development Activities

Payloads for Exploring Planetary Atmospheric Dynamics

SPAV for Solar Occultation Experiments in Venusian Mesosphere-Payload on board Venus Orbiter Mission

Solar occultation Photometry for vertical profiling of Aerosols and thin clouds in the Venusian atmosphere (SPAV) is a multi-wavelength optical payload being jointly developed by SPL and LEOS. As one of the Prime Priority payloads on

board ISRO's Venus Orbiter Mission (VOM), SPAV will obtain high-resolution (~1-2 km) vertical profiles of sulphuric acid aerosols, water vapour, and optically thin clouds & haze layers in the Venusian mesospheric region (~70-100 km). This will be achieved by performing Solar Occultation Experiments (SOE), measuring attenuated solar flux through the atmosphere and unattenuated flux at the top-of-atmosphere (TOA), along the Line-of-Sight (LoS) between the instrument and the sun during spacecraft sunrise/sunset occultation events. Operating in the visible to near-infrared (VIS-NIR) spectral regime (380-1020 nm) in photometric mode, SPAV will enable comprehensive studies of the spectral characteristics of Venusian sub-micron sized aerosols and detached haze layers, offering new insights into dynamical and physical processes in Venusian mesosphere. SPAV has a dual-head configuration, consisting of two identical Optical Heads (SPOH) (Fig.12a) with a common Processing Unit (SPU).

Each SPOH unit consists of three channels: Channel-A (500 nm and 650 nm), Channel-B (850 nm and 935 nm), Channel-C (380 nm and 1020 nm), with each channel comprising of 2 photometric wavelength bands shared by a single CMOS C640 linear array detector, resulting in a total of 6 photometric channels for each SPOH. Each photometric channel has a FOV of 1.4° x 0.01°, viewing a linear strip of the sun-disk. The channels are oriented in such a way that Channels-A and C will image a vertical strip of the sun disk during SOE measurements, whereas Channel-B is oriented perpendicular to A & C, so as to concurrently image a horizontal strip of the sun disk (Fig. 12b). This configuration enables simultaneous imaging of perpendicular linear strips of the sun disk, to derive the sun aspect angles and ensuring that instrument bore sight is precisely pointing towards the sun centre. This will also enable the edge-to-edge correction of the sun image accounting refractive distortions during measurements through the dense atmosphere. The two SPOH units are mounted on opposite sides of the spacecraft (pointing towards +Roll and -Roll axes) to capture maximum number of occultation events via dedicated spacecraft attitude pointing manoeuvres, with the required sun-pointing accuracy (~0.01°) and stability (≤ 1×10^{-4} deg/sec). Presently, the payload configuration and design of SPAV are completed, optimized based on extensive 3D orbital geometry simulations and solar flux simulation studies, and EM development is in progress.

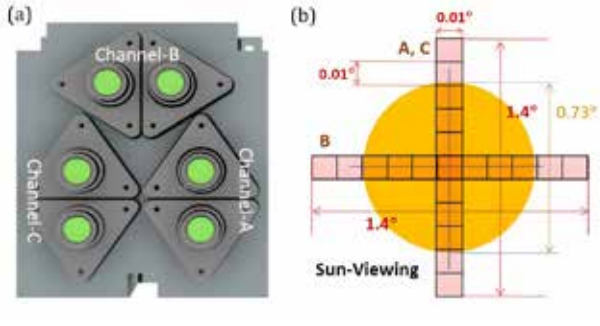

Figure 12: (a) Design of SPAV Optical Head (SPOH) indicating the arrangement of Channels-A, B & C; (b) Visualization of sun-viewing by individual photometric channels.

PIPET-V for In Situ Profiling of Venusian Atmosphere - Payload on board Venus Atmospheric Probe (VAP)

Package for In-situ Profiling of planETary atmospheres for Venus (PIPET-V) is a payload proposed by SPL in collaboration with IISU, to characterize the Venusian atmospheric structure during the entry and descent phases of the Venus Atmospheric Probe (VAP), in the context of ISRO's Venus Orbiter Mission (VOM). PIPET-V consists of a suite of specialized sensors, namely temperature & pressure sensors (resistance temperature sensors and piezoresistive pressure sensors) and inertial sensors (MEMS-based 3-axis accelerometers and gyroscopes) for in-situ vertical profiling of Venusian atmospheric temperature, pressure, density and winds. In the initial hypersonic entry phase of VAP, PIPET will estimate atmospheric density via drag deceleration measurements using 3-axis accelerometers (from~120 km to ~65 km altitude). Subsequently, during the subsonic descent phase (~65 km altitude down to surface), PIPET will measure atmospheric temperature and pressure using high-accuracy sensors ruggedized to operate in the harsh Venusian environment. Further, navigation data from the inertial sensors will be used to derive horizontal winds during the descent phase. In total, PIPET will provide a comprehensive picture of the Venusian atmospheric structure from the surface to the thermosphere (~0-120 km). Presently, the preliminary payload design and identification of suitable sensors for PIPET-V have been completed.

Design and Development of Lidar Systems for Atmospheric Profiling

Lidar for Tropospheric Experiments (LiTE) – TDP R&D

SPL has successfully designed and developed an indigenous portable micro-pulse Lidar for

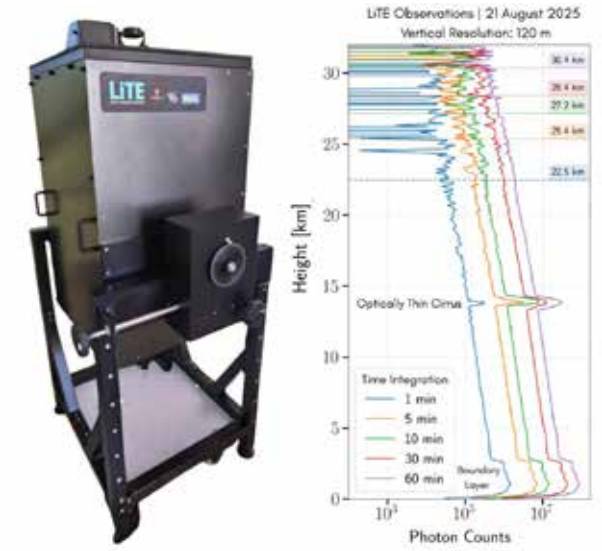

Figure 13: Left: LiTE system developed and operationalized at SPL as part of TDP R&D; Right: Vertical profiles of range-corrected lidar signals (background-removed) at 4:30 – 5:00 IST obtained during a clear-sky night (20-21 August 2025) over Thumba, for different time integrations, with 120 m altitude resolution, depicting the scattering signals up to ~30 km altitude region. The dashed horizontal lines indicate the altitudes at which SNR = 2 for different time-integrated profiles.

Tropospheric Experiments (LiTE), as part of TDP R&D. The system comprises of a laser transmitter (532 nm, ~30 µJ pulse energy, 1000 Hz PRF) and telescope receiver (350 mm dia. Cassegrain-type telescope) in co-axial configuration, along with a ~1.2-nm ultranarrow-band filter, high-gain PMT detector and 40-MHz transient recorder for data acquisition. The system was extensively field-tested and inducted for regular observations from Thumba, providing excellent lidar backscatter profiles in the entire troposphere up to ~18 km altitude during clear-sky nights, at high vertical (~3.75 m) and temporal (~1 minute) resolutions. The unprecedented high-resolution lidar profiles from LiTE reveal intriguing features of lower tropospheric aerosols (persistent ultra-thin layers, small-scale variabilities, and short-period oscillations) and high-altitude cirrus (multi-layered and ultra-thin cirrus in TTL, cirrus uncinus and descending cirrus). The system is also incorporated with a mechanical positioning unit for multi-angle lidar operation. The aft-optics assembly of LiTE has been further augmented by incorporating collimating and focusing (C/F) lens assembly and detector focal plane adjustments, enhancing the altitude coverage up to ~20 km during clear-sky nights at native resolution. Coherent time integration up to ~30-60 minutes and altitude binning to 120 m improved the lidar signals and SNR, enhancing the altitude coverage of LiTE up to ~30 km, enabling the scientific investigation of stratospheric aerosols (Fig. 13).

Mini Lidar: A prelude to LiME Payload for Mars Lander Mission *(*MLM)

As part of TDP R&D, a Mini Lidar has been designed and developed in house at SPL, using a compact ~150 mm dia. Cassegrain telescope, integrated with the same micro-pulse energy laser source, of the LiTE system, in biaxial configuration with ~100 mm laser-telescope separation (Fig. 14). The system has been extensively tested in the field environment using PMT detector and 40-MHz transient recorder, providing high-resolution (~3.75 m, 1 minute) vertical profiles up to ~15 km altitude, revealing ultra-fine features and variabilities of tropospheric aerosols and thin clouds. The system is incorporated with elevation-azimuth scanning capabilities using a computerized 2-axis mechanism, enabling 3-dimensional mapping of aerosol pollutants in the near field (< 5 km). System improvements are in progress, including further miniaturization and incorporation of dual-polarization and dual-wavelength (532 nm & 1064 nm) capabilities to study particle shape and size characteristics. The development of the Mini Lidar is a prelude to the Lidar for Martian Environment (LiME) payload shortlisted for ISRO's upcoming MLM.

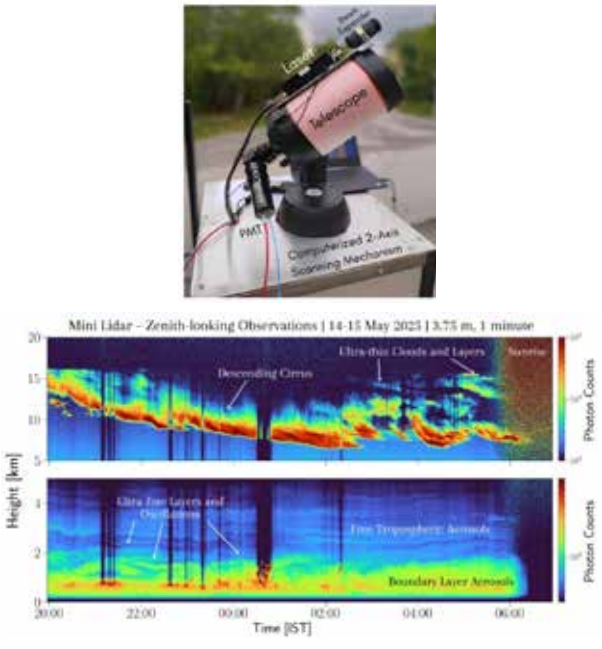

Figure 14: Left: Mini Lidar system in-house developed at SPL; Right: Mini Lidar Zenith-looking observations (range-corrected signals, background corrected) during 14-15 May 2025, revealing fine-scale features of aerosols and cirrus in the troposphere up to ~15 km altitude.

Rayleigh-Mie Lidar System (RMLS)

Design and development of the Rayleigh-Mie Lidar System (RMLS) is an Advanced R&D Project of SPL, being established at SPL Observatory, IPRC Mahendragiri as a state-of-the-art system for profiling middle atmospheric temperature (~30-80 km altitudes), and lower atmospheric aerosols & clouds (~3-30 km altitudes). Design, configuration and system specifications of RMLS were optimized & finalized through theoretical simulations, and recommended by the Inter-Centre Expert Committee (ICEC-RMLS). The 4-channel data acquisition systems (40-MHz Transient Recorders) and PMT detectors (ungated & uncooled for Mie, gated & TE-cooled for Rayleigh) have been procured and extensively tested & characterized in lab and field environments using the in-house developed LiTE system. The high-energy laser (532 nm, ~800 mJ energy per pulse, 30 Hz PRF) has been developed and tested by the OEM (M/s Innolas GmbH, Germany) and is presently ready for shipment. Procurement of 500-mm RC telescope for Mie and large-area (800-mm) Newtonian telescope receiver for Rayleigh are underway. Site-readiness activities are completed to facilitate the integration & installation of RMLS at SPL Observatory, IPRC Mahendragiri.

New Experiments/Campaigns/ Initiatives

RH200 Rocket experiment using aluminium chaff

A RH200 rocket experiment was conducted on 19 November 2025 using aluminium chaff instead of traditionally employed copper chaff over Thumba for the first time. The central objective of the experiment was to increase the altitude of wind measurements by adopting aluminium chaff, which has potential to attain terminal velocity suitable for wind measurements at higher altitudes than copper chaff, owing to its relatively lower density. In order to examine the suitability of the aluminium chaff for wind measurements in the middle atmosphere, a rocket experiment using RH-200 was carried out, successfully.

The radar data comprising of range, elevation and azimuth angles of the aluminum chaff are processed at very high time resolution of 0.1 s, which provided better altitude resolution of winds in the middle atmosphere. The high vertical resolution of winds of the order of 100 m (in case of copper it is 1 km) is attributed to reduced terminal velocity of aluminum chaff, which provided ample samples

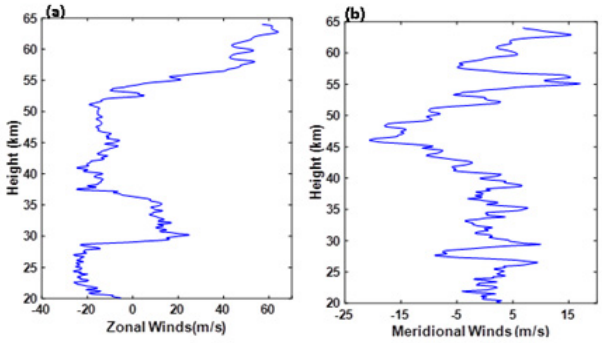

Figure 15: Height profiles of 100 m resolution (a) zonal winds and (b) meridional winds measured using RH-200 with aluminium chaff payload on 19 November 2025.

of wind measurements. Before proceeding with the high-resolution wind measurements, the output of newly developed algorithm for processing the radar data is validated with the existing algorithm at TERLS, which readily showed a good agreement between the two. After validating the algorithm, the zonal and meridional winds with 100 m vertical resolution are estimated (Fig. 15). This is for the first time that the high vertical resolution winds are derived from the rocket soundings over Thumba, which will be useful for investigating the small-scale gravity waves as well as turbulence in the middle atmosphere

CUSAT Radar Experiments for Investigating Vertical Coupling of the Atmosphere

An experimental Monsoon Campaign was conducted during 17-19 July and 4-9 August 2025. This is a joint experimental campaign between SPL-VSSC and Advance Centre for Atmospheric Radar (ACARR)-Cochin University of Science and Technology (CUSAT) to understand the dynamics and chemistry of the tropical lower and upper atmosphere and its coupling during summer monsoon. CUSAT ST radar was operated continuously to probe from lower to the upper atmosphere in different experimental modes, which includes different array configurations. A temporary ozonesonde laboratory was also established at ACARR for ozonesonde preparation. Every day between 14:30-15:30 IST one ozonesonde/radiosonde was launched from ACAAR to get the temperature and ozone profiling from surface to 35 km. Apart from the above radar observations, there are a few other co-located instruments, viz., automatic weather station, Micro rain radar, disdrometer and ceilometer, and radiometer along with the satellite observations will also be used to address the proposed scientific objectives.

Ongoing Activities and Future Projections

- Cluster launching of RH200 sounding rockets for investigating the tides, planetary and gravity waves simultaneously in the tropical middle atmosphere.
- Radiative transfer computations for retrieval of atmospheric temperatures for satellite based middle atmospheric measurements
- Space based measurements of atmospheric turbulence parameters and generation of their three-dimensional maps over India
- Whole Atmosphere Community Model Simulations of middle atmosphere for Re-entry vehicle applications
- Multi-frequency radar observations of vertical structure and microphysical properties of monsoon clouds
- Development and Testing of SPAV Payload (Solar Occultation Experiment) for Venus Orbiter Mission
- Development of Dual-wavelength and Dual polarization Lidar
- Development and Operationalization of Rayleigh-Mie Lidar System

Publications in Peer-Reviewed Journals

1. Anjana, U. and Kumar, K. K., "Impact of Hadley circulation expansion on the distribution of low-level clouds over its descending limbs", Theoretical and Applied Climatology, https://doi.org/10.1007/s00704-025-05544-6, 2025
2. Poddar, N., Das, S. S., Bhattacharjee, S. and Naja M., "Characteristics of Vertical Air Motion During Summer Monsoon Over the Central Himalayan Region Using 206.5 MHz ARIES Stratosphere-Troposphere (ST) Radar", Earth and Space Science, https://doi.org/10.1029/2025EA004232, 2025.
3. Subrahmanyam, K. V., Kumar, K. K., Nayak, R. K., Ramana, M. V., Rao, G. S, "Space-Borne Dual Frequency Radar Observations of Precipitation Microphysics of Extremely Severe and Long-Lived Cyclonic Storm BIPARJOY", Journal of the Indian Society of Remote Sensing, https://doi.org/10.1007/s12524-025-02278-w, 2025.
4. Veenus V. and S. S. Das, "Assessing the impact of the Hunga Tonga-Hunga Ha'apai volcanic eruption on the structure of the Brewer-Dobson circulation: Possible Implications", Advances in Space Research, https://doi.org/10.1016/j.asr.2024.11.075, 2024.
5. Veenus V., and S. S. Das, "The Teleconnection between Brewer-Dobson Circulation and Quasi-Biennial Oscillation: Implications on Ozone and Water Vapor Distribution – A Composite Analysis", Climate Dynamics, https://doi.org/10.1007/s00382-025-07616-9, 2025a.
6. Veenus V., and S. S. Das, Observational evidence of stratospheric cooling and surface warming due to an increase of stratospheric water vapor by Hunga-Tonga Hunga-Ha'apai. Natural Hazard, https://doi.org/10.1007/s11069-025-07320-1, 2025.

Publications in Refereed International Report

1. Mehta, S. K., M. Fujiwara, S. Tegtmeier, M. V. Ratnam, S. Fadnavis, K. K. Kumar, S. S. Das, S. K. Sharma, R. V. Nair, V. Velu, C. Sarangi, N. Ojha, L. K. Sahu, A. Kottyail, T. P. Sabin, M. Gogoi, K. Mohankumar, M. N. Rajeevan, International Conference on the Asian Summer Monsoon Anticyclone: Gateway of Surface Pollutants to the stratosphere, doi:10.13140/RG.2.2.16807.98728, APARC Newsletter, 64 (32), 2025.

Scientific/Technical Reports

1. Sunil Kumar S. V., Jayadev Pradeep, Sachin Prabhakar, Dinakar Prasad Vajja, "Design and Development of a Rayleigh-Mie Lidar System (RMLS) for probing lower and middle atmosphere: Preliminary Design Document", VSSC Technical Report, ISRO-VSSC-TR-0093-0-25, 2025.
2. Jayadev Pradeep, Varun Nikam and Sunil Kumar S. V., "Comparative Analysis of Venusian Atmospheric Models", VSSC Technical Report, ISRO-VSSC-TR-0279-0-25, 2025.
3. Sunil Kumar S. V., AmitMaji, Jayadev Pradeep, et al., "Venus Orbiter Mission Preliminary Design Review Document: Solar occultation Photometry for vertical profiling of Aerosols and thin clouds In Venusian atmosphere (SPAV)", VSSC Design Report, ISRO-VSSC-DR-0621-0-25, 2025.
4. Jayadev Pradeep, Koushik N., Varun Nikam, and VIP Study Team, "Venus Impact Probe: Study Report", VSSC Study Project Report, ISRO-VSSC-SP-0233-0-25, 2025.

Presentation in Symposia/Conferences/Workshops

1. Poddar N., Das, S. S., Naja, M., Bhattacharjee, S., "Characteristics of vertical air motion over the central Himalayan region using 206.5 MHz Stratosphere-Troposphere radar", 16th International Workshop on the Technical and Scientific Aspects of iMST Radar and Lidar (MST16/iMST3), University of Rostock, Rostock, Germany during 9-13 September 2024.
2. Poddar N., Das S. S., Naja, M., Bhattacharjee, S., "Characteristics of vertical air motion over the central Himalayan region using 206.5 MHz Stratosphere-Troposphere Radar", International Symposium on the 40th Anniversary of the MU Radar, University of Kyoto, Kyoto, Japan during 18-21 November 2024
3. Nabarun Poddar, Siddarth Shankar Das, Manish Naja and Samaresh Bhattacharjee (2024), Characteristics of vertical air motion during monsoon over central Himalayan region using 206.5 MHz Stratosphere-Troposphere Radar, 6th URSI Regional Conference on Radio Science (6thURSI-RCRS 2024), which was held in Bhimtal, India, from 22-25 October 2024.
4. Samaresh Bhattacharjee, Siddarth Shankar Das, Priyanka Srivastava, Manish Naja, and Nabarun Poddar (2024), Characteristics of atmospheric boundary layer studied using 206.5 MHz ST Radar over the central Himalayas: Preliminary results, 6th URSI-RCRS2024.
5. Uma, K.N., Bukya Sama, and Siddarth Shankar Das, Jagdish Jena and Veenus Venugopal (2024), Spatial evolution of convection and rainfall using S-band Polarimetric radar over the East Coast of India, 6th URSI-RCRS2024.
6. Koushik, N., K. K. Kumar. An Enigmatic Variability in the Tropical Middle Atmosphere. European Geophysical Union (EGU) General Assembly, Online, 29 April 2025.
7. Jayadev Pradeep, Varun Nikam and Sunil Kumar S. V., "Dynamic Characteristics of the Venusian Atmosphere: Insights for Future Exploratory Missions to Venus", Global Space Exploration Conference (GLEX 2025), organized by International Aeronautics Federation, New Delhi, 7-9 May 2025.
8. Sunil Kumar S. V., Jayadev Pradeep, Varun Nikam, "Solar Occultation Experiments (SOE) for Exploring the Venusian Atmosphere: Methodology and New Insights from Simulations", Global Space Exploration Conference (GLEX 2025), organized by International Aeronautics Federation, New Delhi, 7-9 May 2025.
9. Jayadev Pradeep, Varun Nikam and Sunil Kumar S. V., "Comparative Analysis of Venusian Atmospheric Structure using Models and Observations", Venus Science Conference (Venus-SC 2025), PRL, Ahmedabad, 25-26 September 2025 (online)
10. Varun Nikam, Jayadev Pradeep and Sunil Kumar S. V., "Chemical Species & their Variabilities in the Venusian Atmosphere: Insights from Models and Observations", Venus Science Conference (Venus-SC 2025), PRL, Ahmedabad, 25-26 September 2025 (online)
11. Sunil Kumar S. V., Jayadev Pradeep, Varun Nikam, "A Simulation Framework for Solar Occultation Experiments in the Venusian Atmosphere", Venus Science Conference (Venus-SC 2025), PRL, Ahmedabad, 25-26 September 2025 (online)
12. Hadiya Nawal, C.K and K. Kishore Kumar, Polarimetric Radar Observations of waterspouts over the southern Indian peninsular Coast of the Arabian Sea, International Symposium on Tropical Meteorology (INTROPMET 2025), Indian Institute of Tropical Meteorology during 18-20 November 2025.
13. Anjana U and K. Kishore Kumar, Intertropical Convergence Zone: A regional Perspective using Multi-metric Approach, INTROPMET 2025.
14. Oindrila Nath and K. Kishore Kumar, Quasi-Biennial Oscillations and Indian Summer Monsoon Coupling Mechanisms: A New Perspective, INTROPMET 2025.
15. Siddarth Shankar Das, N. Poddar, M.V. Ratnam, et al. (2024), Recent observations of atmospheric instabilities from the Indian network of ST/MST radars: Results inferred from NetRAD-ASMA campaign, International Symposium on the 40th Anniversary of the MU Radar (MU40)", held at Kyoto University, Kyoto, Japan, during 18-21 November 2024.
16. Siddarth Shankar Das, N. Poddar, M. V. Ratnam, A. Paul, V. Venugopal, P. Nandakumar (2024), Azimuth echo variation in the troposphere and lower stratosphere from multiple Doppler beams and vertical in-beam spatial interferometry: First results from newly established 53 MHZ radar at Haringhata (22.94°N, 88.51°E), 6th URSI-RCRS 2024.
17. JayadevPradeep, Sunil Kumar S. V. and VarunNikam, "Dynamics and Variabilities in the Venusian Atmosphere: Insights from Models and Observations", Workshop on Variability and Stability of the Venus' Atmosphere in Various Spatiotemporal Scales Inferred from Space Missions and Numerical Simulations, International Space Science Institute, Beijing, 5 June 2025.
18. Sunil Kumar S. V. and JayadevPradeep, "Probing Structure and Dynamics of the Stratosphere from High-Altitude Balloons: Test beds for Remote Sensing & In Situ Payloads", 2- Day User Meeting at TIFR balloon Facility, Hyderabad, 27-28 October 2025
19. Sunil Kumar S. V. and JayadevPradeep, "SPAV: Solar occultation Photometry for vertical profiling of Aerosols and thin clouds in Venusian atmosphere", National Meet on ISRO's Venus Orbiter Mission - Science and Enhancing Academia Engagements, ISRO HQ, Bangalore, 29-30 October 2025.

आयनमंडल तापमंडल एवं चुंबकमंडल भौतिकी
Ionosphere Thermosphere Magnetosphere Physics

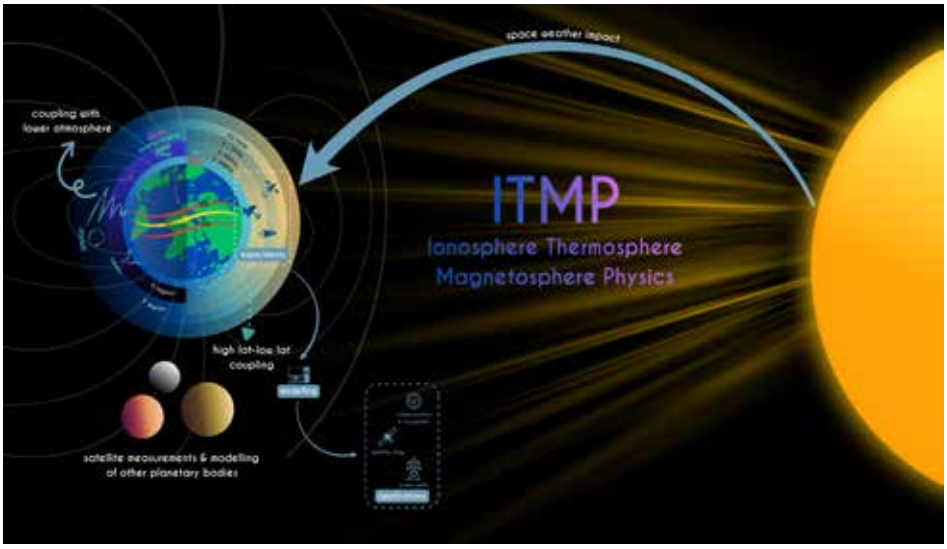

आयनमंडल, तापमंडल एवं चुंबकमंडल भौतिकी (आइटीएमपी) शाखा का लक्ष्य, (क) बदलते अंतरिक्ष मौसम एवं भूचुंबकीय परिस्थितियों तथा इसके अक्षांशीय असमानताओं पर चुबंकमंडल तापमंड़ल-आयनमंड़ल प्रणाली की अनुक्रिया का अध्ययन, (ख) तापमंड़ल, आयनमंड़ल का उसके नीचे प्रसरित वायुमंड़ल के साथ गतिकीय युग्मन पर अध्ययन, (ग) ऊपरि वायुमंड़लीय प्रक्रमों का प्रतिनिधित्व करने के लिए तापमंड़ल-आयनमंड़ल मॉडलों का आंतरिक विकास व उपयोग, और प्रौद्योगिक अनुप्रयोगों के लिए बेहतर इनपुट प्रदान करने हेतु इन अध्ययनों का उपयोग करने पर ध्यान केंद्रित करते हुए, भौमिक ऊपरी वायुमंड़ल की ऊर्जिकी तथा गतिकी की जाँच करना है। आइटीएमपी शाखा का यह प्रयास रहता है कि वह इन अनुसंधान लक्ष्यों को भूमि, रॉकेट तथा अंतरिक्ष आधारित मंचों में प्रयोग हेतु क्षमता रखने वाले स्वदेशी तौर पर विकसित परीक्षणों के माध्यम से तथा अनुसंधान की व्याप्ति को अन्य सौरप्रणाली पिड़ों के चुंबकमंड़ल,तापमंड़ल तथा आयनमंड़ल तक भी बढ़ा कर पूरा करे।

Ionosphere Thermosphere Magnetosphere Physics (ITMP) branch aims at investigation of the energetics and dynamics of terrestrial upper atmosphere, with focus on (a) Study of the response of the magnetosphere thermosphere ionosphere system to varying space weather and geomagnetic conditions and it's latitudinal differences, (b) Study of the dynamical coupling thermosphere ionosphere has with the atmosphere below it, (c) In house development and use of thermosphere-ionosphere models to represent the upper atmospheric processes and make use of these studies to provide better input for technological applications. ITMP strives to meet these research objectives through indigenous development of experiments capable of being used on ground, rocket and space-based platforms and extending the scope of its research to the magnetospheres, thermospheres, and ionospheres of other solar system bodies as well.

वैज्ञानिक टीम / Science Team
तरुण कुमार पंत / Tarun Kumar Pant
राज कुमार चौधरी / Raj Kumar Choudhary
मंजू जी / Manju G.
विनीत सी / Vineeth C.
मो मोसारफ होस्सैन / Md. Mossarraf Hossain
मृदुला एन / Mridula N.
संध्या के नायर / Sandhya K. Nair
अंबिली के एम /Ambili K. M.
अजय अनिल पोटदार / Ajay Anil Potdar
आयिषा एम अश्रफ / Ayisha M. Ashruf
सत्यप्रिय दास / Satyapriya Das[$]

तकनीकी टीम / Technical Team
प्रमोद पी. पी. / Pramod P. P.
मोहम्मद नज़ीर एम / Mohammad Nazeer M.
मणिकंठन नायर एन / Manikantan Nair N.
अनुमोद पी जी / Anumod P. G.

डीएसटी महिला वैज्ञानिक / DST Women Scientist
श्रीबा श्रीकुमार / Sreeba Sreekumar

अनुसन्धान सहयोगी / Research Associates
शिम्ना के / Shimna K.*
स्वाति चौधरी / Swati Chowdhury
अर्चना आर के /Archana R. K.
समीन कादर एस के / Samin Kader S. K.
ललिता जी कृष्णन / Lalitha G. Krishnan

अनुसंधान अध्येता / Research Fellows
श्रुती टी. वी. / Sruthi T. V.[#]
रिचा नाजा जैन / Richa Naja Jain[&]
मनु टी / Manu T.
सौम्यनील बैनर्जी / Soumyaneal Banerjee
आर्या अशोक /Arya Ashok
रूबन सैमसन याकुब / Reuben Samson Yaqub
विष्णुप्रिया के एस / Vishnupriya K. S.

[$]Joined in December 2025
[*]Relieved in April 2025
[#]Relieved in January 2025
[&]Relieved in February 2025

Equatorial Ionosphere Thermosphere Processes

Short and Long-Term Variations in Geomagnetic External Field: Study based on 104 years of Geomagnetic Observations from the Indian Low Latitude Station-Alibag

The variations of all the three components of the geomagnetic field over a low latitude Indian station Alibag (18°N, 72°E) during the past 104 years (1921–2024) have been examined. The quiet time diurnal variations in the northward (ΔX) component represent the solar quiet (Sq) current, while the variations in zonal component (ΔY) represent combined signatures of Sq and Inter-hemispheric Field-Aligned Currents (IHFAC), and the vertical component (ΔZ) is a combination of Sq and induced currents. The response of these components to sunspot numbers in different seasons has been investigated and found that the response is highest during the summer months and lowest during winter. The amplitudes of ΔX components are consistently higher in spring (March) than in autumn (September), which is opposite for ΔY and ΔZ. This study further reveals a reversal in the polarity of ΔY with local time and seasons confirming the contribution of IHFAC. To understand it, the responses of IHFAC to solar activity cycle have also been examined. Additionally, geomagnetic main field (core origin field) variations have also been extracted from quiet days midnight data to examine the secular variations. Overall, the analysis of the long-term trend in the geomagnetic field reveals that (a) the long-term trend in residual Sq and in Sq during low solar activity years shows a decreasing trend (b) this could be associated with dip latitude movement and climate change in upper atmosphere associated with increase in CO_2 (Fig. 1).

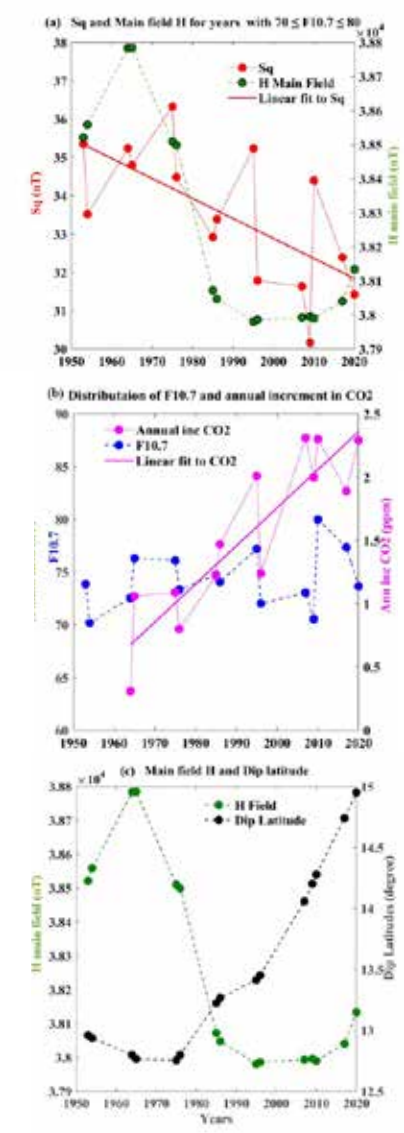

Figure 1: (a) The variations in the amplitude of Sq and H main Field during the years 1950-2020 with the correlation coefficient (R) between them (b) the distribution of F10.7 and annual increment in CO_2 during these years (c) the main field H variations and Dip latitude variations [Archana et al., J. Geophys. Res., 2025].

Do the vertical movements of the peak height of F-region truly represent the vertical E×B plasma drift velocity over the dip-equator?

The reasons for the difference observed between the theoretically estimated E×B plasma drift and the drift calculated by tracing the movement of the ionospheric F2 region peak as inferred through ionograms, are examined, using a quasi two-dimensional theoretical ionospheric model. A comparison of vertical plasma drift velocities during the11 May 2024 superstorm, derived from three independent methods: (i) ΔhmF2/Δt estimated from Digisonde observations at Trivandrum, (ii) ΔhpF/Δt obtained from the QTD model by tracing the motion of the upper plasma peak (hpF), and (iii) the penetration electric field driven vertical drift predicted by the PPEF model has been done (Fig. 2). The close agreement among these three estimates highlights that under extreme storm time conditions, the strong equatorward thermospheric winds and enhanced vertical E×B drifts elevate the F-region peak well above 300 km (diffusion threshold height). In this case, the derived drifts truly represent the vertical drift of the ionosphere. Analysis shows that vertical drift causes the electron density profiles in the F2 region

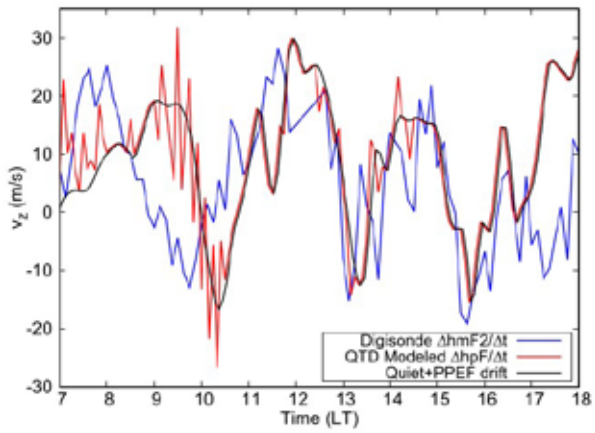

Figure 2: Comparison of vertical plasma drift velocities during the 11 May 2024 superstorm, derived from three independent methods: (i) ΔhmF2/Δt estimated from Digisonde observations at Trivandrum, (ii) ΔhpF/Δt obtained from the QTD model by tracing the motion of the upper plasma peak (hpF), and (iii) the penetration electric field driven vertical drift predicted by the PPEF model [Ashok et al., J. Geophys. Res., 2025].

to steepen. Photochemical processes dominate the lower peak (hmF2), while the upper peak (hpF) is attributed to vertical drift, which is difficult to trace due to diffusion effects. The close agreement between model derived ΔhpF/Δt and Scherliess-Fejer (SF) vertical drifts confirms that the F2 peak movement does not represent the vertical drift if it is below 300 km. The extreme conditions during this superstorm provided a rare opportunity to observe the presence of strong equatorward thermospheric winds and enhanced vertical E×B drifts which elevated the F-region peak well above 300 km.

Impact of an eclipse on the Indian equatorial ionosphere thermosphere system: A case study

The response of the ionosphere thermosphere system in the vicinity of the geomagnetic equator, specifically over Trivandrum (TRV), Kochi, and Madurai, was investigated for the solar eclipse of December 26, 2019, using data from multiple instruments. The HF radar observations in the aftermath of the eclipse peak phase, reveal a sharp increase in the vertical drift of E-region type II irregularities by a factor of 6 at the altitudes of 105 and 114 km. The backscattered power also shows enhanced fluctuations around the eclipse time (Fig.3). The wavelet analyses of the power fluctuations bring out an enhanced presence of wave activity on the eclipse day. The dominant 0.3 h. wave extracted at 105 km and 114 km reveals the oppositely directed amplitude and phase propagation features, indicating the gravity wave origin of the fluctuations. The ICON satellite-based temperature measurements also confirm the existence of waves with a dominant vertical wavelength of ~9–14 km. The observation of blanketing Es layer concurrent to the observation

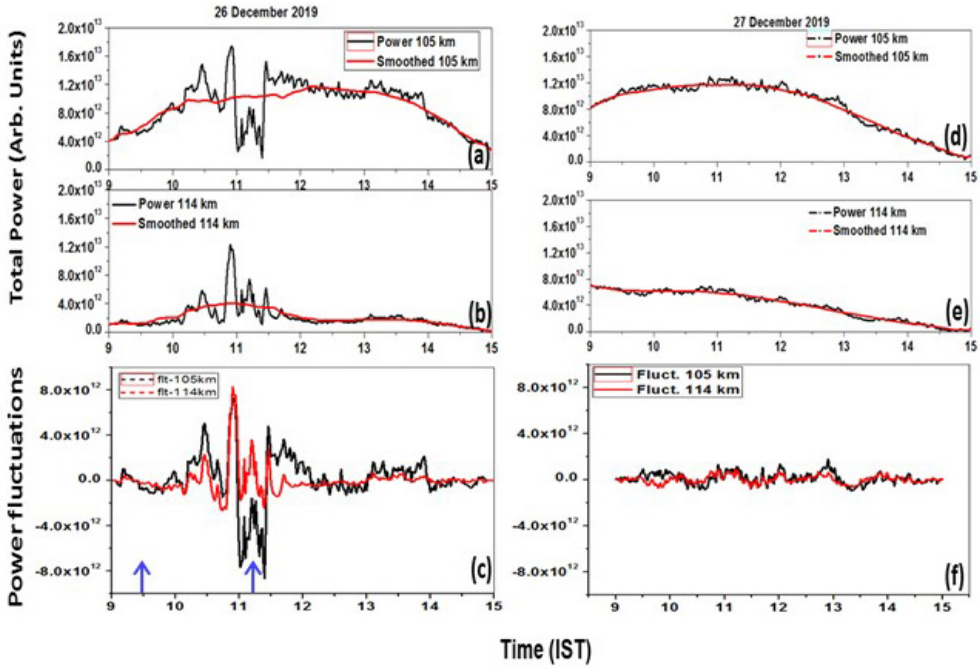

Figure 3: (a) Temporal variations of backscattered power, along with the trend for 105 and 114 km on eclipse day (b) Temporal variations of power fluctuations for 105 and 114 km on eclipse day (c)Same as (a) but for control day (d)Same as (b) but for control day [Manju et al, Adv. Space Res., 2025].

of wave activity in the HF radar irregularity structures reveals the role of gravity wave induced winds in the generation of the irregularities/ layer. The integrated bottom side electron content at TRV during the eclipse peak phase shows a large percentage reduction by as much as 42% with respect to the control day. The percentage reductions observed in Global Positioning System Total Electron Content (GPSTEC) at Kochi and Madurai are found to be ~20%. The lower percentage of reduction at Kochi and Madurai are ascribed to the weakened Equatorial Ionization Anomaly (EIA) and the consequent presence of EIA crest closer to these locations, in addition to the effect of eclipse induced recombination coupled with (albeit) reduced fountain effect related ionization removal, from Trivandrum (the trough location).

Geometric Mean Algebraic Reconstruction Technique: A tool for ionospheric tomography using GNSS receiver system

Ionospheric tomography is a widely utilized technique for investigating the electron density distribution in the ionosphere. This approach primarily relies on multiple line-of-sight total electron content (TEC) measurements from receivers positioned across the region of interest. A comprehensive methodology for formulating linear equations corresponding to each observation is developed. These equations are then simplified into a matrix form, subsequently solved using iterative technique. To determine the electron density distribution through reconstruction of the 3D electron density structure of the local ionosphere, a modified version of the algebraic reconstruction technique (ART) termed as the geometric mean algebraic reconstruction technique (GMART), is adopted. The performance of GMART was evaluated against ART and the multiplicative algebraic reconstruction technique (MART) with a comparative analysis of the convergence behaviour of these iterative methods. Electron density tomograms over the Indian region are generated using (a) a priori constructed using the IRI2016 model, (b) reconstructed using ART, (c) reconstructed using MART, and (d) reconstructed using GMART (Fig. 4). The resulting tomographic images offer an extensive view of the ionospheric structure, facilitating monitoring of spatial variations over the time. The altitude profiles of the ionosphere derived from the GMART technique were further validated against ground-based ionosonde observations of bottom-side electron density profiles. The comparison reveals a strong agreement between the reconstructed electron density profiles and real ionospheric electron density measurements obtained from ionosonde.

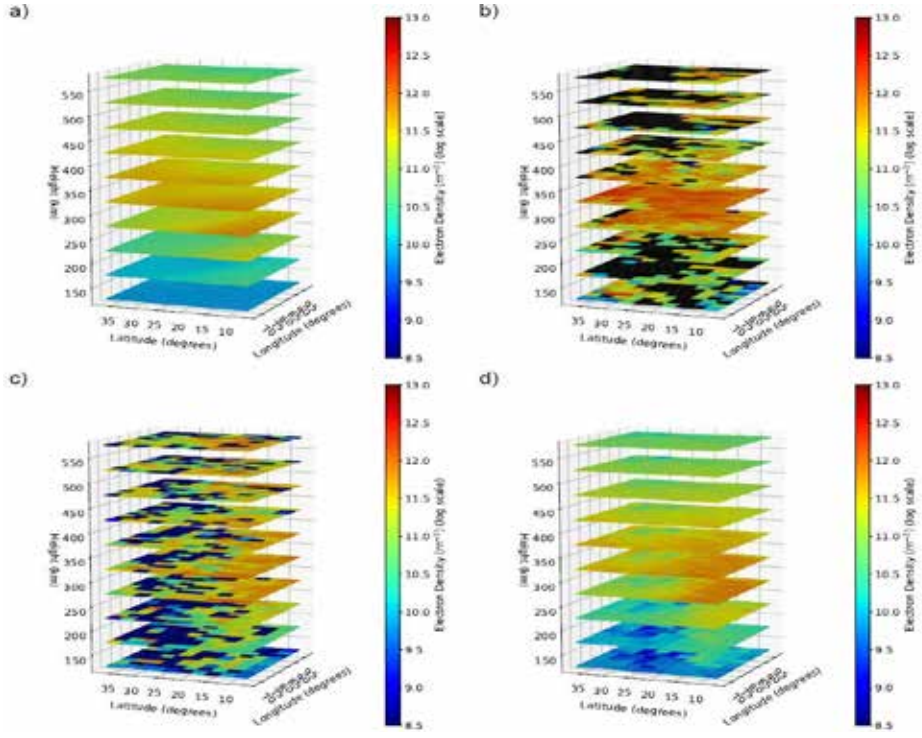

Figure 4: Electron density tomograms over the Indian region (a) a priori constructed using the IRI2016 model (b) reconstructed using ART (c) reconstructed using MART (d) reconstructed using GMART [Potdar et al., RAS Tech. Instr., 2025].

IMF By-driven electric field disturbances over the equator during northward IMFs

The first evidence of equatorial and low-latitude ionospheric electric field disturbances driven by quasi-periodic variations in the interplanetary magnetic field B_y component ((IMF B_y), under a constant northward IMF B_z (~+15 nT), solar wind dynamic pressure (~8 nPa), solar wind velocity (~450 km/s), and positive Sym-H (+10 nT) has been provided. The virtual height of the F layer (h'F), measured by ionosondes at opposite longitudes in the American (Jicamarca, 11.9°S, -76.0°E; Fortaleza, 3.9°S, -38.52°E) and Indian (Trivandrum, 8.5°N, 77.0°E; Tirunelveli, 8.73°N, 77.7°E) sectors, shows electric field disturbances with opposite polarities during the day and night, driven by changes in the IMF. During northward IMF Bz conditions, vertical E × B plasma drifts measured by the Jicamarca Incoherent Scatter Radar (ISR), along with equatorial electrojet (EEJ) observations, reveal westward electric field disturbances on the dayside. Conversely, on the nightside, ionosonde measurements at Trivandrum and Tirunelveli show eastward electric field perturbations (Fig.5). Notably, quasi-periodic electric field fluctuations with prominent periodicities of approximately 15 min are observed in both, the IMF By and ionospheric parameters, such as dh'F/dt and EEJ, in both local time sectors. These fluctuations are driven by modulations in high-latitude disturbance polar (DP2) currents. SuperDARN ionospheric convection maps display enhanced convection, rotation, and expansion, which appear to influence the equatorial electric field. The presence of northward Bz (NBZ) currents and reverse convection patterns likely contributes to the observed westward electric field perturbations at low latitudes.

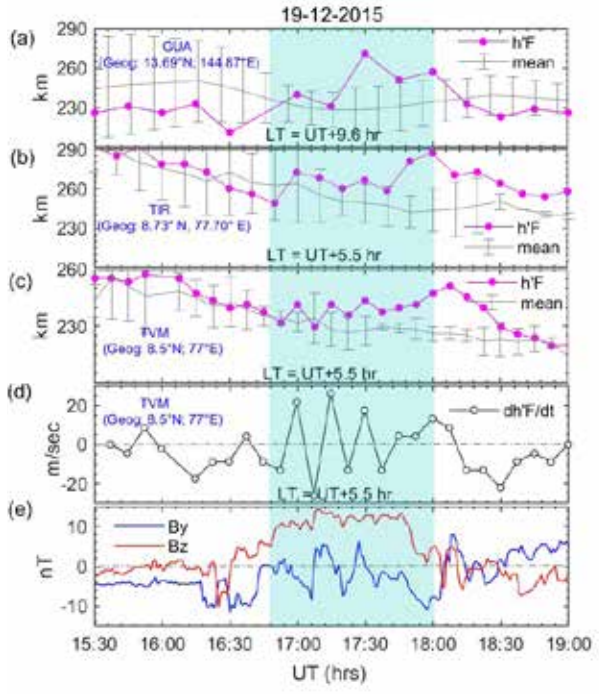

Figure 5:Variations in the virtual height of the F-region (h'F) at (a) Guam (GUA), (b) Tirunelveli (TIR), and (c) Trivandrum (TVM), (d) vertical plasma drift (dh'F/dt) derived from h'F variations, (e) IMF Bz and By components. The grey lines with error bars represent the mean and standard deviation from five International Quiet Days (IQDs). The cyan-shaded region marks the period of significant ionospheric perturbations [Ram et al., J. Atmos. Sol. Terr. Phys., 2025].

Lower Atmosphere-Upper atmosphere Coupling

Response of equatorial and low latitude ionosphere over Indian region to the tropical cyclones

The distinct impacts of two tropical cyclones-Ockhi (2017) and Burevi (2020)-on the equatorial and low-latitude ionosphere using multiple ionospheric parameters, including the Equatorial Electrojet (EEJ)-induced magnetic field, foF2, h'F, and GPS TEC have been examined. The study specifically addressed how the electrodynamics over the dip equator (Trivandrum: 8.5°N, 77°E, 0.5°N dip latitude) gets modified and influence the low-latitude ionosphere (Hyderabad: 17.4°N, 78.4°E, 11.7°N dip latitude) as the cyclones traverse the Indian equatorial region. During the passage of Tropical Cyclone Ockhi, a strong Counter-Electrojet (CEJ) with varying strength (-22 to -5 nT) was observed (Fig.6), accompanied by a decrease in foF2, and TEC at the equatorial site. Correspondingly, the low-latitude ionosphere also exhibited a decrease in TEC. In contrast, Tropical Cyclone Burevi, which was weaker than Ockhi, exhibited a weaker CEJ (-13 to -2.6 nT) along

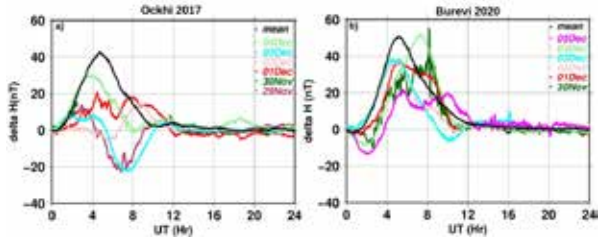

Figure 6: Time variation of ionospheric current induced magnetic field over Tirunelveli and Alibag from (a) 29 November 2017 to 04 December 2017 during the TC Ockhi and (b) 30 November 2020 to 05 December 2020 during the TC Burevi. The black line represents the quiet day mean [Shimna et al., Adv. Space Res., 2025].

with an increase in critical frequency of F2 layer, and TEC at the equatorial site. Similarly, the low-latitude ionosphere also showed an increase in TEC during Burevi's passage. Ockhi, being a more intense cyclonic storm, exhibited presence of strong blanketing Es layers over Trivandrum, particularly near the peak of its cyclonic activity. On these days, despite a weak Pre-Reversal Enhancement (PRE), the presence of Equatorial Spread-F (ESF) was observed. The presence of enhanced terdiurnal tides during these events was inferred through wavelet analysis of TEC over Trivandrum. It is proposed that, gravity waves generated by the cyclones likely caused the observed CEJs and ESF. The observed variability in ionospheric parameters and TEC is attributed to modifications in E-region electrodynamics and subsequent changes in the plasma fountain. Overall, it has been shown that strong tropical cyclones can disrupt the ionosphere through intense convection and lightning activity highlighting the identification of these atmosphere-ionosphere disturbances as crucial for accurate ionospheric modelling and space weather forecasting.

Did the "Tauktae" cyclone impact the upper atmosphere through traveling ionospheric disturbances? A case study over the Arabian sea using measurements from InSWIM network stations

The influence of cycone "Taukte" on ionosphere over the Indian low-latitude region has been examined. During May 2021, the first pre-monsoon tropical cyclone of the year and the fifth strongest ever recorded over the Arabian Sea, Cyclone Tauktae formed and evolved over the Arabian Sea. It originated from a depression near the Lakshadweep Islands on May 14, 2021, rapidly intensified into an extremely severe cyclonic storm by May 17, 2021, and made landfall on May 19, 2021. During its passage, the Arabian Sea experienced highly convective and disturbed conditions. This powerful tropical cyclone amid geomagnetically quiet conditions was studied to explore its potential effects on the ionospheric region. Using the COSMO regional atmospheric model, the movement of Cyclone Tauktae and prevailing lower atmospheric conditions were simulated. Additionally, ionospheric data from three InSWIM network stations namely Kavaratti, GMRT, and NCRA were utilized. Temporal variations in fluctuations in the Vertical Total Electron Content (dVTEC), for the selected GNSS satellites (PRNs) at these stations, as shown (Fig. 7), were estimated. Analysis of the VTEC measurements from May 14 to 18, 2021 (cyclone-influenced days) and May 05, 2021 (non-cyclone day) revealed a prominent presence of Traveling Ionospheric Disturbances (TIDs) during the cyclone days. Spectral analysis of VTEC data showed significant enhancements in TID spectral power on May 16-17, 2021, at NCRA and GMRT, with wave velocities ranging from 100 to 125 m/s. As the geomagnetic conditions remained quiet during both, the non-cyclone day and the cyclone days, the observed TIDs were attributed to the forcing from the lower atmosphere, eventually associated with the presence of Cyclone Tauktae.

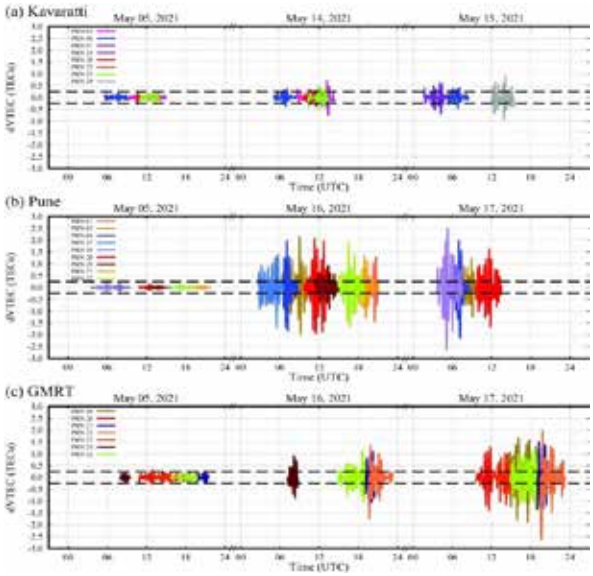

Figure 7: Temporal variations in dVTEC acquired from selected PRNs at the Kavaratti station (a) on May 05, 2021, and May 14–15, 2021; at the Pune station (b) on May 05, 2021, and May 16–17, 2021; and at the GMRT station (c) on May 05, 2021, and May 16–17, 2021. Each PRN (01 to 32) is represented by a distinct color. The X-axis denotes time in UTC, while the Y-axis represents dVTEC in TECu. The black dashed line in (a)–(c) indicates the upper and lower limits (0.25 TECu) for cyclone-induced ionospheric perturbations [Chowdhury et al., Adv. Space Res., 2025a].

First observational investigation on the temporal trends of VTEC over an equatorial station during Tropical Cyclones

The impact of two tropical cyclones (Mora and Ockhi, 2017) over the Northern Indian Ocean on Vertical Total Electron Content (VTEC) over Trivandrum, was examined by comparing data from similar periods in 2018 and 2019. The Daily variations in AVTECmax (i.e. average maximum total electron content in TEC units) observed over Trivandrum were estimated for the year 2017, 2018, and 2019 (Fig. 8). To ensure accuracy, a data screening method was implemented to exclude the potential effects of geomagnetic storms and

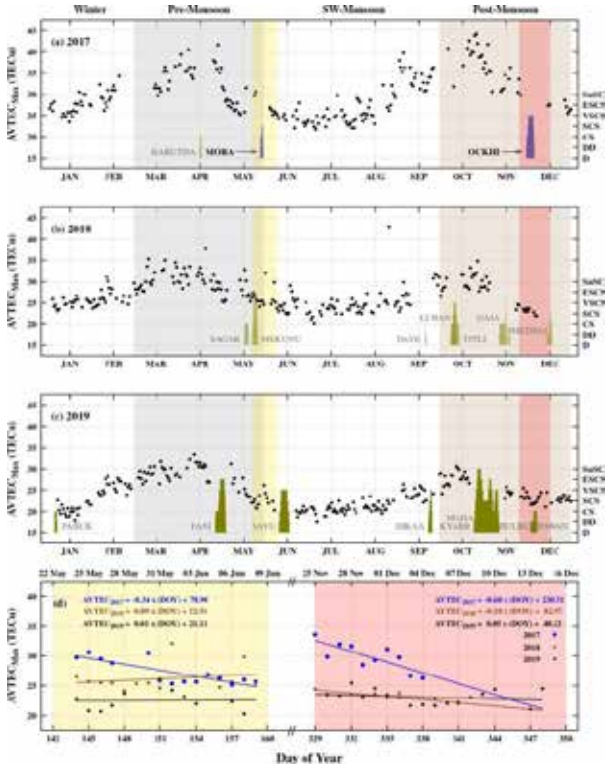

Figure 8: (a-c) Daily variations in AVTECmax (TECu) observed over TVM for the years 2017, 2018, and 2019. Four seasons - winter, pre-monsoon, south-west monsoon, and post-monsoon are marked in different shades on the top X-axis. All the Tropical Cyclones (TC) are marked by their names and are represented as colored vertical bars (right Y- axis). The height of the vertical bars corresponds to the intensity of TC. The study period corresponding to these two cyclones are shown in prominent shades. (d) a linear-fit representing the trend of AVTECmax as a function of day of the year, together with the observed AVTECmax, is shown in different colors [Chowdhury et al., Adv. Space Res., 2025b].

other tropical cyclones on VTEC. Results showed a significant depletion in VTEC, ranging from 7% to 19%, which varied based on the intensity of the cyclones and their distance from the measurement site. The analysis demonstrated a sharp depletion in the VTEC during the passage of the cyclone, the first of its kind, emphasizing the influence on the upper atmosphere, which was seen to extend even after the landfall.

Multi-Instrument Investigation of the Pre-Seismic Ionospheric Response to 2021 Haiti Earthquake

The study of pre-seismic variations in the ionosphere due to 2021 Haiti earthquake (Mw= 7.2) is carried out using ground and space-based instruments. The day time ionospheric response is analyzed using Vertical Total Electron Content (VTEC) from International GNSS Service (IGS) stations and electron density from Swarm satellite data. The results demonstrate that bandpass filtered VTEC reveals clear, pronounced, pre-seismic oscillations with peak magnitudes of ~0.2 TECU on 05 August 2021, that is, 9 days before the earthquake for stations near and just outside the earthquake preparation zone (top panels, Fig. 9). Similarly, enhanced wave-like oscillations are also evident in the filtered VTEC data near the conjugate stations on the same day (bottom panels, Fig. 9). Another unique feature during 05 August 2021 is the anomalous enhancement of northern Equatorial Ionization Anomaly crest shown by Swarm electron density data. Such an enhancement is not observed for other days during August. This is also concurrent with the drop in Relative humidity which occurred during the same day near the impending epicentre region.

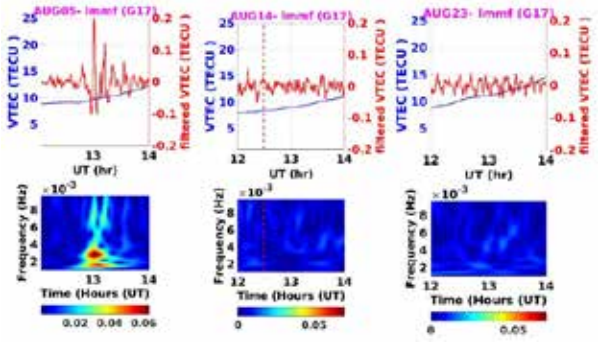

Figure 9: Vertical Total Electron Content (VTEC) (blue curve) and filtered VTEC (red curve) from station PRN pair G17 LMMF for 05 August (left panels), 14 August (middle panels) and 23August 2021(right panels). Red dashed line indicates the Earthquake onset time [Sreeba et al, Earth and Space Sci., 2025].

Hence the concomitant anomalies found in various atmospheric and ionospheric parameters suggest that the anomalies found on 05 August 2021 are plausibly related to the Haiti 2021 earthquake. This study also sheds some light into similarities with the Haiti 2010 event which occurred very close to the epicenter of 2021 event, hence emphasizing the need for detailed studies of the Earthquake prone regions of world using multiple precursor parameters.

Space Weather Impact on Ionosphere

Impact on the plasma distribution over the Indian equatorial/low latitude ionospheric region during the May 2024 Gannon Superstorm

The effects of the superstorm of May 10-11, 2024, on the plasma density distribution in the ionosphere over the Indian equatorial and low-

latitude regions have been investigated. The Vertical Total Electron Content (VTEC) is used as a proxy to understand the plasma density distribution. The VTEC variations observed over four InSWIM stations Trivandrum, Bangalore, Pune and Bhopal during the storm period, 10-13 May 2024 are compared with that on 9 May, pre-storm day (Fig. 10). Analysis of the AE index suggests a strong equatorward wind surge due to intense auroral heating during the storm. In conjunction with the equatorward neutral wind from the auroral region and the storm generated strong convective electric fields penetrating down to the dip-equator, caused VTEC reduction at night (main phase) and enhancement during the day (recovery phase) on 11 May over Trivandrum, Bangalore, Pune. Simultaneously, an overall decrease in VTEC of over 60% was observed in Bhopal, an equatorial ionization anomaly crest region. The undulations observed in the magnetic field (ΔH) at the dip-equator correlated with interplanetary electric field (IEFy) indicating the penetration of IEFy to equatorial ionosphere. Analysis of the AE index suggests a strong equatorward wind surge due to intense auroral heating during the storm. Since the superstorm occurred at night over Indian longitude sector, meridional wind circulation played a prominent role. These results highlighted the need for more comprehensive analysis using multiple instruments and models to understand the response of the Indian equatorial and low-latitude regions during geomagnetic storms.

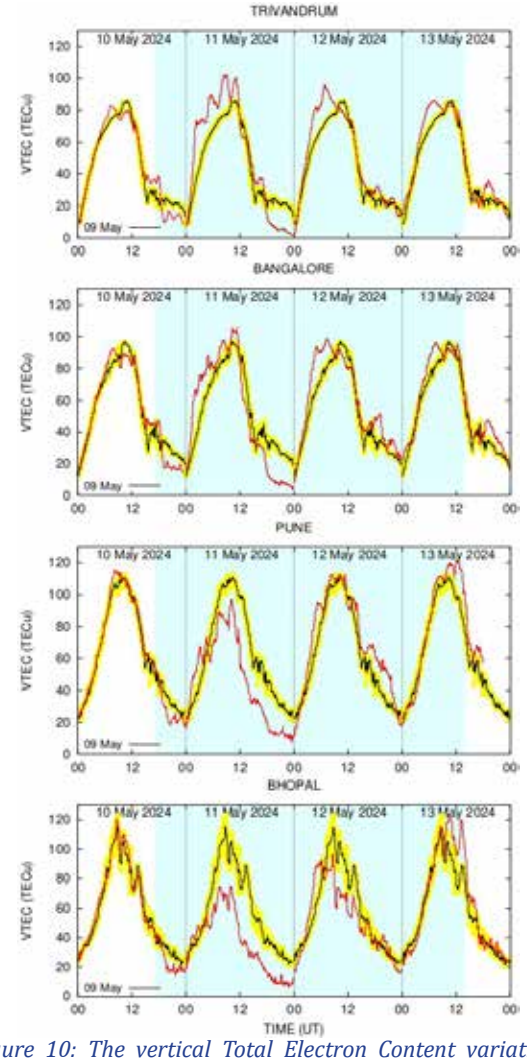

Figure 10: The vertical Total Electron Content variations observed over Trivandrum, Bangalore, Pune and Bhopal during the storm period, 10-13 May 2024. The daily variations are compared with the 9 May, pre-storm day [Ambili et al., J. Geophys. Res., 2025].

Unique Signatures of meridional wind variations on the electron density distribution over the dip equator during May 2024 Gannon Superstorm

The unusual daytime enhancement and undulations observed in Vertical Total Electron Content (VTEC) during the extreme G5 geomagnetic storm (superstorm) on 11 May 2024 over a dip equatorial station in India, Trivandrum is investigated using a physics-based ionospheric model. To isolate the effects of storm-induced electric fields and neutral wind perturbations, the ion continuity and momentum equations for seven ion species are solved using a dipole geomagnetic field approximation. The electron density profile for the combined Prompt Penetration Electric Field-driven vertical drift and storm-time meridional winds during the 11 May 2024 superstorm is simulated (Fig. 11). The model reproduces the strong F-region uplift along with the characteristic wind-induced undulations, and this combined

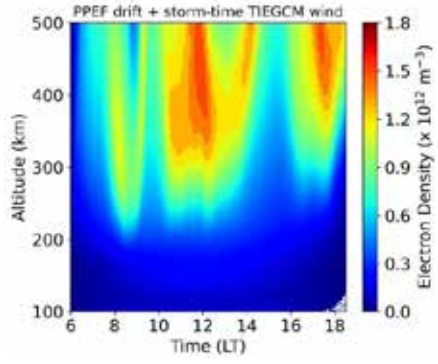

Figure 11: Simulated electron density profile for the combined Prompt Penetration Electric Field-driven vertical drift and storm-time meridional winds during the 11 May 2024 superstorm [Ashok et al., Geophys. Res. Lett., 2025].

forcing provides the best match to the Digisonde observations, capturing both the magnitude of the uplift and the characteristic storm-time structural variations. The results clearly show that fluctuating prompt penetration electric fields primarily drive the strong VTEC enhancement, while storm-time meridional wind reversals cause prominent undulations. The model reproduces the Ionospheric Electron Content (IEC) measured by a co-located Digisonde and the VTEC measurements by the GNSS receiver before noon. However, both the model and Digisonde underestimate GPS-derived VTEC in the post-noon sector, suggesting additional plasmaspheric contributions. This study demonstrates, for the first time, the coupled influence of electric fields and meridional winds in shaping ionospheric responses to severe storms over the Indian dip equatorial region using in house developed physics-based equatorial/low latitude ionospheric model.

Anomalous response of equatorial ionosphere during the recovery phase of May 2024 Gannon Superstorm from GOLD observation

The Gannon superstorm of May 10, 2024 significantly impacted the thermosphere-ionosphere system, causing unusual plasma density redistribution. During the recovery phase of the superstorm on 11 May 2024, the thermosphere ionosphere system experienced dramatic changes marked by an unusual redistribution of plasma density. The satellite based peak electron density (Nmax) from Global-scale Observations of the Limb and Disk (GOLD), ground-based Vertical Total Electron Content (VTEC), and topside VTEC from Swarm C satellite revealed an enhanced electron density at the equator and a complete disappearance of the Equatorial Ionization Anomaly (EIA) crests (Fig.12) over American longitudes. This absence of EIA crests was linked to a strong daytime Counter Electrojet (CEJ) caused by disturbance dynamo that was also observed in ground magnetic data. The unusually strong CEJ means that the electric field and the resultant ExB vertical drift is very weak on that day, thereby eliminating the fountain effect. Thermosphere-Ionosphere-Electrodynamics General Circulation Model (TIEGCM) simulations further indicated the presence of equatorward converging meridional winds from both hemispheres. This converging wind hindered the diffusion of plasma from the dip equatorial region to low latitudes, leading to the formation of a narrow band of enhanced Nmax along the equator. Additionally, a pronounced enhancement in the O/N_2 ratio along the equator

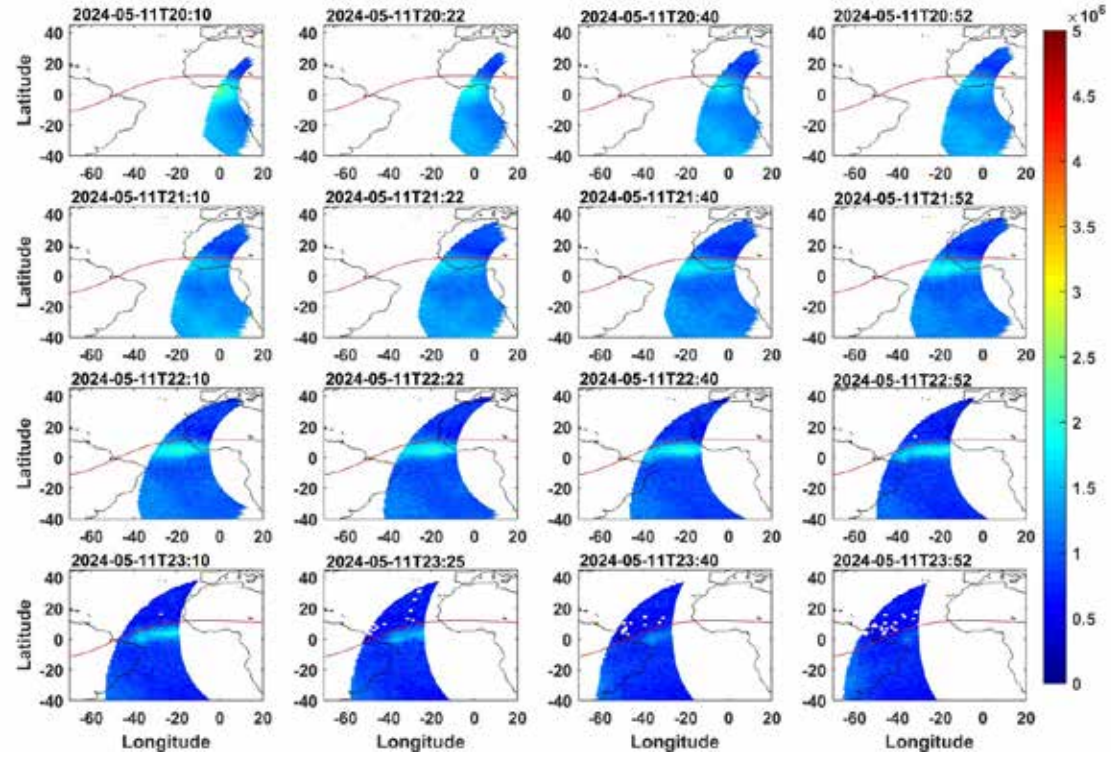

Figure 12: Spatio-temporal variation of peak electron density scan from GOLD observations on 11 May 2024 20:10 UT to 23:52 UT [Shimna et al., Space Weather, 2025].

was observed during the recovery phase, further contributing to this phenomenon. The present study, therefore, for the first time, demonstrates the combined effects of storm induced changes in equatorial electrodynamics, meridional winds, and significant compositional changes during the recovery phase of a superstorm, and their influence on plasma distributions. The corroborative evidence from model simulations further strengthened these observational findings.

Signatures of the long duration prompt penetration electric field in the 18 MHz HF radar observations over Thumba

One of the best proxies to estimate the daytime ionospheric zonal electric field from the dynamo region is the drift of the plasma irregularities in the ionospheric E-region by coherent radars, although there have not been many at HF frequencies. The present study is based on the observations of the anomalous variability in the zonal drift of 8.3 m scale size plasma irregularities in the ionospheric E-region during the daytime on 12 October 2021, and 28 November 2022, as observed by an 18 MHz HF radar at Thumba (8.5°N, 77°E, and dip lat., 1.96°N). While the wind perturbations from the lower atmosphere and the electric field penetrating from the solar wind, can both cause the perturbations in the E-region electric field.

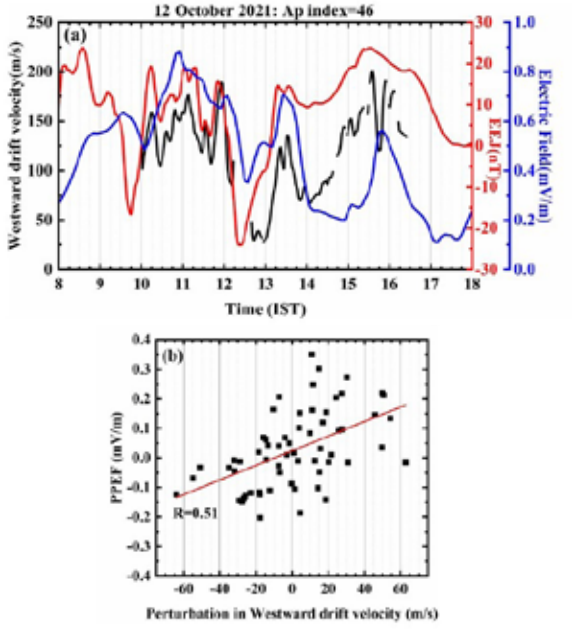

Figure 13: (a) Comparison between the observed westward drift at 96 km altitude, EEJ strength, and the predicted overall Electric field on 12 October 2021. (b) Correlation between the perturbations in the westward drift velocity to the PPEF [Krishnan et al, J. Geophy. Res., 2025a].

Based on a comparison with the predicted Prompt Penetration Equatorial Electric Field (PPEF) as ascribed by Manoj et al. (2008) and the quiet-time dynamo electric field over Thumba, it is concluded that the perturbations in the electric field on these two events are caused by PPEF solely driven by IMF Bz oscillations and mapping to the equatorial region. It is observed that on these days the prompt penetration electric fields were sustained for long time. The former event is a result of a Coronal Mass Ejection, whereas the latter event was caused by a high-speed solar wind associated with coronal hole. The fluctuations in the strength of the Equatorial Electrojet (EEJ) calculated from the magnetic field observations from a pair of equatorial (Tirunelveli) and off-equatorial (Alibag) stations are also found to be well in agreement with the radar observations and modeled PPEF, thereby verifying the E-region observations (Fig. 13).

Responses of the Daytime Low and Equatorial Ionosphere and Thermosphere over the Indian Region During the Geomagnetic Storm of April 2023

Study of the response of Thermosphere–Ionosphere (TI) system over the Indian longitude sector during the geomagnetic storm of April 23–24, 2023, is presented. The ionosonde observations at the dip equatorial station, Trivandrum (8.52°N, 77°E, dip lat. 1.96°N), are found to have unusually high F2 peak plasma density (foF2), with three maxima during the daytime on April 24 (Fig. 14).

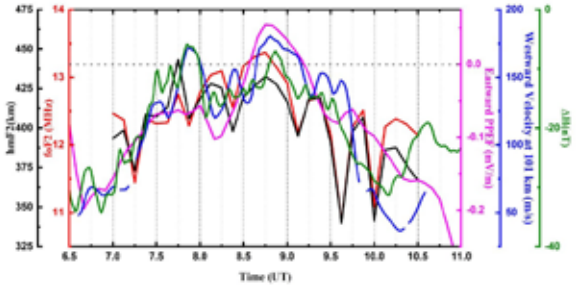

Figure 14: Comparison of hmF2, foF2 variation over Trivandrum to predicted Prompt Penetration Electric Field (PPEF), observed E-region plasma irregularity drifts at 101 km and EEJ strength on 24 April 2023 [Krishnan et al., J. Geophy. Res., 2025b].

The Total Electron Content (TEC) observations from different latitudes showed enhancements temporally progressing from north to south. These features are identified as Traveling Ionospheric Disturbances (TIDs) with speeds 400 to 750 m/s. Two major enhancements in TEC observed over Trivandrum were concurrent to the first and

third maxima in foF2. Simulations of meridional wind and temperature for this storm were carried out using the Thermosphere-Ionosphere-Electrodynamics General Circulation Model (TIEGCM) that was driven with high-latitude inputs derived from the Assimilative Mapping of Ionospheric Electrodynamics (AMIE) technique. Simulations show the signatures of Traveling Atmospheric Disturbances (TADs) in ionospheric F-region, which confirm with the TID observations. The second foF2 peak is found to be simultaneous to the modulation in Prompt Penetration Electric Field (PPEF), which is also observed in the drift of the E-region ionospheric plasma irregularities using the HF radar and the Equatorial Electrojet (EEJ) strength measured by ground-based magnetometer. Simultaneously increasing electric field and foF2 implies the presence of storm-time equatorward wind, inhibiting the plasma fountain. This is the first study comparing comprehensive observations and AMIE-TIEGCM modeling studies of daytime responses of low and equatorial TI during a geomagnetic storm.

Effects of May 2024 Gannon Superstorm on the plasma distribution over the crest of equatorial anomaly region in the Indian ionospheric sector

In this study the Vertical Total Electron Content (VTEC) measurements solely from Bhopal is used to understand the impact of an geomagnetic storm over the Equatorial Anomaly crest region in the Indian ionospheric sector. The VTEC contour map is generated on May 10 to 13, 2024 over the Bhopal region (Fig. 15). Vertical dashed line (red color) shows the Sudden Storm Commencement (SSC) time and two vertical dashed lines (magenta color) show the start and end of the Main Phase (MP) of the storm. It was observed that the superstorm produced positive and negative impacts on VTEC. Approximately +61% deviation in VTEC was observed at ~0500 UT on May 12, 2024 whereas approximately ~ 68.5% deviation in VTEC was observed at ~ 2045 UT on May 11, 2024. The increase in VTEC (+24% to 50%) during the main phase of the storm can be attributed to the prompt penetration of electric fields (PPEFs) and suppression of VTEC during recovery phase of the storm has been attributed to the changes in the thermospheric composition and ionospheric disturbance dynamo electric fields (DDEF). Increase in VTEC and wave-like structures in the VTEC on May 12, 2024 may be due to the combined effect of DDEF and traveling ionospheric

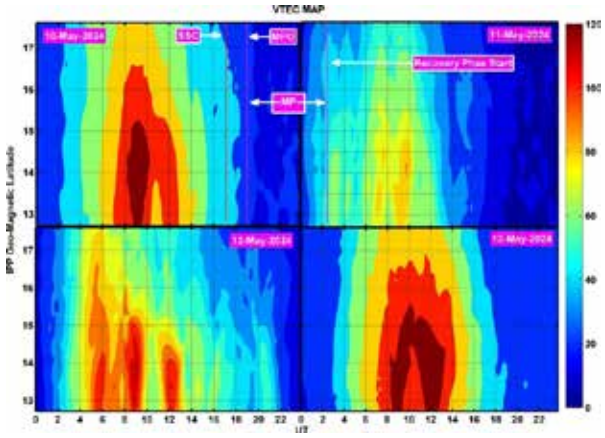

Figure 15: VTEC contour map (May 10 to 13, 2024), vertical dashed line (red color) shows the SSC time and two vertical dashed lines (magenta color) shows Main Phase (MP) of the storm [Jain et al., Adv. Space Res., 2025].

disturbances (TIDs) generated by this geomagnetic storm; however, a separate study is needed to fully characterize these TIDs. We also compared IRI2020 TEC with the observed VTEC and found that IRI-TEC model accurately estimated the suppression in VTEC on May 11 and 12, but could not reflect on the wave-like structure observed in VTEC on May 12.

Rapid Reversal of Hemispheric Asymmetry in the Intensity of EIA Crests During the Geomagnetic Storm of 23 April 2023: A Unique Observation from GOLD satellite

Using the peak electron density of Ionospheric F-region from the Global-scale Observations of the Limb and Disk (GOLD) satellite a unique phenomenon; the rapid reversal of the intensity of the Equatorial Ionization Anomaly (EIA) crests between the hemispheres during the main phase of 23 April 2023, geomagnetic storm has been reported (Fig.16). The Prompt Penetration Electric Field amplified the intensity of both EIA crests. However, the enhancement at the southern crest began to decay within an hour, while the northern crest began to strengthen. Thermosphere Ionosphere Electrodynamics General Circulation Model simulations indicate that trans-equatorial wind played a key role in these variations. Wavelet periodograms of ground-based total electron content measurements confirmed the presence of Travelling Ionospheric Disturbances (TIDs). Storm-induced winds and TIDs likely changed the altitude of the F-peaks and the recombination rates between the crests, and plasma transport by trans-equatorial winds also contributed to this rare phenomenon.

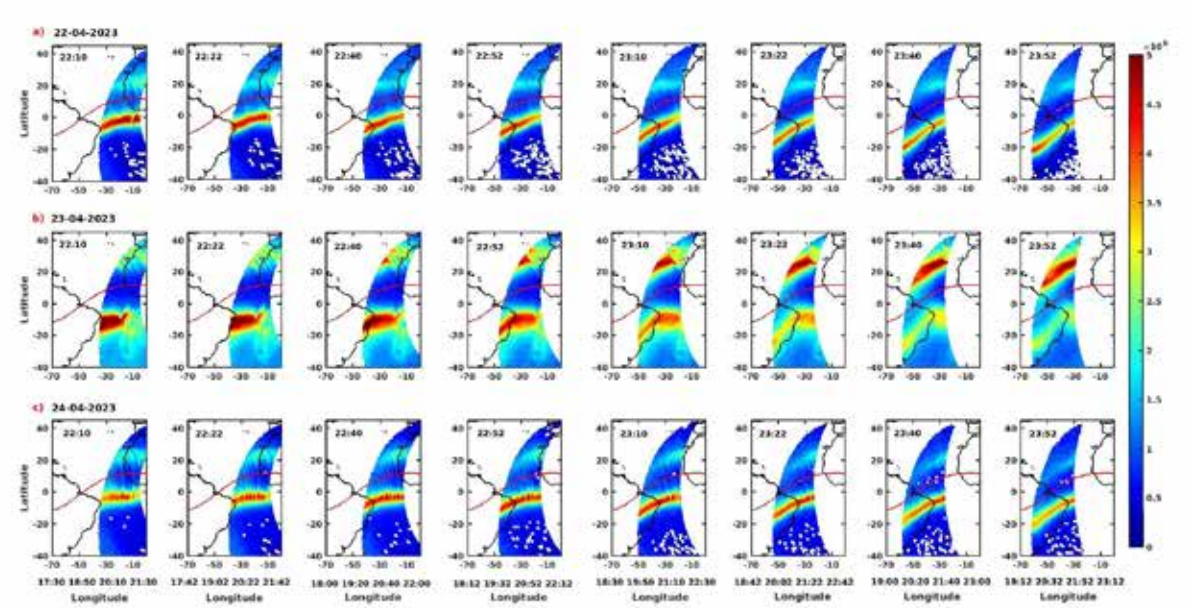

Figure 16: Spatio-temporal variation of Nmax (electrons/cm3) from GOLD observations on (a) 22nd April 2023 22:10 UT to 23:52 UT (b) 23rd April 2023 22:10 UT to 23:52 UT, (c) 24th April 2023 22:10 UT to 23:52 UT. The X and Y axes of the figure correspond to Geographic latitude and longitude, respectively, and the red line represents the geomagnetic equator. The local time at each longitude is mentioned at the bottom of the panel [Shimna et al., Geophys. Res. Lett., 2025].

Indian equatorial ionosphere under the influence of the May 2024 geomagnetic storm: Insights into electric fields, plasma irregularities and F-region dynamics

The study investigates the distinctive features of the daytime equatorial E-region ionosphere using observations of HF radar (18 MHz), ionosonde, and magnetometer at Thumba during the superstorm on 10-11 May 2024. The northward component of the Interplanetary Magnetic field exhibited large-amplitude oscillations throughout the day on May 11 that resulted in sudden changes in the Interplanetary Electric field, in turn manifesting as Prompt Penetration Electric Field (PPEF). The drift measurements of plasma irregularities using the radar indicates that these PPEF modulations effectively mapped onto the equatorial ionosphere in the Indian region. The radar observations of the zonal drift of daytime E-region plasma irregularities exhibited four notable and significant aspects: (a) enhancements in westward drift velocities during eastward electric field to 500 m/s, exceeding the ion acoustic limit by ~140 m/s. (b) eastward reversal of drift with speeds ~200 m/s in response to westward PPEF, (c) occasional disappearance of plasma irregularities, and (d) short-lived westward drifting echoes in east beam of radar suggesting a possible localized alterations in electron density profiles (Fig. 17). Concurrent ionosonde measurements revealed a rise in the ionospheric peak altitude beyond 500 km during local noon, accompanied by the presence of the F3 layer. This alluded to the combined effect of eastward PPEF and equatorward thermospheric wind.

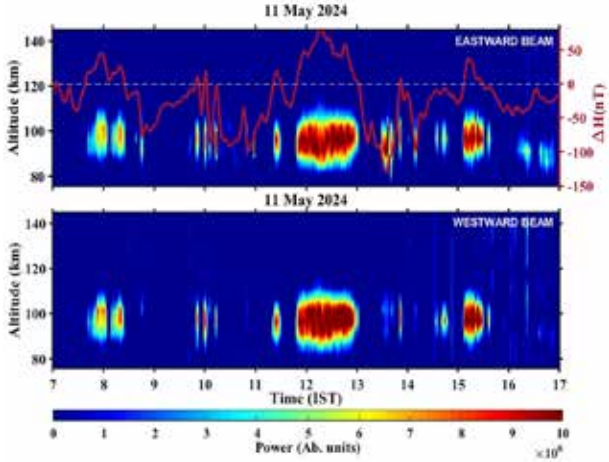

Figure 17: Backscattered power received by the 18 MHz HF radar at Thumba for eastward (top) and westward (bottom) directed beams during daytime on 11 May 2024, as a function of time and altitude. The maroon curve in the top panel represents the EEJ strength over the region [Krishnan et al., Earth and Space Sci., 2025].

Indian Network for Space Weather Monitoring (InSWIM): An initiative to observe and model the low latitude ionosphere over the Indian longitudes

The aim of this paper was to update the world scientific community on the commissioning and scientific utility of Indian Network for Space Weather Monitoring (InSWIM) network for space weather studies. As the name suggests,

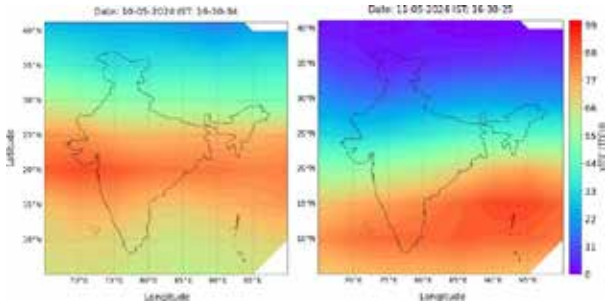

Figure 18: Comparison of the TEC map over the Indian ionospheric region on 10 May and 11 May 2024 at 16:30 IST (11:00 UT) [Choudhary et al., Adv. Space Res., 2025].

this program envisages the study of impact of Space weather on the Indian ionospheric region and develop an Ionospheric Model. The INSWIM network stations will be equipped with instruments such as Global Navigation Satellite Systems (GNSS) receivers, Low Earth Orbit (LEO) receivers, ionosondes, magnetometers, and airglow photometers/imagers. Currently, multi-frequency, multi-constellation GNSS Receiver systems are operational at various stations in India. This network will enable us to understand, (a) the quiet-time variability of the ionosphere over the Indian low-latitude region, (b) comprehensively study the response of the low-latitude ionosphere specific to the Indian longitudes under different space weather conditions, with the goal of understanding the various physical mechanisms causing variability in the ionospheric regions, and (c) develop an ionospheric model to reduce ionospheric errors in GNSS systems. Additionally, this network will provide complementary information for rocket and satellite-based experiments. The Total Electron Content (TEC) map over the Indian ionospheric region on 10 May and 11 May 2024 at 16:30 IST (11:00 UT) is generated and compared (Fig. 18). The impact of the superstorm, which had its onset at 18:00 UT on 10 May 2024, can easily be seen on 11 May 2024. In this work the details of the InSWIM network to the scientific community for its possible use in monitoring and studying the impact of space weather on the near-Earth space environment is provided.

Risk Assessment of Geomagnetically Induced Currents (GICs) Over the Indian Sector in Comparison with American and African Sectors

Geomagnetically Induced Currents (GICs) are the manifestation of adverse space weather events on the ground that pose serious threats to power grids as well as pipelines. Extensive investigations on the impact of GICs at high and mid-latitudes have been undertaken while the effects of GICs at low-latitude regions and geomagnetic equator have been relatively less explored. In this study, ground-based magnetometer data over the equatorial and low-latitude regions of the Indian, American, and African sectors are analyzed for different phases of 30 geomagnetic storm events that occurred from 2002 to 2024. The important findings of the study are summarized as follows. (i) dB/dt values greater than 90 nT/min are observed during intense geomagnetic disturbances at the equatorial regions of Indian, American, and African sectors indicating the possibility of significant GICs (Fig. 19). (ii) dB/dt values in the range of 25–40 nT/min are observed to manifest over low latitude regions during all storm phases at all three longitude sectors. (iii) Enhanced equatorial dB/dt values during daytime at all three longitude sectors during all phases of the storms indicate the role of EEJ in the localized enhancement of magnetic field perturbations. (iv) The role of Prompt penetration and Disturbance dynamo electric fields in producing dB/dt fluctuations are revealed both during day and night times. (v) The role of solar wind dynamic pressure pulses in triggering huge dB/dt values even during night time in addition to day time are unravelled. (vi) The study shows that the equatorial regions of India are also susceptible to the risk of GICs just as in the case of American and African sectors. Since India is developing large power grids which can potentially be affected by GIC effects, the present study is pertinent.

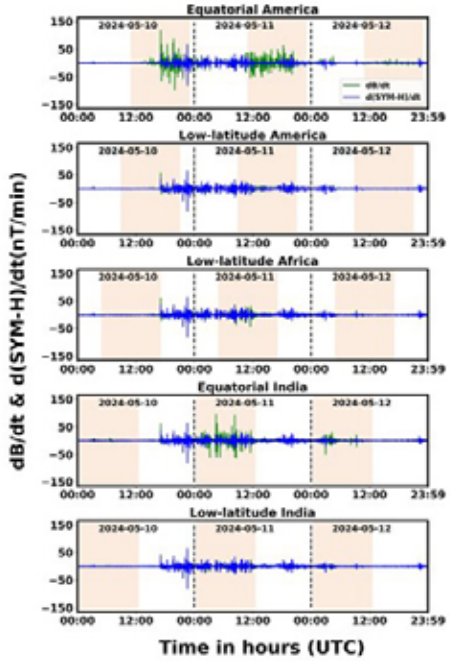

Figure 19: The dB/dt and d(SYM-H)/dt at the American, African, and Indian sectors during the May 2024 Gannon Superstorm [Vishnupriya et al, Space Weather, 2025].

Studies of Sun and Radio Occultation Technique

A novel technique for plasma asymmetry correction in Radio occultation profiling

Radio Occultation (RO) experiments often employ the geometrical optics (GO) approximation and the Abel transformation, assuming spherical symmetry of the planetary atmosphere or ionosphere to retrieve electron density profiles. This assumption is also extended to derive temperature, pressure, and neutral density profiles of the lower atmosphere. However, the assumption of spherical symmetry is not always valid and can introduce significant uncertainties in the retrieved electron density profiles. A simple retrieval algorithm is proposed, called integrated TEC (Total Electron Content) decomposition (ITD) method that accounts for ionospheric asymmetry and demonstrates the effect of solar zenith angle (SZA) variation along the ray path. Unlike traditional methods, it does not rely on the Abel transformation and avoids the assumption of spherical symmetry, making it applicable under diverse geophysical conditions. The method is applied to RO observations around Venus, obtained from the Akatsuki and Venus Express (VEX) radio science experiments. It assumes that plasma is primarily produced by solar radiation and follows the chapman distribution. The top left panel of Fig. 20 shows the electron density profiles retrieved using the ITD method for considering medium as spherically symmetric (blue curve) and asymmetric medium (red curve) for the observation conducted on July 15, 2006. Vertical dotted line shows the uncertainty associated with the observation. The top right panel of the Figure shows percentage variation in the electron density profile due to the assumption of spherical asymmetry, while the bottom panel shows variations in the solar zenith angle (SZA) along the ray path passing through the tangent height of 6051.8 km + 90 km radial distance. Results show the spherical symmetry assumption overestimates the main peak electron density by 2%–5% and the electron density at lower altitudes by 400%–800%. The proposed method offers a more accurate framework for retrieving electron density profiles, particularly in regions where the spherical symmetry assumption breaks down.

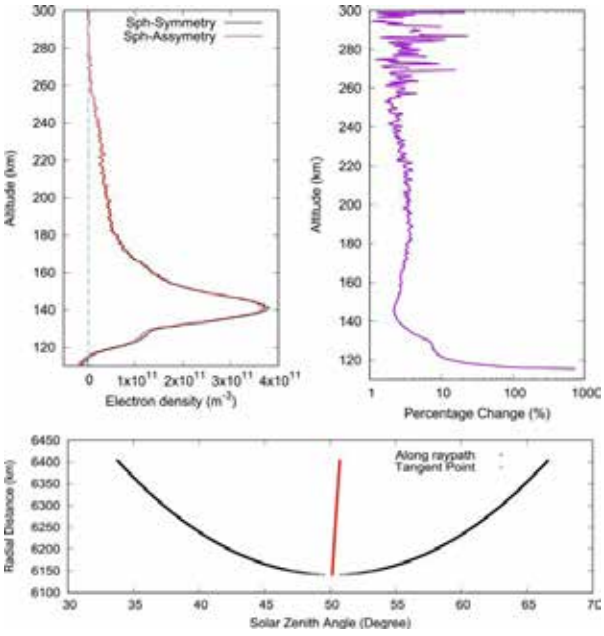

Figure 20: Top left Panel: Electron density profiles retrieved using the ITD method for considering medium as spherically symmetric (blue) and asymmetric medium (red) for the observation conducted on July 15, 2006. Vertical dotted line shows the uncertainty associated with the observation. Top right Panel: Percentage variation in the electron density profile due to the assumption of spherical asymmetry. Bottom Panel : Variation of solar zenith angle (SZA) along the ray path passing through the tangent height of 6051.8 km + 90 km radial distance. Red curve: SZA values at each tangent point [Tripathi et al., Icarus, 2025].

Insights into solar wind flow speeds from the coronal radio occultation experiment: Finding from the Indian Mars Orbiter Mission

Radio occultation measurements from the Indian Mars Orbiter Mission (MOM) during October 2021 were used to estimate solar wind velocities in the near-Sun region. The spectral broadening (second moment) in the received Telecommunication Tele Command (TTC) signal using the S band is calculated from the MOM spacecraft as opposed to the doppler (first moment) which is typically used. An empirical relationship is developed to estimate the electron density and the radial speeds of the solar wind in the near-Sun region. The approach uses only two parameters: the broadening in the received signal, and the geometry of the bodies involved in the experiment, thereby reducing the complexity, as well as getting a better estimate with reduced sources of error. The study focused on observations conducted from 2021 October 2 to October 14, a relatively quiet phase of solar cycle 25. The analysis targeted the coronal region within heliocentric distances of 5–8 R_O, near the ecliptic plane. In this region, solar wind velocities ranged from 100 to 150 km/s, while electron densities were on the order of 10^{10} m^{-3}. The results are compared with electron density observations and

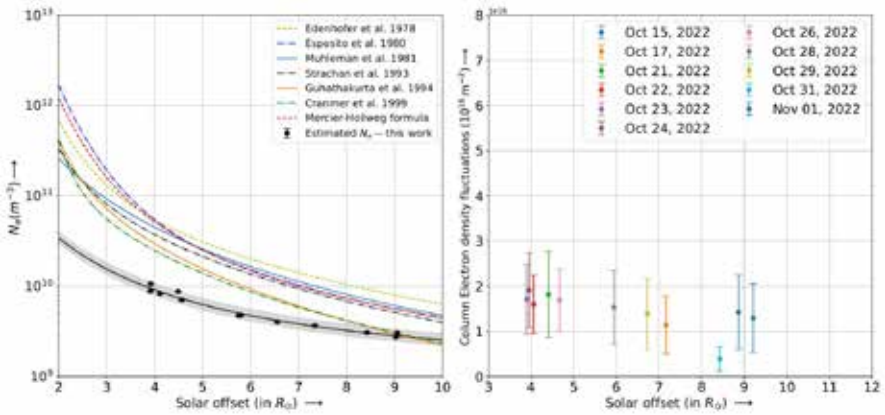

Figure 21: Left panel: Electron density estimates for the 2022 solar occultation experiment compared against other models in the literature. Right panel: Fluctuations in the column density during October 2022 [Aggarwal et al., Astrophys. J., 2025].

models derived from previous studies (Fig. 21). Though the decrease in the electron densities with respect to increasing heliocentric distance matches quite well with the theoretical models, MOM estimates fall at the lower edge of the distribution. This difference was linked to the prolonged weak solar activity during the MOM observations, in contrast to prior studies conducted during periods of comparatively higher solar activity in earlier solar cycles.

Estimation of solar wind velocity under varying solar activity using the radio science experiment

Extending the technique to calculate solar wind parameters from the spectral broadening (second moment), solar wind dynamics is studied based on Doppler spectral width measurements of X-band radio signals from the Japanese Akatsuki spacecraft. The data set included two solar conjunction occultation experiments conducted in 2016 and 2022, capturing the transition from the descending phase of solar cycle 24, a period of low solar activity, to the ascending phase of solar cycle 25, which exhibited moderate to intense activity. The study demonstrated the utility of this technique for estimating both slow and fast solar wind velocities across different phases of solar activity. A key focus was the 2022 experiment, which probed the solar corona near coronal holes at heliocentric distances ranging from 1.4 to 10 $R_\odot$. In addition, the impact of electron density estimates on the accuracy of solar wind speed determinations is investigated. Akatsuki results compared against the solar wind measurements done across a period of more than 50 years, using a variety of methods from in-situ to remote sensing observations (Fig. 22). The velocity profile of the solar wind within a polar coronal hole, derived from observations made using Skylab's white-light instruments is depicted by Curve 1. Additional models for the volume velocity of the solar wind with and without contributions from MHD waves are represented by Curves 2 and 3 defined in previous studies. Present results demonstrated reliable retrieval of both slow and fast solar wind speeds across heliocentric distances of 1.4–10 $R_\odot$, including regions near coronal holes. The results also demonstrated that the accurate solar wind estimates critically depend on improved electron density modelling.

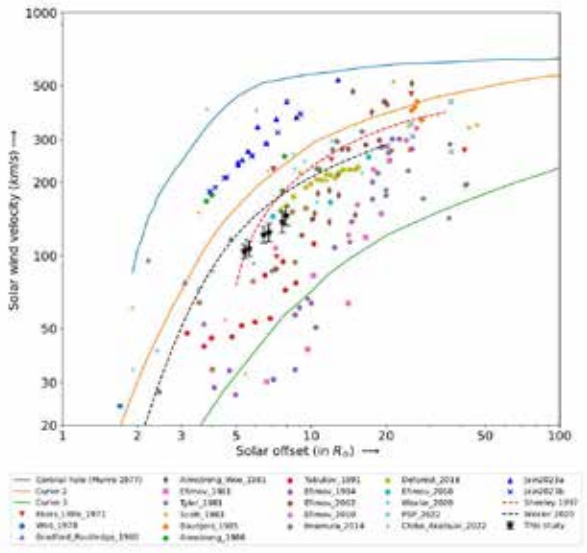

Figure 22: Akatsuki results compared against the solar wind measurements done across a period of more than 50 years, using a variety of methods from in-situ to remote sensing observations. The velocity profile of the solar wind within a polar coronal hole, derived from observations made using Skylab's white-light instruments, is depicted by Curve 1. Additional models for the volume velocity of the solar wind with and without contributions from MHD waves are represented by Curves 2 and 3 from previous studies [Aggarwal et al., Mon. Not. R. Astron. Soc., 2025].

A theoretical perspective on the impact of stochastic plasma in solar flare turbulence under thermal X-ray background

Magnetohydrodynamic (MHD) turbulence during the impulsive phase of solar flares is known to drive stochastic and non-stochastic plasma motions, influencing background x-ray emissions. In the study, the impact of stochastic plasma is investigated by modelling with a Gaussian temperature distribution from 10 to 40 MK, representative of X-class solar flares, using RHESSI observations, on theoretically assumed background X rays in the 1–10 keV range. Using statistical models under the hydrodynamic approximation of turbulence, particularly second-order structure functions, optical turbulence intensity and coherence properties of the X rays is estimated. A consistent ~ 2% reduction in turbulence intensity was observed with increasing turbulence and coherence length scales. A schematic diagram of MHD turbulence during chromospheric evaporation in the solar flare is presented in Fig. 23. Various length scales of the turbulence and paths of scattered thermal X-rays are shown in this sketch. The twisted curve shows the fluctuating magnetic field lines in the solar flare. The pink arrow indicates the direction of chromospheric evaporation in the standard solar flare model. The spatial variation of turbulence intensity is non-linearly distributed. The simulation results demonstrate fluctuations in the X-ray intensity in turbulent solar flare plasmas due to thermal impact and offer new insight into the role of MHD turbulence in shaping background x-ray emission.

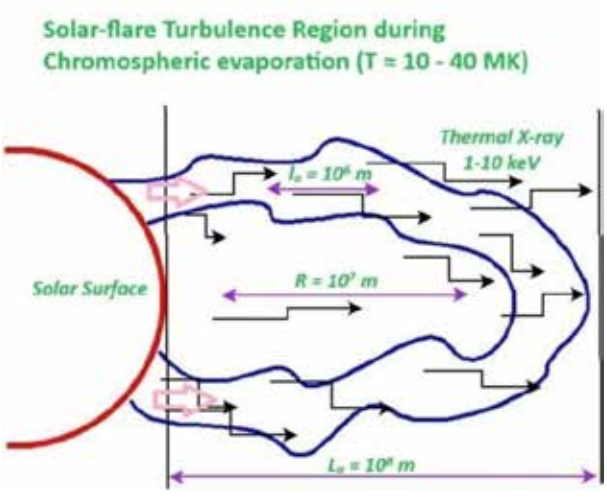

Figure 23: A schematic diagram of MHD turbulence during chromospheric evaporation in the solar flare. Various length scales of the turbulence and paths of scattered thermal X-rays are shown in this sketch. The twisted curve shows the fluctuating magnetic field lines in the solar flare. The pink arrow indicates the direction of chromospheric evaporation in the standard solar flare model. The spatial variation of turbulence intensity is non-linearly distributed [Pramod and Choudhary, Phys. Plasma, 2025].

Lunar Science

In situ ionospheric observations near lunar south pole by the Langmuir Probe on Chandrayaan-3 Lander

In situ measurements of the near surface lunar plasma environment are made using the RAMBHA-LP (Radio Anatomy of the Moon Bound Hypersensitive ionosphere and Atmosphere-Langmuir Probe) payload onboard India's Chandrayaan-3 Lander during lunar daytime (2023 August 24 to 2023 September 2). These observations provide estimates of near surface (2 m above the surface) lunar electron density and electron temperature from the south polar region, 'for the first time'. The estimations reveal the daytime lunar plasma to have mean electron density (*Ne*) in the range of 380–600/cc and mean electron temperature (*Te*) in the range of 3000–8000 K (Fig.24). The critical roles of solar wind and the Earth's magnetospheric particle flux in modulating the lunar dayside ionosphere outside and inside the Earth's geomagnetic tail, respectively, are unravelled using RAMBHA-LP observations and lunar ionospheric model simulations. The study also highlights the role of molecular species in the genesis of lunar near surface plasma environment.

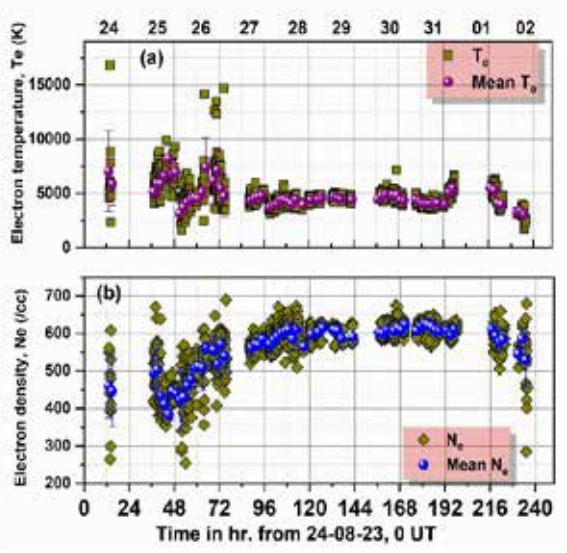

Figure 24. Temporal variations of (a) electron temperature (Te) and its 2 hourly mean, (b) electron density (Ne) and its 2 hourly mean during the period from August 24 to September 2, 2023 [Manju et al,. Mon. Not. R. Astron. Soc., 2025].

Lunar ionosphere in the geotail region as observed by Chandrayaan-2 orbiter using two-way radio occultation measurements

First electron density profile of the Lunar ionosphere when the Moon is inside the geomagnetic tail region has been presented. The S-band telemetry and telecommand radio signals in a two-way mode are used for the radio occultation experiment from Chandrayaan-2 orbiting the Moon. The radio signals were tracked using an 18 m diameter antenna at the Indian Deep Space Network (IDSN). The IDSN served as an active source for generating and receiving the radio signal, while the onboard oscillator on CH-2 was used as a passive receiver and transmitter. The transmitted radio signal passed twice through the lunar plasma medium before reaching the receiver end. The study found a high electron density of approximately 2.5×10^4 cm^{-3} close to the surface of the Moon (~2 km altitude). Three-dimensional lunar ionospheric model simulations showed that to achieve such high plasma density, the plasma should be in photochemical equilibrium, which is possible inside the geomagnetic tail only in the presence of lunar crustal magnetic fields. The integrated Total Electron Content (TEC) observed on 2022 November 8, 18:00 UTC, near the north pole at 74° latitude and 84°W longitude and the corresponding electron density profile (EDP) is obtained (Fig. 25). The model also introduced a localized reduction in Ar and Ne neutral density to align with previous observations near the lunar pole.

Technology Development

Ionospheric D region observations over the equatorial location of Thiruvananthapuram using an in house developed VLF receiver

The lowermost region of ionosphere is referred to as the D region. The integrated conductivity of D & E region determines the Electrojet current as well as Electric fields, thereby affecting the whole equatorial and low latitude electrodynamics. Space weather events like geomagnetic storms, solar flares and eclipses can lead to large enhancement/ depletion of ionization in D region, thereby affecting various ionospheric processes over dip equatorial ionosphere. As a result, Very Low frequency (VLF) radio signals propagating through D region gets modified. These changes in VLF signals can be used to understand the D region ionization density and its variability's. Hence a VLF receiver is developed in-house at SPL, VSSC for understanding the equatorial D region dynamics. The VLF receiver is operational at Ponmudi from 3/02/2025 and has a range of 1 kHz to 50 kHz.

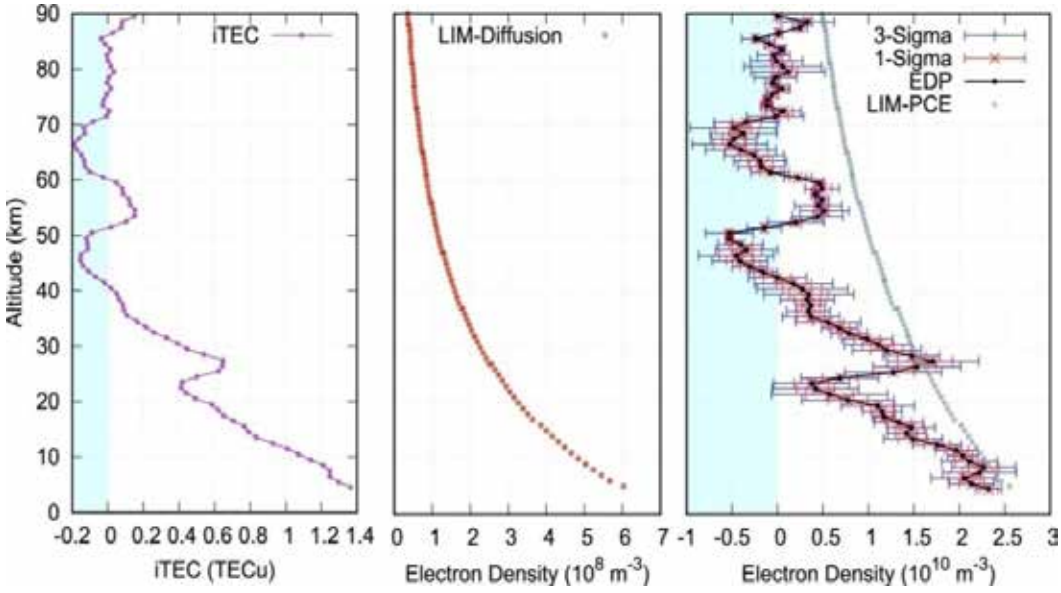

Figure 25: Left panel: the integrated TEC observed on 2022 November 8 at 18:00 UTC, near the north pole at 74° latitude and 84°W longitude, and the corresponding electron density profile (EDP) is shown in the right panel (black curve). The error bar in blue and red color indicate the σ and 3σ variation in electron density, respectively, with σ representing the standard deviation. The area shaded in cyan has negative electron density, which stands for noise. The gray-colored profile represents the lunar ionospheric model (LIM) output, and PCE stands for photochemical equilibrium. Middle panel: simulated EDP at the observation site when the Moon is inside the geotail in the absence of a crustal magnetic field [Thripathi et al., Astrophys. J. Lett., 2025].

Technology Development

ENWi and LP probes for Kulasekarapattinam flight

Development of ENWi probe in ion mode as well as LP probe for constant potential mode and sweep mode is ongoing. The probes have been fabricated and the vibration and constant acceleration tests are completed.

Characterization of the ATomic OXygen Sensor (ATOXS)

The laboratory model of the ATomic OXygen Sensor has been successfully designed, developed and characterized under varying vacuum levels, substrate temperatures, and atomic oxygen (AO) flux levels. The characterization curve of ATOXS sensor is depicted in Fig.26. The performance of ATOXS was found to be nominal across the different AO flux levels tested, ranging from 4.5 x 10^{13} AO cm^{-2} s^{-1} to 25.5 x 10^{13} AO cm^{-2} s^{-1}. The test results demonstrate that the sensor exhibits consistent responses to variations in AO flux levels expected at POEM-4 orbit. These findings indicate that flying the sensor on-board POEM or any Low-Earth Orbit satellite could enable the measurement of AO density profiles in the 250 to 350 km altitude range across multiple geographic locations, depending on the mission's orbital inclination. Furthermore, similar AO flux levels are expected to be encountered by satellites in circular orbits between 400 and 500 km. At 400 km, AO densities range from 6.4×10^{6} /cm^3 to 3.5×10^{8}/cm^3, and at 500 km, from 3.5×10^{5}/cm^3 to 9.9×10/cm^3, varying between solar minimum and maximum conditions. These observations indicate that the sensor could also be effectively utilized onboard such satellites longer duration missions. While the sensor shows promising performance, certain aspects require further refinement. Improvements will be incorporated into forthcoming iterations to get better accuracy and durability. The entire design, development and characterization process has been documented in detail in VSSC technical reports (ISRO-VSSC-TR-0417-0-25, ISRO-VSSC-TR-0369-0-25).

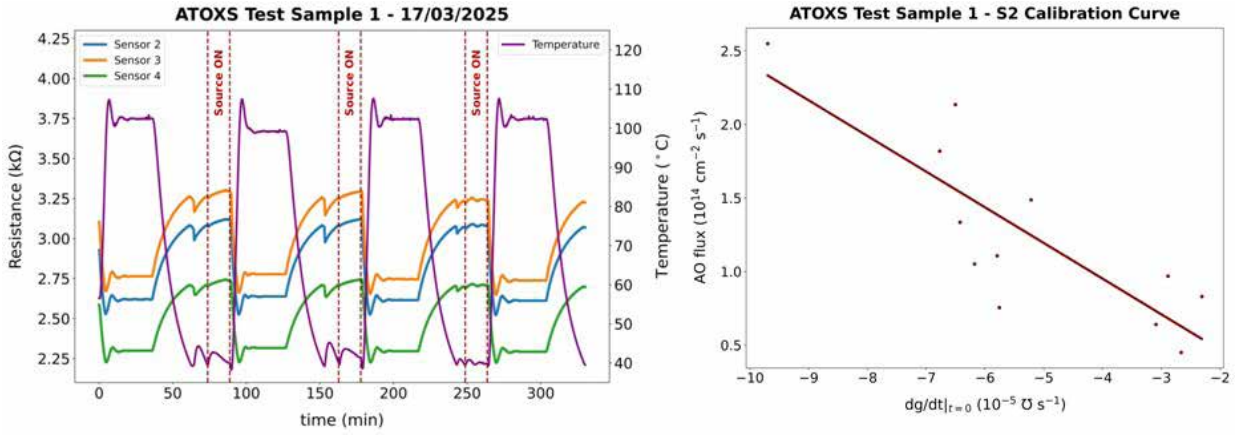

Figure 26: Calibration curves of ATOXS.

Ongoing Activities and Future Projections

- The development of payloads for ISRO's forthcoming earth and planetary missions: NMS and UrVASI for DISHA mission, RAVI for the Venus Orbiter Mission.
- Development, testing and delivery of Reusable Atomic Oxygen Sensor for future POEM orbiter mission.
- Development of an Thermospheric Ion Composition Explorer for the POEM and aeronomy missions.
- Development of mass spectrometer and QCM-based atomic oxygen sensor and Rocket borne Airglow Photometers for sounding Rocket platform (RH300 and RH 560).
- Studies on the manifestations of the interactions of northward oriented interplanetary magnetic field with Earth's magnetosphere in the thermosphere-ionosphere system.
- Integrated studies on Earth's magnetosphere, ionosphere, thermosphere as a system and explore its behaviour as system using data/measurements and models, with new and comprehensive results to follow.

- Addressing the day-to-day variability in the equatorial ionosphere, irregularities therein, their onset, evolution and duration, based on in-situ measurements, space borne observations and modelling.
- Solar wind turbulence in the interplanetary medium involving Radio Science Experiments through ISRO's existing and forthcoming planetary missions.
- Monitoring and modelling the impact of space weather specifically over the Indian region using ionosondes, multi-wavelength nightglow photometers and multi-constellation multi-frequency receivers to be installed at the INSWIM stations.
- Development of AI based model for investigating and predicting the impact of space weather on ionosphere-thermosphere system.

Publications in Peer-Reviewed Journals

1. Aggarval.,K., Choudhary, R. K., Abhirup, D., Roopa M. V., Bijoy K. D., "Insights into Solar Wind Flow Speeds from the Coronal Radio Sounding Experiment : Findings from the Indian Mars Orbiter Mission", The Astrophysical Journal, https://doi.org/10.3847/1538-4357/adb627, 2025.
2. Aggarval.,K., Choudhary, R. K., Abhirup, D., Imamura, T., "On the estimation of solar wind velocity under varying solar activity conditions using Akatsuki measurements", Monthly Notices of the Royal Astronomical Society, https://doi.org/10.1093/mnras/staf1305, 2025.
3. Ajay, P., Choudhary, R. K., Surendra Sunda, "Geometric Mean Algebraic Reconstruction Technique: A tool for ionospheric tomography using GNSS receiver system", RAS Techniques and Instruments, https://doi.org/10.1093/rasti/rzaf015, 2025.
4. Ambili, K. M., Choudhary, R. K., Ashok, A., Ajay, P., Vineeth, C., Pant, T. K., "The impact of 11 May 2024 great geomagnetic storm on the plasma distribution over the Indian equatorial/low latitude ionospheric region", Journal of Geophysical Research: Space Physics, https://doi.org/10.1029/2024JA033368, 2025.
5. Ando H., Noguchi, K., Imamura, T., Takagi, M., Sugimoto, N., Matsuda, Y., Tellmann, S., Patzold, M., Hausler, B., Choudhary, R. K., Antonita, M., "Vertical propagation of Venusian thermal tides above and below clouds revealed by Akatsuki radio occultation", Journal of Geophysical Research: Planets, https://doi.org/10.1029/2025JE009165, 2025.
6. Ando, H., Noguchi, K., Imamura, T., Takagi, M., Sagawa, H., Yamazaki, A., Oschlisniok, J., Tellmann, S., Patzold, M., Hausler, B., Joo Lee, Y., Choudhary, R. K., Antonita, M., "Long-term variability of the thermal structure in Venus's low-latitude atmosphere investigated using Venus Express and Akatsuki radio occultations". Journal of Geophysical Research: Planets, https://doi.org/10.1029/2025JE009218, 2025.
7. Archana, R. K., Vineeth, C., Pant, T. K., "Short and Long-Term Variations in geomagnetic external field: Study based on 104 years of geomagnetic observations from the Indian low latitude station- Alibag, Journal of Geophysical Research: Space Physics, https://doi.org/10.1029/2025JA034632, 2025.
8. Ashna V. M., Bhaskar Ankush, Manju G., Sini R., "Solar wind – magnetosphere coupling efficiency and its dependence on solar activity during geomagnetic storms of 23-24 solar cycles", Journal of Geophysical Research: Space Physics, e2023JA031687, https://doi.org/10.1029/2023JA031687, 2024.
9. Ashok, A., Ambili, K. M., Choudhary, R.K., "Do the vertical movements of the peak height of F region truly represent the vertical E×B plasma drift velocity over the dip equator?", Journal of Geophysical Research: Space Physics, https://doi.org/10.1029/2024JA033202, 2025.
10. Ashok, A., Ambili, K. M., Choudhary, R. K., Lu, G., "Unique signatures of meridional wind variations on the electron density distribution over the dip equator", Geophysical Research Letters, https://doi.org/10.1029/ 2024GL117926, 2025.
11. Choudhary, R. K., Ambili, K. M., Vineeth, C., Potdar, A., Hossain, M. M, Pant, T. K., "Indian Network for Space Weather Impact Monitoring (InSWIM): An initiative to observe and model the low latitude ionosphere over the Indian longitudes", Advances in Space Research, https://doi.org/10.1016/j.asr.2024.11.025, 2025.

12. Chowdhury, S., Choudhary, R.K. and Subrahamanyam, D.B., "Did the 'Tauktae' Cyclone Impact the Upper Atmosphere through Traveling Ionospheric Disturbances? A Case Study Over the Arabian Sea using Measurements from InSWIM Network Stations", Advances in Space Research, https://doi.org/10.1016/j.asr.2024.11.012, 2025a.

13. Chowdhury, S., Subrahamanyam, D. B., Choudhary, R. K., "First Observational Investigation on the Temporal Trends of Vertical Total Electron Content (VTEC) over an Equatorial Station: Discerning the Impacts of Mora and Ockhi-two Tropical Cyclones in 2017", Advances in Space Research, https://doi.org/10.1016/j.asr.2024.11.078, 2025b.

14. Gokularam, M., Prasenjit, K. M., Sheetal, K., Keshav, R. T., Choudhary, R. K., "Improved Frequency Estimation for Radio Occultation through Chirp Z-Transform and Adaptive Slicing", RAS Techniques and Instruments, https://doi.org/10.1093/rasti/rzaf026, 2025.

15. Jain A., Richa, T., Sudhir, J., Choudhary, R.K., "Effects of the Super Intense Geomagnetic Storm on 10-11 May, 2024 on Total Electron Content at Bhopal", Advances in Space Research, https://doi.org/10.1016/j.asr.2024.09.029, 2025.

16. Krishnan, L. G., Shiokawa, K., Pant, T. K., Vichare, G., "Signatures of the long duration prompt penetration electric field in the 18 MHz HF radar observations over Thumba". Journal of Geophysical Research: Space Physics, https://doi.org/10.1029/2024JA033140, 2025a.

17. Krishnan, L. G., Shiokawa, K., Pant, T. K., Lu, G., Shreedevi, P. R., Otsuka, Y., Sunda, S., "Responses of the Daytime Low and Equatorial Ionosphere and Thermosphere over the Indian Region During the Geomagnetic Storm of April 2023". Journal of Geophysical Research: Space Physics, https://doi.org/10.1029/2024JA033141, 2025b.

18. Krishnan, L. G., Pant, T. K., Manu, T., Vineeth, C., Jose, L., Yaqub, R. S., et al., "Indian equatorial ionosphere under the influence of the May 2024 geomagnetic storm: Insights into electric fields, plasma irregularities and F-region dynamics". Earth and Space Science, https://doi.org/10.1029/2024EA004116, 2025.

19. Manju G., Mridula, N., Sruthi, T. V., "Impact of an eclipse on the Indian equatorial ionosphere thermosphere system: A case study", Advances in Space Research, https://doi.org/10.1016/j.asr.2025.03.068, 2025.

20. Manju, G., Pant, T. K., Mridula, N., Md. Mosarraf Hossain, Ambili, K. M., Pradeep Kumar, P., Sruthi, T. V., Vishnupriya, K. S., Satheesh Thampi, R., Aneesh, A. N., Keshav, R. T., Sreelatha, P., Rosmy John, "In situ ionospheric observations near lunar south pole by the Langmuir Probe on Chandrayaan-3 lander", Monthly Notices of the Royal Astronomical Society, https://doi.org/10.1093/mnras/staf1276, 2025.

21. Pant, T. K., Manju G, Nizy Mathew, Pradeepkumar P, Johns Paul, Sreelatha P, Satheesh Thampi, Mridula N, Md. Mosarraf Hossain, Dinakar Prasad Vajja, Aasik V, Satheesh Chandran M, Kiran John Antony, Renju R, Tanmay Singhal, Pramod P.P, Sajeev R, Suresh R, Sunitha K, Jiju John, Thamarai V, Teena Choudhary, M.M. Mehra, K.Durga Prasad. "Chandrayaan-3 Lander Payloads and Science", Journal of Aerospace Sciences and Technologies, https://doi.org/10.61653/joast.v76i3a.2024.1006, 2024.

22. Pramod, K., P. and Choudhary, R. K., "Probing the Impact of Stochastic Plasma in Solar Flare MHD Turbulence on Thermal X-ray Background: A Theoretical Study", Physics of Plasmas, https://doi.org/10.1063/5.0283070, 2025.

23. Ram S.P., T. K., Sripathi, S., Rout, D., Bhaskar, A., Scipion, D. E.,"IMF By-driven electric field disturbances over the equator during northward IMFs: PPEF responses", Journal of Atmospheric and Solar Terrestrial Physics, https://doi.org/10.1016/j.jastp.2025.106642, 2025.

24. Shimna, K., Vineeth, C., Choudhary, R. K. , Pant, T. K., "On the Response of Equatorial and Low Latitude Ionosphere over Indian Region to the Tropical Cyclones", Advances in Space Research, https://doi.org/10.1016/j.asr.2025.03.017, 2025.

25. Shimna, K., Archana, R. K., Vineeth, C., Lu, G., Pant, T. K., Vijayan, M. S. M., "Impact of the Gannon

Superstorm on the equatorial ionization anomaly dynamics during its recovery phase on 11 May 2024", Space Weather, https://doi.org/10.1029/2025SW004428, 2025.

26. Shimna, K., Archana, R. K., Vineeth, C.,Lu, G., Pant, T. K., & Vijayan, M. S. M. "Rapid reversal of hemispheric asymmetry in the intensity of EIA crests during the geomagnetic storm of 23 April2023: A unique observation from GOLD", Geophysical Research Letters, https://doi.org/10.1029/ 2025GL117213, 2025.
27. Sreeba, S., Manju, G., Pant, T. K., "Multi-instrument investigation of the preseismic ionospheric response to 2021 Haiti earthquake", Earth and Space Science, https://doi. org/10.1029/2025EA004394, 2025.
28. Thripathi, K. R., T., Imamura, T., Choudhary, R. K., "A novel technique for plasma asymmetry correction in radio occultation profiling", Icarus, https:// doi.org/ 10.1016/j.icarus.2025.116670, 2025.
29. Thripathi, K. R., Choudhary, R. K., Ambili, K. M., "Lunar ionosphere in the Geotail region as observed by Chandrayaan-2 Orbiter using two-way Radio Occultation measurements", The Astrophysical Journal, Letters, https://doi.org/ 10.3847/ 2041-8213/a db3a7, 2025.
30. Vishnupriya, K. S., Manju, G, "Risk assessment of geomagnetically induced currents (GICs) over the Indian sector in comparison with American and African sectors", Space Weather, https://doi. org/10.1029/ 2024SW004133, 2025.
31. Yadav, V. K., Choudhary, R. K., Midhun Gautam, M., "Observations of the fluctuations in Interplanetary Magnetic Field around L1 point during the solar transient events of 2024 with MAG payload onboard Aditya-L1 spacecraft", The Astrophysical Journal, https://doi.org/10.3847/1538-4357/ae00b6, 2025.

Publications in Proceedings

1. Manju G., Pant, T. K., Mridula, N., Ambili, K. M., Mosarraf Hossain, Sruthi, T. V., Vishnupriya, P., Satheesh Thampi, R., Abhishek, J. K., Aneesh, A. N., Johns Paul, Pradeep Kumar, P., Sreelatha, P., Rosmy John, "Exploration of lunar plasma environment using RAMBHA-LP onboard Chandrayaan-3 lander", Proceedings of GLEX 2025, 7-9 May 2025, New Delhi, India.
2. Ambili, K. M., "Relevance and scope of planetary ionospheric modelling", Proceedings of GLEX 2025, New Delhi, 7-9 May 2025.

Presentation in Symposia/Conferences/Workshops

1. Saumyaneal Banerjee, "Sulfuric Acid and Sulfur Dioxide vapor concentrations in the lower atmosphere of Venus using the Radio Occultation Technique. ", 43rd annual meeting of The Astronomical Society of India, National Institute of Technology Rourkela, 15-19 February 2025.
2. Raj Kumar Choudhary, "Exploring the characteristic Features of the Venus Ionosphere Using Physics based Ionospheric Model and Observations", Interntional conference on Space for Sustainability : Science, Technology, Education and Policy & 6th Indian Planetary Dcience Conference (IPSC-2025) , IIT Roorkee, 04-07 March 2025.
3. Ambili, K. M., Relevance and scope of planetary ionospheric modelling, IAF Global Space Exploration Conference (GLEX 2025), New Delhi, India, 7-9 May 2025.
4. Manju G. Pant, T. K., Mridula, N., Ambili, K. M., Mosarraf Hossain, Sruthi, T. V., Vishnupriya, P., Satheesh Thampi, R., Abhishek, J. K., Aneesh, A. N., Johns Paul, Pradeep Kumar, P., Sreelatha, P., Rosmy John, "Exploration of lunar plasma environment using RAMBHA-LP onboard CHANDRAYAAN-3 Lander," GLEX 2025, New Delhi, India, 7-9 May 2025. '
5. Ambili, K. M., "Radio Anatomy of Venus Ionosphere (RAVI): Ionospheric measurements", National Meet on ISRO's Venus Orbiter Mission- Science and Enhancing Academia Engagements, Science Programme Office, ISRO Headquarters, Bengaluru, 29-30 October 2025.

6. Raj Kumar Choudhary, "Radio Anatomy of Venus Ionosphere (RAVI): Atmospheric measurements", National Meet on ISRO's Venus Orbiter Mission- Science and Enhancing Academia Engagements, Science Programme Office, ISRO Headquarters, Bengaluru, 29-30 October 2025.

Technical Reports

1. Ayisha M Ashruf, "Earth's Radiation Environment in POEM-4 Orbit", ISRO-VSSC-TR-0507-0-24, October 2024.
2. Ayisha M Ashruf, Vineeth, C., Pramod, P. P., Ashok, K., Mahesh, S., Jinesh, K. B., Roshith, K. R., "Characterization of the ATomic OXygen Sensor (ATOXS) for Low-Earth Orbit Applications", ISRO-VSSC-TR-0369-0-25, June 2025.
3. Ayisha M Ashruf, Vineeth, C., Pramod, P. P., "ATomic OXygen Sensor (ATOXS) - Design, Development and Characterization", ISRO-VSSC-TR-0417-0-25, July 2025.

ग्रहीय विज्ञान शाखा
PLANETARY SCIENCE BRANCH

ग्रहीय विज्ञान शाखा (पीएसबी) सूर्य, ग्रहों, चंद्रमाओं तथा धूमकेतुओं के मॉडलिंग तथा प्रयोगात्मक अन्वेषण में प्रयासरत है। यह मुख्यतः तीन प्रमुख विषयों पर केंद्रित होता है। (क) सौर पवन तथा इसका सौरमंडल के ग्रहों तथा अन्य ग्रहीय पिंडों के साथ परस्पर क्रिया (ख) सौर विकिरण की ग्रहीय वायुमंडल के साथ परस्पर क्रिया तथा इनकी परस्पर क्रिया से उत्पन्न प्रक्रम (ग) ग्रहीय पिंडों के वायुमंडल की संरचना तथा इनकी गतिकी। इन उद्देश्यों की पूर्ति हेतु यह समूह, सौर पवन प्लाज़्मा, अंतरग्रहीय तथा ग्रहीय चुंबकीय क्षेत्रों, साथ ही प्लाज़्मा के अभिलक्षणों तथा ग्रहीय वायुमंडल के निरावेशी कणों के मापन हेतु अत्याधुनिक वैज्ञानिक प्रदायभारों की संकल्पना, अनुकरण, अभिकल्पना तथा विकास का कार्य करता है।

The Planetary Science Branch (PSB) carries out experimental and modeling investigations of the Sun, planets, moons and comets, mainly focusing on three major themes: (a) Solar wind and its interaction with solar system planets and planetary bodies, (b) Interaction of solar radiation with planetary atmospheres and the processes initiated through this interaction, and (c) Dynamics and composition of the atmospheres of planetary bodies. To realize these objectives, PSB undertakes the conceptualization, simulations, design, and development of state-of-the-art scientific payloads for the measurement of solar wind plasma, interplanetary and planetary magnetic fields as well as the characteristics of plasma and neutrals in planetary atmospheres.

वैज्ञानिक टीम / Science Team
सतीश तंपी आर / Satheesh Thampi R.
स्मिता वी तंपी / Smitha V. Thampi
विपिन कुमार यादव / Vipin Kumar Yadav
धन्या एम बी / Dhanya M. B.
वेंकटरामन वी / Venkataraman V.
अंकुश तुकाराम भास्कर / Ankush Tukaram Bhaskar
चेमुकुला मात्तिन यादव / Chemukula Mathin Yadav
रूबिया आर / Rubia R.*
प्रितेश मेश्राम / Pritesh Meshram

तकनीकी टीम / Technical Team
दिनकर प्रसाद वज्जा / Dinakar Prasad Vajja
अनीश ए एन / Aneesh A. N.

अनुसन्धान सहयोगी /Research Associate
गोविंद जी नंपूतिरी / Govind G. Nampoothiri#

अनुसन्धान अध्येता /Research Fellows
इंदु वेणुगोपाल / Indu Venugopal
शिबोतोष बिस्वास / Shibotosh Biswas
चॉंदनी पी / Chandhini P$

**Joined in July 2025*
#Relieved in October 2025
$Joined in January 2025

Solar Wind, Interplanetary Magnetic Field and Planetary Space Weather

Simulating the Arrival of Multiple Coronal Mass Ejections that Triggered the Gannon Superstorm on May 10, 2024

The May 10, 2024 space weather event stands out as the most powerful storm recorded during the current solar cycle. This study employs an in-house developed numerical framework based on the open source semi-empirical coronal model, HUXt (Heliospheric Upwind eXtrapolation with time-dependence) and cone models, named the Solar Transient ARrival (STAR) framework, to forecast solar wind velocity and the arrival of coronal mass ejections (CMEs) associated with this event. The simulations were also carried out using Space Weather Adaptive SimulaTion (SWASTi) and a drag-based model (DBM) for this complex event of multiple CMEs. Predicted arrival times and velocities from these models are compared with actual observations at the Sun-Earth L1 point. Fig.1 shows the snapshots of the radial maps from these simulations. These simulations reveal that three CMEs reached Earth nearly simultaneously, resulting in the extreme space weather event, followed by the arrival of a few more eruptions. The simulations accurately predicted arrival times with a discrepancy of approximately 5 hours or less for these CMEs. Further, the ensemble study of DBM shows the sensitivity of the CME arrival time to the background solar wind speed and drag parameters. All three models have done fairly well in reproducing the arrival time closely to the actual observation of the CMEs responsible for the extreme geomagnetic storm of May 10, 2024. These rare solar storms offered a unique opportunity to thoroughly evaluate and validate our advanced models for predicting their arrival on the Earth.

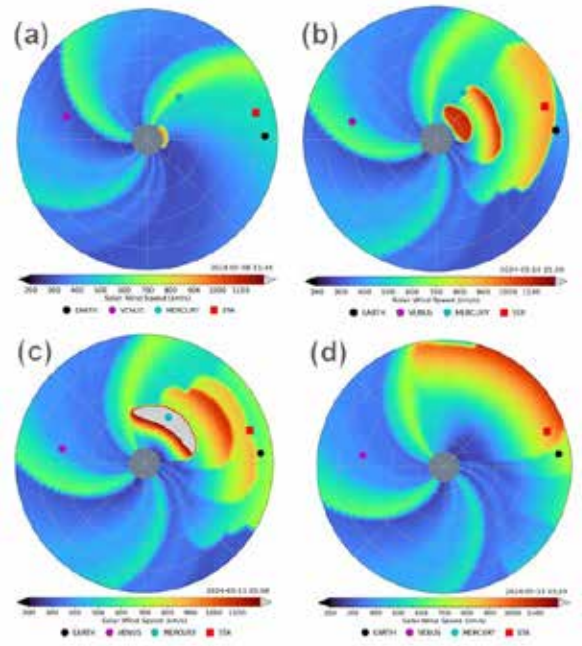

Figure 1: Snapshots from the STAR simulations. The solar wind velocity is shown in color. Different CMEs can be seen. The positions of Mercury, Venus, Earth, and STEREO-A spacecraft are also shown. The UTC corresponding to each snapshot is given in the figure [Thampi et al., Astrophys. J., 2025].

Pinching of ICME flux rope: unprecedented multipoint observation of internal magnetic reconnection during Gannon's superstorm

The large-scale magnetic reorientation of the interplanetary magnetic field (IMF) inside one of the coronal mass ejections (CMEs), during the extreme solar storm on May 10, 2024 is presented in this study. High-resolution multipoint measurements with the help of a total of seven satellites: NASA's ACE, Wind, STEREO-A, ARTEMIS-P2, MMS, NASA-NOAA joint mission DSCOVR, and ISRO's ADITYA-L1, have revealed an ongoing magnetic reconnection process inside a CME magnetic cloud. On 10th May 22:05:00 UT, L1-orbiting spacecraft detected a drastic rotation of the IMF B_y component, along with a sharp change in the orientation of IMF B_z. The plasma density and temperature show local enhancements, with a low plasma beta, confirming that the region is within a magnetic cloud. In situ particle data from WIND spacecraft demonstrate a sudden intensification of both electron and ion flux, and an isotropic pitch-angle distribution of suprathermal electrons confirms the presence of a magnetic reconnection outflow region.STEREO-A, situated at the furthest, displays signatures of two well-separated Magnetic clouds. In contrast, observations at L1 show merging of the two CMEs. Minimum variance analysis and 2D hodograms of the magnetic field also revealed deformation at L1 compared to a relatively smooth variation of the CME flux rope at STEREO-A. It is evident from these observations that, due to the margin of two CMEs, the leading magnetic cloud was compressed and deformed, which induced a large-scale current sheet and subsequently triggered magnetic reconnection. The reconnection extent was as large as 200 RE (~ 1.3 million kilometers) across the GSE (geocentric solar ecliptic) Y direction. Moreover, the same reconnecting feature was tracked near the Moon by ARTEMIS-P2 and near Earth's magnetosphere by MMS, which indicated the reconnection was quasi-steady up to 35

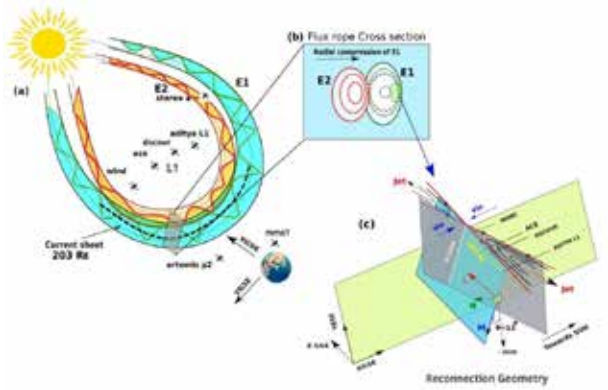

Figure 2: Artistic illustration of the ICME–ICME interaction and embedded magnetic reconnection site. Panel (a) describes the interaction of two ICME MCs on 2024 May 10. Two prominent MCs (E1 and E2) are marked in green and yellow, respectively, in the GSE coordinate system, along with all the spacecraft's tentative positions. The internal magnetic reconnection current sheet is marked with a black dashed line inside E1 MC spanning 203 RE along the dawn–dusk direction. Panel (b) represents the cross-sectional view of the reconnection site, indicating the structural deformation of E1 due to intense compression from the trailing MC E2. Panel (c) displays the 3D reconnection geometry in the GSE and local boundary-normal coordinate system. All spacecraft around the L1 point probed the same reconnection outflow jet. The ecliptic plane is shown in green, while the sky-blue plane represents the plane containing the reconnection X-LINE, which lies along the M direction and is inclined to -ZGSE at 12°. This sketch is for illustration purposes only and not to scale [Biswas et. al., Astrophys. J. Lett., 2025].

minutes. Fig. 2 shows the artistic illustration of the ICME–ICME interaction and embedded magnetic reconnection site. This study holds a significant impact not only on the dynamics of solar extreme events but also on the geo-effectiveness of the solar storms on planetary magnetospheres.

Electrodynamic forcing of the Dusk side ionosphere of Earth and the resulting super-fountain effect during the May 2024 Gannon Superstorm

The Equatorial Ionization Anomaly (EIA) is a large scale ionospheric structure formed by the upward E × B drift near the magnetic equator, which lifts plasma to higher altitudes before it diffuses along magnetic field lines to form two crests on either side of the equator. This process becomes highly sensitive to geomagnetic disturbances, especially when storm-time electric fields penetrate to low latitudes. During the extreme geomagnetic superstorm of 10 to 11 May 2024, this electrodynamic coupling intensified dramatically, allowing the SWARM-A satellite located near the dusk-sector pre-reversal enhancement (PRE) time to capture unprecedented changes in the evening ionosphere. The study shows that strong prompt-penetration electric fields (PPEF), acting simultaneously with the natural PRE, triggered a powerful super-fountain effect between ~20°E and 55°W, with maximum uplift near 55°W. This produced unusually deep equatorial electron density (N_e) troughs, significantly poleward-shifted EIA crests, and clear double-crest signatures even in topside TEC. Another key discovery is the first in-situ evidence of large evening-sector electron temperature (T_e) enhancements linked directly to a super-fountain, along with hemispherically asymmetric mid-latitude T_e increases likely driven by auroral expansion, plasmaspheric erosion, and altered heat conduction. Fig. 3 shows the latitudinal profiles of N_e and T_e measured by the SWARM Langmuir Probe, depicting these two observations. Together, these results demonstrate that extreme electrodynamic forcing during this superstorm produced exceptional uplift, heating, and structural distortion of the EIA, offering new insights into storm-time ionospheric dynamics.

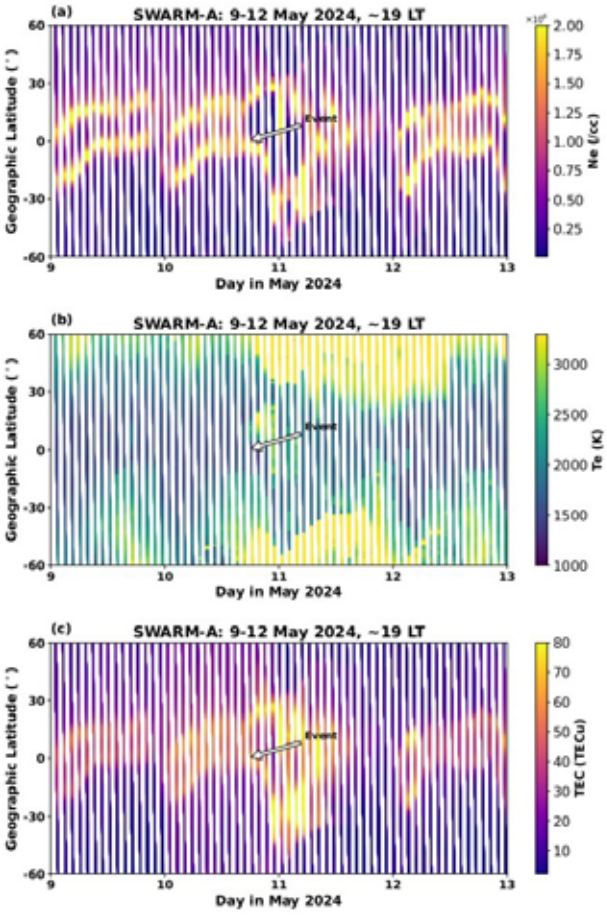

Figure 3: The latitudinal profiles of (a) electron density and (b) electron temperature measured by the SWARM Langmuir Probe are shown. The arrow in each panel indicates the point at which SWARM first detects the storm's influence immediately after its onset [Venugopal et al., Sci. Rep., 2025].

Impact of the May 2024 Gannon Superstorm on the lunar exosphere as observed by CHACE-2 on the Chandrayaan-2 orbiter

Response/variability of lunar exosphere to space weather events was an open question till the recent observations by Chandra's Atmospheric Composition Explorer-2 (CHACE-2) on board Chandrayaan-2 orbiter. CHACE-2 made in-situ observations of the lunar exosphere on 10 May 2024, when the Moon encountered an extreme space weather event (NOAA G5 class), caused by a series of CMEs. Observations showed an increase in the total pressure around the arrival time of the CME impact on the Moon (Fig. 4a). The increase started around the dayside equator, about 45 minutes from the start of observation, and was seen continuously throughout the 4 hours of operation, except for the deep nightside. The altitude of observations was similar to the pre and post event impact days (Fig. 4b). The solar zenith angle, local solar time was also identical on these days. The total number densities derived from these observations showed an enhancement by more than an order of magnitude. This magnitude of enhancement is consistent with the model results, explained by the enhanced solar wind ion sputter process. This is the first observational confirmation of the enhancement in lunar exospheric densities during a CME impact.

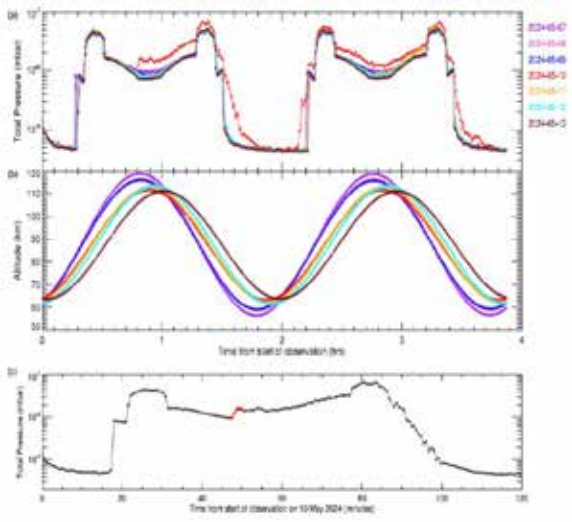

Figure 4: Time series (from start of observations) of (a) the total pressure observed by CHACE-2, for the days from 07 to 13 May 2024, shown in different colors. (b) The altitude of observations for the days from 07 to 13 May 2024 with colors same as in panel (a). (c) The total pressure observed for 10 May 2024, zoomed for the first 2 hrs of observation. The data points used for the computation of number density are shown as red color filled circles. The horizontal axis represents the time from the start of observations expressed in minutes [Dhanya et al., Geophys. Res. Lett., 2025].

Extreme Geoeffectiveness by turbulent Sheath of ICME of October 2024 Space Weather event

The intense space weather event of October 10-11, 2024, was driven by an isolated ICME characterized by well-defined sheath and magnetic cloud structures, offering a unique opportunity to investigate their sequential impacts on the terrestrial space environment. In-situ plasma and magnetic field measurements from NASA's ACE, WIND, and ISRO's Aditya-L1 spacecraft are utilized to identify the structure of this ICME. Concurrently, data from GOES-16 and 18, along with observations from the Magnetospheric Multiscale (MMS) mission, are employed to analyze the magnetosphere's distinct response to the various components of the ICME. Intense magnetic field compression, driven by enhanced solar wind pressure in the ICME sheath, exposed geostationary satellites positioned in the morning and noon local time sectors to interplanetary space as the magnetopause boundary moved Earthward, reaching below 5 R_E. Fig. 5 shows the magnetic field and electron flux data from GOES-16 (a and b) and

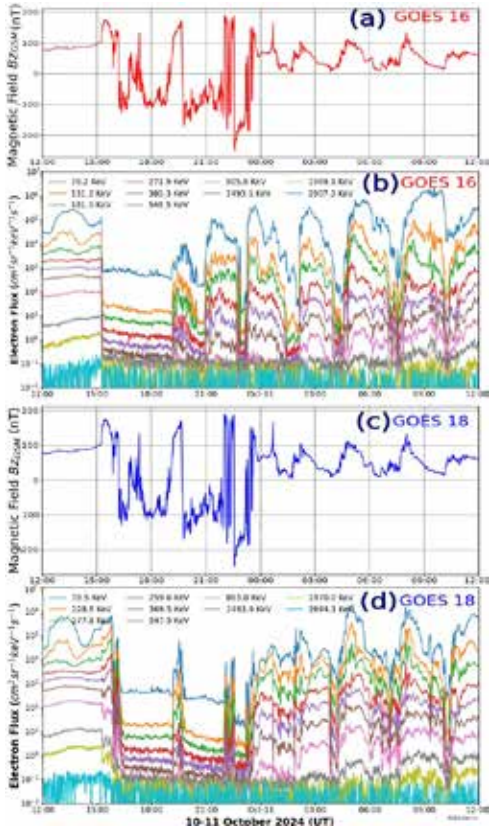

Figure 5: Magnetic field component Bz (GSM) and electron flux data from GOES-16 (a and b) and GOES-18 (c and d). Please note that the magnetic field shown here is a local field in GSM at GEO altitudes [Thampi et al., Astrophys. J., 2025].

GOES-18 (c and d). It can be seen that the severe space weather event is strong enough to produce the geosynchronous magnetopause crossing (GMC) during the sheath phase. Most of the ring current intensification took place within the ICME-sheath transit, indicative of the superior role of the sheath plasma. During the passage of the turbulent ICME-sheath, a severe intensification of field-aligned currents (FACs), equator ward expansion, and multiple bands of FACs were noted within the Earth's magnetosphere-ionosphere system, unlike the magnetic cloud phase. These observations underscore the critical role of the ICME sheath in driving extreme space weather effects on Earth.

Observations of the Fluctuations in the Interplanetary Magnetic Field around L1 Point during Solar Transient Events with MAG Payload onboard Aditya-L1

The MAG instrument onboard Aditya-L1 has observed several solar transient events since January, 2024. This study focused on three such solar events observed in the months of March, May, and October, 2024. The analysis of power spectral density (PSD) or the magnetic field power spectra during the day of solar extreme event (March 24, 2024) reveals the fluctuations consistent with Kolmogorov-type turbulence, characterized by a spectral slope close to −5/3. To emphasize changes in spectral behavior, the event-day spectra are compared with those from a day when the quiet solar wind conditions prevail (March 02, 2024). A marked contrast is observed: while the quiet periods exhibit anisotropic turbulence, the extreme events display quasi-isotropic behavior, with spectral slopes closely following the Kolmogorov spectrum across all three IMF components as shown in Fig. 6. On March 24, the PSS for all components fell within the range −1.64 to −1.76, consistent with the Kolmogorov inertial-range value of (−5/3), indicating fully developed, isotropic turbulence. The similarity in spectral slopes across the IMF components supports the interpretation of an energy cascade that is largely direction independent under disturbed solar wind conditions. To examine contrast in turbulent scaling under quiescent solar conditions, we compared the PSS values during these events with those observed on 2024 March 2, a geomagnetically quiet day (Dst ≈ −10 nT). The PSS on 2024 March 2 ranged from −1.47 to −1.83 across components, with the southward *Bz* component showing the steepest slope, indicative of a more active turbulent cascade in that direction. This suggests that during quiet intervals, the lack of large-scale drivers may allow inherent anisotropic structures to dominate the energy cascade. These results underscore the variability of IMF turbulence under different solar wind driving conditions and point to the need for deeper theoretical investigation into the interplay between isotropic and anisotropic turbulence regimes in both active and quiescent solar wind environments.

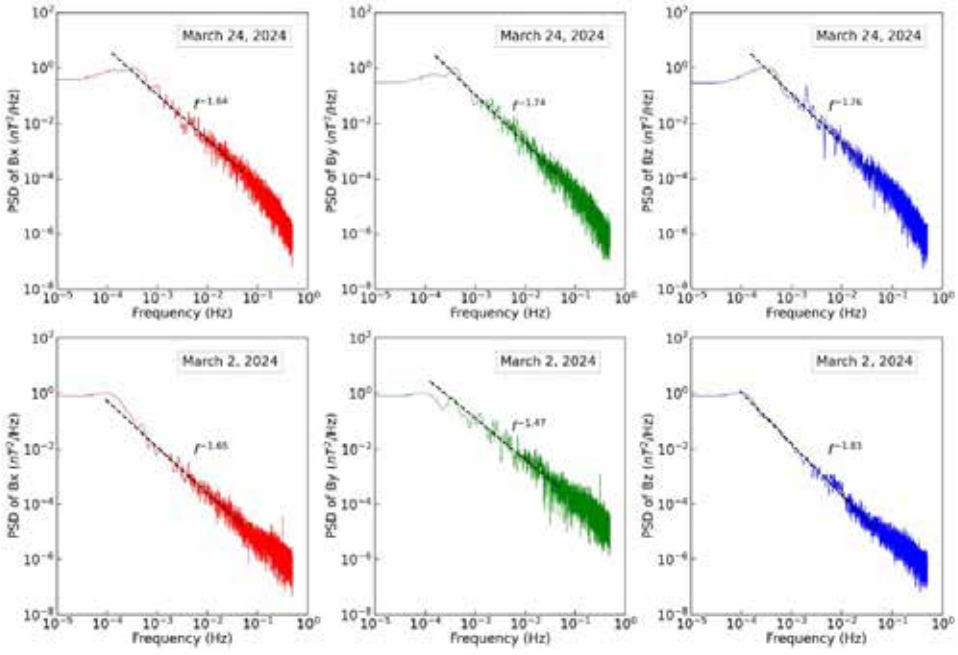

Figure 6: The (an)isotropy in the IMF components during the extreme solar transient event when compared with a quiet day in March, 2024 [Yadav et al., Astrophys. J., 2025].

Energization of Separatrix electrons by plasma double layers during asymmetric magnetic reconnection.

Using the data from Magnetospheric Multiscale (MMS) mission data, for the first time, the presence of multiple plasma double layers (DLs) has been observed at the reconnection separatrix (a boundary layer between reconnected and non-reconnected magnetic field lines) has been reported. DLs consist of two layers of electrons and ions, well separated in plasma, which give rise to an electric field, often parallel to the magnetic field. Such charge separation occurs due to plasma wave-charged-particle interactions; in this case, the Buneman instability drives the wave. The magnetic reconnection separatrix is a potential region where kinetic scale charge separation develops, violating quasi neutrality and eventually accelerating or decelerating the background electrons and ions. Through in-situ electric-field measurements and analysis of particle velocity distributions, electron energization up to the keV range has been observed. Fig. 7 shows the artistic illustration of the magnetic reconnection geometry at Earth's dayside magnetopause (panel a) with the possible trajectory of the MMS spacecraft, along with the parallel component of the electric field of the MMS4 spacecraft with unipolar electric field structures identified as plasma double layers (panel b), and the two-dimensional electron velocity distribution function, with a shift in the distribution along the direction parallel to the magnetic field (panel c), indicating parallel energization.The theoretical model of DLs and numerical simulations has well supported the observational findings. The two-dimensional scales of the DLs (a few hundred meters wide and a few thousand meters long parallel to the magnetic field) have been estimated from observational data. They are qualitatively consistent with numerical simulation results. Further, the study shows the presence of electron phase-space holes (EHs), which develop due to strong two-stream instability. These kinetic-scale features are essential for wave-particle interactions to occur and for the subsequent particle energization in magnetic reconnection.

Impact of high-intensity long-duration continuous auroral electrojet activity (HILDCAAs) on relativistic electrons in Earth's outer radiation belt during the Van Allen Probes era

The multiple High-Intensity Long-Duration Continuous Auroral Electrojet Activity (HILDCAA) events have been analyzed using in situ measurements from NASA's Van Allen Probes to understand how electron fluxes respond across different L-shells, pitch angles, and energy ranges. A superposed epoch analysis was performed to discern common trends in the radiation belt response to HILDCAA activity. It clearly shows that relativistic electron flux enhancements during these events are significant. In most events, the rise seems to occur with a delay of about 0 to 2 days from the onset of the HILDCAA interval, which indicates that acceleration and transport processes act on a time scale of several days. The energy of the accelerated electrons reaches a maximum of

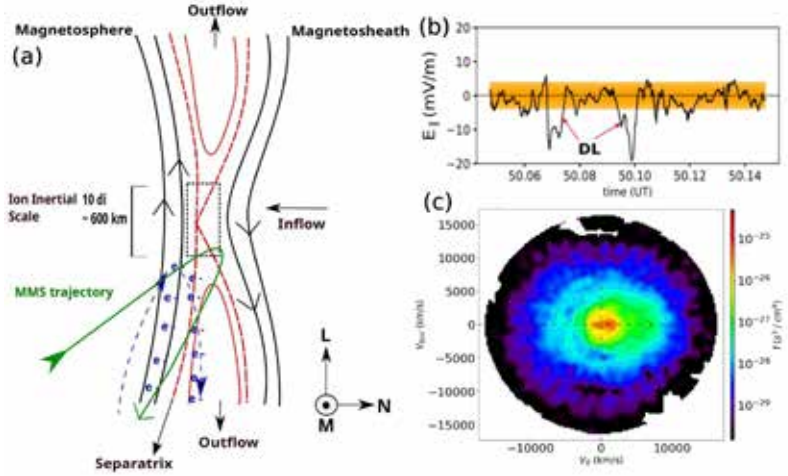

Figure 7: Panel (a) shows the artistic illustration of the magnetic reconnection geometry at Earth's dayside magnetopause with the possible trajectory of the MMS spacecraft. The rectangular box at the centre represents the ion diffusion region. Panel (b) represents the parallel component of the electric field of the MMS4 spacecraft with unipolar electric field structures identified as plasma double layers. Finally, panel (c) shows the two-dimensional electron velocity distribution function, with a shift in the distribution along the direction parallel to the magnetic field, indicating parallel energization [Biswas et. al., Geophys. Res. Lett., 2025].

~6 MeV, which proves that HILDCAA events can drive appreciable energization in the outer belt. Electrons with perpendicular pitch angles show stronger flux enhancements compared to those whose directions are aligned with the magnetic field (Fig. 8). Such behavior implies involvement of acceleration mechanisms dependent on pitch angle rather than uniform radial diffusion alone. The clear distinction in the response of different pitch angle populations highlights how wave-particle interactions drive the evolution of high-energy electrons. Further analysis of plasma waves using ground and space-based magnetic field measurements shows that while VLF waves, especially chorus waves, reveal enhanced power during the HILDCAA periods, timing and pitch angle characteristics point to a dominant role of ultra-low-frequency (ULF) waves. Classical radial diffusion normally requires coherent structures of ULF waves, but our observations indeed show that partially incoherent yet persistent ULF activity can effectively energize electrons during HILDCAAs. These results emphasize that HILDCAA events, though generally less intense than major geomagnetic storms, are highly effective in the energization of outer radiation belt electrons due to the sustained nature of HILDCAA-driven ULF activity. This helps gradual but significant acceleration, thus contributing to prolonged high-energy electron enhancements. This has important implications for space weather, where elevated MeV electron fluxes pose risks to the spacecraft in medium and high Earth orbits. These results are important for a better understanding of radiation belt responses during HILDCAA intervals and have implications for satellite safety and even the interpretation of energetic particle behavior in other Earth-like planetary magnetospheres.

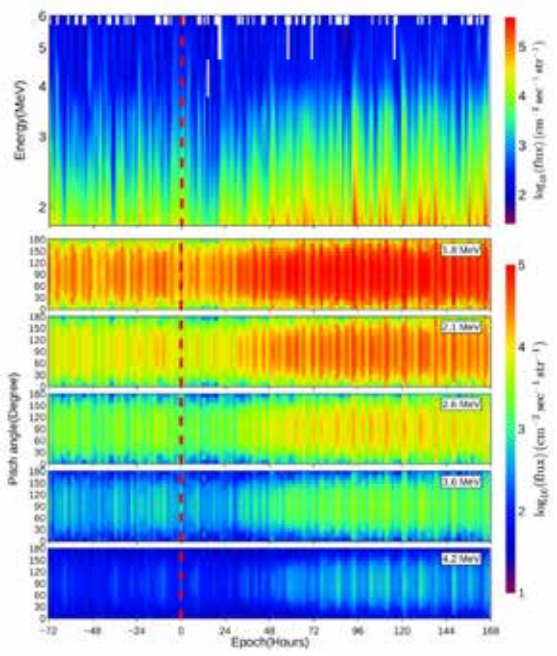

Figure 8: (Top panel) Superposed energy spectrum of electron fluxes. (Bottom panels) Pitch angle variation of fluxes for different energies at L-shell > 4 measured by the Relativistic Electron Proton Telescope (REPT) onboard Van Allen Probes mission. The vertical red-dashed line in the figure is the onset of all events. Distinct enhanced fluxes after the onset were observed [Nema et al., Adv. Space Res., 2025].

Modeling Studies of Planetary Plasma Environments

Investigation of the Dust-Acoustic Nonlinear Periodic Waves in the Saturn's Magnetosphere

Nonlinear periodic structures such as solitons and double layers are ubiquitous in space plasma environments, where they play a crucial role in particle acceleration and in the transfer of energy and momentum across different plasma regions. Observations from the *Cassini* spacecraft have revealed electrostatic solitary waves (ESWs) in Saturn's magnetosphere with electric field amplitudes ranging from a few mV/m up to ~10 mV/m, and with time durations from several hundred microseconds to a few tens of milliseconds. These ESWs are generated at Saturn's bow shock due to counter-streaming between incoming solar-wind protons and ions reflected from the shock. They are also detected within Saturn's dusty E-ring, where they are plausibly produced by the co-rotation of two ion populations drifting at different velocities in the presence of negatively charged dust grains. The present study provides a theoretical investigation of the generation mechanisms of these waves using a two-ion (H^+ and O^+) dusty plasma framework, incorporating dust charge variation from first principles. Fig. 9 shows a schematic of this mechanism. The analysis

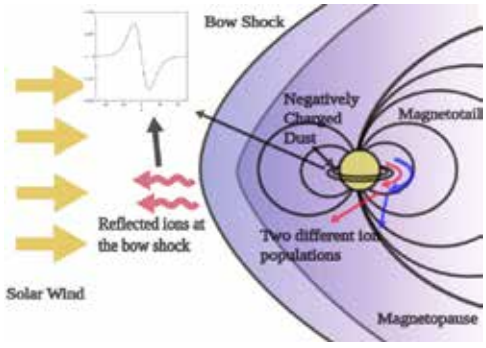

Figure 9: The plausible generation mechanism for the ESWs in the Saturn's magnetosphere with the inset showing the electric field waveform for solitons obtained from the model [Rubia et al., Phys. Plasmas, 2025].

shows that the characteristics of the nonlinear periodic waves are significantly influenced by the temperature and density ratios of the ion species, as well as by their respective charges and masses. The model aptly explains the observed ESWs in Saturn. Because the formulation is generic, it is also applicable to wave phenomena in other planetary dusty plasma environments, including Cometary tails and Jupiter's magnetosphere.

On the effect of H_3^+ ions on the characteristics of electrostatic solitary waves and double layers in the Ganymede wake observed by Juno Spacecraft

Ganymede, the Icy Moon of Jupiter, is the only Moon in the solar system having its own intrinsic magnetic field. On 7th June 2021, Juno Spacecraft performed a historic close flyby (at an altitude of 1046 km) of the Ganymede. During the flyby, Juno traversed through the hitherto unexplored magnetopause and wake regions. For the first time, H_2^+ and H_3^+ ions were observed in the wake, implying that the wake region is influenced by water products from the Ganymede surface. Further, the Juno Waves instrument observed the electrostatic solitary waves (ESWs) in the wake and at the magnetopause boundary. The present study investigates the generation mechanism of the ESWs in the Ganymede wake using a multi-component fluid plasma model consisting of warm H^+, O^+ and H_3^+ ions, electron beam and suprathermal background electrons following κ- distribution. The primary focus of the study is on the role of H_3^+ ions on the characteristics of the ESWs. The model supports the existence of one slow and two fast ion-acoustic modes in the lower frequency regime, and electron-acoustic mode in the higher frequency. Fig.10 shows the variation of the soliton potential f with x(x, t) for solitons, double layers and electric field.

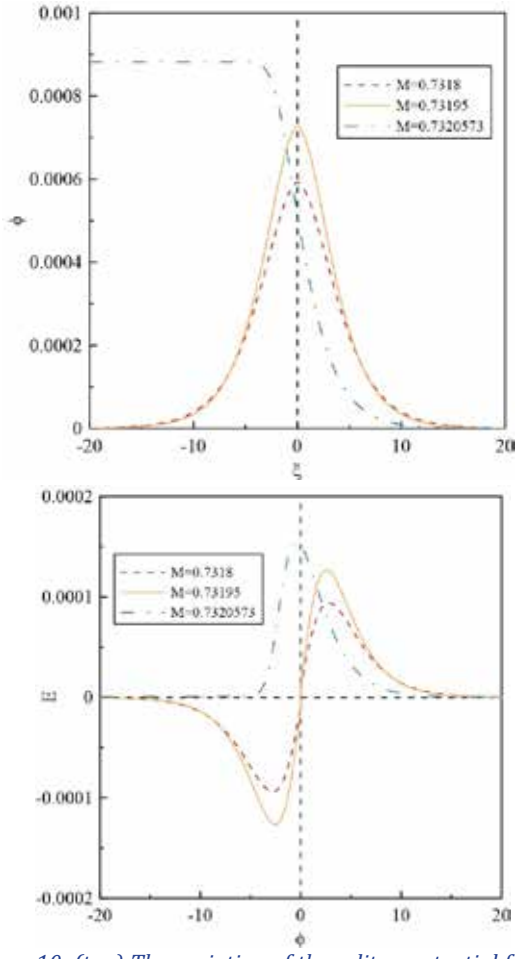

Figure 10: (top) The variation of the soliton potential f with x(x, t) for solitons (red and orange curve) and double layers (blue) and, (bottom) electric field, E vs. x(x, t) [Rubia et al., Astrophys. J., 2025].

It was observed that the number density and temperature of the H_3^+ ions plays a deterministic role in the polarity (i.e. positive or negative) and existence of ESWs and double layers. When the number density of the H_3^+ ions is considered to be zero, one of the fast ion-acoustic modes vanishes.

Studies on electrostatic solitary waves in the Ganymede magnetopause region

Ganymede, the only moon in the solar system known to possess its own intrinsic magnetosphere, is embedded within Jupiter's vast magnetic environment. Near the equator, Ganymede's magnetic field lines are predominantly closed, meaning both foot-points are anchored to the moon's surface. In contrast, the polar regions are characterized by open field lines, with one foot-point connected to Ganymede and the other extending into Jupiter's ionosphere. These closed field lines are oriented approximately anti-parallel to Jupiter's field, making the magnetopause a favorable site for magnetic reconnection. Meanwhile, the open field line topology enables both particle escape and precipitation. On 07 June 2021, the Juno spacecraft detected electrostatic solitary waves (ESWs) near Ganymede's magnetopause. ESWs are frequently interpreted as indicators of ongoing magnetic reconnection. The current study models the observed ESWs from first principles under a fluid-dynamics framework using a plasma composition emulating the conditions during Juno's flyby. The modeled system comprises of warm H^+ and O^+ ions, two counter-streaming electron beams, and a population of suprathermal electrons described by a k-distribution. The findings

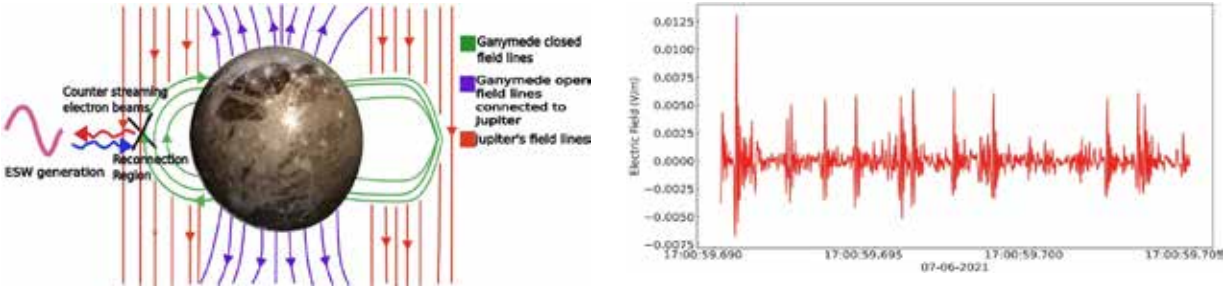

Figure 11: (left) Generation mechanism for ESWs at the Ganymede magnetosphere due to counter-streaming of electrons and (right) ESWs waveform observed by JUNO on 7 June 2021 [Rubia et al., Astrophys. J., 2025].

indicate that symmetric electron beams support the coexistence of both slow and fast ion-acoustic solitons. However, when the electron beams are asymmetric, differing in number density and drift velocity, electron-acoustic solitons also emerge alongside the ion-acoustic modes. Furthermore, the asymmetric beam configuration reproduces the observed characteristics of the ESWs more accurately than the symmetric beam condition. Fig.11 shows a schematic of the generation mechanism for ESWs at the Ganymede magnetosphere due to counter-streaming of electrons along with ESWs waveform observed by JUNO on 07 June 2021.

PAPA Payload onboard Aditya-L1

Solar Wind Bulk parameters retrieval from PAPA Observations

PAPA payload onboard Aditya-L1 started observations of solar wind on December 15, 2023, which included the full scan mode operation of both the sensors in all three, i.e SWEEP-electron, SWICAR-ion and SWICAR-electron mode. Since then PAPA has made measurements of solar wind plasma in different energy domains in phases ,depending on the severity of the solar event and sensitivity of PAPA detectors. Fig.12 shows the SWICAR ion mode measurements for almost 100 days in 2025. The energy time series of STOP counts shows two distinct bands, the first band corresponds to solar wind protons and the second corresponds to alpha particles.

The solar wind bulk parameters are retrieved from the detector count rates recorded by PAPA. The count rates are converted into differential number fluxes using calibration parameters, which are further converted into velocity distribution functions. To derive the plasma moments from this, two different approaches have been applied. The first method employs the moment relations for obtaining density, bulk velocity and temperature directly from the discrete distribution function values. In the alternate method, the discrete distribution function values are fitted with an isotropic Maxwellian distribution function and

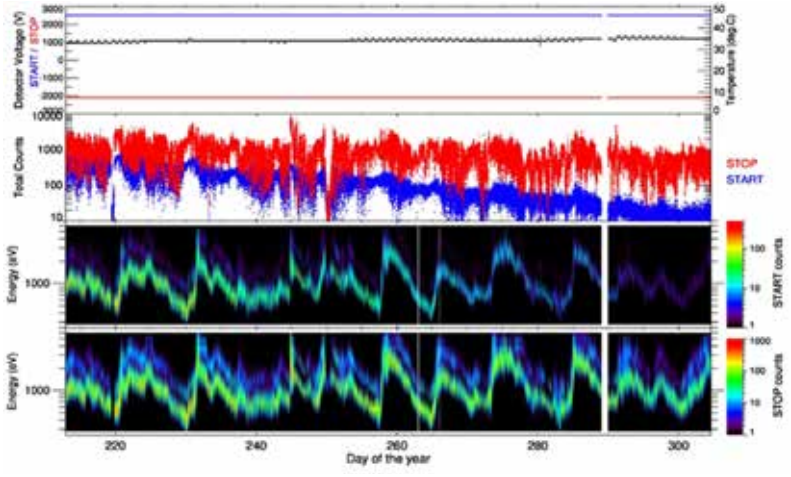

Figure 12: SWICAR ion mode observations for almost 100 days starting from 31 July 2025. Topmost panel shows detector voltages (left Y-axis) as well as temperature (right Y-axis). Second panel from the top shows the total START counts (blue curve) and STOP counts (red curve). Third panel from the top shows the energy-time spectrogram of START counts. Bottom panel shows the energy-time spectrogram of STOP counts.

bulk parameters are obtained from the best fit parameters. The retrieved bulk parameters (proton number density, bulk velocity and temperature) in comparison with that of the contemporary measurements from 3DP/WIND, in Fig. 13. Overall, the parameters derived from PAPA and provided from WIND are in agreement. The minor differences could be associated with the different locations of the two spacecraft, which is indicated by the time differences in the event time responses as well.

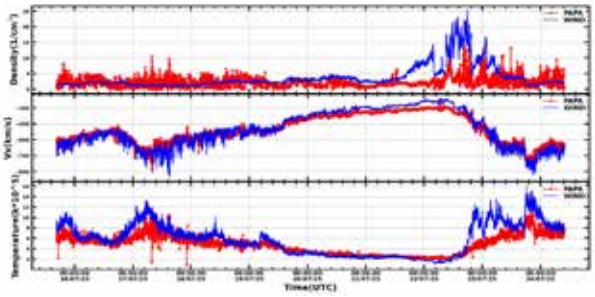

Figure 13: The bulk parameters such as proton density (top panel), x-component of bulk velocity (middle panel), and proton temperature (bottom panel) retrieved from PAPA (red color) and from 3DP/WIND (blue color) for the period from 16-07-2025 to 24-07-2025 [WIND data was taken from NASA CDA web].

Data Products

For PAPA, the data products (level-1 & level-2) are released through PRADAN in a phased manner. Total 192 data products (96 Level-1 and 96 Level-2) containing both ion and electron data spanning from 15 to 25 December 2023, 208 data products containing only ion data (104 Level-1 and 104 Level-2) from 15 July to 02 September 2024, 80 files (40 Level-1 and 40 Level-2) containing only ion data from 12 to 31 December 2024, have been released.

MAG Payload onboard Aditya-L1

Interplanetary Magnetic Field (IMF) observations around the L1 point with MAG payload onboard Aditya-L1 spacecraft

The MAG payload onboard Aditya-L1 spacecraft is continuously measuring the IMF coming from the Sun towards Earth in a halo-orbit around the L1 point. The IMF observations made by MAG are time-to-time compared with the observation made by the instrument onboard DSCOVR spacecraft as shown in Fig.14, for the duration June 1-15, 2025 which depict a well correlated IMF measurement by both the spacecraft. These observations establish the fact that both the MAG sensors and the MAG electronics are satisfactorily performing on the designed parameters.

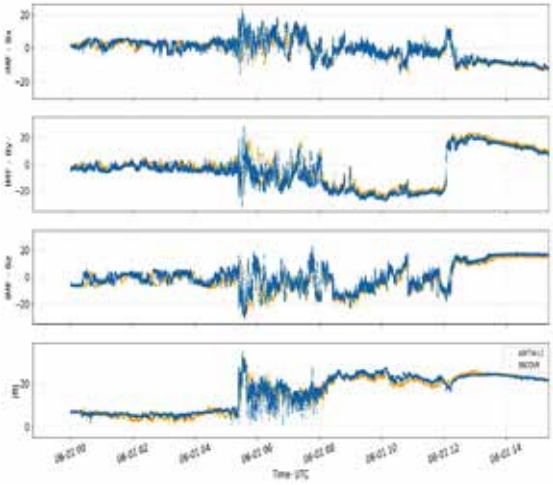

Figure 14: Comparison of the IMF measurements onboard Aditya-L1 with that onboard DSCOVR spacecraft during June 1-15, 2025. All values are in units of nT [Yadav et al., Sol. Phys., 2025].

Data Products

For MAG payload, all the Level-1 and Level-2 data products were released from July 01, 2024 to till date. MAG L1 data products are processed and released daily after receiving the two data files per day (one for the duration 00:00:00 to 12:00:00 UTC and the other for 12:00:00 to 23:59:59 UTC). MAG L2 data products are released once in a week and the data products are generated from last 7 days of observations (one file for the duration 00:00:00 to 23:59:59 UTC per day). A total of 1526 data products for MAG are available in the PRADAN portal.

CHACE-2 onboard Chandrayaan-2

Current status & Data Products

CHACE-2 is being operated regularly and the health parameters are found to be normal. The operation time was increased from ~4 hours to 6 hours on 25/10/2024 and later to 7 hours on 09/07/2025. The data is received at the payload operation centre (POC) of SPL. CHACE-2 data products (level-1a) are being released through PRADAN in a periodic manner, once every month. From August 2024 to October 2025, a total of 437 data products have been released.

Technology Development

Simulations for SAMPAD/MLM using Geant4

To investigate the transport and acceleration of Solar Energetic Particles (SEPs) at 1.5 AU and their impact on the Martian atmosphere, a Solar And

Martian PArticle Detector (SAMPAD) payload is being developed. The calibration curves (deposited energy versus incident energy) for electrons and protons in Avalanche Photo Diodes (APDs) and silicon-cylinder Solid State Detector (SSD) stacks were estimated. Energy deposition logic for inferring incident energy from SSD signals was implemented. Differential channel efficiencies for electrons and protons in the SSDs were calculated (Fig. 15). The effects of varying SSD thickness and area on performance were compared. The performance of a hybrid configuration of SSD stack consisting of both thin and thick detectors was also estimated.

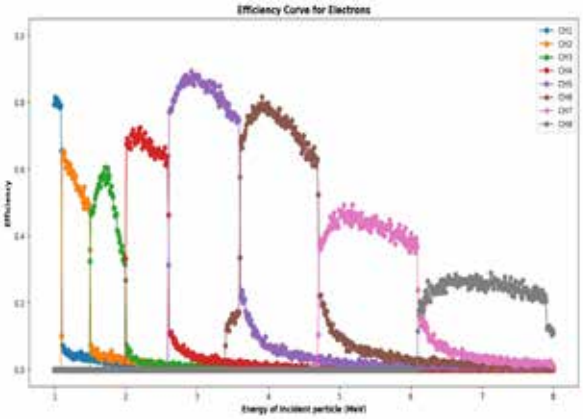

Figure 15: Differential energy-channel efficiencies for electrons.

Venus Ionospheric and Solar Wind particle AnalySer (VISWAS)

SPL, VSSC is developing a novel Plasma Analyser (PA) having electron and ions sensors. This together with the Energetic Neutral Atom (ENA) analyser from IRF, Sweden, is named as 'Venus Ionospheric and Solar Wind Particle Analyser (VISWAS)' for the Venus Orbiter Mission (VOM) of ISRO. This payload will help us to understand the solar wind interaction with Venus and the Venusian Plasma environment. Basically, VISWAS consists of 2 sensors; VISWAS-PA and VNA. Plasma analyser is capable of measuring both ions as well as electrons. Venusian Neutrals Analyser (VNA) is an energetic neutral atom analyser developed by IRF, Sweden that will measure energetic neutral atoms (ENAs) from Venus. SPL will develop the plasma analysers and their power and processing electronics with support from various entities of VSSC. All the three sensors interface to a common VISWAS Control Unit (VCU), developed by Avionics entity of VSSC, which in turn interfaces to the spacecraft. The mechanical configuration of both PA and VNA sensors are shown in Fig. 16.

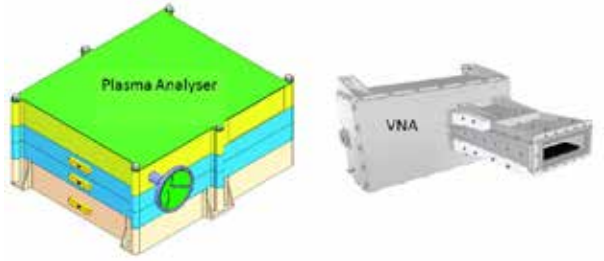

Figure 16: Mechanical configuration of VISWAS payload having Plasma Analyser (left) and Venusian Neutral Analyser (VNA) sensor (right).

VISWAS will carry out the in-situ measurement of ions which are of Venus Ionospheric/solar wind origin in the energy range from 10 eV to 30 keV in the mass range of 1- 60 amu, electrons in the energy range 10 eV to 3 keV, and energetic neutral atoms in the energy range 1of 10 eV to 10 keV in the mass range of 1-44 amu. In the PA, the energy analysis of the incoming ions/electrons is carried out by electrostatic analyser and the mass analysis of ions using time-of-flight (TOF) technique. Using multiple electrodes at the entrance section of the analyser, a field of view of 180° (azimuth) × 180° (elevation) will be achieved by suitable voltage scanning at the electrodes, which gives the directional information of the incoming ions/ electrons.

The primary objective of VISWAS payload is to investigate the solar wind interaction with upper atmosphere of Venus by in-situ observation of ions, electrons and to understand the plasma dynamics in the Venusian magnetosphere, the loss of upper atmosphere/ionosphere (ions as well as non-thermal neutrals) and the role of different escape mechanisms and to investigate, using energetic neutral atoms, variability of the main domains of the Venusian induced magnetosphere and processes responsible for atmospheric sputtering, potentially a very important channel of the atmospheric escape.

Simulations for VISWAS-PA/VOM using SIMION

The VISWAS payload is currently being developed for the upcoming Venus Orbiter Mission (VOM). A three electrode deflection system was designed for the Plasma Analyser (PA) specifically to enable angular scanning across a hemispherical FOV. This system consists of three identical electrodes arranged in a funnel-like geometry, allowing it to cover approximately 2π steradians. Funnel design

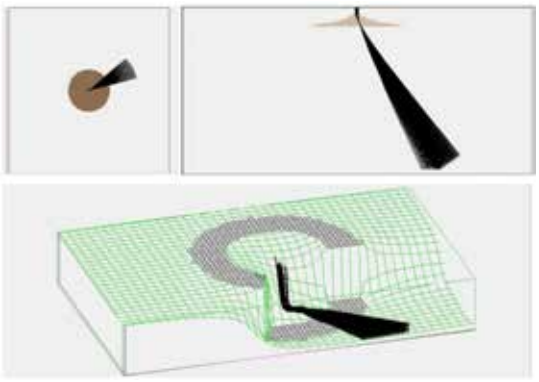

Figure 17: The front and top views of the funnel, along with the Potential Energy (PE) view. Particles with 5 keV energy, launched within an azimuthal range of 15°–41° and a zenith range of 29°–37°, were deflected under an electrode voltage configuration of (-2, 0, 0) kV.

parameters, which include curvature, entrance and exit diameters, were optimized through simulations to provide broad FOV coverage, reduce voltage requirements, and to obtain a good angular resolution (Fig. 17).

Payload Operation Centre (POC)

The payload Operation Centre (POC) serves as the nodal point connecting the payload, mission, and ISSDC teams. The data from PAPA and MAG payloads on the Aditya-L1 and CHACE-2 on Chandrayaan-2 orbiter are being received continuously at POC. The POC chain for each payload is operated on a daily basis. POC is equipped with NKN-VRF for receiving the science data. POC has been augmented with TM-VRF link for real-time monitoring of payload telemetry and a data storage system.

Ongoing Activities and Future Projections

- Extension of the analytical and numerical work pertaining to plasma instability studies in the lunar ionosphere by including the magnetic field in the analysis.
- Realization of the Venus fluxgate magnetometer (VFGM) payload onboard Venus Orbiter Mission (VOM).
- Extension of the HUXt based solar wind velocity prediction model to Mars.
- Study of the ion outflow from Earth and Mars during space weather events.
- Extension the plasma instability and plasma wave studies to other planetary and solar system bodies such as Mars, Venus and comets using experimental and theoretical techniques.
- Comparative investigation of variation in heavy elements in the solar wind during quiescent and passage of CME at L1 point using PAPA onboard Aditya-L1
- Development of a compact payload to measure distribution of energetic particles in Earth and planetary magnetospheres.
- Development of space weather forecasting models using machine learning and physics-based models.
- Characterize the processes governing ion-outflow at Mars. Study the origin of the Magnetic switchbacks and Alfvénic fluctuations in the solar wind.
- Development of a plasma wave detector (PWD) which constitutes a customized LP, triaxial electric field sensor, fluxgate and search-coil magnetometers for plasma wave observations in space.
- Establishment of an advanced high vacuum space simulation laboratory (AHVSSL) in SPL.
- Development of models for the prediction of different Solar wind parameters using physics based and AL/ML approaches.

Publications in Peer-Reviewed Journals

1. Ashna, V. M., Bhaskar, A., Manju, G., Sini, R., "Solar wind – magnetosphere coupling efficiency and its dependence on solar activity during geomagnetic storms of 23-24 solar cycles", Journal of Geophysical Research: Space Physics, https://doi.org/10.1029/2023JA031687, 2024.
2. Vichare, G., Bhaskar, A., Rawat, R., Yadav, V., Mishra, W., Angchuk, D., Anand K.,"Low-latitude auroras: insights from 2023 April 23 solar storm", The Astrophysical Journal, https://doi.og/10.3847/1538-4357/ad8dd3, 2024.
3. Thampi, R. S., Abhishek, J. K., Sasidharan, D., Varma, G., Sen, V. K., Ray, S., Dhanya, M. B., Pandey, U., Chandra, S. K. S., Akash, J. B., Aneesh, A. N., Wilson, T. M., Naresh, S., Naik, N., Yadav, M. C., Venkataraman, V., John, R., Manoj, R., Nampoothiri, G. G., Meshram, P., George, M., Ramdas, V., George, G. V., Pillai, A. M., Dey, A., Das, S., Varier, G. S., Sajitha, G., Mathews, S., Kumar, P. P., Nisha, G. R., Nandi, A., Sundar, B., Sethunadh, R., Rajendra,

A., Saleem, H., Samad, A. K. A., "Plasma Analyser Package for Aditya (PAPA) onboard the Indian Aditya-L1 Mission", Solar Physics, https://doi.org/10.1007/s11207-024-02414-8, 2025.

4. Manju, G., Pant, T. K., Mridula, N., Hossain, M. M., Ambili, K. M., Pradeep K. P., Sruthi, T. V., Vishnupriya, K. S., Thampi, R. S., Aneesh, A. N., Keshav, R. T., Sreelatha, P., Rosmy J., "In situ ionospheric observations near lunar south pole by the Langmuir Probe on Chandrayaan-3 Lander", Monthly Notices of the Royal Astronomical Society, https://doi.org/10.1093/mnras/staf1276, 2025.
5. Yadav, V.K., Vijaya, Y., Krishnam Prasad, B., Srikar, P.T., Mahajan, M., Mallikarjun, K.V.L.N., Zamani, S.N., Lohar, K.A., Kandpal, M.M., Narendra, S., Rai, V.S., Abhijit A. A., Veeresha, D. R., Smaran T.S., Kalpana A., Srivastava, N., Vichare, G., "The Fluxgate Magnetometer (MAG) onboard Aditya-L1 Spacecraft", Solar Physics, https://doi.org/10.1007/s11207-025-02440-0, 2025.
6. Thampi, S. V., Bhaskar, A., Mayank, P., Vaidya, B., Venugopal, I.,"Simulating the Arrival of Multiple Coronal Mass Ejections That Triggered the Gannon Superstorm on 2024 May 10", The Astrophysical Journal, https://doi.org/10.3847/1538-4357/ada93c, 2025.
7. Biswas, S., Bhaskar, A., Shuster, J. R., Ahmadi, N., Wilder, V. D., Thampi, S. V., Thampi, R. S., "Energization ofseparatrix electrons by plasma doublelayers during asymmetric magneticreconnection". Geophysical Research Letters, https://doi.org/10.1029/2025GL115285, 2025.
8. Venugopal, I., Thampi, S. V., Bhaskar, A., "Electrodynamic forcing of the Duskside ionosphere and the super fountain effect during the superstorm of May 10 to 11 2024", Scientific Reports, https://doi.org/10.1038/s41598-025-08843-0, 2025.
9. Nandy, D., Pant, V., Anand, M., Jithu J. A., Arun K. A., Bane, K., Banerjee, D., Ravindra, B., Bhaskar, A., Bhattacharyya, R., Bhowmik, P., Chandra, R., Chatterjee, P., Chatterjee,S., Dimri, A. P., Sneha A. G., Hanasoge, S., Hazra, S., Jain, R., Joshi, B., Nagaraju, K., Kansabanik, D., Karak, B. B., Kathiravan, C., Khan, R., Krishnan, H., Brajesh, K., Sanjay, K., Anshu, K., Majumdar, S., Mayank, P., Mishra, S., Mishra, W., Atul, M., Surajit, M., Mugundhan, V., Narendranath, S., Divya, O., Megha, P., Ritesh, P., Arghyadeep, P., Prasad, A., Raja, K, S., Rajhans, A., Ramesh, R., Saha, C., Sankarasanubramanian, K., Selvakumaran, R., Sharma, R., Sharma, R., Arpit, K. S., Nishant, S., Soni, S., L., Abhishek, K. S., Srivastava, N., Tripathi, D., Uddin, W., Vaidya, P. B., Vemareddy, Vichare, G., Vigeesh, G., Nitin, Y., Yadav, V.K., "The Indian Solar and Heliospheric Physics Vision: Fundamental Science to a Space Weather Resilient Society", Journal of Astronomy and Astrophysics, https://doi.org/10.1007/s12036-025-10064-w, 2025.
10. Biswas, S., Bhaskar, A., Raghav, A., Kumar, A., Ghag, K., Thampi, S. V., Yadav, V. K., "Pinching of the Flux Rope: Unprecedented Multipoint Observations of Internal Magnetic Reconnection during Gannon's Superstorm", The Astrophysical Journal Letters, https://doi.org/10.3847/2041-8213/adfe60, 2025.
11. Yadav, V. K., Choudhary, R. K., Goutham, M. M.,"Observation of the fluctuations in Interplanetary Magnetic Field around the L1 point during the solar transient events of 2024 with MAG payload onboard Aditya-L1 spacecraft", The Astrophysical Journal, https://doi.org/10.3847/1538-4357/ae00b6, 2025.
12. Rubia, R., Dhanya, M. B., Singh, K., Kourakis, I., "Theoretical perspective on the occurrence of electrostatic solitary waves and double layers in the Ganymede Wake", The Astrophysical Journal, https://doi.org/10.3847/1538-4357/adff57, 2025.
13. Mahajan, M., Yadav, V.K., Vijaya, Y., Prasad, B.K., Mallikarjun, K.V.L.N., Zamani, S.N., Lohar, K.A., Kandpal, M.M. Srikar, P.T., "The Design and Realisation of the Electronics Package for the MAG Payload on Board Aditya-L1 Spacecraft", Review of Scientific Instruments, https://doi.org/10.1063/5.0273204, 2025.
14. Rubia, R., Dhanya, M. B., Singh, K., Kourakis, Rubia, R., Dhanya, M. B., Singh, K., Kourakis, I., "A mechanism for electrostatic solitary waves observed in the Ganymede's magnetopause", The Astrophysical Journal, https://doi.org/10.3847/1538-4357/ae0a1b, 2025.
15. Thampi, S. V., Bhaskar, A., Venugopal, I., Biswas, S., Yadav, V. K., "Extreme Geoeffectiveness by Turbulent Sheath of ICME of October 2024 Space Weather Event", The Astrophysical Journal, https://doi.org/10.3847/1538-4357/ae1974, 2025.
16. Dhanya, M. B., Yadav, C. M., Thampi, S. V., Das, T. P., Thampi, R. S., Bhardwaj, A., "Impact of a coronal mass ejection on the lunar exosphere as observed by CHACE-2 on the Chandrayaan-2 orbiter", Geophysical Research Letters, https://doi.org/10.1029/2025GL115737, 2025.
17. Rubia, R., Yadav, L. L., Singh, S. V., Devanandhan, S., Dhanya, M. B., "Dust-acoustic nonlinear periodic waves in a two-ion dusty plasma with dust charge variation: Application to Saturn's magnetosphere", Physics of Plasmas,https://doi.org/1063/5.0269669, 2025.
18. Mukundan, V., Withers, P., Thampi, S. V., Bhardwaj, A. , "Decoupling the influence of solar cycle and seasons on Mars' dayside ionosphere: Insights from MAVEN observations during the declining phase of solar cycle 24", Icarus, https://doi.org/10.1016/j.icarus.2025.116470, 2025.
19. Remya, S. N., Unnikrishnan, K. Thampi, S. V., Sreekumar, H., "Ionospheric responses to two consecutive geomagnetic storms of the ascending phase of the solar cycle 25 over the Indian sector", Journal of Geophysical Research: Space Physics, doi: https://doi.org/10.1029/2024JA033159, 2025.
20. Khan, W., Ramachandran, R., Gupta, S., Meka, J.K., Venkataraman, V., Hill, H., Rajasekhar, B.N., Janardhan,

P., Bhardwaj, A., Mason, N.J., Sivaraman, B., "Infrared spectroscopy reveals ethylene glycol is an anti-crystallizer in water mixed astrochemical ices", Life Sciences in Space Research,, https://doi.org/10.1016/j.lssr.2025.01.006, 2025.
21. Khan, W., Ramachandran, R., Gupta, S., Meka, J.K., Venkataraman, V., Rajasekhar, B.N., Janardhan, P., Bhardwaj, A., Mason, N.J. Sivaraman, B., "Irradiation of condensed CO reveals a new pathway for the formation of aromatic molecules in astrochemical ices", Life Sciences in Space Research,https://doi.org/10.1016/j.lssr.2025.09.007, 2025.
22. Roy, A., Singh, S.V., Ramachandran, R., Meka, J.K., Ambresh, M., Vijay, T., Janardhan, P., Jayaram, V., Venkatraman, V., Das, A. Hill, H., "Instantaneous formation of interstellar minerals and mineral quantum dots", Royal Society of Chemistry Advances, https://doi.org/10.1039/d5ra01088h, 2025.
23. Nema, A., Bhaskar, A., Pathak, K. N., Thampi, S. V., Datta, A. , "Impact of High-Intensity Long-Duration Continuous Auroral Electrojet Activity (HILDCAAs) on Relativistic Electrons in Earth's OuterRadiation Belt during Van AllenProbes Era", Advances in Space Research, https://doi.org/10.1016/j.asr.2025.06.041, 2025.
24. Pandya, M., Bhaskar, A., Samara, M., Michell, R., Mirizio, E., Kang, S. B., Blum, L. W., "Spatio-temporal evolution of pulsating aurora observed using a ground-based imagers", Frontiers in Astronomy and Space Sciences, https://doi.org/10.3389/fspas.2025.1561439, 2025.
25. Pandya, M., Ebihara, Y., Oliveira, D.M., Samara, M., Fok, M.C., Bhaskar, A., Ferradas, C.P., Tanaka, T., Michell, R., Reeves, G., Manweiler, J.W., , "First simultaneous multi-point observation of the local-time asymmetry of keV ions in the dayside magnetosphere during the main phase of the geomagnetic storm", Journal of Geophysical Research: Space Physics, https://doi.org/10.1029/2025JA033793, 2025.
26. Shah, M., Raghav, A., Ghag, K., Dhamane, O., Kumbhar, K., Nicolaou, G., Bhaskar, A., Allen, R.C. Shaikh, Z., "Thermodynamic Characterization of Solar Wind Interaction Regions Using PSP Observations: Evidence of Subadiabatic and Superadiabatic States", The Astrophysical Journal, https://doi.org/10.3847/1538-4357/ade9a3, 2025.
27. Singh, R., Pant, T. K., Sripathi, S., Rout, D., Bhaskar, A., Scipion, D. E. , "IMF By-driven electric field disturbances over the equator during northward IMFs: PPEF responses", Journal of Atmospheric and Solar–Terrestrial Physics, https://doi.org/10.1016/j.jastp.2025.106642, 2025.

Publications in Conference Proceedings

1. Vipin K. Yadav, Mahima Agarwal, Mehul Chakraborty, Rajneesh Kumar; "Generation of Streaming Beam-Plasma Instability in Variable Lunar Plasma around Moon", URSI Regional Conference on Radio Science (URSI-RCRS 2024), October 22-25, 2024; ARIES / GEHU, Bhimtal, India; Page: 1-4; doi:10.46620/URSI_RSRC24/0039KVI5957
2. Vipin K. Yadav, Y. Vijaya, P.T. Srikar, B. Krishnam Prasad, Monika Mahajan, K.V.L.N. Mallikarjun, S. Narendra, Abhijit A. Adoni, Vijay S. Rai, D.R. Veeresha and Syeeda N. Zamani;"First Results of the Magnetometer (MAG) Payload onboard Aditya-L1 Spacecraft", URSI Regional Conference on Radio Science (URSI-RCRS 2024), October 22-25, 2024; ARIES/ GEHU, Bhimtal, Uttarakhand, India; Page: 1-4; doi:10.23919/URSI-RCRS63970.2024.11201161.
3. Thampi, R. S., Dhanya, M. B., Yadav, M. C., Aneesh, A. N., Meshram, P., Samad, A. K. A., Varier, G. S., Sajitha, G., Sundar, B., Mathews, S., Kumar, P. P., Nandi, A., Pandey, U., Naik, N., Ray, S., Sen, V. V., Chandra, S. K. S., Varma, G., Manoj, R., Akash, J. B., Sasidharan, D., John, R., Wilson, T. M., Naresh, S., "Impact of CME on solar wind: First results from Plasma Analyser Package for Aditya (PAPA) payload onboard, Aditya-L1 mission", Proceedings of GLEX 2025, New Delhi, 7-9 May 2025, (GLEX-25-2, 2, 6, x93540).

Technical Reports

1. PAPA- PV phase operations, status and results, AdityaL1-PAPA-PV issue 4, , 07 October 2024..
2. Spaceweather flag estimation for PAPA, AL1-PAPA-SW-FLAG issue 1.0, 04th October 2024
3. PAPA Data products User Manual, Issue 1, Revision 3, January 01, 2025.

Presentation in Symposia/Conferences/Workshops

1. Ankush Bhaskar, "Solar Storms and Space Weather: Navigating the Sun's Impact on Our World", International Conference on the Emerging Role of Mathematics in Science and Technology, Jawaharlal Nehru College, Boko, Assam, 24-26 October, 2024.
2. Rubia, R., M. B. Dhanya, S. V. Singh and G. S. Lakhina, "Existence of electrostatic solitary waves over the lunar magnetic anomaly region", International Union of Radio Science (URSI) Regional conference on Radio Science (URSI RCRS 2024), ARIES/GEHU, Bhimtal, Uttarakhand, 22-25 October, 2024.
3. Rubia, R., S. V. Singh, G. S. Lakhina, S. Devanandhan, M. B. Dhanya and T. Kamalam, "Occurrence of Electrostatic Solitary Waves in the Venusian, Plasma Environment", Asia-Pacific Conference on Plasma Physics (AAPPS), Malacca, Malaysia, 3-8 November, 2024.
4. Vipin K. Yadav, "Streaming Beam-Plasma Instability Generation around Moon in Variable Lunar Plasma Environment", 8th Asia-Pacific Conference on Plasma Physics (AAPPS-DPP 2024), Malacca, Malaysia, 03-08 November, 2024.
5. Vipin K. Yadav, "Plasma Wave Studies at Lagrangian Points: L4 and/or L5"; Discussion on India's Next Leap in Solar and Heliospheric Exploration, Indian Institute of Astrophysics (IIA), Bengaluru, 30 July, 2024.

वायुमंडल प्रौद्योगिकी प्रभाग
ATMOSPHERE TECHNOLOGY DIVISION

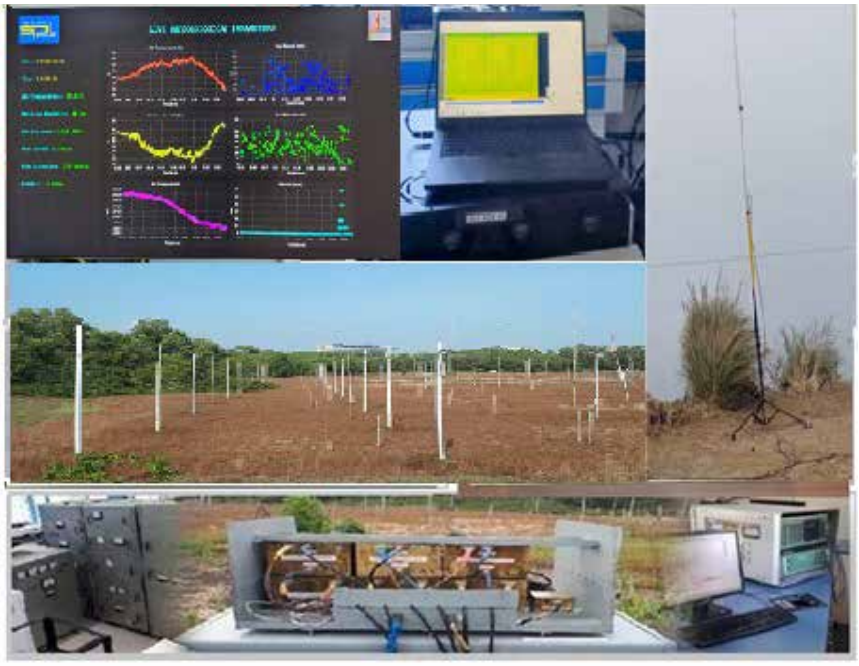

वायुमंडल प्रौद्योगिकी प्रभाग (एटीडी) गुब्बारे, रॉकेट तथा अंतरिक्ष उन्मुख प्रदायभारों की अवधारणा स्तर से लेकर अभिकल्पना, विकास तथा परीक्षण सहित वायुमंडलीय, अंतरिक्ष तथा ग्रहीय विज्ञान क्षेत्रों के लिए अभिकल्पित प्रयोगात्मक प्रणालियों के प्रौद्योगिकी पक्ष पर तथा स्वस्थाने अन्वेषण हेतु भू-आधारित प्रणालियों के विकास और वायुमंडल के सुदूर संवेदन पर ध्यान केंद्रित करता है। सक्रिय प्रयोगात्मक प्रणलियों के संवर्धन तथा रखरखाव, एसपीएल के वैज्ञानिक गतिविधियों को तकनीकी समर्थन देने तथा सामान्य तकनीकी सुविधाओं के अनुरक्षण के लिए भी एटीडी उत्तरदायी है। यह एसपीएल की वैज्ञानिक शाखाओं के साथ निकट समन्वय करते हुए कार्य करता है तथा वैज्ञानिक विचारों को मूर्तरूप देने हेतु तकनीकी विशेषज्ञता प्रदान करता है।

Atmosphere Technology Division (ATD) focuses on the technological aspects of experimental systems designed for atmospheric, space and planetary science areas, including the development and testing of balloon-, rocket-, and space-borne payloads from the proof-of-concept and development of ground-based systems for in-situ probing and remote sensing of the atmosphere. ATD is also responsible for the augmentation and maintenance of the ongoing experimental systems, providing technical support to the scientific activities of SPL and maintenance of the common technical facilities. It works in close coordination with the scientific branches of SPL and provides technical expertise for realization of scientific ideas.

वैज्ञानिक/इंजीनीयर / Scientists/Engineers
दिनकर प्रसाद वज्जा / Dinakar Prasad Vajja
प्रमोद पी पी / Pramod P.P.
मोहम्मद नज़ीर एम / Mohammed Nazeer M.
मणिकंठन नायर एन / Manikantan Nair N.
लाली पी टी / Lali P.T.
अनीष ए एन / Aneesh A.N.

तकनीकी टीम / Technical Team
अनुमोद पी जी / Anumod P.G.
सतीश कुमार बी / Satheesh Kumar B.

Executive Summary

Atmosphere Technology Division (ATD) has made significant contributions to the scientific and technical activities of SPL during the reporting period. These include contributions to the following activities: (i) Design of onboard electronics for the TAAP payload of the Chandrayaan-5/Lupex Lander, (ii) Design of onboard electronics for the PIPPET-V payload of the Venus Impact Probe, (iii) Design of onboard processing electronics for the NMS payload for the upcoming ISRO's scientific missions, (iv) Development of automatic data dissemination system for weather monitor station, (v) Design, development, field testing and regular operation of VLF receiver, (vi) Operation and maintenance of HF radar and Digisonde system (vii) Fabrication of mechanical systems, fixtures, generation of CAD drawings and installation of various scientific instruments. ATD is also carrying out the operation, maintenance and upgradation of the common facilities and looked after the safety aspects of SPL.

Payloads for Space Missions

Onboard Electronics for the TAAP Payload of the Chandrayaan-5/LuPEX Lander

The Thermophysical Analysis of lunAr Polar regolith (TAAP) is one of the payloads to be flown onboard forthcoming ISRO-JAXA LuPEX lander. It draws heritage from the ChaSTE payload onboard Chandrayaan-3 lander. Scientific objectives of the payload are (i) temperature profiling of the lunar regolith up to a depth of 200mm with an accuracy of better than ±0.5 ^{o}C in the range from -200 ^{o}C to +100 ^{o}C, (ii) estimation of thermal conductivity of the regolith at different depths. The payload consists of mechanism unit with a thermal probe and the electronics unit. The mechanism is a motorized unit for probe deployment and penetration operations. The thermal probe consists of twelve Pt-1000 RTD sensors for the temperature profile measurement and two foil heaters for the thermal conductivity experiment.

Functional Requirements of the TAAP Payload Electronics

The onboard electronics for the payload is being designed and developed with the functional requirements: (i) power ON and OFF interface, (ii) deployment motor drive for the payload deployment operation from stowed condition to 180^{o} vertically downward position, (iii) penetration motor drive for inserting the probe into the regolith up to 200 mm depth, (iv) precision current excitation with negligible self-heating effect for the RTD sensors, (v) signal conditioning and accurate digitization of the analog voltages, (vi) probe heaters drive, (vii) payload data transfer periodically to the lander, (viii) telecommands reception and execution for the payload operations and (ix) telemetry generation for the payload status.

Electrical Interfaces of the TAAP Payload Electronics

The electrical interfaces of the TAAP payload electronics were reviewed and finalized. The defined interfaces support pulse- and level-type telecommands, analog and digital telemetry, and a +5 V serial CMOS interface for payload data transfer to the Baseband Data Handling (BDH) system of the lander. Payload data are transmitted at a data rate of 1 kbps with a packet size of 67 bytes per second.

The telecommand interface includes pulse-type commands operating at +5 V with a pulse width of 64 ms for payload ON/OFF, payload reset, deployment and penetration motor selection, and motor drive ON/OFF functions. Level-type commands at 0 V / +5 V are implemented for motor direction control (CW/ACW) and independent ON/OFF control of the two probe heaters.

The telemetry interface comprises both analog and digital-bit signals. Analog telemetry (0 to +5 V), sampled at 2 s intervals, is used for monitoring probe deployment and displacement, as well as RTD-based temperature measurements. Digital-bit telemetry (0 V / +5 V), sampled at 32 s intervals, provides payload ON/OFF status, motor peak current status, and motor selection status.

Payload data transfer to the BDH system is implemented through a dual-redundant serial CMOS interface operating at +5 V. Each channel employs a continuous 1 kHz clock, a data-valid signal with 670 ms ON and 330 ms OFF durations, and NRZ-coded data transmitted at 1 kbps. The timing characteristics of the BDH interface signals are illustrated in Fig. 1.

The payload electronics incorporate multiple interface connectors to support power, command, telemetry, and mechanism interfaces. These include a 9-pin D-sub connector for raw bus power input, a 26-pin high-density D-sub connector for BDH, telecommand, and telemetry interfaces, a 25-pin D-sub connector for payload mechanism interfacing, and a 62-pin high-density D-sub connector for payload probe interfacing.

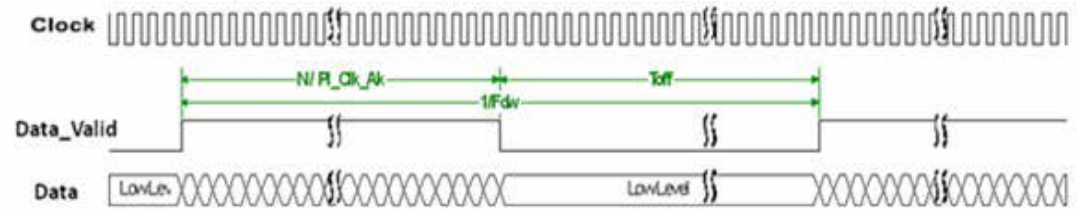

Figure 1: Timing diagram of the BDH signals of the TAAP payload electronics.

Design of the TAAP Payload Electronics

The onboard electronics is built around a FPGA with embedded 8051 processor core. A 3-phase half H-bridge drives two BLDC motors for the probe deployment and the penetration operations. Selection of the motors is done by using two latch relays. 4-wire ratiometric measurement method is adopted for the RTD sensors. A precision current source excites the sensors sequentially with 16x1 analog multiplexer. The RTD signals are properly signal conditioned with buffers and noise filters. A high resolution ADC accurately digitizes the analog signals. Selection of the RTD signals to the ADC is done by using two 16x1 analog multiplexers. Reference voltage for the ADC is derived from a precision external resistor. Two N-channel MOSFETS drive the probe heaters. Currents drawn by the motors and the heaters are also measured during their operations. 4.096 MHz crystal oscillator provides master clock to the circuit. On-chip PLL of the FPGA generates the required clocks for both the ADC and the 8051 processor. Onboard software resides in a PROM of size 32KB. The implemented BDH, TC and TM interface circuits are compatible with the lander electronics. JTAG interface facilitates programming the FPGA and debugging the processor code. URSC make 30W DC-DC converter powers the electronics. A latch relay with pulse telecommands switches ON/OFF the converter. Necessary operating voltages for the circuit are derived from linear low dropout voltage regulators. All the electronic components used are space qualified and part of the PPL of the URSC/SAC/IISU. The electronics has the features of broken sensor wire detection, on-chip calibration for the ADC and safety interlock to limit any excess current drawn during the probe penetration. Design of the electronics (Engineering Model) has been completed and its PCB layout is in progress. Its block diagram is shown in Fig. 2.

Onboard Electronics for the PIPPET-V Payload of the Venus Atmospheric Probe

The PIPET-V (Package for In-situ Profiling of PlanETary atmospheres – Venus) payload was proposed onboard ISRO's Venus Atmospheric Probe (VAP) for profiling pressure and temperature of the Venusian atmosphere from ~ 60 km altitude to surface. The payload has up to

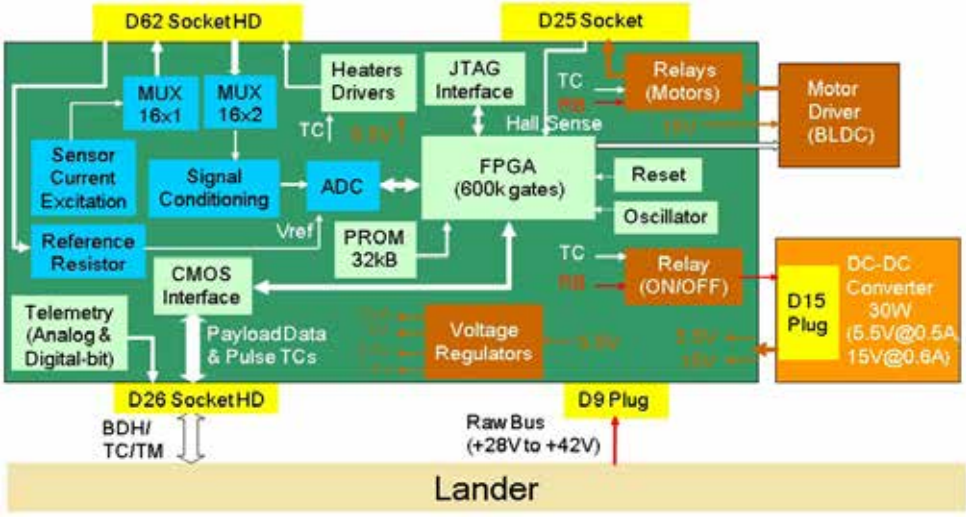

Figure 2: Block diagram of the TAAP payload electronics.

twelve Piezoresistive type pressure sensors and two thin platinum wires with suitable mounts for measuring its atmosphere's pressure with an accuracy of better than ±0.5 % in the range from a few mbar to 100 bar and temperature with an accuracy of better than ±0.5 °C in the range from 200 K to 800 K.

Functional Requirements of the PIPPET-V Payload Electronics

The onboard electronics for the payload is being designed and developed with the functional requirements: (i) precision voltage excitations for the pressure sensors, (ii) precision current excitation with low self-heating effect for the temperature sensors, (iii) signal conditioning and accurate digitization of the analog voltages, (iv) payload data transfer, (v) telemetry generation for the payload status.

Electrical Interfaces of the PIPPET-V Payload Electronics

The electrical interfaces of the PIPPET-V payload electronics were finalised. The interfaces support analog and digital-bit telemetry, along with a +5 V three-line serial CMOS interface for payload data transfer to the Baseband Data Handling (BDH) system of the VAP. Payload data are transmitted at a data rate of 1 kbps with a packet size of 55 bytes per second. The telemetry interface includes digital-bit telemetry at 0 V / +5 V for monitoring the PIPPET-V payload ON/OFF status, with a sampling interval of 32 s. In addition, analog telemetry in the range of 0 to +5 V, sampled every 32 s, is used for monitoring the temperature of the PIPPET-V electronics.

Payload data transfer to the BDH system is implemented through a dual-redundant three-line serial CMOS interface operating at +5 V. Each channel employs a continuous 1 kHz clock and a data-valid signal with ON and OFF durations of 550 ms and 450 ms, respectively. The payload data are transmitted at a rate of 1 kbps using NRZ coding. The payload electronics incorporate dedicated interface connectors to support power, telemetry, BDH communication, and sensor interfaces. These include a 9-pin D-sub connector for power input, a 15-pin high-density D-sub connector for BDH and telemetry interfaces, and a 62-pin high-density D-sub connector for interfacing with payload sensors.

Design of the PIPPET-V Payload Electronics

4-wire ratiometric measurement method is adopted for both the pressure and the temperature sensors. The payload electronics has a precision linear voltage regulator for exciting the pressure sensors. Two precision current sources provide excitation for the temperature sensors. A high resolution ADC accurately digitizes analog signals of the sensors with proper signal conditioning. Selection of the analog signals to the ADC is done by using two 16x1 analog multiplexers. The signal conditioning chain consists of a differential-mode filter, two common-mode filters, two buffer amplifiers and two charge reservoirs. 4.096 MHz crystal oscillator generates master clock to the circuit. JTAG interface facilitates programming the FPGA. The VIP power system provides the required input power supply to the electronics. Necessary operating voltages for the circuit are derived from linear low dropout voltage regulators. All the electronic components used are space qualified and part of the PPL of the URSC/SAC/IISU. The electronics has the features of broken sensor wire detection and on-chip calibration for the ADC. Design of the electronics (Proto Model) has been completed and its PCB layout is initiated. Block diagram of the electronics is shown in Fig. 3.

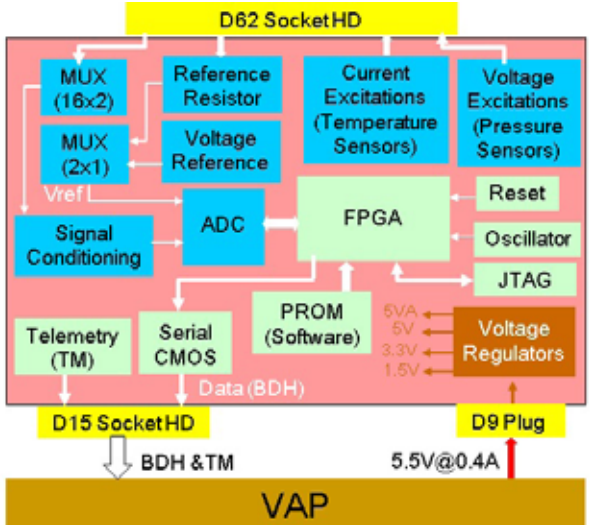

Figure 3: Block diagram of the PIPPET-V payload electronics.

Processing Electronics for the NMS Payload of the DISHA Mission

The NMS (Neutral Mass Spectrometer) payload has been proposed for the DISHA mission. Its objective is to study neutral composition of a tenuous atmosphere. It draws heritage from CHACE-1, MENCA and CHACE-2 payloads.

Functional Requirements of the NMS Payload Processing Electronics

The processing electronics for the payload is being designed and developed with the functional

requirements: (i) data acquisition from the mass spectrometer by initializing its PCCU (Probe Control and Communication Unit), (ii) data transfer to the spacecraft periodically, (iii) reception and execution of data telecommands (16-bit) for selecting operating parameter of the payload and (iv) generation of data telemetry (8-bit) for updating operating the payload status.

Electrical Interfaces of the NMS Payload Processing Electronics

The proposed electrical interfaces for the NMS payload electronics were defined to support serial telecommand, telemetry, and high-speed payload data transfer to the Baseband Data Handling (BDH) system. The interfaces include +5 V serial CMOS data-word telecommand and telemetry links, along with a +5 V three-line serial LVDS (Low Voltage Differential Signalling) interface for payload data transmission. The payload data are transferred at a data rate of 128 kbps with a data packet size of 2048 bytes. The serial telecommand and telemetry interfaces are implemented using +5 V CMOS data-word formats. The timing characteristics of the telecommand and telemetry signals are illustrated in Fig. 4 and Fig. 5, respectively, demonstrating compliance with the specified data-word protocol and interface timing requirements.

Payload data transfer to the BDH system is realized through a dual-redundant three-line LVDS interface. Each channel operates with a continuous 128 kHz clock and a data-valid signal having ON and OFF durations of 128 ms and 384 ms, respectively. The payload data are transmitted at 128 kbps using NRZ coding. The NMS payload electronics incorporate dedicated interface connectors to support power, telecommand, telemetry, and BDH interfaces. A 9-pin D-sub connector is provided for power input, while a 44-pin high-density D-sub connector is used for BDH, telecommand, and telemetry interfacing.

Design of the NMS Payload Processing Electronics

The processing electronics is built around a FPGA with 8051 processor core. It has RS-232 transceiver for communication with the PCCU for data acquisition. Onboard software and initial configuration parameters of the mass spectrometer reside in a PROM of size 32KB. EEPROM of size

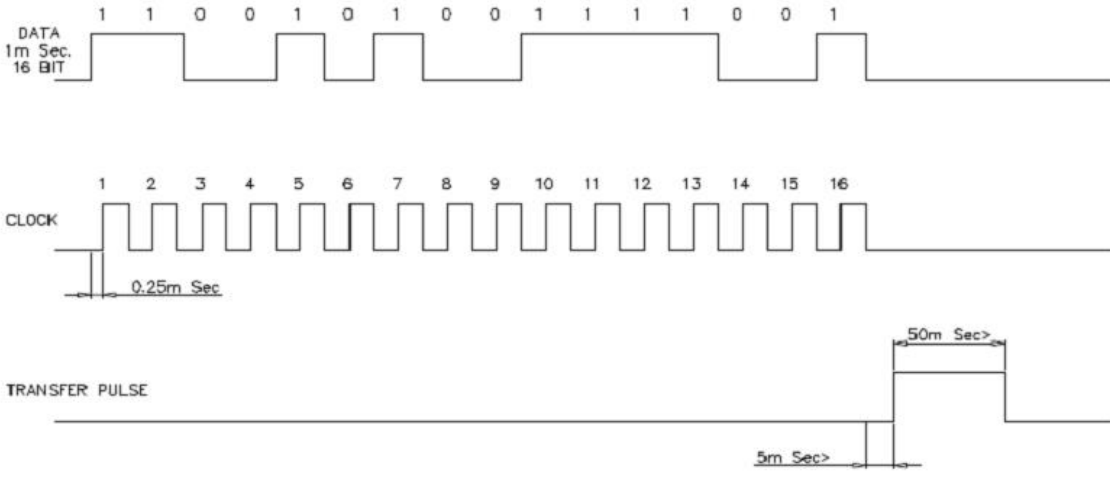

Figure 4: Timing diagram of the telecommand signals of the NMS payload electronics.

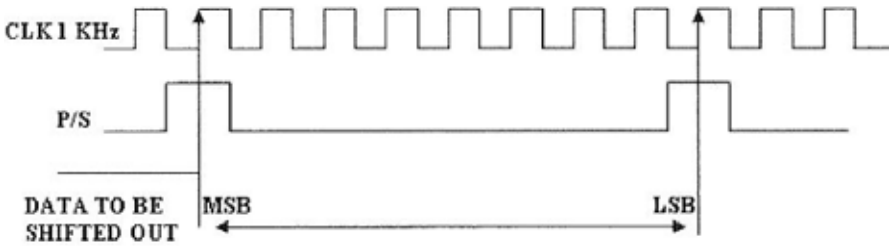

Figure 5: Timing diagram of the telemetry signals of the NMS payload electronics.

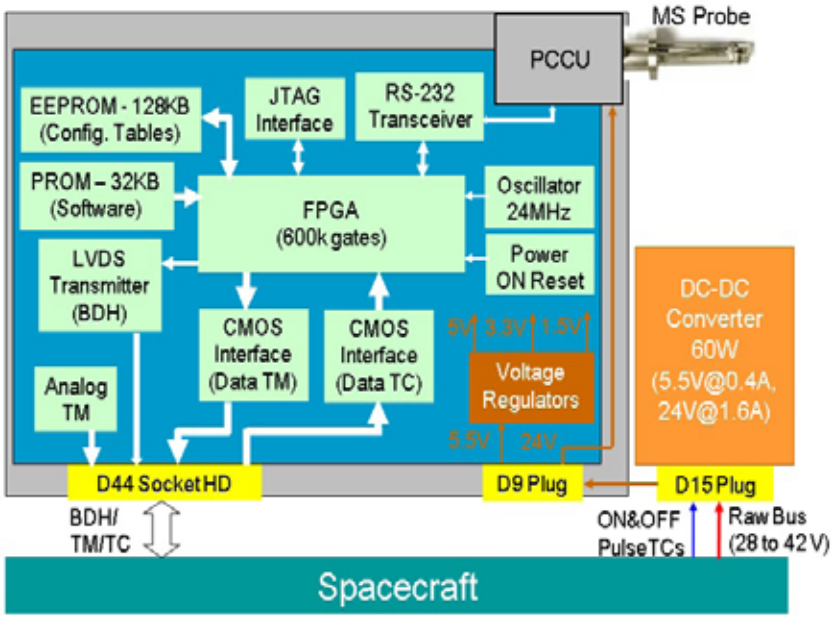

Figure 6: Block diagram of the NMS payload electronics.

128KB stores final configuration parameters of the mass spectrometer. 24MHz crystal oscillator generates master clock to the processor. JTAG interface facilitates programming the FPGA and debugging the processor code. URSC make 60W DC-DC converter powers the electronics. Necessary operating voltages for the circuit are derived from linear low dropout voltage regulators. All the electronic components used are space qualified and part of the PPL of the URSC/SAC/IISU. Design of the electronics (Proto Model) has been completed and its PCB layout is initiated as per the following block diagram (Fig. 6).

Onboard Electronics for the ATOXS Payload of the POEM Mission

ATOXS (ATomic OXygen Sensor) payload measures atomic oxygen concentration in the Earth's atmosphere. The payload consists of a sensor unit and an electronics unit. A Zinc Oxide (ZnO) thin film based sensor unit has been in-house developed for the measurement of atomic oxygen concentration. Sensor electronics (Flight Model-FM) and its electrical interfaces have been finalized after thorough testing of its Proto Model and detailed review by an expert committee in VSSC. Fabrication of the FM electronics is in progress. All the electronics components are selected from the PPL of the VSSC. A 6-layer PCB of 100x100x2 mm^3 size has been designed and its QC inspection has also been completed. Mechanical design of the PCB and chassis have been completed. Calibration and characterization of the sensor is in progress.

Onboard Electronics for the RoBOT Payload for Sounding Rocket Experiments

RoBOT (Rocket-Borne atomic Oxygen sensor for Thermosphere) payload has been proposed to measure the atomic oxygen concentration at 80-120 km altitude onboard RH300 and 80-500 km onboard RH560. The payload consists of a Quartz Crystal Microbalance (QCM) based sensor unit and an electronics unit for data acquisition. The sensor unit contains silver coated QCM as a measuring sensor and gold coated QCM as a reference sensor. Frequency of the measuring QCM decreases as it interacts with atomic oxygen whereas the reference QCM remains unaltered. The reference QCM is employed to nullify frequency changes due to temperature and aging. Reduction in the frequency is calibrated against the atomic oxygen concentration.

Design of the RoBOT Payload Electronics

The electronics (Proto Model) has been designed with the functional requirements, i) generation of regulated voltage (+5 V) from raw bus supply, ii) excitation for QCM oscillators for frequency signal generation, iii) counting the pulses of the reference and the measurement QCM oscillators, iv) transfer the payload data to rocket telemetry system through RS485 interface.

The electronics is built around a PIC microcontroller. The microcontroller is selected due to its small size, less power consumption and easy implementation. It has 32 kB of program memory and 2048 bytes

of data memory. A DC-DC micro-module convertor generates regulated +5 V supply from the raw power for the electronics. Two Pierce crystal oscillator circuits are used to produce square wave pulses from the QCMs. The pulses are counted with an accuracy of 1pulse by using two built-in counters of the microcontroller. Pulses counting period of 100 ms is finalized to obtain 50 to 100 m for RH300 flight and 300 to 500 m for RH560 flight. The pulse count data is stored in the internal data memory of the microcontroller. RS485 protocol is implemented to transfer the payload data to the rocket telemetry system. The electronics receives RS-485 commands periodically from data processing unit (DPU) of the sounding rocket for transferring the data. The payload has one D-sub 9-pin plug connector to interface with raw power system of the rocket and one D-sub 9-pin socket connector to interface with the rocket telemetry. All the electronics components are selected from the PPL of the VSSC. Onboard software for the electronics is developed in embedded C. Block diagram of the payload electronics is shown in Fig 7.

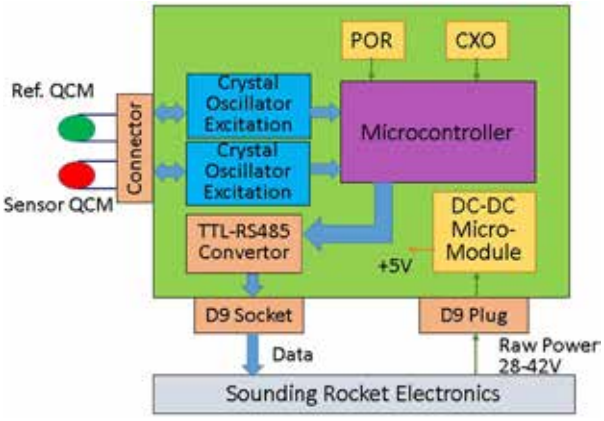

Figure 7: Block diagram of the RoBOT payload electronics.

Ground-based Systems

Development of Automatic Data Dissemination System for Weather Monitoring Station

An automatic data dissemination system was developed for remote weather monitoring applications to enable real-time acquisition, transmission, archiving, and visualization of meteorological data. The system autonomously acquires weather data from the monitoring station and disseminates it to a remote location through Ethernet communication, thereby eliminating the need for manual data downloads and facilitating continuous real-time monitoring. The system comprises stand-alone transmitter, receiver, and remote data display units. The transmitter unit, installed at the weather monitoring site, periodically acquires data via an RS-232 interface and wirelessly transmits the data using LoRa communication operating in the license-free 866 MHz band. The receiver unit, located nearby, receives the data packets and forwards them to a remote location through Ethernet.

The remote data display unit receives the data via Ethernet, archives it, and presents key meteorological parameters—temperature, relative humidity, pressure, wind speed, wind direction, and rainfall—in real-time graphical format. The system has been successfully implemented and is operational. The developed transmitter card is shown in Fig. 8.

Figure 8: Transmitter card of the data dissemination system.

Development of VLF Receiver

An in-house Very Low Frequency (VLF) receiver has been designed and developed to investigate the dynamics of the equatorial ionospheric D region. The receiver is designed to detect radio waves in the 1 kHz to 50 kHz frequency range and employs a 2 m non-resonant electric-field monopole antenna. The system comprises an advanced low-noise amplifier for high-sensitivity signal amplification, followed by analog and digital filtering to suppress unwanted noise, and a high-sampling-rate data acquisition module for accurate digitization of the received signals. The internal configuration of the VLF receiver is shown in Fig. 9.

The developed VLF receiver has been operational at Ponmudi since 03 February, 2025. Initial

Figure 9: Inside view of the developed VLF receiver.

observations demonstrate the capability of the system to capture fine ionospheric signatures. Fig. 10 shows a representative spectrogram illustrating the occurrence of two tweak events. These features arise due to dispersion in the Earth–ionosphere waveguide, where higher-frequency components arrive earlier than lower-frequency components. The dispersion persists up to the cutoff frequency, beyond which wave propagation is not supported. In the present observations, first- and second-order modes are identified.

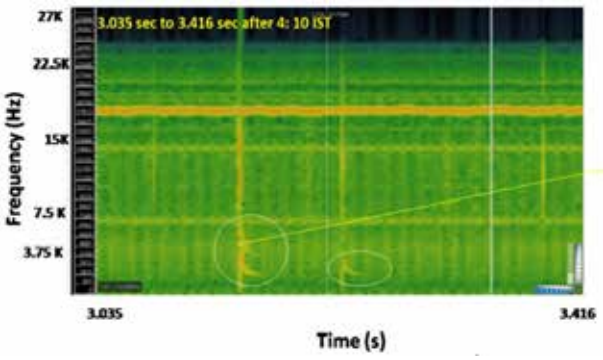

Figure 10: Spectrogram illustrating the occurrence of two tweak events.

Operation and Maintenance of HF Radar System

The in-house developed HF radar is a phase-coherent, monostatic, pulsed system operating at 18 MHz, designed to study plasma instability processes associated with Equatorial Electrojet (EEJ) and Equatorial Spread-F (ESF) irregularities in the ionosphere. The radar operates with a peak transmitter power of 50 kW and employs an interlaced phased-array antenna consisting of 72 wire dipoles arranged in a 12×6 configuration over an area of ~10,000 m^2. Doppler beam swinging is implemented with beam directions at the zenith, 30° East, and 30° West. Backscattered signals are processed using a digital receiver and a PC-based data acquisition system.

Periodic breakdown and preventive maintenance were carried out during the year, including the replacement of 18 damaged antenna masts and reinstallation of dipole antennas (Fig. 11) and restoring the system to reliable operation. The radar was operated routinely and continuously (24×7) during observation campaigns. During January-December 2025, the system operated for 248 days with a total observation time of approximately 2,000 hours. Representative ESF power spectra observed in the zenith beam on 03 January 2025 are shown in Fig. 12.

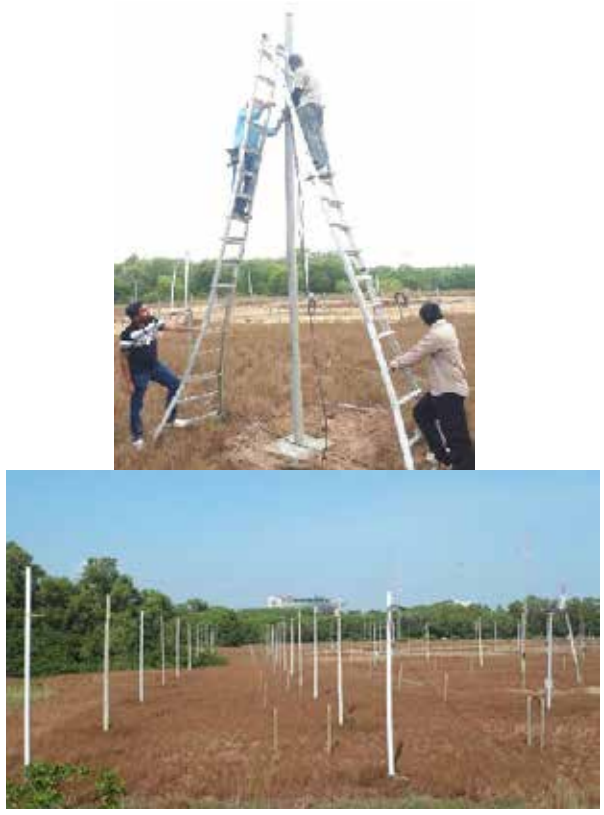

Figure 11: Refurbished masts of the HF radar antenna.

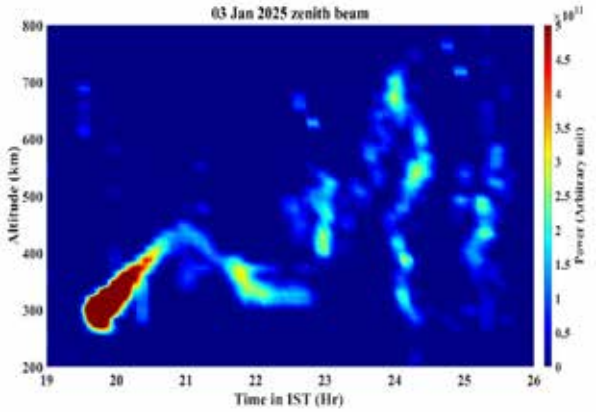

Figure 12: Received power spectra of ESF for zenith beam on 03 January, 2025.

Operation and Maintenance of Digisonde System

Digisonde is an Ionospheric radar that uses high frequency radio waves (2 to 20 MHz) for monitoring electron density in the ionosphere. It generates 300 W peak transmission power. Signal transmission is performed with two (NE–SW and NW–SE) crossed delta antennas of 30 m in height. Signal reception is done with an array of four crossed magnetic dipole receive antennas in a triangular arrangement.

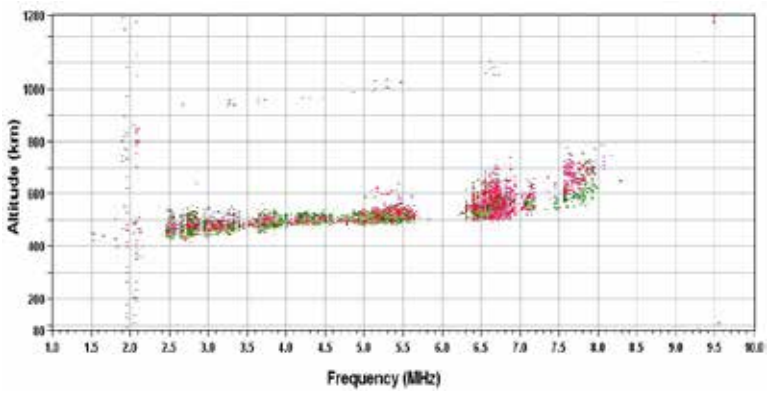

Figure 13: Ionogram observed by the Digisonde on 03 January, 2025.

Ionogram observed by the system on 03 January, 2025 is shown in Fig. 13.

Experimental and Common Facilities

Operation and Maintenance of HVSSF

The HVSSF (High Vacuum Space Simulation Facility) is operated, maintained and augmented with sub-systems for the development, testing, calibration and characterization of scientific payloads. Technical support has been provided for the following activities which include: (i) verification of the revised energy levels of the PAPA payload from 400 eV to 5 keV with its proto-FM for uploading to its FM operation, (ii) calibration of atomic Oxygen sensor being developed at SPL and (iii) testing of Silicone-based substrates by illuminating with UV radiation which were developed by PSCG/VSSC. The photograph of the test setup of the Silicone-based substrate in the HVSSF is shown in Fig. 14.

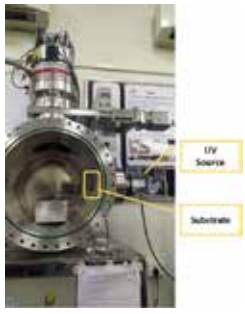

Figure 14: Test setup for the Silicone-based substrates in the HVSSF.

Operation and Maintenance of Clean Room Facility

The clean room facility of SPL is equipped with two clean rooms of class 10000 and class 100000 and two work benches (Laminar flow tables) of class 100 and class 1000. Regular up-keep and maintenance of the facility have been carried out.

Mechanical Engineering Activities

The following mechanical engineering activities were carried out at SPL workshop and CAD design unit: (i) Coordinated fabrication activities of SPL's ENWi and LP probes for RH560 flight from Kulasekharapatnam, (Fig. 15), (ii) Coordinated fabrication activities of detector flange for Monochromator, (iii) Prepared CAD drawings and generated 3D model for fabrication of mask assembly for daytime airglow photometer and (iv) Prepared CAD drawings for fabrication of mono lens photometer.

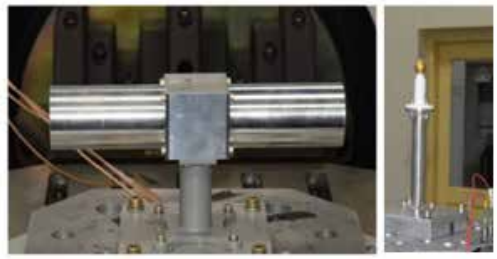

Figure 15: The fabricated ENWi and LP probes for the RH560 flight.

Ongoing Activities and Future Projections

- Qualification of sensor for profiling middle atmosphere temperature onboard RH200.
- Qualification of electronics for Atomic Oxygen Sensor onboard POEM and Sounding Rockets.
- Qualification of electronics for the TAAP payload of the LuPEX mission.
- Qualification of electronics for the PIPPET-V payload of the VAP.
- Qualification of electronics for the NMS payload of the DISHA mission.
- Development of digisonde system.

Publications in Peer-Reviewed Journals

1. Mathew, N., K. Durga Prasad, Dinakar Prasad Vajja , V. Aasik , Fazil Mohammad , P.P. Pramod, M. Satheesh Chandran, Kiran John Antony, M. Ram Prabhu , M.B. Dhanya , Manu V. Unnithan, Shiju G. Thomas , Chandan Kumar, Dona Mathew, R. Suresh , K.P. Subhajayan, P.S. Ajeeshkumar, P. Kalyana Reddy, Samik Jash, K. Kannan, K. Sunitha , Sanjeev Mishra, Janmejay Kumar, V. Sathiyamoorthy and Anil Bhardwaj, Chandra's Surface Thermophysical Experiment (ChaSTE) onboard Chandrayaan-3 Lander, Advances in Space Research, https://doi.org/10.1016/j.asr.2025.01.022, 2025.
2. Mathew, N., M. RamPrabhu, V. Aasik , Fazil Mohammad , Dinakar PrasadVajja, P.P. Pramod, Kiran John Antony, M.Satheesh Chandran, K.P. Subhajayan and V. Sathiyamoorthy, Operational insights and measurements of ChaSTE on the Chandrayaan-3 Vikram Lander, Advances in Space Research, https://doi.org/10.1016/ j.asr. 2025.05.024, 2025.
3. Mathew, N., K. Durga Prasad, Fazil Mohammad, V. Aasik, Dinakar Prasad Vajja, M. Ram Prabhu, M. Satheesh Chandran, K. P. Subhajayan, Kiran John Antony, P. P. Pramod, Chandan Kumar, Dona Mathew, R. Suresh, U. A. Subramanian, V. Sathiyamoorthy, Manu V. Unnithan, V. Preethakumari, Vinitha Ramdas, Ajay Salas, P. S. Ajeeshkumar, Neha Naik, Vinu Paul, P. Kalyana Reddy, G. Ambily, K. Kannan, M. B. Dhanya, Sanjeev Mishra, P. T. Lali, K. Sunitha, Samik Jash, Tanmay Singhal, Janmejay Kumar, Manoj Kumar Mishra, R. Renju, C. Suresh Raju and Anil Bhardwaj, Thermal conductivity of high latitude lunar regolith measured by Chandra's Surface Thermophysical Experiment (ChaSTE) onboard Chandrayaan-3 lander, Scientific Reports, https://doi.org/10.1038/s41598-025-91866-4, 2025.

Technical Reports

1. Pramod P. P. and Ayisha M. Ashruf, Requirement specifications of electronics for Rocket-Borne atomic Oxygen Sensor for Thermosphere (RoBOT) payload onboard sounding rocket, ISRO-VSSC-DR-0402-0-25, July 2025.
2. Ayisha M. Ashruf, C. Vineeth, Pramod P. P, Ashok K., Mahesh S., Jinesh K. B. and Roshit K. R., Characterization of the Atomic Oxygen sensor (ATOXS) for low-earth orbit applications, ISRO-VSSC-TR-0369-0-25, June 2025.

योजना और समन्वय प्रकोष्ठ
Planning and Coordination Cell

The Planning and Coordination Cell of SPL (SPL – PCC) is responsible for the overall planning of the activities at SPL, annual budget preparation and presentations for approval, coordination of need aspect review of scientific and technical items required for SPL activities, monitoring of procurement status and budget utilisation, coordination with other entities of VSSC and ISRO HQ and the periodic progress report preparation of the laboratory for submission to higher management.

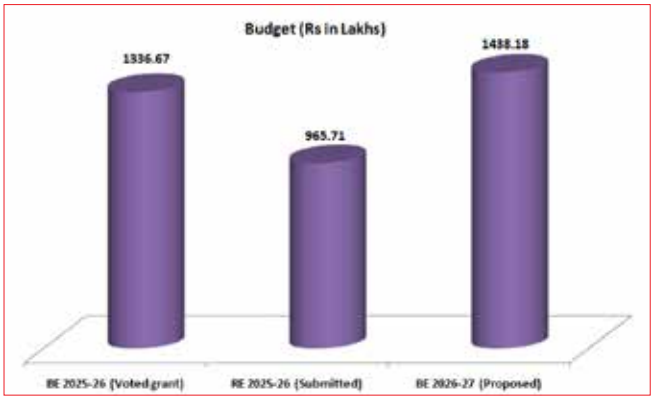

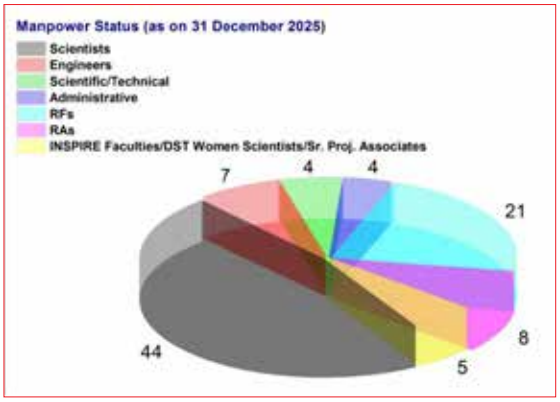

एसपीएल पीसीसी टीम / SPL – PCC Team

सुरेश बाबू एस, प्रधान, पीसीसी / Suresh Babu S., Head, PCC
विजयकुमार एस नायर / Vijayakumar S. Nair
अजीषकुमार पी एस / Ajeeshkumar P. S.
षिजी एन डी / Shiji N. D.

कार्यालय और प्रशासनिक सहायता
Office and Administrative Support

एसपीएल कार्यालय टीम / SPL Office Team

शालिनी एम एस / Salini M. S.
षिजी एन डी / Shiji N. D.
सिमी इस्माइल / Simi Ismail
यूसफ एन / Yoosaf N.

SPL administration facilitates the administrative and secretarial requirements for a smooth and effective functioning of SPL by providing co-ordination, communication and logistics. Besides the general administration, office management and housekeeping of SPL, it caters to the necessary official assistance to different ISRO projects such as ARFI and NOBLE. It co-ordinates and provides logistic support for different national observation campaigns of SPL. Also, SPL administration is responsible for coordinating activities within SPL, involving other divisions, facilities of VSSC and/or other ISRO centers and different Institutions/Universities. It meets the administrative requirements of different payload development for ISRO's space missions.

Research programme facilitated by ISRO fellowship program including research fellowship program and research associate program is a major activity of SPL. SPL administration provides the required assistance interms of documentation and organizing Ph.D. synopsis/defense, doctoral committee meetings, student reviews, regular student/faculty seminars and Central Level Monitoring Committee meeting of VSSC. It also supports for arranging seminars/invited talks in SPL by leading scientists from India and abroad and arranges necessary logistics required during their visit and stay.

क्षमता निर्माण गतिविधियां
CAPACITY BUILDING ACTIVITIES

SPL is dedicated to advancing research and development in atmospheric, space, and planetary sciences. As part of its capacity-building activities, SPL supports a range of activities aimed at developing expertise in these fields. This includes providing opportunities for doctoral research leading to a PhD degree and post-doctoral research conducted through ISRO's Research Associate Scheme and other national initiatives such as the INSPIRE Fellowship, Ramanujan Fellowship, National Postdoctoral Fellowship, and DST Women Fellowship. SPL also organizes internship programs and academic projects for college and university students as part of their graduate and post- graduate courses.

Additionally, SPL scientists engage with educational institutions by delivering lectures on advanced and fundamental topics in atmospheric, space, and planetary sciences as part of National Space Day, National Science Day, International Moon Day, World Environment Day and World Space Week programs.SPL scientists give interviews and lectures on the importance and challenges of scientific space missions in national media for public awareness These efforts aim to foster scientific knowledge, inspire future researchers, and strengthen India's capabilities in space science and technology.

अकादमिक परियोजनाएं / ACADEMIC PROJECTS

पीएच.डी.प्रशिक्षण / Ph.D. INTERNSHIP

1. Ayushi Nema, Department of Physics, Sardar Vallabhbhai National Institute of Technology, Surat, India, "Impact of HILDCAAS on the Earth's Outer Radiation Belt", July - August, 2024 [Supervisor: Ankush Bhaskar]

एम.एससी/बी.एससी/परियोजना/प्रशिक्षण / M.Sc./B.Sc. PROJECTS/INTERNSHIP

1. Rincy Roy., University of Kerala, "A satellite-based study on the fog occurrence over the south Peninsular India", May-July 2025 [Supervisor: SathiyamoorthyV.].
2. Lekshmi R Mohan., "Impact of Clouds on Surface Radiation Balance over a Dry Peninsular Indian Region" March-May, 2025 [Supervisor: Dr. Kiran Kumar NVP].
3. Athira AA., University of Kerala, "Identification of Overshooting convective clouds using passive Microwave observations by Megha-Tropiques SAPHIR at 183.31 GHz" April -May, 2025 [Supervisor: Nizy Mathew].
4. Achin Sarkar., IISER, Kolkata, "Atmospheric Boundary layer over an urban location (New Delhi) during winter season", December 2024 - January 2025 [Supervisor: Santosh Muralidharan].
5. Viswajith Alex., IIT, Bhubaneshwar, "Structure and dynamics of Eastern India Coastal Current in Bay of Bengal". May- June 2025. [Supervisor: Santosh Muralidharan].
6. Aleesha K. B., Cochin University of Science & Technology, Kochi "Estimation of Soil Moisture from SAR Observations Using Machine Learning Techniques over the Different Regions of India", August 2024 - February, 2025 [Supervisor: Renju R.].
7. Gayathri M, Sacred Heart College, Thevara, "Investigating the relationship between soil moisture and rainfall over Indian region", April-June, 2025 [Supervisor: Renju R.]
8. Infant Nishant., Madras Christian College, "Lunar Thermal Energy Storage and Power Generation", December 2024 - January 2025. [Supervisor: Renju R.].
9. Revathy S., Sacred Heart College, Thevara, "Impact of rain drop axis ratio on attenuation of GSAT-14/Ka band signals over Thumba", April-June 2025 [Supervisor: Renju R.].
10. Ann Maria., Sacred Heart College, Thevara. "Vertical structure of Cumulonimbus clouds and intense convective clouds over Thumba using C-band polarimetric radar", April-June, 2025 [Supervisor: Shailendra Kumar].
11. Arthay V. S., All Saint's College, Thiruvananthapuram, "Intercomparison of rainfall data form INSAT and GPM IMERGE over India", April-June, 2025 [Supervisor: Shailendra Kumar].
12. Sahana K., NSS Hindu College, Changanacherry, "A Study on the Attenuation of Solar Radiation on Mars due to Dust", March-May, 2025. [Supervisor: Vijayakumar S. Nair]
13. Deepanshu Meena, Indian Institute of Space Science and Technology, Thiruvananthapuram, "Impact of Dust on Solar Radiation Reaching the Martian Surface", June-July, 2025. [Supervisor: Vijayakumar S. Nair]
14. Aishik Parna Borah, Indian Institute of Technology, Madras, "Impact of black carbon deposition on Himalayan snow albedo: a case study from December 2010", May-July, 2025. [Supervisor: Vijayakumar S. Nair]

15. Rupankar Mitra, Kerala University of Digital Sciences Innovation and Technology, Thiruvananthapuram, "Application of AI/ML techniques for fast radiative transfer computations", July-August, 2025. [Supervisor: Vijayakumar S. Nair]
16. Elsa Maria Nobi, Sacred Heart College, Thevara, "Chemical Characterisation of atmospheric Aerosols at a High-altitude Site on the Southwest coast of India", April 2025 [Supervisor: Prashant Hegde].
17. Pratik Sahu, Indian Institute of Science, Education and Research, Kolkata, "Sensitivity study on the satellite reaching radiance using 6S Radiative Transfer Model", June-August, 2025 [Supervisor: Mukunda Gogoi].
18. Anupjyoti Sarma, Dibrugarh University, Assam, "Satellite remote sensing of atmospheric aerosols", January 2025 [Supervisor: Mukunda Gogoi].
19. Jugnu Shukkur, Indian Institute of Science Education and Research, Tirupati, "A study on observational techniques for the measurement of SO_2 from the Space", December 2024-January 2025. [Supervisor: Sobhan Kumar Kompalli]
20. Rajagopal, L., PSG College of Arts and Science, Coimbatore, "A study on cloud condensation nuclei over tropical coastal atmosphere", November-December, 2025 [Supervisor: Sobhan Kumar Kompalli]
21. Dhatchanamoorthi, M., PSG College of Arts and Science, Coimbatore, "A study on cloud condensation nuclei over tropical coastal atmosphere", November-December, 2025 [Supervisor: Sobhan Kumar Kompalli]
22. Kanishka Karunakaran, PSG College of Arts and Science, Coimbatore, "A study on cloud condensation nuclei over tropical coastal atmosphere", November-December, 2025 [Supervisor: Sobhan Kumar Kompalli]
23. Adithya Santhosh, All Saint's College, Thiruvananthapuram, "Distribution and Characteristics of Dust Aerosols in Martian Atmosphere", February–June, 2025 [Supervisor: Prijith S. S.]
24. Revathy A. S., St. Xavier's College, Thumba, "Characteristics of Marian dust aerosols under different scenarios" July-October, 2025 [Supervisor: Prijith S. S.]
25. Archana P. J., Government College, Kariavattom, "Investigating the structural signatures of Atmospheric Organic Aerosols using 1 H Nmr", September 2024 - January 2025. [Supervisor: Boreddy Suresh Kumar Reddy]
26. Moulidharan S., Alagappa University, Thondi, "Chemical characterization of water-soluble organic carbon and water-soluble total nitrogen aerosols", December 2024-January 2025. [Supervisor: Boreddy Suresh Kumar Reddy]
27. Felsa Ann, SRM Institute of Science and Technology, Chennai, "Terrestrial and Extraterrestrial Origin of PAHs", May- June, 2025. [Supervisor: Boreddy Suresh Kumar Reddy]
28. Jonnalagadda Gayatri, Amrita Vishwa Vidyapeetham, Ettimadai, "Future climate projections over the Indian subcontinent", June - July 2025 [Supervisor: Sijikumar S.]
29. Sandra Divya Rajesh, Vellore Institute of Technology, Vellore, "Lower Atmospheric Dynamics", May - June 2025 [Supervisor: Sijikumar S.]
30. Kavyasree, M. S., All Saints College, Thiruvananthapuram, "Upper Tropospheric Humidity: A Panoramic View from INSAT 3DR and INSAT 3DS", July 2025 [Supervisor: Uma K. N.]
31. Abhinav A B, Department of Physics, Cochin University of Science and Technology, Kochi, "Exploring the Thermal Impact of Global Dust Storms on the Surface and Atmosphere of Mars", January-May 2025 [Supervisor: S. V. Sunil Kumar].
32. Anand J, Amrita Vishwa Vidhyapeetham, Kollam, "A statistical study on the coupling between the Quasi Biennial Oscillation, the El-Nino Southern Oscillation and the Madden Julian Oscillation", January 2025 [Supervisor: N. Koushik].
33. Ancy Antony, All Saint's College, Thiruvananthapuram,"Characteristics of Semi-annual and Annual Oscillations over the Sub-tropical station 'Balasore' using RH-200 Sounding Rocket Observations", April-July 2025 [Supervisor: Siddarth Shankar Das].
34. Arya S,Department of Physics, University of Kerala, Thiruvananthapuram, "Representation of Atmospheric Dynamics during the Sudden Stratospheric Warming event of January 2009 in the whole atmosphere reanalysis JAWARA", March-June 2025 [Supervisor: N. Koushik].
35. Gagan S., MS Ramiah University of Applies Sciences, Bangalore, "Exploring Aerosols and Clouds using EarthCARE Atmospheric Lidar Data", November-December 2025 [Supervisor: Varun Nikam].
36. Harsh Kumar, Indian Institute of Space Science and Technology, Thiruvananthapuram "Optical Characterisation of Laser Systems for Atmospheric Lidar Application", June-August 2025 [Supervisor: S. V.Sunil Kumar].
37. Nandhana Narayanan, Cochin University of Science and Technology, Kochi, "Study on the distributions of relative humidity during the passage of tropical cyclone using SAPHIR on-board Megha-Tropiques", April-June 2025 [Supervisor: Siddarth Shankar Das].

38. Niranjana Varma S, Amrita Vishwa Vidyapeetham, Kollam, “Cold Collar: An Enigmatic Thermal Structure in the Venusian Atmosphere”, November-December 2024 [Supervisors: K. Kishore Kumar & S. V. Sunil Kumar].
39. Vishnudhasan G, KSR Institute for Engineering and Technology, Namakkal, Tamil Nadu, “Development of a Real-time Data Visualization and Analysis Software for Atmospheric Lidar Application", February-May 2025 [Supervisor: JayadevPradeep].
40. Prudhvi Teja, National Institute of Technology, Surat “A study on the Variations in the Topside Ionosphere Using PLASDEM onboard PSLV-POEM Mission”, January - June 2025 [Supervisor: Raj Kumar Choudhary].
41. Arjun Aditya, National Institute of Technology, Raipur, “Development of ionospheric tomography technique to generate three-dimensional distribution of plasma density over the Indian Low latitude ionospheric region using GNSS satellite system”, July-October 2025 [Supervisor: Raj Kumar Choudhary].
42. Farha, F., MES Kalladi College, Mannarkad, Department of Physics, University of Calicut, Kerala, “Ionospheric response during magnetic disturbances and quiet periods: effects on occurrence of irregularities” [Supervisor: Manju G.].
43. Hemashree, University of Bangalore " Study of ionospheric scintillations using Kp and Ap indices", 1-30 May 2025 [Supervisor: Manju G.].
44. Stebin Sunny, Mar Ivanios College, Trivandrum, “Application of high-resolution grating monochromator for measurement of mesospheric dayglow emissions”, July 2025 – Jan 2026 [Supervisor: Mosarraf Hossain Md].
45. Karthika M, Rathinam College of Arts and Science, Coimbatore, “Prediction of Dst index three hours in advances using AIML techniques”, July-October 2025 [Supervisor: Ambili K. M.].
46. Huda Rana A, University of Kerala Karyavattam Campus, Trivandrum, “Response of the dip equatorial and low latitude ionosphere to the severe geomagnetic storm occurred on 12 August 2024”, March-May 2025 [Supervisor: Ambili K. M.].
47. Rajamahanthi Tejaswini, SASTRA Deemed to be University, Thankavur, “Response of equatorial and low latitude ionosphere to the intense storms”, June-August 2025-06.08.2025 [Supervisor: Ambili K. M.].
48. Midhun Gowtham M., Sardar Vallabhbhai National Institute of Technology, Surat, Gujarat; “Studies on solar transient phenomena with MAG IMF measurements onboard Aditya-L1”, November – December, 2024. [Supervisor: Vipin K. Yadav]
49. Rohit Mathew Titus, IISER, Trivandrum, Kerala; “Observations of Solar Alfven wave signatures from various spacecrafts with plasma and IMF data”, December, 2024 – January, 2025. [Supervisor: Vipin K. Yadav]
50. Shreya Varsha Arun, Amritha Vishwa Vidyapeetham, Kollam, Kerala; “Observations of Extreme Solar Transient Events from IMF Data measured by the MAG Payload onboard Aditya-L1 Spacecraft”; July, 2024. [Supervisor: Vipin K. Yadav]
51. Yuvasree Vydhyanathan,"Prediction geomagnetic indices using AI/ML", CUSAT, Kochi, December 2024 - January 2025. [Supervisor: Dhanya M B]
52. Keerthy. S. A, Dept. of Physics, All Saints College, ““Study of Variation of the Alpha-Proton Ratio in the Solar Wind during Solar Activity””, Thiruvananthapuram, April-June 2025. [Supervisor: Dhanya M B]
53. Roshna. N, Dept. of Physics, University of Kerala, ““Simulation of Carbon Foil for the Space Based Mass Spectrometers””, Thiruvananthapuram, April-June 2025. [Supervisor: Dhanya M B]
54. Arathy V. Nair, Sri Sathya Sai Arts and Science College, Kerala; “Response of the Martian Upper Atmosphere to the impact of coronal mass ejection: A case study”; April, 2024. [Supervisor: V. Venkataraman]
55. Abhita, University of Kerala, Trivandrum, “Turbulence in ICME multi-point observations.”; March - July 2025. [Supervisor: Ankush Bhaskar]
56. Govind G B, IUCAA, Pune, “Solar wind acceleration”, June - July 2025. [Supervisor: Ankush Bhaskar]
57. Noora Rafeeq, St Xavier’s College, Thumba, “Impact of Interplanetary Coronal Mass Ejection on Venusian Induced Magnetosphere”, July - October 2025. [Supervisor: Ankush Bhaskar]
58. Akash Bhaskar; Mahatma Gandhi College, Udupi, Karnataka; “Study of Coronal Mass Ejection (CME) event on October 10, 2024”, May–June, 2025. [Supervisor: Chemukula Mathin Yadav]
59. Priyanka Priyadarshini; NIT, Surathkal, Karnataka; “Study of Solar Wind and its Variabilities”; September 2024 – January 2025. [Supervisor: Chemukula Mathin Yadav]
60. Bhaminy Krishnan G. and Ms. Divya S. John, Govt. College Karyavattom, Trivandrum, Kerala; “Machine Learning for Solar Flare Forecasting: A Comparative Study”; June – August, 2025. [Supervisor: Pritesh Meshram]

एम.टेक/बी.टेक परियोजना/ M.Tech/B.Tech PROJECT

1. Nada Basheer, "Predicting the solar flares from magnetograms and magnetic parameters Using Deep Learning Models", Department of Computer Science, Cochin University of Science and Technology, September 2024 - February 2025. [Supervisor: Dhanya M B]
2. ApparajuKedari Sri Vyshnavi, Amritha Viswa Vidyapeetham, Chennai, **"**Development of embedded software for Sun angles computation by using GPS time and position information", July-September, 2025 [Supervisor: Pramod PP].
3. ArahamAbeddin, NSHM Knowledge Campus, Durgapur, "Development of frequency counter for quartz crystal-based sensor"**,** January-April, 2025 [Supervisor: Pramod PP].
4. Pulimi Keerthi, Amrita School of Engineering, Chennai, "Automatic Data Retrieval and Wireless Data Transfer System for Weather Stations", January-April, 2025 [Supervisor: Lali PT].
5. Rengapriyaa L, Thiagarajar College of Engineering, Madurai, "Application of AIML techniques to the prediction of solar flares", December-January 2025 [Supervisor:Ambili K. M.].
6. Sowndarya M, KSR Institute of Engg& Technology, Tiruchengode, "Prediction of Dst index using AIML techniques", February-May 2025 [Supervisor: Ambili K. M.].

आईएएससी-आईएनएसए-एनएएसआई ग्रीष्मकालीन अनुसंधान फैलोशिप योजना / IASc-INSA-NASI SUMMER RESEARCH FELLOWSHIP PROGRAMME

1. Shruti Bhattacharya, University of Calcutta, Kolkata, "Characteristics of turbulence during the passage of a very severe Cyclonic Storm Nivar-2020", September-November 2025 [Supervisor: Siddarth Shankar Das].
2. Ananthakrishnan, G, Detection of Pyroxene in different Craters in Moon using Moon Mineralogy Mapper (M3), Department of Geology, University of Kerala, Joint Science Academies Summer Research Fellowship Program, May-July 2025. [Supervisor: Uma, K. N.]
3. Kovvuri Vijaya Ishwarya, INSAT-3DR: A New Perspective on the Classification of Clouds, Department of Meteorology and Oceanography, Andhra University, Joint Science Academies Summer Research Fellowship Program, May-July 2025. [Supervisor: Uma, K. N.]

स्कूल, कॉलेजों एवं विश्वविद्यालयों में व्याख्यान / LECTURES at SCHOOLS/COLLEGES/UNIVERSITIES

Sathiyamoorthy V.

- "Weather & Climate Satellites of India" Department of Remote Sensing, Bharathidasan University, Tiruchirappalli, 20 March 2025.
- "Roll clouds of the Arabian Sea", Atmospheric and Oceanic Sciences Group, Space Applications Centre, Ahmedabad, 23 September 2025.

Satheesh Thampi R.

- "Unraveling the mysteries of the Sun and solar wind using the Plasma Analyser Package for Aditya (PAPA) onboard Aditya-L1 solar mission",Pioneer Kumaraswamy College, Nagercoil, 27 February 2025.

Bala Subrahamanyam D.

- "Evolution of a new science stream – Enroute inhibitions – and the destiny", National Space Day 2024 Lecture, Department of Physics, Govt College for Women, Thiruvananthapuram, 23 August 2024.

Smitha V. Thampi

- Chandrayaan-3: Touching the Moon, Inspiring a Nation, National Space Day 2025, SN College, Varkala, 12 August, 2025.

Vijayakumar S. Nair

- "Air quality monitoring in urban areas", Amity University, UP, December 2, 2024.
- "Exploring Climate Change from Space", Mar Ivanios College, Thiruvananthapuram, October, 7, 2024.
- "Space for Earth" National Space Day Celebrations, St. Thomas College Palai, August 27, 2025.
- "Exploring Climate from Space", Central University of Kerala, Kasargod, August 18, 2025.

Vipin K. Yadav

- "MAG (Aditya-L1) Data Analysis", IUCAA Hands-on Workshop on Solar Astronomy using Aditya-L1, Department of Physics, University College, Thiruvananthapuram, 20-22 August, 2025.
- "Hands-on Training: MAG (Aditya-L1) Data Analysis", 8th Aditya-L1 Workshop, IIT, Indore, 27-29 September, 2024.

Mukunda M Gogoi

- “Safeguarding Our Planet & Transforming Lives through Earth Observation Satellites: From Space to Society”, Keynote Speaker, National Space Day, Dibrugarh University, Assam, August 22, 2025.
- "Bridging Observations from Ground to Space: The Role of Aerosols in Climate Dynamics", DDU Gorakhpur University, Gorakhpur, September 17, 2024.

Dhanya M. B.

- Plasma Environment of the Moon as revealed by Chandrayaan-1, National Conference on Plasma Physics and Space Science, Department of Physics, Bharata Mata College, Thrikkakara, 8-9 October, 2024 (online).

Prijith S. S.

- ‘Space and Climate Change’, Inaugural programme of World Space Week - 2024 Reaching out to students, Jawahar Navodaya Vidyalaya, Calicut, September 30, 2024.
- ‘Application of Space Technology in Climate Science’, NASA Space Apps - 2024, Amrita Vishwa Vidhyapeetham, Kollam, October 06, 2024.

Renju, R.

- “Exploring Space: India’s Lunar Journey and Beyond”, National Space Day Celebration-2025, Assumption College, Changanassery, 14 August 2025.

Chemukula Mathin Yadav

- "PAPA (Aditya-L1) Data Analysis", IUCAA Hands-on Workshop on Solar Astronomy using Aditya-L1; Department of Physics, University College, Thiruvananthapuram, 20-22 August, 2025.
- "Hands-on Training: PAPA (Aditya-L1) Data Analysis", 8th Aditya-L1 Workshop; IIT, Indore, 27-29 September, 2024

वीएसएससी के युविका कार्यक्रम 2025 में व्याख्यान/ LECTURES IN YUVIKA PROGRAMME - 2025 at VSSC

Suresh Babu S.

- “Introduction to Space”, May18, 2025

Smitha V. Thampi

- “Chandrayaan and Mangalyaan", May22, 2025

Dhanya M. B.

- "Exoplanets & Life Component", May 24, 2025.

प्रशिक्षण कार्यक्रम में भागीदारी / PARTICIPATION IN TRAINING PROGRAMME

Sathiyamoorthy, V.

- ISRO Structured Training Programme-2025 on ‘Emerging Technologies & Trends for Geospatial Applications’, Regional Remote Sensing Centre-West, NRSC, Jodhpur, Rajasthan, 06-10 October 2025.

Vijayakumar S. Nair

- Helicopter Design for Martian Environment, Training Programme, VSSC, October 18, 2024.

Sijikumar S.

- ISRO Structured Training Program on Evolution of Inner Solar System: Remote Sensing Data Analysis and Instruments for Space Missions, Physical Research Laboratory, Ahmedabad, November 10-14, 2025.

Mukunda Gogoi

- Short-Term course on Quantum Technology, VSSC,Thiruvananthapuram, April 2-4, 2025.
- Space science and Technology Awareness Training (START) and IIRS Academia Meet, Indian Institute of Remote Sensing (IIRS), Dehradun, March 20-21, 2025.

Sobhan Kumar Kompalli

- ISRO Structured Training Program on ‘Evolution of Inner Solar System: Remote Sensing Data Analysis and Instruments for Space Missions’, Physical Research Laboratory, Ahmedabad, November 10-14, 2025.

Prijith S. S.

- ISRO Structured Training Programme on ‘Multi-Wavelength Astronomy with Ground and Space based facilities’, Physical Research Laboratory, Ahmedabad, November 25-29, 2024
- Short-Term course on ‘Quantum Technology’, VSSC, Thiruvananthapuram, April 2 - 4, 2025.
- Short course on ‘Radiative Energy Transfer’, URSC, Bengaluru, April 20-25, 2025

Pramod P. P

- ISRO Structured Training Program on Evolution of Inner Solar System: Remote Sensing, Data Analysis and Instrumentation for Space Missions", 10-14 November, 2025 at PRL, Ahmedabad.

Ambili K. M.

- ISRO Structured Training ProgrammeonEmerging Technology Trends in Geospatial Applications, RRSC-West, Jodhpur, October 06-10, 2025.

Renju, R.

- ISRO Structured Training Programmeon Advances in Satellite Radar Imaging, , Indian Institute of Remote Sensing, Dehradun, 23-27 September 2024.

Aneesh A. N.

- 'Software Training Programme on MATLAB', VSSC,August20-22, 2025.
- 'Microchip India MASTERs 2025', Bangalore, December16-19, 2025.

Suresh Kumar Reddy B.

- A Short-Term Programme on 'Polymer Chemistry, Processing and Characterization Techniques', VSSC,Thiruvananthapuram, January 20-23, 2025.
- A three-day Technology Update Programme on 'Spectroscopy and its Applications to Material Science, VSSC,Thiruvananthapuram,July08-10, 2025.

Koushik N.

- Short course on Radiative Energy Transfer, URSC, Bengaluru, 20-25 April 2025.

Santosh Kumar Pandey

- A three-day Technology Update Programme on "Spectroscopy and its Applications to Material Science", VSSC, Thiruvananthapuram, July 08-10, 2025.

Satheesh Kumar B

- Autodesk Inventor Training Programme, 22-26 September, 2025, HRDD/VSSC.
- FEAST Training Programme, 11-13 June, 2025, HRDD/VSSC.

Athul A. K.

- A five-day training on "Remote Sensing of Atmospheric Composition and Air Quality", at Space Application Centre, Ahmedabad, 04-08 August 2025.

Chandhini. P

- Centre for Space Science and Technology Education in Asia and the Pacific (CSSTEAP) short course on 'Solar Physics & Planetary Science', conducted by Physical Research Laboratory, Ahmedabad, 13-27 June, 2025.

संगोष्ठीयों एवं कार्यशालाओं में भागीदारी / PARTICIPATION IN SYMPOSIA/WORKSHOPS

K. Kishore Kumar

- TIFR Two-day User Meeting, Hyderabad, 27-28 October 2025
- NDACC-IRWG-TCCON-COCCON Annual Meeting, ARIES, Nainital, 16-20 June 2025
- International Symposium on Tropical Meteorology (INTROPMET 2025), Indian Institute of Tropical Meteorology, Pune, 18-20 November 2025.
- National Meet on Venus Orbiter Mission, ISRO HQ, Bangalore, October 29-30, 2025.

Siddarth Shankar Das

- International Symposium on Tropical Meteorology (INTROPMET 2025), Indian Institute of Tropical Meteorology, Pune, 18-20 November 2025.

Vijayakumar S. Nair

- Two Day User meeting, TIFR, Hyderabad, October 27-28, 2025.

Vineeth C.

- "Overview of science plan from UrVASIpayload", SAC Astronomy, Microgravity, Heliophysics, Ionosphere VaarTA (SAMHITA), SAC, ISRO, Ahmedabad, 05-06 May 2025.
- "National Meet on "ISRO's Venus Orbiter Mission-Science and Enhancing Academia Engagements", Science Programme Office, ISRO Headquarters, 29-30 October 2025.

Sunil Kumar S. V.

- National Meet on Venus Orbiter Mission, ISRO HQ, Bangalore, October 29-30, 2025.

Mukunda M. Gogoi

- Satellite Technology Day, U R Rao Satellite Centre (URSC), Bangalore, April 21, 2025.
- National Seminar on "The Role of Space Technology in Disaster Risk Management", Institute of Land and Disaster Management (ILDM), Thiruvananthapuram, March 11-12, 2025.
- Data Science and Technologies: Applications in Atmospheric and Space Sciences, NARL, Gadanki, January 20-31, 2025.

Prijith S. S.

- National Seminar on 'The Role of Space Technology in Disaster Risk Management', Institute of Land and Disaster Management, Thiruvananthapuram, 10-11 March, 2025.
- Grant Finale,BharathiyaAnthariksh Hackathon-2025, NRSC, Hyderabad, August 7-8, 2025.
- EOS-06 Utilization Projects Review Meeting, Space Application Centre, Ahmedabad, October 14, 2025 (Online).
- National Meet on Venus Orbiter Mission, ISRO HQ, Bangalore, October 29-30, 2025.

Renju, R.

- Workshop on Leadership for Early Career Women Researchers in Science, Technology, Engineering and Mathematics (STEM), Indian Institute of Space Science and Technology, Trivandrum, 14 July 2025.

Koushik N.

- National Meet on Venus Orbiter Mission, ISRO HQ, Bangalore, October 29-30, 2025.

Jayadev Pradeep

- TIFR Two-day User Meeting, Hyderabad, 27-28 October 2025
- Workshop on Variability and Stability of the Venus' Atmosphere in Various Spatiotemporal Scales Inferred from Space Missions and Numerical Simulations, International Space Science Institute, Beijing, 2-6 June, 2025 (online).
- National Meet on Venus Orbiter Mission, ISRO HQ, Bangalore, October 29-30, 2025.

Ramya C. B.

- Emerging Science, Technology and Innovation Conclave (ESTIC-2025), Bharat Mandapam, New Delhi, November 03-05, 2025.

Lima C. B.

- Emerging Science, Technology and Innovation Conclave (ESTIC-2025), Bharat Mandapam, New Delhi, November 03-05, 2025.

Oindrila Nath

- International Symposium on Tropical Meteorology (INTROPMET 2025), Indian Institute of Tropical Meteorology, Pune, 18-20 November 2025.

Athul A. K.

- "Satellite, Ground and Column Data for Air Quality Applications", 5-day workshop by National Institute of Technology, Calicut, December 08 – 12, 2025.

Nabarun Poddar

- National Training Workshop on Weather Radar: Theory, Calibration, Maintenance, Data analysis and Applications (NT Radar), Indian Institute of Tropical Meteorology, Pune, during 7-10 April 2025

Hadiya Nawal C. K.

- National Training Workshop on Weather Radar: Theory, Calibration, Maintenance, Data analysis and Applications (NT Radar), Indian Institute of Tropical Meteorology, Pune, during 7-10 April 2025
- International Symposium on Tropical Meteorology (INTROPMET 2025), Indian Institute of Tropical Meteorology, Pune, 18-20 November 2025.

हिंदी गतिविधियाँ / HINDI ACTIVITIES

विपिन कुमार यादव

I. वीएसएससी की हिन्दी समितियों की सदस्यता

1. सदस्य, वीएसएससी अंतर्जाल वेबसाइट पर हिन्दी अंतर्वस्तु की विवीक्षा समिति; मई, 2016 से.
2. सदस्य, वीएसएससी आंतरजाल वेबसाइट पर हिन्दी अंतर्वस्तु की विवीक्षा समिति; सितंबर, 2018 से.

II. हिन्दी में तकनीकी लेख एवं मौखिक प्रस्तुतियाँ

1. "प्रथम भारतीय सौर अभियान आदित्य-एल1 पर अवस्थित प्रवाहद्वार चुम्बकमापी मैग (MAG) प्रदायभार"; विपिन कुमार यादव, एवं अन्य; हिन्दी तकनीकी संगोष्ठी: अंतरग्रहीय मिशनों के लिए उन्नत प्रौद्योगिकी एवं चुनौतियाँ; अक्तूबर 18, 2024; द्रव नोदन प्रणाली केंद्र, वलियामला, केरल, पृष्ठ: 035:1-7
2. "आदित्य-एल1 पर अवस्थित मैग्नेटोमीटर (मैग, MAG) के प्रथम परिणाम"; विपिन कुमार यादव, एवं अन्य; अंतर केंद्र तकनीकी हिन्दी संगोष्ठी: विकसित भारत 2047 हेतु इसरो स्वदेशी पहल; नवंबर 13-14, 2024; अन्तरिक्ष उपयोग केंद्र, अहमदाबाद, गुजरात, पृष्ठ: 433-436

III. वीएसएससी की हिन्दी में गृह-पत्रिका "गगन" में लेख

1. "मेरी प्रथम मलेशिया यात्रा" गगन-59; अप्रैल – सितंबर 2024, पृष्ठ: 23-26

IV. हिन्दी प्रतियोगिताओं में निर्णायक

1. "कर्मचारियों के समूह 4 (कक्षा XI & XII) के बच्चों के लिए हिन्दी वक्तृता प्रतियोगिता"; हिन्दी माह समारोह; सितंबर 19, 2024; विक्रम साराभाई अन्तरिक्ष केंद्र, तिरुवनन्तपुरम.
2. "कर्मचारियों के समूह 4 (कक्षा XI & XII) के बच्चों के लिए हिन्दी देशभक्ति-गान गायन प्रतियोगिता"; हिन्दी माह समारोह; सितंबर 19, 2024; विक्रम साराभाई अन्तरिक्ष केंद्र, तिरुवनन्तपुरम.
3. "कर्मचारियों के समूह 1 (कक्षा IV & V) के बच्चों के लिए हिन्दी पाठन प्रतियोगिता"; हिन्दी माह समारोह; सितंबर 19, 2024; विक्रम साराभाई अन्तरिक्ष केंद्र, तिरुवनन्तपुरम, केरल.
4. "कर्मचारियों के समूह 1 (कक्षा IV & V) के बच्चों के लिए हिन्दी देशभक्ति-गान गायन प्रतियोगिता"; हिन्दी माह समारोह; सितंबर 19, 2024; विक्रम साराभाई अन्तरिक्ष केंद्र, तिरुवनन्तपुरम.
5. "कर्मचारियों के समूह 3 (कक्षा VIII, IX & X) के बच्चों के लिए हिन्दी वक्तृता प्रतियोगिता"; हिन्दी माह समारोह; सितंबर 20, 2024; विक्रम साराभाई अन्तरिक्ष केंद्र, तिरुवनन्तपुरम.
6. "कर्मचारियों के समूह 3 (कक्षा VIII, IX & X) के बच्चों के लिए हिन्दी देशभक्ति-गान गायन प्रतियोगिता"; हिन्दी माह समारोह; सितंबर 20, 2024; विक्रम साराभाई अन्तरिक्ष केंद्र, तिरुवनन्तपुरम.
7. "कर्मचारियों के समूह 2 (कक्षा VI & VII) के बच्चों के लिए हिन्दी पाठन प्रतियोगिता"; हिन्दी माह समारोह; सितंबर 20, 2024; विक्रम साराभाई अन्तरिक्ष केंद्र, तिरुवनन्तपुरम, केरल.
8. "कर्मचारियों के समूह 2 (कक्षा VI & VII) के बच्चों के लिए हिन्दी देशभक्ति-गान गायन प्रतियोगिता"; हिन्दी माह समारोह; सितंबर 20, 2024; विक्रम साराभाई अन्तरिक्ष केंद्र, तिरुवनन्तपुरम.
9. "वीएसएससी के वाहन-चालकों के लिए हिन्दी समाचार-पत्र वाचन प्रतियोगिता"; हिन्दी माह समारोह; अक्तूबर 01, 2024; विक्रम साराभाई अन्तरिक्ष केंद्र, तिरुवनन्तपुरम, केरल.
10. तकनीकी सत्र 1ब; तकनीकी हिन्दी संगोष्ठी: "अंतर-ग्रहीय अभियानों के लिए उन्नत प्रौद्योगिकी एवं चुनौतियाँ"; अक्तूबर 18, 2024; द्रव नोदन प्रणाली केंद्र, वलियमला, केरल.

V. हिन्दी लेखों के लिए पुरस्कार

1. प्रथम पुरस्कार; "प्रथम भारतीय सौर अभियान आदित्य-एल1 पर अवस्थित प्रवाहद्वार चुम्बकमापी मैग (MAG) प्रदायभार"; हिन्दी तकनीकी संगोष्ठी: अंतरग्रहीय मिशनों के लिए उन्नत प्रौद्योगिकी एवं चुनौतियाँ; अक्तूबर 18, 2024; द्रव नोदन प्रणाली केंद्र, वलियामला, केरल.
2. प्रथम पुरस्कार; "मेरी प्रथम मलेशिया यात्रा"; वीएसएससी हिन्दी गृह पत्रिका गगन-59; अप्रैल – सितंबर 2024.

राष्ट्रीय एवं अंतरराष्ट्रीय समारोह में सहभागिता/
PARTICIPATION IN NATIONAL AND INTERNATIONAL EVENTS

सम्मेलनों, संगोष्ठियों एवं कार्यशालाओं में आमंत्रित व्याख्यान/
INVITED LECTURES IN CONFERENCES/SYMPOSIA /WORKSHOPS

S. Suresh Babu

- "Aerosols – Tiny particles, Big Impacts", IIRS Academia Meet (IAM -2025), Indian Institute of Remote Sensing, Dehradun, 21 March, 2025.
- "Aerosol Radiative Forcing over India and Regional Climate", Keynote Address, Annual Day Event of the Department of Earth and Environmental Science, Indian Institute of Science Education Research (IISER), Bhopal, 24 -25, March, 2025.
- "Satellite Remote Sensing of Aerosols over South Asia" 24th lecture of IASTA monthly online lecture series, 31 July, 2025
- "Aerosols at the 'three' poles and their climate impacts", Keynote Speaker, Session on Space Weather and Meteorology, National Conference on Polar Sciences, National Centre for Polar and Ocean Research, Goa, 16 – 18, September, 2025
- "Aerosol–Cloud Interaction over Indian Region: Current Understanding and Future Perspective", Invited Talk, Session on Aerosols, Clouds & Precipitation Processes, INTROMET 2025, Indian Institute of Tropical Meteorology, Pune, 18 – 20, November, 2025.
- "Aerosols: Tiny particles, big impacts", Eminent Scholar in Resident Programme, CUSAT, 10 November 2025.
- "High Altitude Ballooning for Stratospheric Aerosol and Climate Research", Users Meeting at TIFR National Balloon Facility, Hyderabad.

K. Kishore Kumar

- "A Review of Remote Sensing of Atmospheric Gravity Waves and their Role in the Vertical Coupling of Atmosphere", 6th URSI Regional Conference on Radio Science (6thURSI-RCRS 2024), Bhimtal, 22-25 October 2024.
- "Meteor Radar Network for Middle and Upper Atmospheric Monitoring in India", International Conference on Meteoroids, Meteors, Meteorites: Messengers from Space (MetMeSS-2024), Physical Research Laboratory, Ahmedabad, 20-22 November 2024.
- "Earth Observations to Planetary Exploration: A Regime shift in Space Programs", Telangana Science Congress, Warangal, 19-21, August 2025
- "Spatial Mapping of Stratospheric Dynamics in the Lagrangian Frame of Reference", Two-Day User Meeting at TIFR balloon Facility, Hyderabad, 27-28 October 2025.
- "Best of Both Worlds: An integrated approach using space and ground-based radars for investigating monsoon clouds", International Symposium on Tropical Meteorology (INTROPMET 2025), Indian Institute of Tropical Meteorology, Pune, 18-20 November 2025.

Sathiyamoorthy V.

- "Indian Meteorological Satellites for Weather and Climate Monitoring" World Meteorological Day celebration, IISER, Thiruvananthapuram, 25 March 2025.
- "Introduction to Satellite Meteorology (Part-I and Part-II)" NCESS Training Course on Introduction to Meteorology & Convective Storms, NCESS, Thiruvananthapuram, 18-19 August 2025.
- "Rolls and Closed Convective Cloud Cells: Lesser-known Monsoon Clouds" NCESS Lecture Series –NCESS, Thiruvananthapuram, 19 August 2025.
- "Earth Radiation Balance Monitoring from Satellites (Part - I and II)' UN-Centre for Space Science and Technology Education in Asia and the Pacific (CSSTE-AP) course on 'Satellite Meteorology and Global Climate', Space Applications Centre, Ahmedabad, 22-23 September 2025.

Satheesh Thampi R.

- Science from Plasma Analyser Package for Aditya (PAPA) onboard Aditya-L1, The Variable Sun: Past, Present and Future, IIST, 13-17 October, 2025.
- Science from Plasma Analyser Package for Aditya (PAPA) onboard Aditya-L1, IUCAA Hands-on Workshop on Solar Astronomy using Aditya-L1, Department of Physics, University College, Thiruvananthapuram, 20-22 August, 2025.

Raj Kumar Choudhary

- "From Doubt to Discovery: The Story of the Lunar Ionosphere and Chandrayaan", International Conference on Emerging Trends in Physical and Life Sciences (ICETPLS 2025), IEHE, Bhopal, 8–9 October 2025.

Smitha V. Thampi

- In-situ techniques for Space Exploration, IIRS, Dehradun, October 12, 2025 (online).
- In-situ techniques for Space Exploration, IIRS, Dehradun, May 7, 2025 (Online).

Siddarth Shankar Das

- "Decoding Stratosphere-Troposphere Interactions over the Asian Summer Monsoon Region: A Radar and Satellite Perspectives" INTROPMET-2025,Indian Institute of Tropical Meteorology, Pune, 19 November 2025.
- "The ozone paradox in the extreme weather conditions", Workshop on Feedbacks of uncertain components on the extreme weather and climate, SRM Institute of Science and Technology, Chennai, 20 June 2025.
- "Dynamics and Chemistry of the Upper Troposphere and Lower Stratosphere", 3rdInternational Conference on Higher Education Institute Challenges Solution for Sustainable Development Goal 2024 (ICSDG-2024) held at SRM Institute of Science and Technology, Chennai during 3-5 December 2024.

Vijayakumar S. Nair

- "Aerosol-Fog Interactions over India: Uncertainty in Hygroscopicity modelling", International symposium NANO - Extremes on Ultrafine Aerosol Processes and Numerical Modeling of Urban Climate - Extreme, IIT Madras, February 24–26, 2025.
- "Space and Climate Change", Public lecture organized by Kerala State Science and Technology Museum in association with Break through Society, October 5, 2024.

Vipin K. Yadav

- Magnetic Field Measurements in Space: Indian Perspective, 10th Plasma Science Society of India – Plasma Scholars Colloquium (PSSI-PSC-2024), Indian Institute of Technology (IIT), Delhi, 04 July, 2024.
- Streaming Plasma Instabilities in the Interplanetary Space and the Interstellar Medium, The 2nd Global Forum and International Conference on Industrial Plasma Processes and Diagnostics 2025 (IPPD 2025), Indian Institute of Technology (IIT), Delhi, 18-20 May, 2025 [Keynote address].
- In-situ measurements of magnetic fields, using Aditya-L1, IUCAA Hands-on Workshop on Solar Astronomy using Aditya-L1, Department of Physics, University College, Thiruvananthapuram, 20-22 August, 2025.
- Interplanetary Magnetic Field (IMF) Fluctuations during Solar Transients Events: Observations by MAG onboard Aditya-L1 Spacecraft, Astronomical Society of India (ASI) Symposium on Cosmic Vision 2047: Solar and Planetary Dynamics through Observations and AI/ML, JECRC University, Jaipur, 08-10 September, 2025.
- Observations of Extreme Solar Transient Events by MAG Payload onboard Aditya-L1 Spacecraft around L1 Point, 9th Asia-Pacific Conference on Plasma Physics (AAPPS-DPP 2025), Fukuoka, Japan, 26 September, 2025.
- Science with Aditya-L1 MAG, The Variable Sun: Past, Present, and Future, IIST, Thiruvananthapuram, 13-17 October, 2025.
- Plasma Wave Studies at Lagrangian Points: L4 and/or L5; Discussion on India's Next Leap in Solar and Heliospheric Exploration; Indian Institute of Astrophysics (IIA), Bengaluru; 30 July, 2024.

Kiran Kumar N.V.P.

- "Atmospheric Boundary Layer Dynamics: Characterization and Climate Impacts", Second Frontiers Symposium in Earth, Environmental and Sustainability Sciences 2025, IISER, Thiruvananthapuram, 8 February, 2025.

Dhanya M. B.

- Lunar Plasma Environment: Breakthrough Observations and Simulations" at the 4th Conference on Plasma Simulation (CPS-2024), Indian Institute of Geomagnetism, 11-13November, 2024.
- Lunar Exosphere: Findings from CHACE-2/Chandrayaan-2, Indo-Japanese Lupex science team meeting, 5 Dec 2025 (online).
- Practices in Mass Spectrometry Data Analysis Demonstration & case Study for Mass Spectrometry Data Analysis, CSSTEAP Online Short Course on 'Introduction to Space Science Data Analysis from Space-Borne Experiments', 17 November 2025 (online).
- Demonstration: Case Study for Mass Spectrometry Data Analysis - an example of in-situ study", Online course on "Archival and Access of Space Science Data, being organized by the Indian Institute of Remote Sensing (IIRS), Dehradun, 09 - 13 June, 2025.

Mukunda M.Gogoi

- "Black carbon aerosols over the Himalayas", Keynote Speaker, 1st National Him school on 'Cryosphere & Climate Change Studies' (NHC3S-1: 2025), National Institute of Hydrology (NIH), Roorkee, March 26, 2025.
- "Spaceborne Technology for Earth Meteorology", Special Lecture on World Meteorological Day, Regional Meteorological Centre, Guwahati, March 24, 2025.

Uma K.N.

- "Tracking the Rhythm of Storms: A Perspective from Radar Observations", Brainstorming Workshop on Organization of convection, Tropical storms, disturbances, and extreme weather, Cochin University of Science and Technology, Cochin, 7 July 2025.

Prijith S.S.

- 'Retrieval of Aerosol Properties from Space', Training Program on Air Pollution Hotspots using Satellite Data Set, Indian Institute of Technology, Bhubaneswar, December 28, 2024.

Renju R.

- "Introduction to Microwave Remote Sensing", NCESS Training Course on Introduction to Meteorology & Convective Storms, NCESS, Thiruvananthapuram,20 August 2025.

Ankush Bhaskar

- Solar Wind Transients and Geomagnetic Storms, International Conference on Solar cycle variability: From understanding to making a prediction, ARIES, Nainital, 14-18 October, 2024.
- AuroraMag and Future Magnetosphere Mission, Brainstorming meeting on Indian Satellite mission for Magnetosphere Exploration", IIG, Mumbai, 24-25 April, 2025.
- Modeling the arrival of the Multiple CMEs that triggered the 2024 May 10 Gannon Superstorm, Conference on Solar Wind-Magnetosphere-Ionosphere Coupling (COSMIC), IIG, Mumbai, 22-23 May, 2025.
- Space Science for a Space Weather Resilient Society, INYAS National Symposium and Mid-Year Meeting (MYM-2025) on "Advances in Science and Technology for Sustainable Future (ASTSF-2025)", VIT, Vellore, 18-20 September, 2025.

Rubia R

- Generation of electrostatic waves over the Lunar magnetic anomaly, Asia-Pacific Conference on Plasma Physics (AAPPS), Malacca, Malaysia, November 3-8, 2024.

संगोष्ठियों, सम्मेलनों, एवं कार्यशालाओं में सत्र आयोजन एवं अध्यक्षता / Organisational role in Symposia/Conferences/Workshops

Suresh Babu S.

- Member, Scientific Program Committee, National Conference on Polar Science (NCPS-2025), 16 -18, September, 2025, NCPOR, Goa.
- Member, Technical Program Committee, 14th Asian Aerosol Conference (AAC-2025), 1 -4, December, 2025, Taj The Trees, Mumbai.
- Member, Steering Committee for Bharatiya Antariksh Hackathon - 2025.
- Member, Organizing Committees for Outreach Events during ISRO-NASA Mission to ISS (Axiom-4)
- Mentor, Problem statement titled, 'Monitoring Air Pollution from Space: An integrated approach using Satellite observations and AI/ML techniques',Bharatiya Antariksh Hackathon-2025.

Kishore Kumar K.

- Moderator for a Panel Discussion on 'Venusian atmosphere modelling, retrieval techniques, image processing and simulations and significance of archival data analysis for Venusian Atmosphere', Venus Orbiter Mission-National Meet, ISRO HQ, Bengaluru, 29-30 October 2025

Siddarth Shankar Das

- Member of Scientific Organising Committee, Commission-F, Co-Convener: F06 and Session Chairs for Commission-F and G, 6th URSI Regional Conference on Radio Science (URSI-RCRS 2024), Bhimtal, India, 22-25 October 2024.

Satheesh Thampi R.

- Member, Scientific Organising Committee (SOC) of Astronautical Society of India - ASI-2025, JCERC University, Jaipur, September 2025.
- Member, Scientific Organising Committee (SOC) of Venus Science Congress–Venus-SC-2025, Physical research Laboratory (PRL), Ahmedabad, October 2025.
- Session Chair for Session 1-A: Atmosphere and Ionosphere, Venus Science Conference 2024 (Venus – SC-2024), PRL, Ahmedabad, 23-24 September, 2024.

Vipin. K. Yadav

- Chair for Session 8 on "Fundamentals of Plasmas and Sources, Space/Astrophysical Plasmas, Energy Conversion and Environment Technologies"; The 2nd Global Forum and International Conference on Industrial Plasma Processes and Diagnostics 2025 (IPPD 2025), Indian Institute of Technology (IIT), Delhi, 18-20 May, 2025.

- Chair for Session 5 on "Introduction to Sun; IUCAA Hands-on Workshop on Solar Astronomy using Aditya-L1", Department of Physics, University College, Thiruvananthapuram, 20-22 August, 2025.
- Convener for the session on 'Lunar Ambient Environment' of the brainstorming meeting on 'Habitat Design and Construction on the Moon's Surface', organised jointly by IIT Roorkee and ISRO during 7-8 August 2025 at Greater Noida Campus (GNEC) of IIT Roorkee, New Delhi.
- Member, Scientific Organizing Committee (SOC); 8th Aditya-L1 Support Cell Workshop, IIT, Indore, 27-29 September, 2024.
- Member, Scientific Programme Committee (SPC); "The 2nd Global Forum and International Conference on Industrial Plasma Processes and Diagnostics 2025", IIT, Delhi,18-20 May, 2025.

Mukunda M Gogoi

- Panelist, "Chambers of Space Science and Technology: Opportunities for the students in India", National workshop on Space Science Exploration and career Opportunities, Indian Institute of Remote Sensing (IIRS), Dehradun, March 20, 2025.
- Guest Editor, Atmosphere, Special issue on "Dynamics of Aerosol Distribution and Transport", 2025-2027.
- Member, National Advisory Committee, International Conference on Environmental Sustainability (ICES 2025), TNAU, Coimbatore, 2025.

Prijith S. S.

- Mentor, Problem statement titled, 'Monitoring Air Pollution from Space: An integrated approach using Satellite observations and AI/ML techniques',Bharatiya Antariksh Hackathon-2025.
- Convener, Functional Committee for Thematic Workshop on 'Space and Climate Change', World Space Week -2024. VSSC, Thiruvananthapuram, October 09, 2024.
- Judge, NASA Space Apps-2024 Hackathon, Amrita Vishwa Vidhyapeetham, Kollam, October 06, 2024.

Revathy Ajayakumar

- Conducted One day Training on "RashtriyaKarmyogi", on October 15 and 23, 2025; HRDD, VSSC, Thiruvananthapuram.

Tandule Chakradhar Rao

- Panelist, "Deliberations on Collaborative Effects to Enhance SOLAS Science in the Indian Ocean Region", SOLAS Open Science Conference 2024, CSIR - National Institute of Oceanography, Goa, India, November 10-14, 2024.

VenkataramanV.

- Conducted One day Training on "RashtriyaKarmyogi", on October 15 and 23, 2025; HRDD, VSSC, Thiruvananthapuram.

Ankush Bhaskar

- Resource person for the Sky Watch program organized by IISER-Trivandrum for the school Students from Vithura Panchayath, Trivandrum, and interaction with IISER students, IISER-Trivandrum, 03 February 2025.
- Co-convener, Session: "Geomagnetic observations, indices and products for Space Science, Space Weather, and Space Climate Applications", International Association of Geomagnetism and Aeronomy (IAGA), Portugal, 31 August - 5 September, 2025.
- LOC member and Chair of session "Solar Energetic Phenomena", The Variable Sun: Past, Present and Future, IIST/VSSC, 13-17 October, 2025.

डॉ के राजीव को धन्यवाद / Thanks to Dr. K. Rajeev

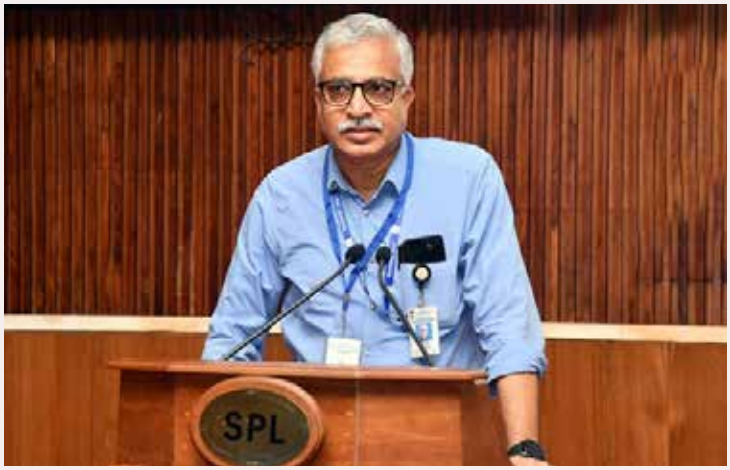

Dr. K. Rajeev, after spearheading SPL as Director during February 2021 to May 2025 laid down office on 31 May 2025. Dr. Rajeev joined SPL, VSSC in December, 1994 after obtaining PhD in Physics from the University of Kerala under ISRO Research Fellowship scheme. He has made major scientific contributions in various domains of research in SPL including boundary layer physics, tropical meteorology, middle atmospheric dynamics, aerosols, clouds and radiation transfer. He led the ISRO-GBP-NOBLE Project, a national project, to characterize atmospheric boundary layer at distinct geographical and climate zones in India. Representing India in COSPAR Council, he brought Indian space science initiatives to International forums. We sincerely thank and acknowledge the services of Dr. K. Rajeev for the progress of SPL.

Dr. K. Rajeev joined VSSC as Prof. Satish Dawan Professor on October 6, 2025.

एसपीएल के वैज्ञानिक सलाहकार समिति की 41 वी बैठक / 41st Meeting of the Scientific Advisory Committee of Space Physics Laboratory, VSSC, 16-17 January 2025


चंद्रयान 2 ने किया कमाल
ISRO को हाथ लगी बड़ी सफलता
Coronal Mass Ejection (CME)
Enhancement of the day-side lunar exosphere
Moon
गोमन्तक
THE TIMES OF INDIA
Chandrayaan-2 detects solar ejection's impact on moon's atmosphere
THE NEW INDIAN EXPRESS
Chandrayaan-2 Makes First Ever Observation Of Sun's Coronal Mass Ejections' Effects On The Moon
Coronal Mass Ejection (CME)
BREAKING NEWS
FLARES ON MOON
POSTED BY ISRO
ThePrint
ISRO's Aditya-L1 decodes how solar storms impact Earth's magnetic field
Sun
Coronal Mass Ejection (CME)
Enhancement of the day-side lunar exosphere
Moon
THE HINDU
ETPrime
Chandrayaan-2 makes first ever observation of impact on Moon, says ISRO
दिप्रिंट
इसरो के आदित्य-एल1 से सौर तूफान के पृथ्वी के चुंबकीय क्षेत्र को प्रभावित
मिली जानकारी
CHANDRAYAAN-2 MAKES SCIENTIFIC BREAKTHROUGH
Chandrayaan-2 observes Sun's impact on moon
NDTV
ISRO's Aditya-L1 Study Reveals How October 2024 Solar Storm Affected Earth's Magnetic Field
PRESSURE SPIKE IN LUNAR ATMOSPHERE
CHANDRAYAAN-2 DETECTS SUN'S IMPACT ON MOON
Chandrayaan-2 detects first CME impact on Moon
news nine
PRESS TRUST OF INDIA
India's premier news agency
Back
Home > National > ISRO's A... how solar storms...
जागरण
भारत के 'आदित्य' ने खुलवाई सौर तूफानों की पहेली, पृथ्वी के चुंबकीय क्षेत्र पर पड़ने वाले प्रभाव को समझने में की मदद
DECCAN Chronicle
ISRO's Aditya-L1 Decodes ... Storm on Earth's Invis...
nature index
Home News Current Index Research leaders Supplements Further analysis
Impact of a Coronal Mass Ejection on the Lunar Exosphere as Observed by CHACE-2 on the Chandrayaan-2 Orbiter
Journal: Geophysical Research Letters
Published: 2025-08-16
DOI: 10.1029/2025GL115737
Affiliations: 1
हिंदुस्तान

SPL in NEWS

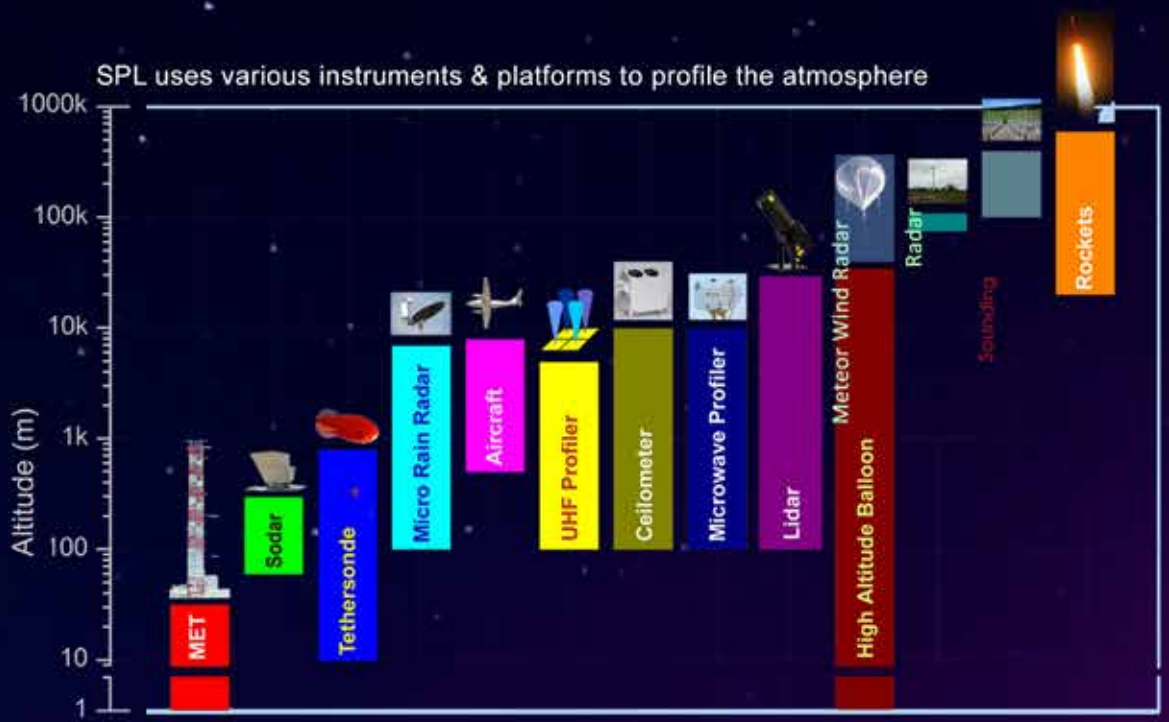

SPACE PHYSICS LABORATORY

Vikram Sarabhai Space Centre, Thiruvananthapuram - 695 022, INDIA

Email: directorspl@vssc.gov.in, Ph: +91 471 256 3663

https://spl.gov.in